Rockefeller University
Digital Commons @ RU

Student Theses and Dissertations

2016

Analysis of Hepatocyte Secretion Pathways: A Case Study on Hepatic Apolipoproteins, Serum Albumin, and Hepatitis C Virus

Constantin N. Takacs

Follow this and additional works at: https://digitalcommons.rockefeller.edu/student_theses_and_dissertations

 Part of the Life Sciences Commons

Recommended Citation

Takacs, Constantin N., "Analysis of Hepatocyte Secretion Pathways: A Case Study on Hepatic Apolipoproteins, Serum Albumin, and Hepatitis C Virus" (2016). *Student Theses and Dissertations*. 305.
https://digitalcommons.rockefeller.edu/student_theses_and_dissertations/305

This Thesis is brought to you for free and open access by Digital Commons @ RU. It has been accepted for inclusion in Student Theses and Dissertations by an authorized administrator of Digital Commons @ RU. For more information, please contact mcsweej@mail.rockefeller.edu.

ANALYSIS OF HEPATOCYTE SECRETION PATHWAYS: A CASE STUDY ON HEPATIC APOLIPOPROTEINS, SERUM ALBUMIN, AND HEPATITIS C VIRUS

A Thesis Presented to the Faculty of

The Rockefeller University

in Partial Fulfillment of the Requirements for

the degree of Doctor of Philosophy

by

Constantin N. Takacs

June 2016

© Copyright by Constantin N. Takacs 2016

ANALYSIS OF HEPATOCYTE SECRETION PATHWAYS: A CASE STUDY ON HEPATIC APOLIPOPROTEINS, SERUM ALBUMIN, AND HEPATITIS C VIRUS

Constantin N. Takacs, Ph.D.

The Rockefeller University 2016

The hepatocyte is one of the major secretory cell types in the body. It fulfills many of the liver's essential functions in protein secretion, lipid storage and transport, and excretion. Some of these functions are carried out via polarized secretion of simple protein cargo, such as serum albumin, or large macromolecular lipid-protein complexes, the lipoproteins. The hepatocyte is also the site of infection of several hepatotropic viruses. Of these, hepatitis C virus (HCV) is peculiar due to its close structural and functional association with the hepatic lipoproteins. All these cargoes are transported from the endoplasmic reticulum (ER) to the cell surface by the vesicular secretory pathway, yet insufficient knowledge exists regarding the molecular regulation of their secretion by the hepatocyte. Furthermore, differential modalities of regulation may be involved in the shuttling of such a diverse set of cargoes as albumin, the lipoproteins and HCV.

The work presented here head-starts a comprehensive examination of how the hepatocyte regulates the secretion of the following cargoes: serum albumin, the apolipoproteins E and B100 (ApoE and ApoB100, respectively, both lipoprotein components, and surrogate markers for these complex macromolecular particles), and HCV, a lipoprotein-associated virus. I propose to combine genetic, biochemical, virological and imaging approaches to identify which vesicular secretory pathways are

utilized by each of these cargoes. These approaches include inactivation of specific vesicular transport pathways, accompanied by measurements of their effects on cargo secretion efficiencies, and establishment of functional fluorescent protein-tagged cargo markers to be used in live cell imaging experiments.

I begin by describing a dominant negative (DN) Rab GTPase screen that I performed to identify Rab proteins involved in ApoE, ApoB100 or albumin secretion. The small Rab GTPases control individual steps of vesicular transport. I analyzed how expression of individual dominant negative Rab proteins affected cargo secretion compared to expression of their wild type (WT) counterparts. I identified several Rabs that caused significant changes in secretion, many of which had previously been described as regulators of various exocytic vesicular transport steps.

I next present ongoing work that aims to define the involvement of the Rabs 11a, 11b, 8a, and 8b in hepatic cargo secretion. Their dominant negative mutants exhibited some of the largest secretion phenotypes in my dominant negative Rab screen. These Rabs have been implicated in various aspects of post-Golgi secretion in polarized and non-polarized cell types. I thus discuss the implications of their involvement in cargo secretion in the polarized hepatocyte and outline my ongoing efforts to define the parameters of this involvement.

I also investigated the function of Rab1b in hepatic secretion. I show that inactivation of Rab1 function, by expression of a set of dominant negative mutants, or by expression of a bacterial effector which affects Rab1 function, led to impairment of albumin, ApoE, ApoB100 and HCV secretion. I implicate Rab1, for the first time to my knowledge, in the transport of these cargoes. I also document differences in the

sensitivity of cargo secretion to the various means of Rab1 inactivation. ApoE secretion, in particular, was insensitive to several means of transport inactivation, consistent with existing models of differential regulation of hepatic cargo transport.

Lastly, I functionally characterize an ApoE-green fluorescent protein fusion (ApoE-GFP). I show that while ApoE-GFP does not support infectious HCV release, a hallmark function of untagged ApoE, ApoE-GFP nevertheless reproduces several known behaviors of ApoE that have been associated with lipoprotein release. I thus conclude that ApoE-GFP may be a useful marker for live cell imaging of lipoprotein release.

This work therefore identifies potential regulators of hepatic cargo transport, establishes molecular tools useful for the continued study of cargo secretion in hepatocytes and elsewhere, and advances the understanding of the involvement of Rabs 11, 8, and, in particular, Rab1, in the regulation of hepatic cargo transport. I propose that this work forms a solid foundation for extensive studies on how these biomedically relevant hepatic cargoes are secreted.

To my grandmother, Aurica Ardelean (1926-1996)

For all the hardship that you went through, while on your own and on a janitress' income having raised two daughters and having helped raise three grandchildren. We have achieved much in our lives, in great part thanks to you.

Thank you, wherever you are!

ACKNOWLEDGEMENTS

I would not have reached this threshold in my professional life without the guidance of Drs. Sanford Simon and Charles Rice, my dissertation advisers. Thank you for mentoring me during the past six years! Thank you for allowing me to pursue this ambitious project, for nurturing my ideas and for steering me through the rough waters of scientific inquiry. Thank you for your brilliant ideas, for making your labs such welcoming places, and for providing wonderful examples of leadership. Thank you for believing in me, and for pushing me to believe in myself as well.

To Drs. Paul Bieniasz and Elaine Fuchs, my thesis committee chair and faculty member, respectively, thank you for being there for me with advice, for evaluating my work year in and year out, and for providing such insightful views on what it means to become and to be a scientist. To Dr. William Balch, thank you for traveling to New York from sunny Southern California to be present during my defense, for reading and evaluating my thesis work, and for having produced such an impressive body of work that I heavily relied upon during my own research expeditions.

I send thanks to everyone in the Rockefeller University's Dean's Office, for offering me the chance to be a part of the wonderful scientific community here at Rockefeller, and for helping make the life of a graduate student so seamlessly easy.

Many thanks also go to my lab mentors and collaborators. To Dr. Margaret Scull, equally for her endless knowledge of HCV biology and for her ever smiley demeanor. Meg, I foresee you will become an extraordinary mentor to all your future grad students, as you have been a mentor, a colleague and a friend to me. To Dr. Ursula Andreo, for

sharing her wonderful expertise in all things lipoprotein, for reading and commenting on my entire thesis, and for her ever charming French demeanor. To Caroline Gleason, Brenna Flatley, Rachel Belote, Colin Belanger for amazing help with all things experimental. To Jenna Lobby and Adam Fuller for being wonderful students. To Dr. Marina Bleck for teaching me so patiently so many techniques. To Drs. Viet Loan Dao Thi and Xianfang Wu for our joint involvement in defining new hepatic cell culture models. To Dr. Michelle Itano for being fluent in statistics and such a wonderful lab neighbor and friend. To Dr. Joseph Luna, for being an example of erudition and endless enthusiasm. To Ursula Andreo, Margaret Scull, Michelle Itano, Gabriella Spitz, Viet Loan Dao Thi and Caroline Gleason for reading my thesis. To Drs. Alison North, Kaye Thomas and Svetlana Mazel, for running amazingly useful Resource Centers, and for being wonderful teachers. To Dr. Craig Roy of Yale University, for sharing his DrrA construct. To everyone in the Simon and Rice labs, who have been my friends and my colleagues, and without whom my past seven years would not have been the same.

I am very grateful to the Howard Hughes Medical Institute for its generosity in providing me with a predoctoral fellowship over three years of my graduate student tenure. A significant part of this project was sponsored by the Center for Basic and Translational Research on Disorders of the Digestive System Through the generosity of the Leona M. and Harry B. Helmsley Charitable Trust. I am thankful to Dr. Barry Coller, Dr. Jan Breslow, and to Maija Neville-Williams of the Rockefeller University Hospital for their continued support and assistance.

I next wish to thank two amazing past mentors. First to Dr. Christine Jacobs-Wagner, of Yale University, my undergraduate adviser. Christine has been a wonderful

scientific and writing mentor during my early years of formation as a bench scientist, and she has taught me many lessons that will stay with me forever. I also thank my middle-school math teacher Elena Corbeanu for the numerous times she found herself devoting incredible amounts of extra effort to the task of teaching me and helping me succeed. Of all my teachers and mentors she has been responsible, in the largest part, for my choice to follow a scientific career path.

I would not be reaching this milestone without incredible support from my friends and from my family. My mother and father, Maria and Alexandru have sacrificed so much throughout their lives such that my brother Ducu and I have the opportunities that they lacked. It saddens me that our success takes us so far away from them. I also thank my aunt and uncle, Elena and Horia Cobzaş, my cousin Ioana Ţunaş, my niece Ana-Maria, and my little cousin Bogdănel. They have been bringing endless joy into my life.

Many friends have also been here for me, at times of difficulty and at times of happiness. I have been made a better person for knowing them, and they have brought rays of sunshine into my life. Silvia Caballero, I shall never forget our after-dinner chat in the Annenberg Hall in Cambridge - we have not stopped being friends since that night, and I do not see how this will ever change. Rachel Belote, we have shared ups and downs, in life, or while doing science in the lab. Now and forever, you shall be my wisest friend. Casandra Panea, you have been a comfort so many times, and a great friend, both here and in college. Lastly, I thank Mary Jo Worthey-Warren and her late husband Richard Warren, Matthew Tjajadi, Lavanya Raghavan and many other friends that have been with me through tough times and through joyous times, and whom I love dearly.

TABLE OF CONTENTS

Chapter 2: Materials and Methods

Chapter 3: A Dominant Negative Rab GTPase Screen Identifies Regulators of Hepatic Cargo Secretion

Chapter 4: Ongoing Characterization of the Involvement of Rab11 and Rab8 in Hepatic Cargo Secretion

Chapter 5: Involvement of Rab1 in Hepatic Cargo Transport

Chapter 6: Functional Characterization of an ApoE-GFP Fusion

LIST OF FIGURES

LIST OF TABLES

LIST OF GENERAL ABBREVIATIONS

ApoB	Apolipoprotein B
ApoB100	Apolipoprotein B100
ApoB48	Apolipoprotein B48
ApoE	Apolipoprotein E
ApoE2	Apolipoprotein E, isoform 2
ApoE3	Apolipoprotein E, isoform 3
ApoE4	Apolipoprotein E, isoform 4
Arf	ADP ribosylation factor
cDNA	Complementary DNA
CMV	Cytomegalovirus
COPI	Coat protein complex I
COPII	Coat protein complex II
DN	Dominant negative
DNA	Deoxyribonucleic acid
EGFP	Enhanced green fluorescent protein
ELISA	Enzyme-linked immunosorbent assay
Endo H	Endoglycosidase H
ER	Endoplasmic reticulum
ERGIC	ER-Golgi intermediate compartment
FLuc	Firefly luciferase
GAP	GTPase activating protein
GEF	Guanine nucleotide exchange factor
GDI	Guanine nucleotide dissociation inhibitor
GDP	Guanosine diphosphate
GFP	Green fluorescent protein
GTP	Guanosine triphosphate
GTPase	GTP hydrolase (GTP γ-phosphatase)
HCV	Hepatitis C virus
HDL	High-density lipoprotein
HFLC	Human fetal liver cultures
HIV-1	Human immunodeficiency virus 1
Huh-7.5	Human hepatoma 7.5 cell line
IDL	Intermediate-density lipoprotein
iHeps	Induced, hepatocyte-like cells
IRES	Internal ribosome entry site
I.U.	Infection units
LDL	Low-density lipoprotein
LDLR	Low-density lipoprotein receptor; LDL receptor
MCS	Multicloning site
mEGFP	Monomeric enhanced green fluorescent protein
MOI	Multiplicity of infection
mRNA	Messenger RNA
NS	Nonstructural protein

PCR	Polymerase chain reaction
PGK	Phosphoglycerate kinase
PNGase F	Peptide-*N*-glycosidase F
qRT-PCR	Quantitative reverse transcription polymerase chain reaction
RFP	Red fluorescent protein
RNA	Ribonucleic acid
RNAseq	RNA sequencing
s.d.	Standard deviation
SDM	Site-directed mutagenesis
SDS-PAGE	Sodium dodecyl sulfate polyacrylamide gel electrophoresis
siRNA	Small interfering RNA
TGN	Trans-Golgi network
UTR	Untranslated region
VLDL	Very low-density lipoprotein
VSVg	Vesicular stomatitis virus glycoprotein
$VSVg_{tsO45}$	VSVg temperature sensitive mutant, strain Orsay, mutation tsO45
WPRE	Woodchuck hepatitis virus posttranscriptional regulatory element
WT	Wild type

Chapter 1

Introduction

1.1 General overview

This thesis describes my efforts, part of a larger and more ambitious endeavor, to molecularly characterize the regulation of the secretion of some complex and biomedically important hepatocyte-derived cargoes. My work focused on understanding the release of the following hepatic cargoes: serum albumin, the lipoprotein components ApoE and ApoB100, and the lipoprotein-associated HCV. My work also touched on the regulation of intracellular secretory vesicular transport, in part in the context of cell polarization. To place these efforts into greater context, and to introduce relevant facts and concepts regarding the major players in this work, I start by providing some background information. I first introduce some general principles of intracellular vesicular traffic regulation and I mention peculiarities of transport regulation in polarized cell systems. Since the greatest part of my work focused on how members of the Rab family of small GTPases control hepatic cargo secretion, I describe the general functional principles applicable to these proteins in greater details, and also introduce some widely used methods to investigate Rab function. I next discuss the hepatocyte, the cell type whose secretory function I investigate, and draw connections between its organization and the processes it carries out. I more extensively introduce the hepatic secretory cargoes that this work focuses on, namely serum albumin, the hepatic lipoproteins, and HCV. For HCV, I place particular emphasis on the functional association between the virion assembly and release portions of the viral life cycle, and the assembly and release

of the hepatic lipoproteins. I conclude by summarizing the goals of this project, the study of which will be expanded upon in greater detail in the following chapters.

1.2. Intracellular vesicular transport

A hallmark organizational principle governing eukaryotic cell structure and function is compartmentalization. For example, the nucleus stores and expresses genetic information, the ER fulfills numerous biosynthetic functions, mitochondria deal with energy production, and lysosomes carry out many degradative processes. Functional segregation is in part achieved by encasing the respective functions in membranous compartments: the membrane-bound organelles. Integration of function also requires communication between the various systems, ensuring that distinct or even opposite processes, such as protein synthesis and degradation, nevertheless occur under harmonious regulation.

An important process that ensures communication between distinct organelles and integration of their functions is vesicular transport (Bonifacino and Glick, 2004; Palade, 1975). The paradigm is simple, as depicted in Figure 1.1A: a portion of the limiting membrane of a donor organelle pinches off as a sealed vesicle, or even as a bigger and pleiomorphic tubulo-vesicular structure. This transport carrier then travels to a target compartment, tethers to it, and the carrier and target membranes fuse, thus releasing the contents of the carrier. The cargo transported may be a soluble lumenal component, such as a secreted protein, a membrane-associated molecule, such as a transmembrane receptor, or the very lipids that form the membrane.

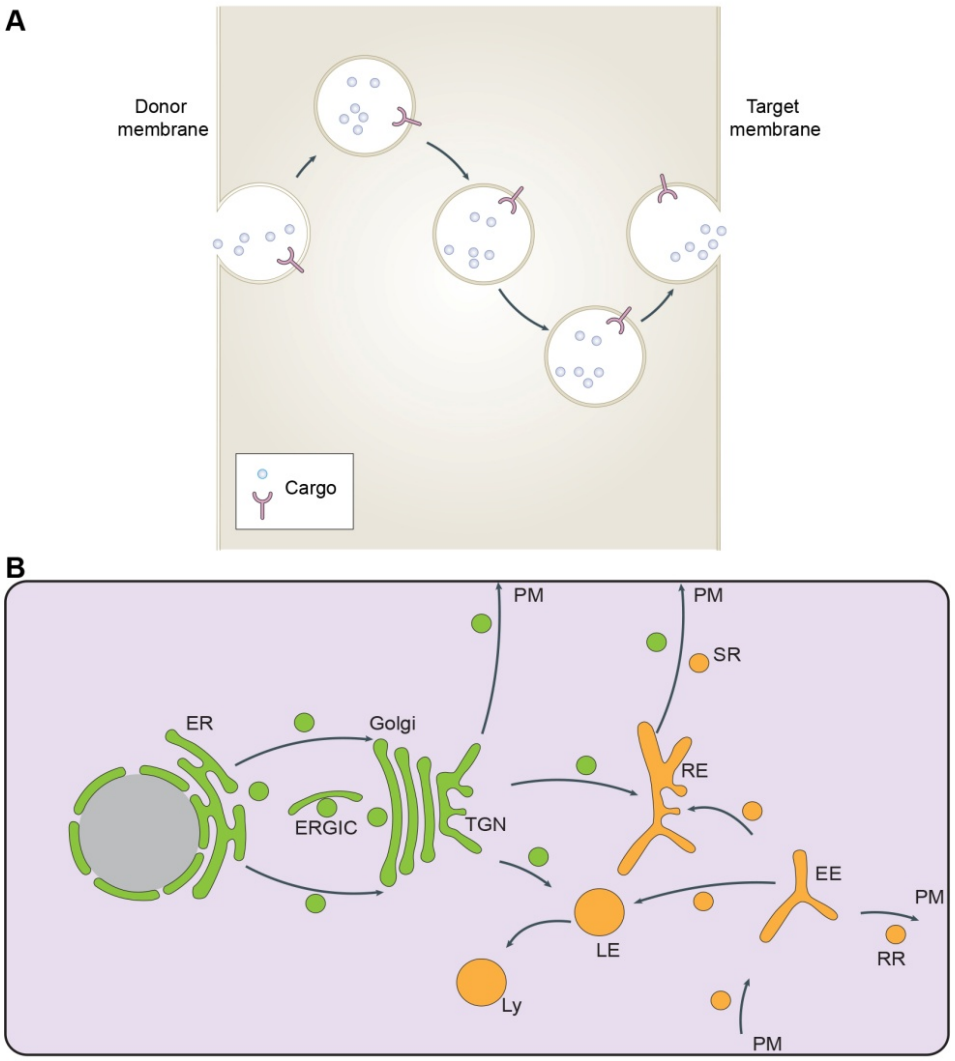

Figure 1.1. Principles of intracellular vesicular transport. (A) Simplified schematic of vesicular traffic between membrane-bound intracellular organelles (for detailed model see Figure 1.3). A vesicle loaded with cargo pinches off a donor organelle membrane, then travels to a target compartment, where the vesicle and target membranes fuse, releasing the cargo. (B) Simplified depiction of major vesicular transport pathways. Green, the biosynthetic or secretory pathway; orange, the endocytic pathway. ERGIC, ER-Golgi intermediate compartment; TGN, trans-Golgi network; PM, plasma membrane; EE, early endosome; LE, late endosome; Ly, lysosome; RE, recycling endosome; RR, rapid recycling from an early endosome; SR, slow recycling from a recycling endosome. Figures adapted by permission from Macmillan Publishers Ltd: Nature Rev. Mol. Cell. Biol. (Stenmark, 2009) ©2009.

In an overly simplified model of intracellular transport, several major vesicular transport pathways can be easily identified (Figure 1.1B). The secretory (or biosynthetic) route transports cargo from a major biosynthetic site, the ER, to the plasma membrane (Palade, 1975). Important way stations along this route are the protein synthesis organelle, the ER, as well as the Golgi system and the trans-Golgi network (TGN), where cargo sorting and processing may occur (Brandizzi and Barlowe, 2013; Glick and Nakano, 2009; Guo et al., 2014). The degradative route, on the other hand, commences at the plasma membrane with an endocytic event (Doherty and McMahon, 2009). The endocytosed cargo is then shuttled through a succession of endosomes (Huotari and Helenius, 2011) before it is delivered to lysosomes, where final degradation occurs (Luzio et al., 2007). Endocytosed cargo may also be recycled in one of two predominant ways: in rapid recycling, the cargo returns back to the plasma membrane directly from an early endosome; in slow recycling, the cargo first travels to a specialized recycling endosome, from where it can then return to the plasma membrane (Grant and Donaldson, 2009; Ren et al., 1998). Importantly, none of these pathways functions in isolation. For example, the last steps of recycling perform a function similar to that of the late secretory pathway, namely delivery of cargo to the plasma membrane. Indeed, some biosynthetic cargoes may traverse the recycling endosome during their secretion (Ang et al., 2004). The interconnectedness of the major intracellular transport pathways is also evident in the delivery of biosynthetic cargo to the endolysosomal degradative or related compartments (Anitei et al., 2010; Bonifacino and Traub, 2003; Raposo et al., 2007).

While this simplified description introduces some of the major players and functions that occur at various stages of vesicular transport, the structural and functional

details of this system are much more complex. More minute functional and structural divisions of the vesicular transport system exist. For example, ER-derived vesicles may fuse together to form an ER-Golgi intermediate compartment (ERGIC) before they reach the Golgi system (Appenzeller-Herzog and Hauri, 2006; Xu and Hay, 2004). Similarly, the transition from endocytic vesicles to lysosomes may include several functionally and structurally distinct stages, from early to late endosomes and then to lysosomes (Huotari and Helenius, 2011). Post-Golgi secretory intermediates may include specialized vesicles, such as those loaded with neurotransmitters, endocrine hormones, or cytotoxic immune cell products, whose release is tightly regulated (de Saint Basile et al., 2010; Sudhof, 2004). Conceptually, the progression from one compartment to another may be viewed as delivery of cargo to a pre-existing target compartment. The same process may be also described as the transformation, or maturation, of a given vesicular compartment. For example, transport vesicle fusion may lead to the formation of the compartment, as in the case of ERGIC formation following fusion of ER-derived vesicles (Appenzeller-Herzog and Hauri, 2006; Xu and Hay, 2004) or of early endosome formation following homotypic fusion of endocytic vesicles (Bucci et al., 1992; Gorvel et al., 1991). Because they lose certain vesicle-specific markers and properties, and acquire new ones, such intermediate compartments may be viewed as being formed by maturation of the original carriers. Regardless of whether membrane transport occurs through cargo shuttling from one compartment to another, through maturation of the cargo transport carrier, or through a mix of these two processes, the dynamically regulated essence of the transport process remains unchanged.

1.3. Vesicular transport in polarized cells

The simplified eukaryotic transport system described above assumes that all sides of a cell are identical. Often this is not true, as many cells have a polar structural and functional organization. An intensely studied type of polarity is that found across columnar epithelia (Rodriguez-Boulan and Macara, 2014), but neurons (Namba et al., 2015) and migrating cells (Petrie et al., 2009) are also the focus of extensive investigation. In columnar epithelia, such as those lining the digestive or respiratory tracts, a sheet of cells separates two distinct environments: the tissue-facing side of the epithelial sheet, which comprises the juxtaposed basal surfaces of individual cells, and the outside- or lumen-facing side of the epithelial sheet, which comprises the juxtaposed apical surfaces of individual cells (Figure 1.2A). The apical surface of a cell is separated from the contiguous basolateral surface by tight junctions (Farquhar and Palade, 1963). These tight junctions (Figure 1.2B) simultaneously restrict trans-epithelial diffusion and prevent mixing of apical and basolateral membrane components (Madara, 1998; Shin et al., 2006). The tight junctions alone would likely not be able to maintain polarity if the cells did not possess mechanisms that allow them to concentrate basolateral and apical components at the appropriate poles (Goldenring, 2013; Rodriguez-Boulan and Macara, 2014). Such mechanisms include polarized secretion (Figure 1.2B), by which apical markers are transported from the TGN directly to the apical surface, and basolateral markers are transported directly to the basolateral surface. Cells may also target cargo to the correct surface by transcytosis (Preston et al., 2014; Rojas and Apodaca, 2002). In this case, cargo initially delivered to one surface is endocytosed and transported across the cell to the opposite surface (Figure 1.2C-D). The presence of polar surfaces

complicates endocytic recycling the most, and several partly interconnected endosome-type compartments have been identified and shown to control recycling and, in some cases, biosynthetic transport at both poles (Goldenring, 2013, 2015). Thus, basal early endosomes function in recycling and some secretory transport to the basolateral surface, apical early endosomes and apical recycling endosomes function at the apical pole, and common recycling endosomes function in both recycling and transcytosis (Figure 1.2C-E). The recycling endosome system may be composed of separate membrane compartments, or may consist of a contiguous compartment with specific functions performed by distinct domains (Goldenring, 2015; Sonnichsen et al., 2000).

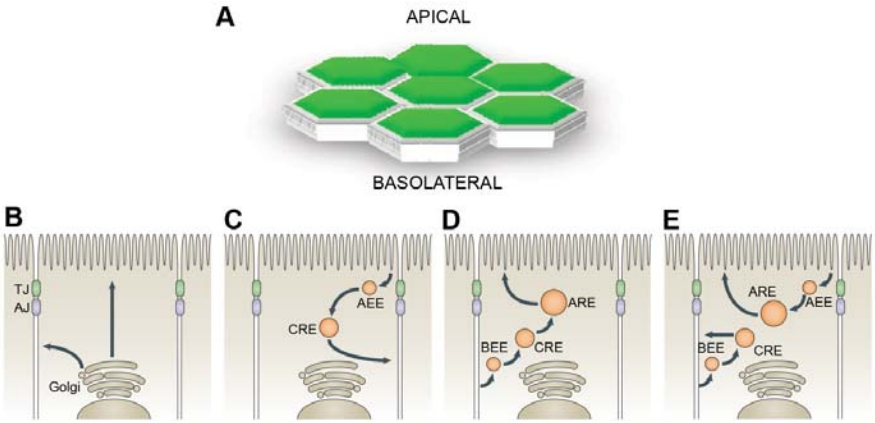

Figure 1.2. Polarized transport. (A) Schematic representation of a columnar epithelium. Cells are packed tightly in a monolayer, with the apical surfaces (top, green) facing a lumenal or exterior space, and the basolateral surfaces (bottom) facing the interior. Figure adapted from (Treyer and Musch, 2013), with the permission from Wiley-Blackwell. Copyright © American Physiological Society. (B-E) Selected types of post-Golgi vesicular transport occurring in polarized cells. Figures adapted by permission from Macmillan Publishers Ltd: Nature Rev. Cancer (Goldenring, 2013) ©2013 (B) Apical and basolateral secretion from the Golgi compartment. (C) Apical to basolateral transcytosis. (D) Basolateral to apical transcytosis. (E) Apical and basolateral recycling; TJ, tight junction; AJ, adherens junction; AEE, apical early endosome; BEE, basolateral early endosome; ARE, apical recycling endosome; CRE, common recycling endosome.

1.4. Regulation of vesicular transport

The vesicular transport steps that connect the major organelles of the secretory pathway are regulated according to well-established principles. The process encompasses cargo sorting at the donor compartment into a budding vesicle, vesicle scission, transport, tethering to the target compartment, and fusion of the vesicle and target compartment membranes (Figure 1.3).

Vesicle budding, accompanied by recruitment of a vesicle coat complex to the nascent transport carrier, is followed by scission of the vesicle membrane form the donor compartment membrane (Figure 1.3a-b). Transmembrane cargoes may be recognized by the sorting machinery due to specific amino acid sorting signals that they possess in their cytosolic domains. Soluble cargoes, on the other hand, may bind to transmembrane sorting receptors, such as the KDEL receptor (Lewis and Pelham, 1992) or the manose-6-phosphate receptor (Guo et al., 2014). These receptors in turn possess cytosolic sorting signals required for transport (Dancourt and Barlowe, 2010; Guo et al., 2014).

Recruitment of the vesicle coats to the site of vesicle budding may be initiated by the GTP-loaded, active form of a small GTPase of the Sar/Arf family (Gillingham and Munro, 2007). Sar1 GTPases recruit coat protein complex II, or COPII, at the ER to mediate anterograde traffic to the Golgi (Aridor et al., 1995; Gillingham and Munro, 2007; Kuge et al., 1994; Nakano and Muramatsu, 1989; Stagg et al., 2006; Stagg et al., 2008). The Arf1 (ADP ribosylation factor 1) GTPase recruits the coat protein complex I, or COPI, at Golgi membranes to mediate intra-Golgi transport and retrograde ER-to-Golgi transport (Aridor et al., 1995; Gillingham and Munro, 2007; Presley et al., 2002; Stearns et al., 1990). Arf proteins may also recruit adaptor protein (AP) complexes and

clathrin cages that mediate late exocytic transport out of the TGN compartment (Gillingham and Munro, 2007; Guo et al., 2014). Lastly, several factors may induce vesicle scission from the donor compartment, including the large GTPases of the dynamin family (Campelo and Malhotra, 2012; Morlot and Roux, 2013; Schmid et al., 2015). Some of these events may occur sequentially, while others may occur simultaneously. Thus, vesicle scission from the donor compartment obligatorily occurs after cargo sorting, but cargo sorting may occur concurrently and in conjunction with vesicle coat formation (Macro et al., 2012), or cargo may be recruited to pre-existent vesicle coats (Rappoport and Simon, 2009).

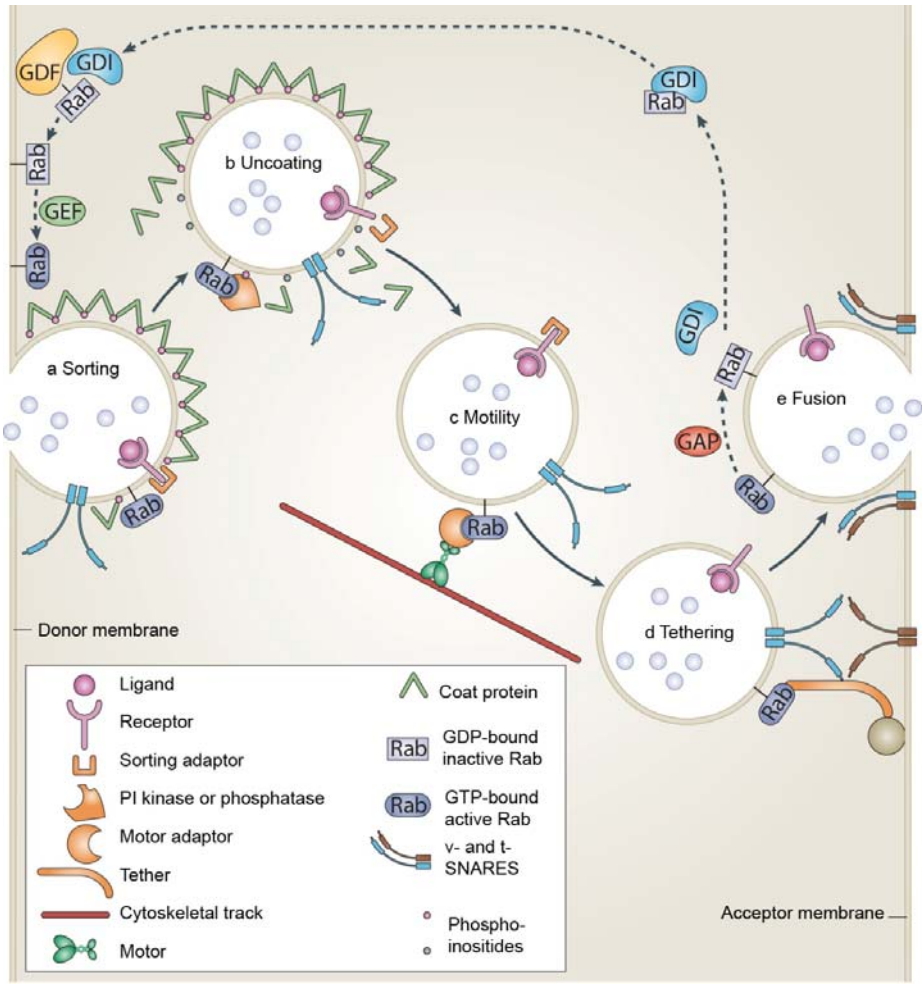

Figure 1.3. Details of vesicular transport. Detailed depiction of the steps involved in vesicular transport between a donor and a target organelle. (a) Cargo is sorted into a budding vesicle while coat proteins promote budding. (b) After scission, the coat proteins are released. (c) The vesicle travels along the cytoskeleton; (d) The vesicle tethers to a target compartment. (e) SNARE proteins mediate vesicle fusion to the target compartment. Throughout transport, the vesicle associated Rab protein is found in the GTP-bound active form and is membrane associated. Upon GTPase activating protein (GAP)-induced GTP hydrolysis, the inactive Rab-GDP binds a GDP-dissociation inhibitor (GDI). The resulting complex is cytosolic. The Rab activity cycle resumes when a GDI displacement factor (GDF) and a Rab guanine exchange factor (GEF) act to promote release of GDP and loading of GTP onto the Rab, returning it to a membrane-bound active state. Figure adapted by permission from Macmillan Publishers Ltd: Nature Rev. Mol. Cell. Biol. (Stenmark, 2009) ©2009.

Transport carrier formation is followed by its movement towards and fusion to a target compartment (Figure 1.3c-d). This process is regulated by the Rab family of small Rab GTPases (Hutagalung and Novick, 2011; Stenmark, 2009; Takai et al., 2001). Their functional cycle will be described in greater detail in the next section. It is sufficient to note here that an active, GTP-loaded Rab protein becomes associated with the budding or budded transport carrier. The active Rab protein will then recruit various types of effector molecules that directly influence vesicle behavior. For example, Rabs may recruit motor proteins of the dynein, kinesin, or myosin families (Hutagalung and Novick, 2011), which will determine whether the transport carriers utilize actin fibers or microtubules for their movement, and whether this movement is directed towards the (+) end or (-) end of microtubules. Similarly, Rabs may recruit tethering and vesicle fusion factors, which will recognize the appropriate target compartment, tether the transport carrier to that compartment, and mediate the fusion of the two membranes and delivery of the cargo (Figure 1.3d-e). For example, Rab1 on ER-to-Golgi transport vesicles recruits p115 (Allan et al., 2000), which tethers anterograde transport vesicles to the Golgi, while Rab8 recruits the exocyst complex to post-Golgi vesicles (Mazelova et al., 2009b). Various SNARE systems control vesicle fusion at various subcellular locations (Martens and McMahon, 2008; Rizo and Rosenmund, 2008; Rizo and Xu, 2015; Wickner and Schekman, 2008).

1.5. The Rab GTPases

While the major regulators of transport carrier formation at the donor compartment are the Sar/Arf GTPases, the major regulators of transport carrier behavior are the Rab GTPases (Hutagalung and Novick, 2011; Stenmark, 2009). They form the largest family of small GTPase in eukaryotes, with over 60 encoded by the human genome (Diekmann et al., 2011; Gurkan et al., 2005). They are somewhat specifically associated with discrete steps of vesicular trafficking (Figure 1.4). Rab1, for example, regulates early anterograde traffic, from the ER to the Golgi (Plutner et al., 1991), while Rab5 regulates the initial steps of endocytic traffic (Bucci et al., 1992; Gorvel et al., 1991). Several Rabs may act together within a given pathway, such as Rab11 and Rab8 in post-Golgi transport to the primary cilium (Knodler et al., 2010; Westlake et al., 2011), while several isoforms may be differentially expressed in various tissues and regulate related but distinct processes (Diekmann et al., 2011; Gurkan et al., 2005).

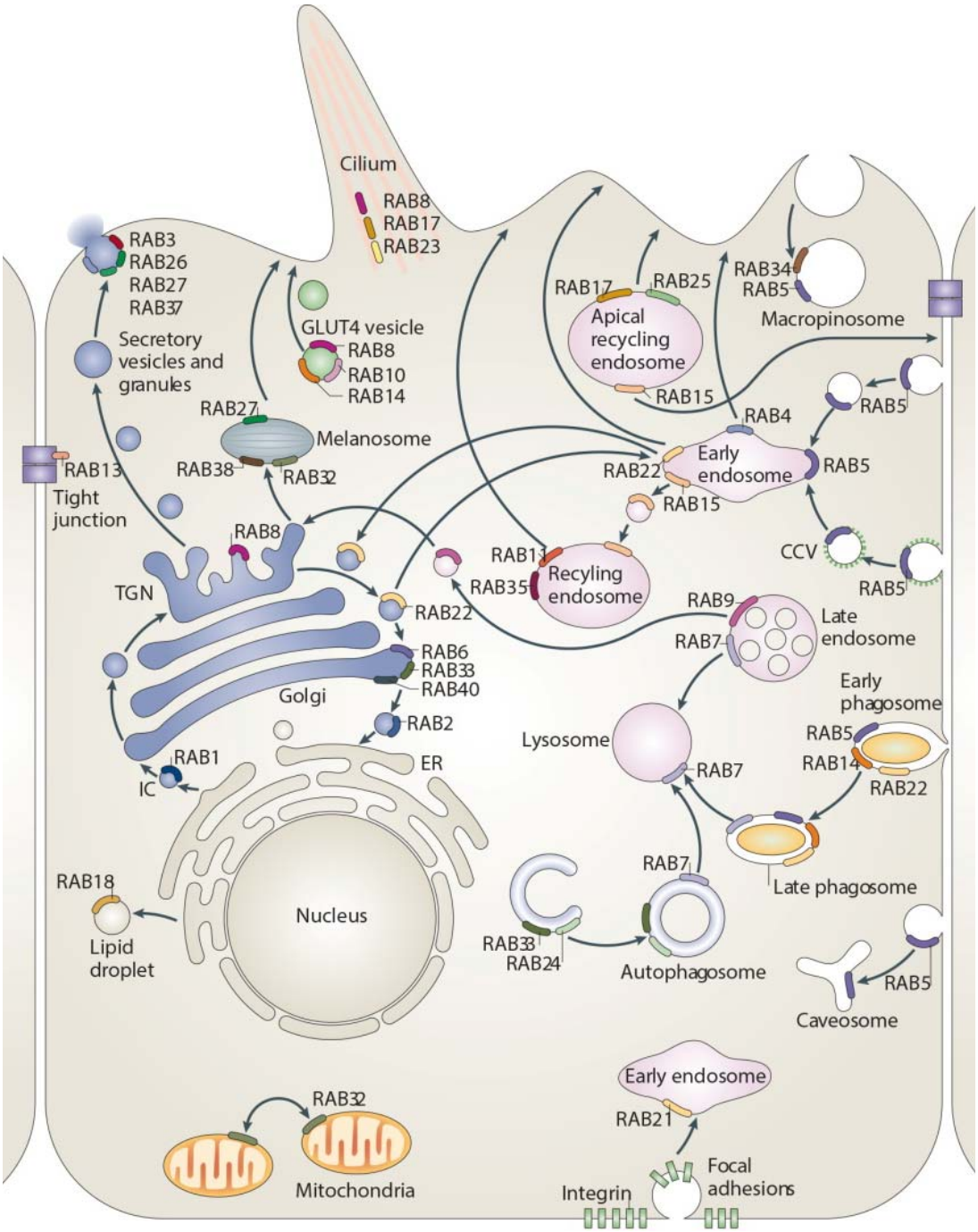

Figure 1.4. Subcellular localization of Rab GTPase functions. The major organelles of a polarized eukaryotic cells are depicted, together with vesicular traffic pathways that connect them. The many Rab GTPases are depicted at their site of function or localization. Figure adapted by permission from Macmillan Publishers Ltd: Nature Rev. Mol. Cell. Biol. (Stenmark, 2009) ©2009. For detailed references, please see the original review article (Stenmark, 2009).

The Rabs amino-terminal domain is the best conserved and contains the GTPase domain. This domain is related to the GTPase domains of other small GTPases of the Rho, Rac and Sar/Arf families (Takai et al., 2001; Wittinghofer and Vetter, 2011), and is involved in GTP or GDP binding and GTP hydrolysis. Sequences connected to the GTPase domain change conformation depending on the nucleotide load of the GTPase and are involved in effector molecule recognition and binding (Takai et al., 2001). The carboxyl-terminal domain of the Rabs has a more divergent primary sequence and may be involved in the localization of the Rab to a given organelle or vesicle (Chavrier et al., 1991). Lastly, conserved cysteines at or very near to the carboxyl-terminus of the Rabs are prenylated with prenyl (usually geranylgeranyl) lipid tails (Khosravi-Far et al., 1991; Leung et al., 2006). These lipid tails mediate the association of the Rabs with target membranes and are essential for function (Khosravi-Far et al., 1991; Nuoffer et al., 1994).

The Rab nucleotide exchange and hydrolysis cycle (Figures 1.3 and 1.5) is similar to that of other small GTPases (Hutagalung and Novick, 2011; Stenmark, 2009; Takai et al., 2001). The active form is the GTP-bound form; active Rab-GTP complexes are membrane bound and mediate effector recruitment (Figure 1.3a-d). Intrinsic Rab GTPase activities are generally slow (Ingmundson et al., 2007), ensuring that inactivation of the Rabs does not occur prematurely. When Rab function needs to cease, however, a Rab GTPase activating protein, or GAP, will bind to the active Rab and stimulate its GTPase activity (Barr and Lambright, 2010). The resulting Rab GDP is inactive, and it detaches from the membrane, creating a cytosolic, inactive, GDP-bound pool of Rab molecules. A GDP dissociation inhibitor, or GDI, accelerates the extraction of prenylated, GDP-loaded,

inactive Rabs from the membrane (Gavriljuk et al., 2013), and, in the process, shields the hydrophobic Rab prenyl moiety in the otherwise hydrophilic cytoplasm (Pylypenko et al., 2006; Rak et al., 2003). The Rabs are returned to their active by exchange of the GDP for a GTP. This is facilitated by proteins called guanine nucleotide exchange factors, or GEFs, which may also ensure recruitment and activation of a given Rab at the appropriate membrane compartment (Barr and Lambright, 2010; Blumer et al., 2013). The Rabs are thus recycled back into a new round of activity.

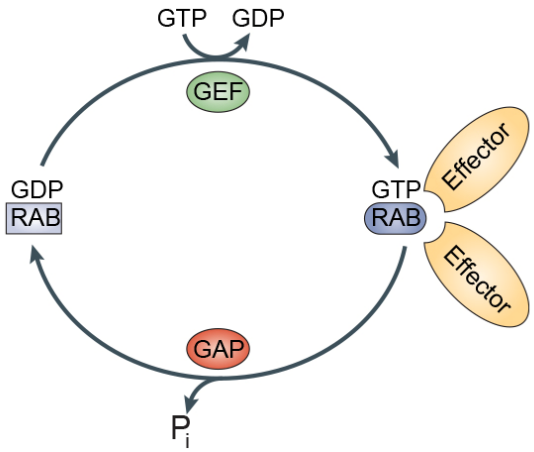

Figure 1.5. The Rab GDP-GTP cycle. An inactive GDP-bound Rab releases GDP and binds GTP, a process promoted by a GEF. The active Rab-GTP is membrane bound and recruits effector molecules. Upon stimulation by a GAP, GTP hydrolysis occurs and the Rab returns to the inactive GDP-bound state. Figure adapted by permission from Macmillan Publishers Ltd: Nature Rev. Mol. Cell. Biol. (Stenmark, 2009) ©2009.

An ongoing debate focuses on which factors determine membrane identity. It is clear by now that the Rabs, due to their somewhat specific association with discrete subcellular compartments, are obvious membrane identity marker candidates, but they are not the only ones (Barr, 2013; Pfeffer, 2013). Other factors that establish membrane identity include the lipid and protein composition of an organelle and vesicle. As traffic is

by necessity continuously dynamic, it is likely that membrane identity is too. Indeed, one Rab may direct the recruitment of another Rab's GEF, which in turn activates the latter onto the membrane and therefore changes membrane identity (Blumer et al., 2013). Rabs may also recruit phosphoinositide kinases or phosphatases, which modify the lipid head groups on a membrane and therefore change the nature of that membrane (Shin et al., 2005). Regardless of the spatio-temporally, morphologically and compositionally dynamic nature of vesicular transport networks, the generally specific functional association between a given Rab and a given organelle or transport carrier render the Rabs obvious targets during investigations aimed at defining a specific cargo's transport pathway(s).

1.6. Selected methods to study Rab function

Study of Rab GTPase involvement in vesicular transport is facilitated by the availability of several well-established experimental approaches. These include, but are not limited to, expression of DN Rab mutants, expression of fluorescent protein-tagged Rab constructs, and overexpression of Rab GAPs and GEFs, including bacterial effectors that have evolved to target specific Rabs.

Introducing any one of several mutations into the Rab protein sequence can abrogate the Rab functional cycle. This is most commonly done using mutations that interfere with the guanine nucleotide exchange and hydrolysis cycle. Shown in Table 1.1 below are these three major mutant classes, along with references to publications where the noted Rab1 mutations have been characterized in greater detail. The amino acids mutated are indicated on a crystal structure of Rab1b in Figure 1.6. The mutations mirror those used in the study of the prototypic small GTPase, H-Ras.

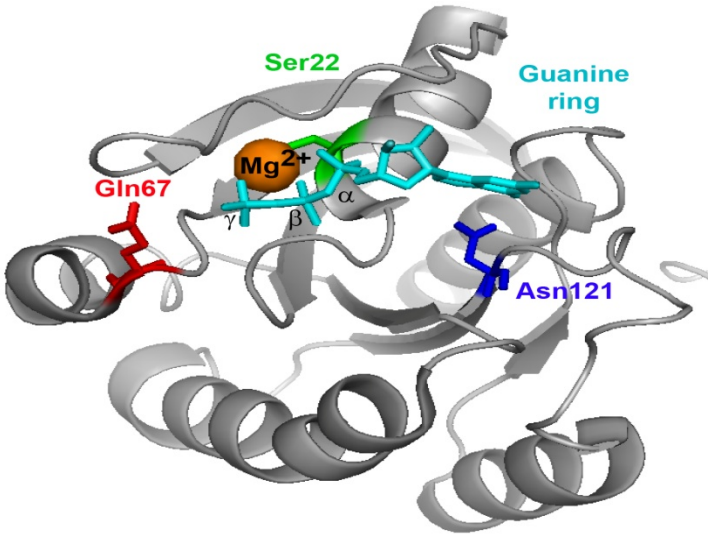

Figure 1.6. Rab1b crystal structure. Crystal structure of Rab1b at 1.7 Å resolution (Protein Data Bank structure 3NKV). Structure initially published in (Muller et al., 2010). Shown is the Rab1b backbone (in gray), together with several features highlighted. The GTP analog GppNHp (guanosine 5'-β,γ-imidotriphosphate, is in cyan. The guanine ring is at the right, and the alpha, beta and gamma phosphates are indicated at the left. The Gln67 residue involved in GTP hydrolysis is in red. The Ser22 residue involved in Mg^{2+} coordination is in green, while the Mg^{2+} ion is in orange. The Asn121 residue involved in guanine ring binding is in blue. Original structure was processed using PyMOL.

A conserved asparagine residue in the guanine ring binding site of the Rab proteins (Figure 1.6, equivalent to H-Ras_{N116}) may be mutated and replaced with the bulkier and hydrophobic isoleucine residue. This change prevents the resulting mutant protein from stably binding GDP or GTP (Pind et al., 1994; Walter et al., 1986). Indeed, it is thought that this mutant may exchange GDP and GTP too rapidly and in an unregulated manner (Pind et al., 1994; Walter et al., 1986). This mutation may induce unregulated recruitment of GTPase effectors, possibly at ectopic locations, thus affecting their dynamics and function. Expression of this nucleotide-binding Rab1 mutant affected

the dynamics of Rab1 effector (p115, GBF1) association with membranes (Alvarez et al., 2003; Brandon et al., 2006; Garcia-Mata et al., 2003; Monetta et al., 2007).

A conserved serine or threonine residue of the nucleotide binding pocket is located close to the β- and γ-phosphates of GTP (Figure 1.6) and is involved in Mg^{2+} coordination in H-Ras (Farnsworth and Feig, 1991). Replacement of the equivalent Rab residue, for example $Rab1a_{S25}$, with an asparagine residue does not allow GTP binding, but permits GDP binding (Nuoffer et al., 1994). As such, this GTP-binding mutant is locked in the inactive GDP-bound form. $Rab1a_{S25N}$ (or $Rab1b_{S22N}$) has been proposed to compete with the WT Rab1a or Rab1b for binding of either a Rab1 GEF or a Rab1 GDI (Nuoffer et al., 1994), in a model mirroring that proposed to explain $H\text{-}Ras_{S17N}$ activity (Farnsworth and Feig, 1991). This mutant may be interchangeably referred to either as a GTP-binding or as a GDP-restricted mutant; throughout this work, I will refer to it as a GDP-restricted mutant. Both it, and the above-mentioned nucleotide-binding mutant, are widely referred to in the literature as DN mutants.

A third, well conserved glutamine residue also close to the γ-phosphate of GTP (Figure 1.6) performs intrinsic GTPase activity of the Rabs, and at times also the stimulated GTPase activity (Gavriljuk et al., 2012; Mihai Gazdag et al., 2013; Mishra et al., 2013; Yu et al., 2013). Its mutation to a leucine (or another hydrophobic residue) abrogates intrinsic Rab GTPase activity, resulting in a mutant that becomes locked in the GTP-bound, active form (Mishra et al., 2013). This GTP-restricted/GTPase mutant is at times referred to as dominant active mutant. Since the expression of these mutants may result in abrogation of the normal Rab function, albeit at a different stage within the GTP cycle, I will refer to the GTPase mutants as DN mutants as well.

Table 1.1 Widely used Rab mutations

Rab process inhibited	Nucleotide load	Activity	Rab1(a or b) mutation	Reference
None (WT)	Normal exchange GDP-GTP	Normal activity cycle	None	
Nucleotide binding	Nucleotide-free	Inactive	$Rab1a_{N124I}$ $Rab1b_{N121I}$	(Pind et al., 1994)
GTP-binding	GDP-restricted	Inactive	$Rab1a_{S25N}$ $Rab1b_{S22N}$	(Nuoffer et al., 1994)
GTPase activity	GTP-restricted	Active	$Rab1a_{Q70L}$ $Rab1b_{Q67L}$	(Gavriljuk et al., 2012)

The general effectiveness of these mutants in inhibiting Rab function in transport is in part due to their ability to interfere with the normal dynamics of the Rab functional GTP/GDP exchange and hydrolysis cycle. The Rab regulators GEF and GAP also interfere with the dynamics of this cycle by skewing the Rab-GDP/Rab-GTP ratio towards the active form (the Rab GEFs) or the inactive form (the Rab GAPs). Overexpression of either has been successfully used to modulate and investigate Rab function (Fuchs et al., 2007; Udayar et al., 2013; Yoshimura et al., 2010). Proteins with GEF or GAP activity have also evolved in some bacterial pathogens that replicate intracellularly, in vesicles derived from the cellular organelles (Hicks and Galan, 2013). *Legionella pneumophila* is an extensively studied example, and has been shown to inject into the host cell cytoplasm several proteins that modulate Rab1 function (Hardiman et al., 2012). Other examples of bacteria that have evolved capabilities to control intracellular vesicular transport include *Coxiella burnetii* (Campoy et al., 2011; Hardiman et al., 2012), *Salmonella typhi* (Spano and Galan, 2012), *Shigella flexneri* and *Escherichia coli* (Dong et al., 2012). That the activities of these bacterial effectors have been fine-tuned over many cycles of evolution informs both their specificity and their

efficacy, and recommends them for use in experiments aimed at modulating Rab function.

Lastly, Rab proteins have generally been proven to tolerate fluorescent protein-tagging very well. Many fluorescent protein-Rab fusions have been shown to retain the localization patterns of the parental Rab, as well as its function (Chen and Wandinger-Ness, 2001; Feng et al., 2001; Moyer et al., 2001b; Peranen and Furuhjelm, 2001). This is however not true across the board, since examples exist where attachment of even a small epitope tag has resulted in a non-functional Rab chimera (Tisdale and Balch, 1996). However, the general usefulness of such fusions remains uncontested, since the many functional fusions allow detailed spatial and temporal analyses of Rab involvement in traffic (Huang et al., 2010; Rzomp et al., 2003; Sonnichsen et al., 2000), as well as a means for monitoring expression levels.

1.7. A case study in complex transport regulation: the hepatocyte

This work specifically focuses on analyzing the secretion pathways utilized by hepatic lipoproteins and HCV, a hepatotropic virus. In order to properly contextualize any experimental findings regarding the regulation of transport of these cargoes, one must consider the function and architecture of the hepatocyte. I therefore introduce here a few notions regarding liver function, architecture and how the hepatocyte functional and structural polarization relate to these.

1.8. Liver function and architecture

The liver carries out a number of complex and often essential functions in the animal body (Strain and Neuberger, 2002; Treyer and Musch, 2013). Among these are energy storage, excretion, drug processing, and the synthesis of numerous serum

components, such as albumin, alpha-1-antitrypsin, complement, coagulation factors, and lipoproteins. The convergence of these functions in one organ is informed by the liver's complex architecture (Figure 1.7). Blood enters the organ through the portal vein, which collects nutrient-rich venous blood from most of the intestine, and through the hepatic artery, which brings in oxygenated blood from the heart. The blood intake supply divides and bathes the liver cells in a system of sinusoids, then reunites to exit the organ through the hepatic vein, and thus re-enters into the general circulation. As such, the liver serves as one of several filters of the circulatory system: it takes up components from the afferent blood supply and releases its own products into efferent blood. The other major liver function, excretion, is achieved through the bile canaliculi system, which converges into the bile ducts and transports the bile (which includes digestive aids and waste products) to the proximal intestine (Boyer, 2013). The function of the organ is predicated on the separation of the blood-related functions of the liver from its excretory function, resulting in an architecture of inter-weaved biliary duct tree branches and afferent and efferent blood vessel tree branches.

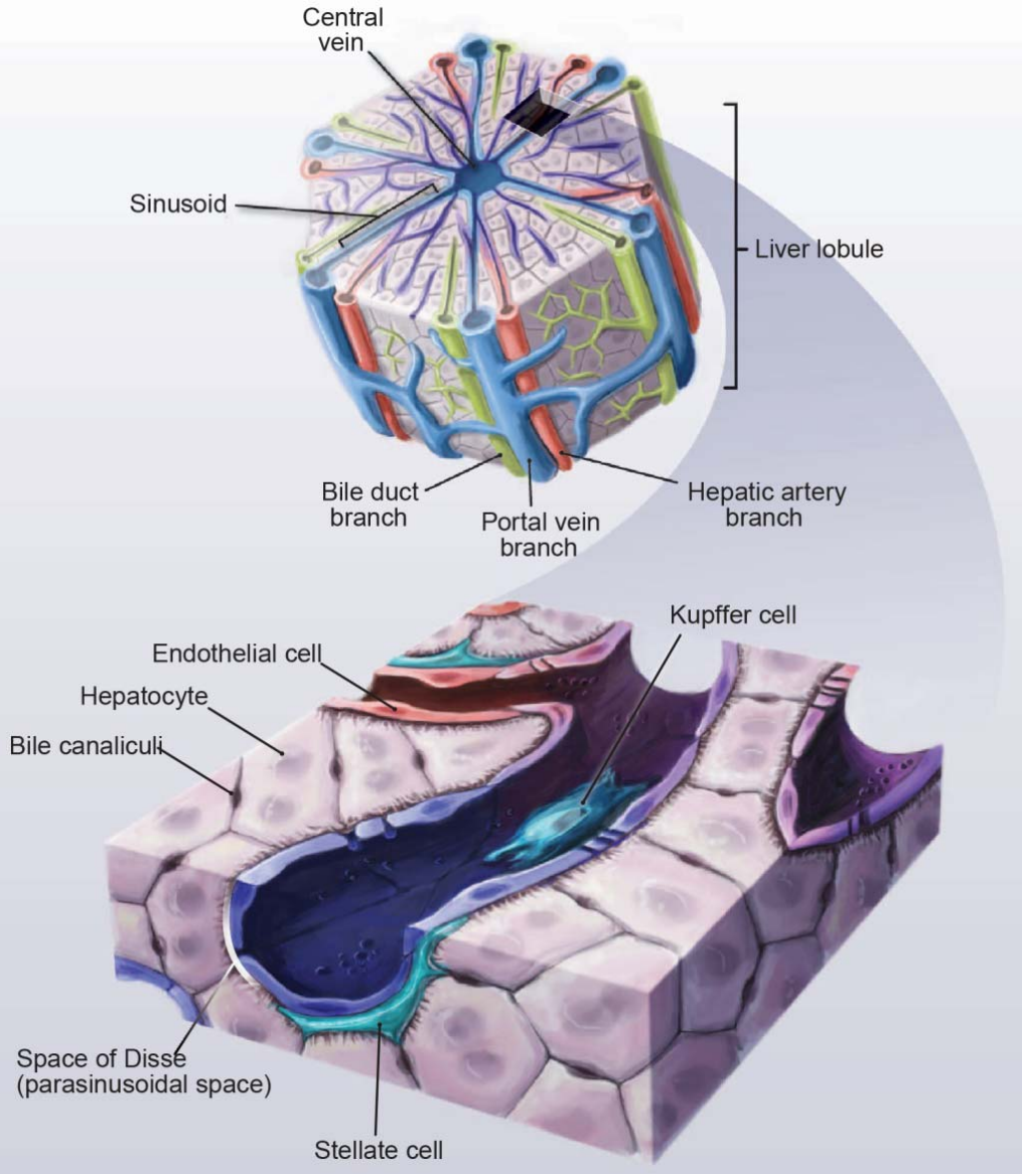

Figure 1.7. Liver architecture. Schematic of liver structural organization. Shown at the top in blue and red are the blood vessels. Blood flows from branches of the portal vein and the hepatic artery, into the hepatic sinusoids, and then into the central veins, which return the blood into general circulation. Shown in green is the bile duct system, which collects bile from the bile canaliculi. The hepatocytes (in purple) separate the biliary (apical) compartment and the sinusoidal (basolateral) compartment. Other liver-resident cell types (endothelial, Kupffer and stellate cells) are indicated, but discussion of their function is beyond the scope of this work. Figure adapted from (Bhatia et al., 2014). Reprinted with permission from AAAS.

1.9. Hepatocyte organization

The separation between the blood-related and bile-related functions of the liver occurs at the level of the hepatocyte (Figure 1.8), which is the functional unit of this organ. Hepatocytes are polarized cells with apical (biliary) and basolateral (sinusoid) surfaces (Gissen and Arias, 2015; Musch, 2014; Treyer and Musch, 2013). While this structural and functional division of the hepatocyte is related to the organization of the cells of simpler, columnar epithelia, such as those of the lung or of the intestine (Marchiando et al., 2010; Rodriguez-Boulan and Macara, 2014), the hepatic cells display a more complex architecture. Thus, at contact sites between hepatocytes, rows of tight junctions delineate narrow apical intercellular lumens, called bile canaliculi (Gissen and Arias, 2015; Musch, 2014; Treyer and Musch, 2013). These canals converge to form the bile duct system and transport the bile, which contains the excretory and digestive products of the hepatocytes (Boyer, 2013). Several canaliculi may flank a given hepatocyte, while the rest of the hepatocyte surface, outside the tight junctions which delineate the bile canaliculi, forms basolateral surfaces oriented towards other hepatocytes or towards the sinusoidal space (Gissen and Arias, 2015; Musch, 2014; Ogawa et al., 1979; Treyer and Musch, 2013). Given the cell's essential role in so many aspects of animal life, it is important to understand how hepatocytes regulate secretion in the context of their architecture and of their other functions.

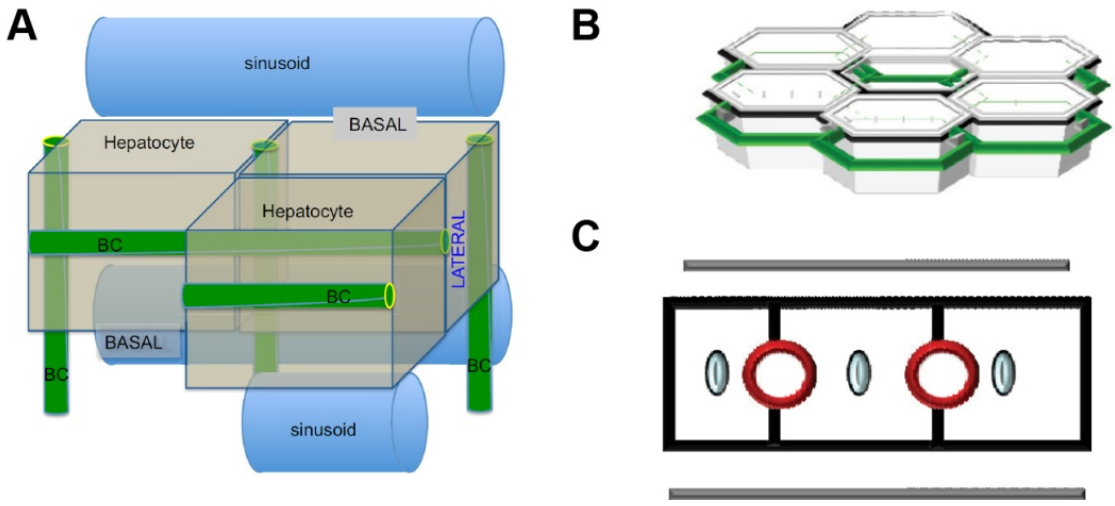

Figure 1.8. Hepatocyte polarity. (A) Three-dimensional schematic of spatial relationships between hepatocytes, bile canaliculi, and hepatic sinusoids. The narrow apical (biliary) domains, in green, are sequestered between adjacent hepatocytes and form a complex network of canaliculi, while the basolateral domains encompass the remaining hepatocyte surfaces. Figure from (Gissen and Arias, 2015), DOI 10.1016/j.jhep.2015.06.015, reproduced under the Creative Commons Attribution License (CC BY, http://creativecommons.org/licenses/by/4.0/, accessed on February 10, 2016). (B) Simplified depiction of a sheet of hepatocytes surrounded by apical canalicular domains (in green) sequestered between adjacent cells. Top and bottom surfaces are formed by basolateral domains. (C) Schematic section, perpendicular on the apical lumen, through a hepatocyte-like polarity system. The apical lumen (red) is found between adjacent cells, while basolateral domains (top and bottom) sandwich the cells. (B) and (C) images adapted from (Treyer and Musch, 2013), with the permission from Wiley-Blackwell. Copyright © American Physiological Society.

1.10. Hepatic secretory cargoes of interest

My interest has long been in studying biological phenomena related to disease. In the context of hepatic secretion, the lipoproteins and HCV have stood out as ideal study candidates. I have also included albumin in this analysis, since its physico-chemical properties diverge from those of the lipoproteins and of HCV. This work therefore focuses on identifying the transport pathways involved in the secretion of a model monomeric protein, albumin, and of the larger and more complex macromolecular assemblies that are the lipoproteins and the HCV particles. I now describe some relevant known features of these cargoes.

1.11. Albumin

I selected serum albumin as a model for the secretion of small, monomeric proteinaceous cargo. Albumin is the most abundant protein in plasma, where it helps maintain homeostasis of the circulatory system while also binding to and transporting various small molecules throughout the body (Ha and Bhagavan, 2013; Quinlan et al., 2005; Rothschild et al., 1988; Yamasaki et al., 2013). The albumin mRNA is translated by ER-associated ribosomes. The amino-terminal signal peptide directs translocation of the nascent protein into the lumen of the ER, resulting in a form termed proalbumin (Judah et al., 1973; Quinn et al., 1975), which is then transported by the vesicular secretory system. During transport, proalbumin is further proteolytically processed into the mature form, albumin (Bathurst et al., 1987; Brennan and Peach, 1988). No glycosylation sites are predicted in the primary amino-acid sequence of albumin; it is secreted mainly in a non-glycosylated form (Struck et al., 1978).

1.12. Hepatic lipoproteins

Definition, general features and metabolic functions. Lipoproteins are large, complex, macromolecular assemblies that employ the lipid-binding and amphipathic properties of their protein components, the apolipoproteins, to solubilize and transport otherwise poorly soluble lipids, such as triglycerides, sphingolipids, cholesterol and cholesterol esters (Mahley et al., 1984). The major lipoproteins produced in the body are the chylomicrons, the very low-density lipoproteins (VLDL) and the high-density lipoproteins (HDL). Chylomicrons are produced by enterocytes and transport dietary lipids from the intestine to the rest of the body. They are the largest of the lipoproteins produced in the body, with diameters over 100 nm (Mahley et al., 1984). As they become depleted of their lipid cargo, they become denser and are termed (chylomicron) remnants. The VLDL fulfill similar lipid transport functions as the chylomicrons, but are produced by hepatocytes. They have densities below 1.006 g/mL and are the largest among the non-chylomicron lipoproteins, with diameters in the range of 30 to 90 nm (Mahley et al., 1984). As VLDL deliver their lipid cargo to cells throughout the body, they too become gradually denser and are therefore termed intermediate-density lipoproteins (IDL, with densities in the range of 1.006 to 1.019 g/mL), or low-density lipoproteins (LDL, with densities between 1.019 and 1.063 g/mL). Lipid loss by VLDL is accompanied by a reduction in particle size, down to LDL diameters of about 20 nm (Mahley et al., 1984). Lastly, HDL are the smallest (8-12 nm in diameter) and densest (densities in the range of 1.063 g/mL to 1.21 g/mL) of the plasma lipoproteins. HDL particles fulfill a major role in a process termed reverse cholesterol transport, which consists of the shuttling of

cholesterol from cells throughout the body to the liver, where cholesterol processing and excretion occurs (Zannis et al., 2015).

The lipid transport function of the lipoproteins is facilitated by their structural organization. At the core of the particle are neutral lipids such as triglycerides and cholesterol esters. This hydrophobic core is similar to that of intracellular lipid droplets (Welte, 2015; Wilfling et al., 2014), in which the hydrophobic fats are also segregated from the aqueous cellular environment with which the neutral lipids are immiscible. The lipid core is surrounded by a polar lipid monolayer, organized similarly to a single leaflet of a membrane that has been wrapped around the neutral lipid center. Apolipoproteins can also on the surface of lipoprotein particles (Mahley et al., 1984). These proteinaceous components utilize lipid-binding domains, most commonly amphipathic helices (Segrest et al., 1992), to associate with the lipid particle. Apolipoproteins are involved both in lipoprotein formation and in their functional processing throughout the body.

Apolipoproteins and their disease associations. Serum lipoproteins contain several proteins components, termed apolipoproteins. ApoB100 is expressed in hepatocytes and is essential for VLDL formation, serving as its defining structural component. It is a very large protein of over 4500 amino acids and contains hydrophobic β-sheet domains involved in lipid binding (Chen et al., 1986; Cladaras et al., 1986; Law et al., 1986; Yang et al., 1986). Apolipoprotein B48 (ApoB48) synthesis results from citidine deamination of the ApoB100 mRNA by Apobec-1, which creates a premature STOP codon in the sequence (Teng et al., 1993; Tennyson et al., 1989). ApoB48 is produced in enterocytes in humans, and in both enterocytes and hepatocytes in rodents (Davidson and Shelness, 2000). Enterocyte-made ApoB48 is involved in chylomicron

biogenesis, while hepatic ApoB100 drives VLDL particle formation (Mansbach and Siddiqi, 2010; Olofsson and Boren, 2005). Other apolipoproteins include those belonging to the A, C and E classes (Kohan, 2015; Kohan et al., 2015; Mahley, 1988; Mahley et al., 1984; Maiga et al., 2014; Norata et al., 2015; Phillips, 2014; Sacks, 2015; Sundaram and Yao, 2012; Zannis et al., 2015). Some of these may undergo cycles of association with and dissociation from the surface of the large ApoB-containing lipoproteins: the chylomicrons, the VLDL and the LDL, and are therefore referred to as exchangeable apolipoproteins. They may also participate in the formation of HDL particles (Zannis et al., 2015). They have been shown to regulate, at least in part, ApoB-containing lipoprotein biogenesis, receptor binding of the lipoproteins, and lipolysis (Kohan, 2015; Kohan et al., 2015; Mahley, 1988; Mahley et al., 1984; Maiga et al., 2014; Norata et al., 2015; Phillips, 2014; Sacks, 2015; Sundaram and Yao, 2012; Zannis et al., 2015).

Among the most extensively investigated apolipoproteins, and components of both VLDL and HCV particles, are ApoB100 and ApoE. Since the work I present here deals exclusively with these two lipoprotein components, I restrict myself to providing detailed background information regarding only these two. The investigation principles that I present throughout this work are nonetheless transferable to the analysis of the secretion of other exchangeable apolipoproteins.

In humans, VLDL obligatorily contains ApoB100, a component that likely has a structural function. VLDL also contains ApoE and other exchangeable apolipoprotein components (Utermann, 1975). Proper regulation of VLDL formation (assembly), secretion, and metabolism are tightly controlled; defects in these processes have been associated with numerous metabolic disease syndromes. Such conditions include

abetalipoproteinemia (Berriot-Varoqueaux et al., 2000; Wetterau et al., 1992), which results from a defect in the lipidation of ApoB100, and hypobetalipoproteinemia (Schonfeld, 2003; Schonfeld et al., 2005; Young et al., 1989), which results from missense mutations in the ApoB100 sequence. These and other types of primary lipoproteinemias may cause atherosclerosis and coronary artery disease (Lusis et al., 2004).

ApoE, the other apolipoprotein I investigate here, occurs in humans as several major isoforms, termed ApoE2, ApoE3 and ApoE4, respectively (Utermann et al., 1977; Weisgraber et al., 1981). While ApoE3 is the most common isoform and is considered "neutral" with respect to disease association, ApoE2 is associated with type III hyperlipoproteinemia and ApoE4 is associated with type V hyperlipoproteinemia (Ghiselli et al., 1982a; Ghiselli et al., 1982b; Utermann et al., 1977). Furthermore, the minor isoform ApoE3-Leiden is a dominant predictor of type III hyperlipoproteinemia (Havekes et al., 1986). Type III disease association is correlated with low clearance rate of ApoE-containing lipoproteins due to defects in LDL receptor (LDLR) binding (Gregg et al., 1981); indeed, ApoE contains a well defined LDLR-binding domain (Wilson et al., 1991). The absence of ApoE expression, or expression of LDLR-binding defective ApoE isoforms, results in accumulation of VLDL, triglycerides, and cholesterol in plasma (Mahley et al., 1999; Plump et al., 1992; Zhang et al., 1992), and increases the likelihood of developing atherosclerosis and coronary artery disease. In these conditions, large amounts of plasma LDL, including its oxidized forms, are deposited in arterial walls. The arterial wall thus accumulates plaque, loses elasticity, and the arterial lumen narrows, eventually leading to cardiovascular morbidity (Breslow, 2000, 2001).

Besides its role in cholesterol transport and metabolism, ApoE has many other functions. Some of these functions are related to its expression by a wide variety of cells in many tissues. For example, macrophages express ApoE and may use it to deliver necessary lipids at sites of nerve regeneration (Ignatius et al., 1986; Snipes et al., 1986). Similarly, astrocytes express ApoE (Murakami et al., 1988; Pitas et al., 1987), which may be involved in sustaining proper neuronal physiology. Indeed, ApoE has been implicated in neurodegenerative disease conditions (Corder et al., 1994; Corder et al., 1993; Greenberg et al., 1995; Martinez et al., 2005; Vance and Hayashi, 2010), with ApoE4 being associated with higher risk of developing late onset Alzheimer's disease, while ApoE2 protecting against the same condition (Corder et al., 1994; Corder et al., 1993). ApoE has also been shown to modulate cell activation and migration (Ali et al., 2005; Kelly et al., 1994; Kothapalli et al., 2004; van den Elzen et al., 2005), and just recently, increased ApoE expression by melanoma cells was shown to increase aggressive tumor behavior and metastatic potential (Pencheva et al., 2012). ApoE-dependent modulation of cell activation may be achieved through direct transcriptional control (Theendakara et al., 2016) or through cell-surface receptor-mediated signaling (Pencheva et al., 2012).

1.13. Lipoprotein assembly and secretion

VLDL assembly and secretion. VLDL assembly commences with the translation of the ApoB100 mRNA and the concurrent translocation of the resulting protein (Chen et al., 1986; Cladaras et al., 1986; Law et al., 1986; Yang et al., 1986) into the lumen of the ER. Efficient translocation requires concomitant loading of lipids onto the nascent polypeptide; this lipidation process is catalyzed by the microsomal triglyceride transport protein (Boren et al., 1992; Wetterau et al., 1992). From the ER, ApoB100-containing

VLDL transits the Golgi system (Ehrenreich et al., 1973) en route to the basolateral plasma membrane, where it is secreted. The complex processes of assembly and maturation of the VLDL particle that occur during its journey through the secretory pathway may include further lipidation, association with exchangeable apolipoproteins, including ApoE, and various post-translational modifications (Olofsson and Boren, 2005; Sundaram and Yao, 2010, 2012; Tiwari and Siddiqi, 2012). VLDL progression through the secretory pathway is also controlled by at least two degradative processes (Ginsberg and Fisher, 2009; Rutledge et al., 2010). When lipid sources are insufficient to achieve proper initial lipidation or if the microsomal triglyceride transport protein activity is reduced or abolished, ApoB100 translocation stalls. The nascent polypeptide then becomes exposed to the cytoplasm and is ubiquitinylated and targeted for proteasome-mediated ER-associated degradation (Benoist and Grand-Perret, 1997; Fisher et al., 2011; Fisher et al., 1997; Zhou et al., 1998). When pre-VLDL formation is completed, but the nascent lipoprotein becomes exposed to poly-unsaturated fatty acids or is oxidized, then the particle is targeted for degradation by the autophagosome (Pan et al., 2008a). Only VLDL molecules that survive this strict quality control process are secreted.

ApoE secretion in the presence or absence of VLDL. Secreted VLDL particles also contain ApoE, a 299-amino-acid, O-glycosylated exchangeable apolipoprotein (Rall et al., 1982; Utermann, 1975; Wernette-Hammond et al., 1989; Zanni et al., 1989). ApoE can be secreted on its own from many cell types, including hepatocytes (Dashti et al., 1980), macrophages (Basu et al., 1981), and astrocytes (Pitas et al., 1987), and can form HDL particles involved in cholesterol transport. Indeed, a major function of lipoprotein-associated ApoE is to tightly bind LDLR family receptors and to promote clearance of

cholesterol-rich lipoprotein particles from circulation (Mahley, 1988; Plump et al., 1992; Zhang et al., 1992). ApoE isoforms or mutants with low LDLR-binding affinity are associated with type III hyperlipoproteinemia and coronary artery disease (Breslow, 2000; Mahley et al., 1999). ApoE is synthesized on ER-associated ribosomes, is translocated into the lumen of the ER, and is transported through the Golgi to the cell surface in secretory vesicles that travel along microtubules (Kockx et al., 2007). A fraction of newly-synthesized ApoE is degraded intracellularly in a post-ER compartment (Deng et al., 1995; Ye et al., 1993). Once secreted, ApoE may associate with the cell surface (Lilly-Stauderman et al., 1993), and may become re-internalized and recycled (Heeren et al., 2003; Laatsch et al., 2012). Lastly, beyond simply being associated with VLDL particles, ApoE was also shown to promote their secretion (Kuipers et al., 1997; Mensenkamp et al., 2001). Various lipoprotein components thus display a complex functional interplay during the assembly and egress of VLDL, with major implications for human disease.

1.14. Hepatitis C virus

Another known cargo of the secretory pathway in hepatocytes is HCV. Infection with HCV may be the cause of several very serious disease conditions, and it was, until recently, very difficult to cure (Thomas, 2013). Furthermore, HCV is peculiar in that it very closely associates with host lipoproteins, including ApoE and ApoB100 (Lindenbach, 2013; Lindenbach and Rice, 2013). HCV has thus become an obvious target in our investigation into how hepatocytes regulate cargo secretion. I provide here a summary of relevant aspects of the HCV life cycle that I hope will inform the

understanding of the investigations I have commenced into the regulation of HCV particle secretion.

1.15. Hepatitis C

Hepatitis - the inflammation of the liver - can have widely varied etiologies, with viral infections being a major cause (Protzer et al., 2012). Several hepatotropic viruses have been identified and shown to be etiologic agents of viral hepatitis. Hepatitis A virus (Matheny and Kingery, 2012) and hepatitis E virus (Khuroo and Khuroo, 2016; Perez-Gracia et al., 2014; Sayed et al., 2015) generally cause self-limiting acute hepatitis, while hepatitis B virus, HCV and the hepatitis B virus-dependent hepatitis delta virus, in turn, often establish chronic infections that may remain active over several decades (MacLachlan and Cowie, 2015; MacLachlan et al., 2015; Rizzetto, 2015; Thomas, 2013). The usual progression of HCV infection is depicted in Figure 1.9. While some patients clear HCV infections spontaneously, the virus often causes chronic infection, which may further progress through the following stages: liver fibrosis, liver cirrhosis, and hepatocellular carcinoma (Hoofnagle, 1997; Thomas, 2000). Liver failure secondary to advanced chronic viral hepatitis remains a major indication for liver transplantation (Neuberger, 2016). Given the severity of HCV-dependent pathologies, HCV infection remains a major health burden worldwide, with over 185 million people (or almost 3% of the world population) thought to be chronically infected with the virus (Mohd Hanafiah et al., 2013). This problem is exacerbated by the failure to develop a protective anti-HCV vaccine (Honegger et al., 2014; Walker and Grakoui, 2015), and by the high costs of effective and well tolerated treatments that have only recently become available (Ayoub and Tran, 2015; Holmes and Thompson, 2015; Scheel and Rice, 2013).

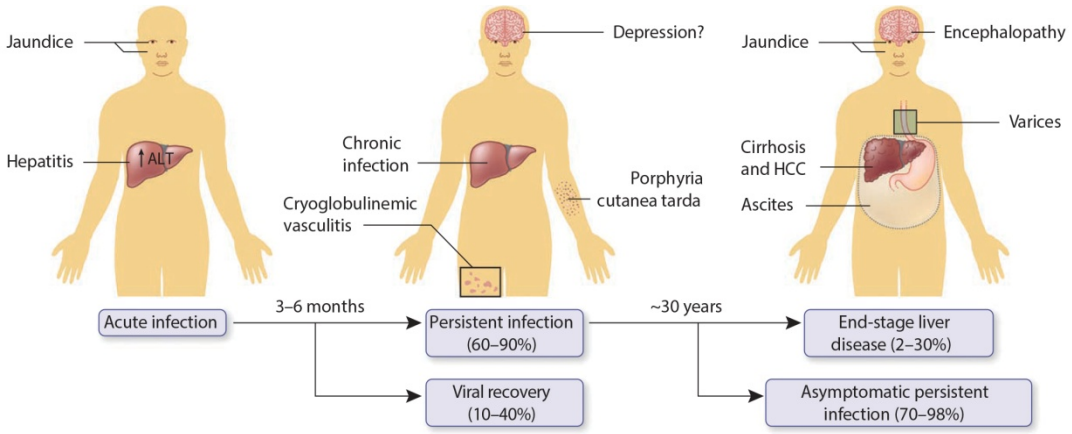

Figure 1.9. HCV disease progression. Symptoms associated with the successive stages of HCV infection. ALT, alanine aminotransferase plasma levels; HCC, hepatocellular carcinoma. Figure adapted by permission from Macmillan Publishers Ltd: Nature Med. (Thomas, 2013) ©2013.

1.16. The HCV virion: structure and composition

HCV is an enveloped virus and has a single-stranded, positive-sense RNA genome; it belongs to the genus *Hepacivirus* within the *Flaviviridae* family (Bartenschlager et al., 2011; Moradpour et al., 2007; Scheel and Rice, 2013). Notable related viruses include the recently identified hepaciviruses (Kapoor et al., 2011; Kapoor et al., 2013; Pybus and Theze, 2015), as well as the more distantly related flaviviruses, pestiviruses, and pegiviruses (Knipe and Howley, 2013).

The HCV particle contains the positive polarity RNA genome, virus-encoded proteins, namely the capsid protein Core and the glycoproteins E1 and E2, and host cell derived proteins and lipid membranes (Bartenschlager et al., 2011; Lindenbach, 2013; Lindenbach and Rice, 2013; Scheel and Rice, 2013). Of the host-cell derived viral particle protein components, most notable are ApoE and ApoB100. The virus association with hepatocyte-derived lipoproteins confers it light, lipoprotein-like densities,

particularly *in vivo* (Andre et al., 2002; Lindenbach, 2013; Lindenbach et al., 2006; Lindenbach and Rice, 2013; Nielsen et al., 2006). The HCV-lipoprotein chimeric entity is called a lipoviroparticle (Andre et al., 2002).

Unlike the more highly and uniformly organized flavivirus particles (Kuhn et al., 2002; Mukhopadhyay et al., 2003; Mukhopadhyay et al., 2005; Zhang et al., 2003a; Zhang et al., 2003b), HCV presents a more amorphous structure, not easily resolved by conventional structural techniques (Catanese et al., 2013). This may be due in part to lipoprotein association, the nature of which has not been unambiguously described as of yet (Lindenbach, 2013; Lindenbach and Rice, 2013). Highly purified infectious particles are about 70 nm (40-100 nm range) in diameter (Catanese et al., 2013), although earlier reports have described a significantly more heterogeneous (both in size and shape) particle population found in more crude viral preparations (Gastaminza et al., 2010; Merz et al., 2011; Yu et al., 2007).

1.17. HCV life cycle

The HCV life cycle follows the classical paradigm of virus propagation, as depicted in Figure 1.10. At a cellular level, the infectious HCV particle enters a host cell, primarily the human hepatocyte, where the virus replicates its genome, and assembles and releases new infectious particles that further propagate the cycle (Scheel and Rice, 2013). To survive inside the host, the virus has developed mechanisms to counteract the host's antiviral defenses, both innate and adaptive (Dustin et al., 2014; Dustin and Rice, 2007; Horner and Gale, 2013). Lastly, to spread within the human population, the virus must be able to infect new hosts. A major driving force for the ongoing epidemic was transmission through non-sterile medical procedures and the lack of screening blood for

transfusion, organs for transplant, and similar other human donor-derived biomedical products (Thomas, 2000, 2013). More recently, injection drug habits in conjunction with use of non-sterile paraphernalia has constituted a major cause of new transmissions (Thomas, 2013), and reports have emerged linking HCV transmission with unsafe sexual practices in at-risk populations (Danta et al., 2007; Schmidt et al., 2011; Thomas, 2013; Urbanus et al., 2009; van de Laar et al., 2009; van de Laar et al., 2010; van de Laar et al., 2007). The mode of HCV transmission prior to the modern medicine-facilitated and relatively recent spread remains unclear (Pybus and Theze, 2015).

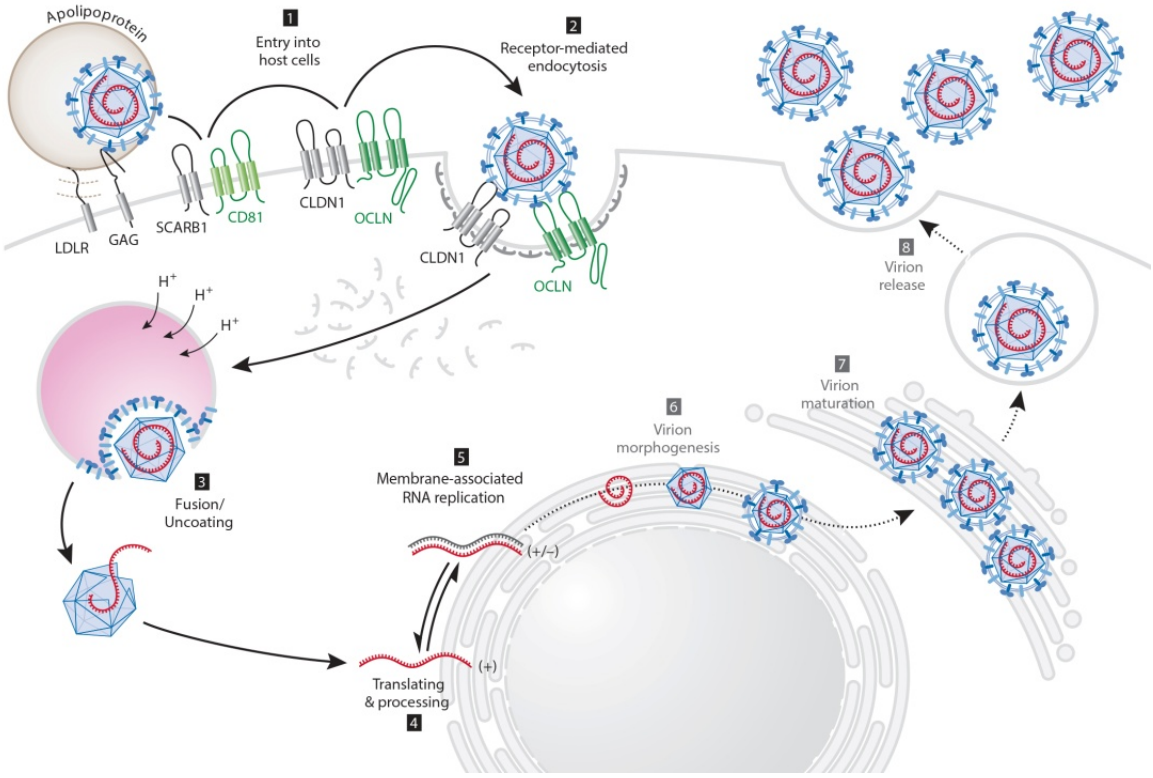

Figure 1.10. The HCV life cycle. The cycle of cellular infection by HCV: (1) The lipoprotein-associated virus binds a series of co-receptors, then undergoes receptor-mediated endocytosis (2), to mediate entry into the target cells. Acid mediated fusion of the viral and host cell membrane within an endosomal compartment leads to release of the viral capsid into the cytosol and uncoating of the genome (3). The genome is translated on ER-associated ribosomes (4), then undergoes replication (5) via a (-) strand RNA intermediate. Virion morphogenesis (6) occurs in an ER-related compartment. The newly formed viruses mature (7) as they are secreted by the host cell vesicular transport system (8), to be released into the extracellular space. LDLR, LDL receptor; GAG, glucosaminoglycans; SCARB1, scavenger receptor B1, CLDN1, claudin1; OCLN, occludin. Figure adapted by permission from (Ploss and Rice, 2009), ©2009 European Molecular Biology Organization.

HCV Entry. The virus enters the target hepatocytes via receptor-mediated endocytosis, followed by acid-mediated fusion of viral and cellular membranes (Lindenbach and Rice, 2013; Scheel and Rice, 2013). Binding to hepatocytes is mediated by several cell-surface co-receptors and may involve a cascade of binding and transport events before the virus is internalized (Lindenbach and Rice, 2013; Scheel and Rice, 2013). Ligands on the surface of the viral particles include the E2 envelope glycoprotein and potentially the associated host lipoproteins, while the cellular receptors include: glucosaminoglycans, LDLR (Andre et al., 2002; Monazahian et al., 1999), the tetraspanin membrane proteins CD81 (Pileri et al., 1998), and scavenger receptor B1 (Bartosch et al., 2003), the tight junction proteins claudin-1 (Evans et al., 2007) and occludin (Ploss et al., 2009), the epidermal growth factor receptor and the ephrin type-A receptor 2 (Lupberger et al., 2011), and the Niemann-Pick C1-like 1 cholesterol absorption receptor (Sainz et al., 2012). Following receptor-mediated endocytosis, acidification of virus-containing endosomal compartments is thought to mediate conformational changes within the viral glycoproteins, which mediate virus-host membrane fusion (Takikawa et al., 2000), leading to release of the RNA genome into the target cell's cytoplasm, thus initiating HCV infection.

Translation and polyprotein processing. The HCV protein is encoded by the positive sense viral genome, in which the protein-coding region is flanked by highly structured 5'- and 3'- end untranslated regions, or UTRs (Figure 1.11A). The HCV genome is translated on ER-associated ribosomes (Hijikata et al., 1991), which recognize the 5'-UTR-contained HCV internal ribosome entry site (IRES) structure (Tsukiyama-Kohara et al., 1992). Translation of the viral RNA results in the synthesis of a single

precursor polyprotein (Figure 1.11B). This HCV polyprotein contains, in order of translation, the following viral proteins (Figure 1.11B-C): the capsid protein Core, the envelope glycoproteins E1 and E2, the viroporin p7, and the nonstructural proteins (NS) 2, 3, 4A, 4B, 5A and 5B (Grakoui et al., 1993c; Lin et al., 1994). These 10 mature HCV proteins are released from the precursor polyprotein by four proteases (Figure 1.11B), two expressed by the host cell and two by the virus. The host cell proteases involved in HCV polyprotein processing are the signal peptidase, which cleaves the viral polyprotein at the junctions between Core and E1, between E1 and E2, between E2 and p7, and between p7 and NS2 (Hijikata et al., 1991; Lin et al., 1994; Mizushima et al., 1994a; Mizushima et al., 1994b), and the signal peptide peptidase, which removes the E1 signal peptide from the carboxyl terminus of the Core protein (McLauchlan et al., 2002). The virus encodes the remaining protease activities required for the processing of its polyprotein, namely a cysteine protease formed by NS2 and the amino terminus of NS3 (Grakoui et al., 1993b; Hijikata et al., 1993a; Lorenz et al., 2006), and a serine protease formed by NS3 and its cofactor NS4A (Bartenschlager et al., 1995; Hijikata et al., 1993a; Kim et al., 1996; Lin et al., 1995; Love et al., 1996; Tomei et al., 1993). The NS2-3 cysteine protease cleaves the NS2/3 junction (Grakoui et al., 1993b; Hijikata et al., 1993a), while the NS3-4A serine protease cleaves the NS3/4A, 4A/4B, 4B/5A and 5A/5B junctions (Bartenschlager et al., 1993; Grakoui et al., 1993a; Hijikata et al., 1993a; Hijikata et al., 1993b; Tomei et al., 1993). The resulting mature HCV proteins are then involved in viral genome replication, virion assembly, and release of assembled progeny virus particles, as well as modulation of host innate immune responses (Scheel and Rice, 2013).

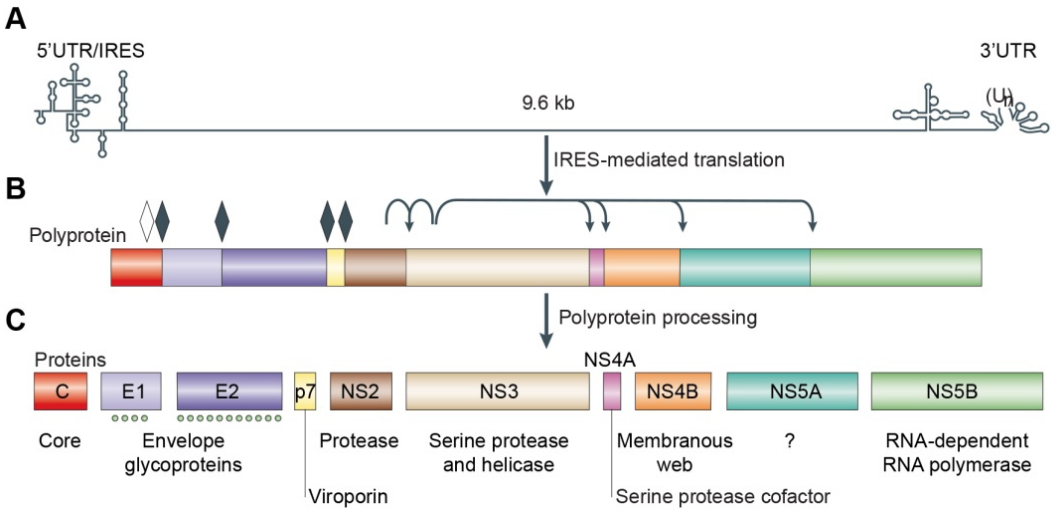

Figure 1.11. The HCV genome and the encoded proteins. (A) Depiction of the HCV RNA genome. The open reading frame is flanked by 5' and 3' UTRs. The 5'UTR contains an IRES. (B) IRES-mediated translation results in the synthesis of a large polyprotein, which undergoes proteolytic processing. Arrows indicate the sites of cleavage by the two viral proteases. Filled diamonds indicate the sites of cleavage by the host signal peptidase, while the empty diamond indicates the site of cleavage by the host signal peptide peptidase. (C) The 10 major HCV proteins are shown. Known selected functions are listed under each protein. Figure adapted by permission from Macmillan Publishers Ltd: Nature Rev. Microbiol. (Moradpour et al., 2007) ©2007.

The replication organelle and genome replication. A characteristic of many cytoplasm-replicating RNA viruses is that they reorganize host cell membranes to create new functional entities dedicated to the replication of the viral genome (Romero-Brey and Bartenschlager, 2014). This adaptation may serve several purposes. For example, by concentrating the enzymatic activities in a small volume or on a small surface, the efficiency of the genome replication process would also be increased. Since many of these viruses are enveloped viruses, the final stages of particle assembly, namely the envelopment of the capsid and the concurrent loading of the envelope glycoproteins,

would also benefit from the spatial coupling of genome replication with the membrane-dependent particle envelopment step on an organelle of the vesicular secretory pathway. Lastly, by segregating, to some extent, the viral replication process from the rest of the cytoplasm, the viruses may have achieved a spatial separation of the genome and its replication intermediates - both potent activators of cytoplasmic innate immune signaling pathways - and the cytosolic innate immune sensor molecules, such as those belonging to the RIG-I family of cytoplasmic innate immune receptors. The creation of a specialized membranous organelle to perform viral genome replication would thus shield the virus and the virus-infected cell from the immediate and long-term anti-viral effects of an activated innate immune system.

HCV, like other flaviviruses, replicates its genome on an ER-derived membranous formation, which has been described as a network of small, interconnected vesicular structures, also called a membranous web (Egger et al., 2002; Romero-Brey and Bartenschlager, 2014; Romero-Brey et al., 2012). The replication activities occurring within it require the non-structural proteins NS3 through NS5B, the 5' and 3' viral genome UTRs, as well as some RNA secondary structure-forming sequences present within the HCV ORF (Lohmann, 2013). The NS3-5B proteins are the viral proteins both necessary and sufficient for genome replication (Egger et al., 2002; Lohmann et al., 1999; Moradpour et al., 2004; Moradpour et al., 2003). The NS3/4A dimer cleaves the polyprotein and releases the other individual NS proteins such that they can perform their respective functions (Kim et al., 1996; Love et al., 1996). NS3 also contains a helicase domain, likely involved in RNA unwinding (Raney et al., 2010). NS4A targets NS3 to membranes due to its amphipathic helix (Wolk et al., 2000). NS4B has a major function

in organizing host membranes into the replication complex (Egger et al., 2002; Romero-Brey et al., 2012). NS5A has RNA binding properties and is essential for both replication and assembly of the viral particle, but does not possess a known enzymatic activity (Appel et al., 2008; Love et al., 2009; Tellinghuisen et al., 2008; Tellinghuisen et al., 2004; Tellinghuisen et al., 2005). Lastly, NS5B is the RNA-dependent RNA polymerase that replicates the viral genome (Behrens et al., 1996; Lesburg et al., 1999). This process involves the synthesis of a complementary, negative sense copy of the viral genome, which then serves as a template for the production of more copies of the positive sense RNA genome. A major requirement for genome replication is the involvement of the host cell microRNA miR-122, a tropism determinant that is also utilized by the virus to modulate host cell gene expression (Jopling et al., 2005; Luna et al., 2015).

HCV assembly and lipoprotein association. Assembly of HCV particles is currently believed to occur at or near cytoplasmic lipid droplets or on ER-derived membranes (Bartenschlager et al., 2011; Lindenbach, 2013; Lindenbach and Rice, 2013). This model is based on several observations. The HCV Core protein, which is required for the formation of the HCV virion (Miyanari et al., 2007; Murray et al., 2007), localizes onto lipid droplets and ER membranes (Boson et al., 2011; Miyanari et al., 2007; Murray et al., 2007). The ability of Core to associate with the cytoplasmic surfaces of the lipid droplets and of the ER membrane is required for viral particle assembly (Boulant et al., 2007; Targett-Adams et al., 2008). Second, in pulse-chase time course experiments, fluorescently labeled Core molecules were observed to relocate from their site of synthesis (ER-bound ribosomes) to the surface of lipid droplets and then back to the ER (Counihan et al., 2011). Furthermore, the E1/E2 glycoprotein heterodimer, required for

particle production and entry, localizes specifically within the ER (Cocquerel et al., 1999; Cocquerel et al., 1998), where it is presumably loaded onto the nascent viral particles during particle envelopment. Particle assembly involves tight coordination of the structural viral particle components (Core, E1 and E2) and some nonstructural HCV proteins (p7, NS2, NS3, NS5A), as evidenced by their colocalization and interaction networks, the later revealed both biochemically and genetically (Appel et al., 2008; Gentzsch et al., 2013; Jirasko et al., 2010; Jones et al., 2011; Kim et al., 2011; Lindenbach, 2013; Lindenbach and Rice, 2013; Ma et al., 2008; Masaki et al., 2008; Miyanari et al., 2007; Murray et al., 2008; Popescu et al., 2011).

Production of infectious HCV also requires that cells express apolipoproteins, such as ApoE and/or ApoB100 (Chang et al., 2007; Fukuhara et al., 2014; Gastaminza et al., 2008; Hishiki et al., 2010; Huang et al., 2007; Hueging et al., 2014; Lee et al., 2014; Long et al., 2011; Vogt et al., 2013). These apolipoproteins are incorporated into the virus particles (Andre et al., 2002; Catanese et al., 2013; Chang et al., 2007; Nielsen et al., 2006) and confer them lipoprotein-like properties, such as a light density (Andre et al., 2002; Gastaminza et al., 2008; Gastaminza et al., 2006; Lindenbach et al., 2006; Nielsen et al., 2006), resulting in the formation of lipoviroparticles (Andre et al., 2002). Knockdown of ApoE or ApoB100, or inhibition of their lipidation, impairs HCV particle production (Chang et al., 2007; Gastaminza et al., 2008; Jiang and Luo, 2009), and Core punctate signals were shown to colocalize with ApoE punctate signals in infected cells (Coller et al., 2012). Additionally, the E2 transmembrane domain was shown to interact with ApoE (Lee et al., 2014). Association of ApoE and ApoB100 with HCV may serve several functions in the viral life cycle: they may help prevent intracellular degradation of

newly assembled HCV particles (Gastaminza et al., 2008), mediate transport of HCV through the secretory pathway (Hishiki et al., 2010), and facilitate entry into target cells through interactions with viral co-receptors, including LDLR (Agnello et al., 1999; Monazahian et al., 1999), glucosaminoglycans (Germi et al., 2002) and scavenger receptor B1 (Scarselli et al., 2002). Overall, the uniquely tight associations between HCV and the liver-derived apolipoproteins ApoE and ApoB100, as well as the complex nature of VLDL and HCV particle assembly and secretion from hepatocytes, invites the inquiry of how the secretion routes of these entities are molecularly regulated.

1.18. Regulation of HCV and lipoprotein release

HCV and lipoprotein secretion has been characterized in broad terms, but molecular details of the regulation of these processes remain somewhat sparse. Both VLDL and HCV transit through the Golgi as they are being secreted, as both ApoB100 and HCV glycoproteins acquire glycan chain modifications that require Golgi-resident enzyme activity (Tran et al., 2002; Vieyres et al., 2010). Furthermore, VLDL particles, HCV and ApoE have each been colocalized or co-isolated with the Golgi (Coller et al., 2012; Ehrenreich et al., 1973; Kockx et al., 2007). Brefeldin A, a potent and widely used inhibitor of ER to Golgi traffic, has been shown to impair the secretion of HCV, ApoE and ApoB100 (Deng et al., 1995; Gastaminza et al., 2008; Rustaeus et al., 1995; Ye et al., 1992; Ye et al., 1993). Lastly, transport of ApoE and of HCV appears to occur along microtubules, since the movement of fluorescently labeled HCV (Coller et al., 2012) or ApoE (Kockx et al., 2007) is severely reduced by treatment with the microtubule poison nocodazole.

Investigation into how HCV and lipoproteins are transported from the ER to the Golgi remains an area of continued interest. Experiments in several systems have documented that both HCV (Coller et al., 2012) and lipoprotein (Gusarova et al., 2003; Jones et al., 2003; Siddiqi et al., 2003) transport depend on the activity of Sar1 GTPases. This is consistent with the particles - at least initially - being transported by a COPII membrane carrier, since Sar1 is the GTPase that specifically recruits COPII at the site of vesicle formation at ER exit sites (Kuge et al., 1994; Nakano and Muramatsu, 1989). There, VLDL may be loaded into a specialized transport vesicle, the VLDL transport vesicle, which was found to be larger than a regular protein transport vesicle, and of a lighter density (Siddiqi, 2008). Albumin has been shown to be transported by such protein transport vesicles, and it was absent from the VLDL transport vesicle (Siddiqi, 2008). It is unclear at the moment whether exclusion of regular proteins from the VLDL transport vesicle is due to passive phenomena (i.e. once a VLDL is sorted there is not much room left in the nascent VLDL transport vesicle to package more cargo) or active processes (i.e. the VLDL is actively concentrated into VLDL transport vesicles while the regular proteins are actively excluded from VLDL transport vesicles and/or actively and specifically concentrated into protein transport vesicles). Also intriguing is the finding that ApoB100 and ApoE segregated into distinct subpopulations of *in vitro*-made ER-derived vesicles, but were found in the same Golgi-derived vesicle population (Gusarova et al., 2007). Since at least a fraction of the hepatic ApoE may be secreted as part of VLDL particles (Dolphin, 1981; Reardon et al., 1998; Vance et al., 1984; Wilcox and Heimberg, 1987), these findings suggest that ApoE-VLDL association occurs in the Golgi, and that their transport from the ER to the Golgi occurs in separate carriers.

Less is known about these cargoes' post-Golgi routes of secretion. They have been shown to be partly degraded intracellularly in a post-Golgi compartment, since degradation was sensitive to inactivation of ER to Golgi transport by brefeldin A treatment (Deng et al., 1995; Gastaminza et al., 2008; Ye et al., 1993). Furthermore, this post-ER degradation has been shown to be inhibited by treatment with protease inhibitors that target endosomal cathepsin and calpain proteases (Deng et al., 1995; Gastaminza et al., 2008; Hiwasa et al., 1990; Ye et al., 1993). It may be the case that some of these cargoes are targeted for endolysosomal degradation, which may be reduced in the presence of said protease inhibitors. It may also be the case that the secretion pathway(s) of these cargoes passes through an endosomal compartment, where some cargo becomes degraded. Indeed, release of HCV particles has been shown to be reduced when Rab11a expression was impaired (Coller et al., 2012). Rab11a is a defining marker of recycling endosomes (Ullrich et al., 1996), as I will more fully explain in Chapter 4. HCV secretion was also reduced when Rab3d expression was knocked down (Coller et al., 2012). Rab3d (also known as Rab16) is known to function at late exocytic steps (Fukuda, 2008) and may thus regulate the final transport steps of HCV secretion. Differences nevertheless do appear to exist between post-Golgi HCV and VLDL transport, since HCV transport was impaired when expression of the γ-1 subunit of the clathrin adaptor protein complex AP-1 was knocked down, while VLDL secretion was unaffected (Benedicto et al., 2015).

Characterization in greater detail of the molecular basis of post-Golgi transport of HCV and of lipoprotein particles is in order. Such work also needs to account for other known aspects of intracellular transport of HCV and of lipoprotein components. A major concern is the need to distinguish, particularly in imaging experiments, between secretory

behavior of newly synthesized cargo and endocytic recycling of cargo up-taken from the extracellular space. ApoE, for example, was shown to be a recycled cargo, although ApoB was not, but was instead targeted for lysosomal degradation (Heeren et al., 2003; Laatsch et al., 2012). HCV, in turn, enters cells through receptor mediated endocytosis (Coller et al., 2009). It is unclear to what extent newly endocytosed particles may reach a compartment that may also function in secretion, such as the recycling endosome (Coller et al., 2012), and how transport of endocytosed infectious viruses differs, if at all, from transport of endocytosed non-infectious viruses, which form the majority of the particles even in some of the most enriched infectious virus preparations (Catanese et al., 2013; Gastaminza et al., 2010).

Any interpretation of experimental findings documenting the involvement of one pathway or the other in HCV or lipoprotein secretion must also account for the possibility that one single pathway may not be exclusively or even primarily responsible for cargo release.

1.19. Significance

As repeatedly emphasized above, the hepatic cargoes that are the focus of the studies I present here serve essential functions in the human body. Maintenance of circulatory system homeostasis and lipid transport are the most obvious of these functions (Ha and Bhagavan, 2013; Olofsson and Boren, 2005; Yamasaki et al., 2013; Zannis et al., 2015). The disease association of these cargoes is extensive. Atherosclerotic cardiovascular disease is a leading cause of morbidity and mortality worldwide (Barquera et al., 2015). The pathologies associated with HCV infection are also numerous and can severely affect human life (Hoofnagle, 1997; Thomas, 2013). Understanding the

processes involved in the production of these bioparticles is thus necessary, and may, in the long run, provide avenues for therapeutic intervention.

From a cell biological perspective, this topic is of interest because it deals with a particularly challenging question: how are large cargoes, such as VLDL or HCV particles, transported by the secretory pathway, given that documented sizes of transport vesicles appear to be insufficient to allow for packaging of these large cargoes (Miller and Schekman, 2013)? Indeed, intensive recent research efforts have dealt with how such cargoes are packaged into COPII-dependent ER-derived vesicles (Jin et al., 2012; Mansbach and Siddiqi, 2010). While my work does not address the sorting of large cargoes into the transport carriers *per se*, it nevertheless touches on the question of whether there are any differences between the transport regulation of carriers that shuttle regularly-sized proteins, such as albumin, and those that transport the large lipoprotein and viral particles. This body of work also lays the groundwork for addressing the question of how polarized transport of lipoproteins and of HCV is regulated by the hepatocyte.

Lastly, the analysis of HCV and lipoprotein secretion must be undertaken while considering the evolutionary history of the virus. That HCV has evolved to be so closely associated with the hepatic lipoproteins is a testimony to how well the virus has "learned" the cell biology of the hepatocyte (Lindenbach, 2013; Lindenbach and Rice, 2013; Scheel and Rice, 2013). Delineating which transport pathways are common for HCV and lipoproteins, and which are distinct, may well advance the understanding of both host and pathogen cell biology. This line of inquiry conceptually mirrors the study of the exocytic transport of the vesicular stomatitis virus glycoprotein (VSVg), which has helped define

major features of secretory vesicular traffic (Bergmann, 1989), or the study of viral and bacterial toxin entry, which have facilitated the investigation of important endocytic processes (Pelkmans, 2005; Schiavo and van der Goot, 2001).

1.20. Aims

Given the biomedical importance of the lipoproteins and HCV alike, and given the complex and interconnected cell biology that is involved in the production of these cargoes by hepatocytes, I set out to define and characterize molecular, spatial and temporal aspects of lipoprotein and HCV egress. My work aimed to: (i) identify the transport regulators of HCV and lipoprotein particle secretion by means of performing a screen using DN mutants of the Rab GTPases; (ii) confirm and describe the involvement of specified members of the Rab family in these secretory processes,; and (iii) validate fluorescent protein-tagged versions of the Rab GTPases and of cargoes as useful tools in live-cell imaging analyses of hepatic cargo secretion. I now compile the work I have performed to date, and describe some avenues of investigation that I believe future work could successfully pursue. This thesis will thus describe at length the methodology used to advance this project. I will then present the design and the results of the DN Rab GTPase screen that I used to unbiasedly identify regulators of hepatic cargo secretion. I will describe ongoing investigations into how Rab11 and Rab8 GTPases may control lipoprotein and HCV secretion, and the characterization of Rab1 involvement in the same processes. I will also describe the tests I performed to determine whether fluorescent protein-tagged ApoE might be used in the study of hepatic lipoprotein and HCV secretion. Throughout the pages, I will also discuss how the approaches and the assays that I have utilized may be improved and adapted to other lines of investigation.

Chapter 2.

Materials and Methods.

2.1. DNA manipulations

Standard molecular biology protocols were used to construct or modify the plasmids used in this work, as described below. Polymerase chain reaction (PCR) using Platinum PCR Supermix (Life Technologies) or Takara polymerase (Clontech) was performed to amplify DNA fragments, which were then digested using New England Biolabs restriction endonucleases and ligated (Quick Ligase, New England Biolabs) into target vectors. Alternatively, the In-Fusion HD kit (Clontech) was employed, according to the manufacturer's instructions, to insert DNA fragments into target vectors. Site-directed mutagenesis (SDM) was performed using the Quick Change Lightning Site Directed Mutagenesis kit (Agilent) according to the manufacturer's instructions. Plasmids were transformed and grown in the DH5α *E. coli* strain at 30°C (retroviral and lentiviral vectors) or at 37°C (all other vectors) in LB medium or terrific broth (Difco). Ampicillin was used at 100 μg/mL and kanamycin was used at 50 μg/mL for selection. DNA was isolated using Purelink Quick Plasmid Miniprep, Quick Gel Extraction or HiPure Plasmid Maxiprep kits (Life Technologies). Plasmids and some of their relevant features are listed in Table 2.1, while the text below also describes the steps undertaken to make these constructs. Table 2.1 also includes a series of plasmids that were used as templates for amplification of various DNA sequences, or as vector backbones. The references or commercial sources for the various plasmids used in this work are also listed in Table 2.1. For the Rab-encoding plasmids that I used in the DN Rab screen part of this work, I

also list in Table 2.1 the NCBI reference sequence number of the respective WT human Rab proteins. The nucleotide sequences of the DNA primers employed during the plasmid construction process are listed in Table 2.2, and the primers are referred to in the text by their names. They were chemically synthesized by IDT. The nucleotide sequences of the relevant features of both intermediate and final constructs were confirmed using DNA sequencing by Genewiz or Macrogen.

Table 2.1. Plasmids

Construct	Relevant Features	Notes	Source or Reference
Non-viral plasmids			
pCR3.1 SynGag	HIV-1 Gag		(Graf et al., 2000)
pMLV GagPol	MLV GagPol	Retrovirus packaging vector	(Jouvenet et al., 2009)
pVSVg	VSVg	Pseudotyping vectors	Clontech
pHCMV-VSVg	VSVg		(Beyer et al., 2002)
pVSVg$_{tsO45}$-GFP	P_{CMV} VSVg$_{tsO45}$-GFP	Retained in the ER at 39.5°C	(Presley et al., 1997)
pmEGFP-N1	P_{CMV} MCS-mEGFP	EGFP$_{A206K}$	Lab plasmid
pmCherry-N1	P_{CMV} MCS-mCherry		Clontech
pGFP-DrrA$_{61-647}$	P_{CMV} GFP-DrrA$_{61-647}$	*L. pneumophila* effector	(Murata et al., 2006)
pCMV-XL5 Rab10	Rab10		Origene
pCMV-XL5 Rab12	Rab12		
pCMV-XL5 Calnexin	Calnexin		
pCMV-SPORT6 Rab1a	Rab1a		Mammalian Gene Collection, Open Biosystems
pCMV-SPORT6 Rab1b	Rab1b		
pCMV-SPORT6 Rab1c/35	Rab1c/35		
pCMV-SPORT6 Rab3d/16	Rab3d/16		
pCMV-SPORT6 Rab5b	Rab5b		
pCMV-SPORT6 Rab5c	Rab5c		
pCMV-SPORT6 Rab13	Rab13		
pCMV-SPORT6 Rab21	Rab21		
pCMV-SPORT6 Rab22a	Rab22a		
pCMV-SPORT6 Rab23	Rab23		
pCMV-SPORT6 Rab27a	Rab27a		
pCMV-SPORT6 Rab27b	Rab27b		
pCMV-SPORT6 Rab38	Rab38		
pOTB7-Rab2a	Rab2a		

Table 2.1. Plasmids

Construct	Relevant Features	Notes	Source or Reference
pOTB7-Rab3b	Rab3b		
pOTB7-Rab4b	Rab4b		
pOTB7-Rab6a	Rab6a		
pOTB7-Rab7a	Rab7a		
pOTB7-Rab8a	Rab8a		
pOTB7-Rab11c/25	Rab11c/25		
pOTB7-Rab22b/31	Rab22b/31		
pOTB7-Rab24	Rab24		
pOTB7-Rab33a	Rab33a		
pOTB7-Rab43	Rab43		
pDNR-LIB-Rab2b	Rab2b		
pDNR-LIB-Rab8b	Rab8b		
pDNR-LIB-Rab32	Rab32		
pBlueScriptR-Rab15	Rab15		
pBlueScriptR-Rab33b	Rab33b		
pCR-TOPO-Rab11b	Rab11b		
pCR-TOPO-Rab36	Rab36		
pCDNA5 Flag3-Rab5a	Rab5a	Obtained from Addgene	(Sun et al., 2010a)
pEGFP-Rab11a$_{WT}$	Rab11a		(Choudhury et al., 2002)
pEGFP-Rab18	Rab18		Lab plasmid
HCV plasmids			
pFL J6/JFH1	P_{T7} HCV J6/JFH1 cDNA	For *in vitro* transcription	(Lindenbach et al., 2005)
Lentiviral plasmids			
pCR/V1 NL GagPol	HIV-1 GagPol + accessory genes	Lentivirus packaging vector	(Zennou et al., 2004)
pLX304 Rab3a	Rab3a		(Yang et al., 2011)
pLX304 Rab3c	Rab3c		
pLX304 Rab4a	Rab4a		
pLX304 Rab6b	Rab6b		
pLX304 Rab6c	Rab6c		
pLX304 Rab7b	Rab7b		
pLX304 Rab9a	Rab9a		
pLX304 Rab9b	Rab9b		
pLX304 Rab14	Rab14		
pLX304 Rab17	Rab17		
pLX304 Rab19b	Rab19b		
pLX304 Rab20	Rab20		
pLX304 Rab26	Rab26		
pLX304 Rab7L1/29	Rab7L1/29		
pLX304 Rab30	Rab30		

Table 2.1. Plasmids

Construct	Relevant Features	Notes	Source or Reference
pLX304 Rab34	Rab34		
pLX304 Rab37	Rab37		
pLX304 Rab39a	Rab39a		
pLX304 Rab39b	Rab39b		
pLX304 Rab40a	Rab40a		
pLX304 Rab40al	Rab40al		
pLX304 Rab40b	Rab40b		
pLX304 Rab40c	Rab40c		
pLX304 Rab41	Rab41		
pLVX Puro	P_{CMV} MCS; P_{PGK} PuroR		Clontech
pLenti4/V5-Dest	ZeoR		Invitrogen
pLVX Bhi3	P_{CMV} MCS; P_{PGK} BlastR	Improved MCS and varied eukaryotic antibiotic selection markers	This study
pLVX Hhi3	P_{CMV} MCS; P_{PGK} HygroR		This study
pLVX Nhi3	P_{CMV} MCS; P_{PGK} NeoR		This study
pLVX Phi3	P_{CMV} MCS; P_{PGK} PuroR		This study
pLVX Zhi3	P_{CMV} MCS; P_{PGK} ZeoR		This study
pLVX Che-hi3	P_{CMV} MCS; P_{PGK} mCherry	mCherry reporter vector	This study
pLVX Hhi3 ApoE3	P_{CMV} ApoE3	ApoE3 engineered to be knockdown - resistant	This study
pLVX Hhi3 ApoE3-mEGFP	P_{CMV} ApoE3-mEGFP		This study
pLVX Bhi3 mEGFP-ApoE3	P_{CMV} SP-mEGFP-ApoE3		This study
pLVX Phi3 mCherry	P_{CMV} mCherry	mCherry control expression vector	This study
pLVX Phi3 FLuc	P_{CMV} FLuc		This study
pLVX Bhi3 FLuc			This study
OL135 pLVX Phi3 mCherry-Rab1b	P_{CMV} mCherry-Rab1b		This study
OL115 pLVX Phi3 mCherry-Rab1b$_{Q67L}$	P_{CMV} mCherry-Rab1b$_{Q67L}$		This study
OL142 pLVX Phi3 mCherry-Rab1b$_{S22N}$	P_{CMV} mCherry-Rab1b$_{S22N}$		This study
OL143 pLVX Phi3 mCherry-Rab1b$_{N121I}$	P_{CMV} mCherry-Rab1b$_{N121I}$		This study
OL177 pLVX Che-hi3 Rab1b	P_{CMV} hab1b	NP_112243.1	This study

Table 2.1. Plasmids

Construct	Relevant Features	Notes	Source or Reference
OL178 pLVX Che-hi3 Rab1b$_{N121I}$	P_{CMV} Rab1b$_{N121I}$		This study
OL249 pLVX Che-hi3 Rab1b$_{Q67L}$	P_{CMV} Rab1b$_{Q67L}$		This study
OL250 pLVX Che-hi3 Rab1b$_{S22N}$	P_{CMV} Rab1b$_{S22N}$		This study
OL 175 pLVX Che-hi3 Rab1a	P_{CMV} Rab1a	NP_004152.1	This study
OL 176 pLVX Che-hi3 Rab1a$_{N124I}$	P_{CMV} Rab1a$_{N124I}$		This study
OL179 pLVX Che-hi3 Rab1c/35	P_{CMV} Rab1c/35	NP_006852.1	This study
OL180 pLVX Che-hi3 Rab1c/35$_{N120I}$	P_{CMV} Rab1c/35$_{N120I}$		This study
OL181 pLVX Che-hi3 Rab2a	P_{CMV} Rab2a	NP_002856.1	This study
OL182 pLVX Che-hi3 Rab2a$_{N119I}$	P_{CMV} Rab2a$_{N119I}$		This study
OL183 pLVX Che-hi3 Rab3a	P_{CMV} Rab3a	NP_002857.1	This study
OL184 pLVX Che-hi3 Rab3a$_{N135I}$	P_{CMV} Rab3a$_{N135I}$		This study
OL185 pLVX Che-hi3 Rab3b	P_{CMV} Rab3b	NP_002858.2	This study
OL186 pLVX Che-hi3 Rab3b$_{N135I}$	P_{CMV} Rab3b$_{N135I}$		This study
OL187 pLVX Che-hi3 Rab3c	P_{CMV} Rab3c	NP_612462.1	This study
OL188 pLVX Che-hi3 Rab3c$_{N143I}$	P_{CMV} Rab3c$_{N143I}$		This study
OL189 pLVX Che-hi3 Rab3d/16	P_{CMV} Rab3d/16	NP_004274.1	This study
OL190 pLVX Che-hi3 Rab3d/16$_{N135I}$	P_{CMV} Rab3d/16$_{N135I}$		This study
OL191 pLVX Che-hi3 Rab4a	P_{CMV} Rab4a	NP_004569.2	This study
OL192 pLVX Che-hi3 Rab4a$_{N126I}$	P_{CMV} Rab4a$_{N126I}$		This study
OL193 pLVX Che-hi3 Rab5a	P_{CMV} Rab5a	NP_004153.2	This study
OL194 pLVX Che-hi3 Rab5a$_{N133I}$	P_{CMV} Rab5a$_{N133I}$		This study

Table 2.1. Plasmids

Construct	Relevant Features	Notes	Source or Reference
OL195 pLVX Che-hi3 Rab6a	P_{CMV} Rab6a	NP_002860.2	This study
OL196 pLVX Che-hi3 Rab6a$_{N126I}$	P_{CMV} Rab6a$_{N126I}$		This study
OL197 pLVX Che-hi3 Rab7b	P_{CMV} Rab7b	NP_796377.3	This study
OL198 pLVX Che-hi3 Rab7b$_{N124I}$	P_{CMV} Rab7b$_{N124I}$		This study
OL199 pLVX Che-hi3 Rab8a	P_{CMV} Rab8a	NP_005361.2	This study
OL200 pLVX Che-hi3 Rab8a$_{N121I}$	P_{CMV} Rab8a$_{N121I}$		This study
OL319 pLVX Che-hi3 Rab8a$_{Q67L}$	P_{CMV} Rab8a$_{Q67L}$		This study
OL320 pLVX Che-hi3 Rab8a$_{T22N}$	P_{CMV} Rab8a$_{T22N}$		This study
OL201 pLVX Che-hi3 Rab8b	P_{CMV} Rab8b	NP_057614.1	This study
OL202 pLVX Che-hi3 Rab8b$_{N121I}$	P_{CMV} Rab8b$_{N121I}$		This study
OL321 pLVX Che-hi3 Rab8b$_{Q67L}$	P_{CMV} Rab8b$_{Q67L}$		This study
OL322 pLVX Che-hi3 Rab8b$_{T22N}$	P_{CMV} Rab8b$_{T22N}$		This study
OL203 pLVX Che-hi3 Rab9a	P_{CMV} Rab9a	NP_004242.1	This study
OL204 pLVX Che-hi3 Rab9a$_{N124I}$	P_{CMV} Rab9a$_{N124I}$		This study
OL205 pLVX Che-hi3 Rab10	P_{CMV} Rab10	NP_057215.3	This study
OL206 pLVX Che-hi3 Rab10$_{N122I}$	P_{CMV} Rab10$_{N122I}$		This study
OL207 pLVX Che-hi3 Rab11a	P_{CMV} Rab11a	NP_004654.1	This study
OL208 pLVX Che-hi3 Rab11a$_{N124I}$	P_{CMV} Rab11a$_{N124I}$		This study
OL313 pLVX Che-hi3 Rab11a$_{Q70L}$	P_{CMV} Rab11a$_{Q70L}$		This study
OL314 pLVX Che-hi3 Rab11a$_{S25N}$	P_{CMV} Rab11a$_{S25N}$		This study
OL209 pLVX Che-hi3 Rab11b	P_{CMV} Rab11b	NP_004209.2	This study

Table 2.1. Plasmids

Construct	Relevant Features	Notes	Source or Reference
OL210 pLVX Che-hi3 Rab11b$_{N124I}$	P_{CMV} Rab11b$_{N124I}$		This study
OL315 pLVX Che-hi3 Rab11b$_{Q70L}$	P_{CMV} Rab11b$_{Q70L}$		This study
OL316 pLVX Che-hi3 Rab11b$_{S25N}$	P_{CMV} Rab11b$_{S25N}$		This study
OL211 pLVX Che-hi3 Rab11c/25	P_{CMV} Rab11c/25	NP_065120.2	This study
OL212 pLVX Che-hi3 Rab11c/25$_{N125I}$	P_{CMV} Rab11c/25$_{N125I}$		This study
OL213 pLVX Che-hi3 Rab12	P_{CMV} Rab12	NP_001020471.2	This study
OL214 pLVX Che-hi3 Rab12$_{N155I}$	P_{CMV} Rab12$_{N155I}$		This study
OL215 pLVX Che-hi3 Rab13	P_{CMV} Rab13	NP_002861.1	This study
OL216 pLVX Che-hi3 Rab13$_{N121I}$	P_{CMV} Rab13$_{N121I}$		This study
OL217 pLVX Che-hi3 Rab14	P_{CMV} Rab14	NP_057406.2	This study
OL218 pLVX Che-hi3 Rab14$_{N124I}$	P_{CMV} Rab14$_{N124I}$		This study
OL219 pLVX Che-hi3 Rab18	P_{CMV} Rab18	NP_067075.1	This study
OL220 pLVX Che-hi3 Rab18$_{N122I}$	P_{CMV} Rab18$_{N122I}$		This study
OL221 pLVX Che-hi3 Rab19b	P_{CMV} Rab19b	NP_001008749.2	This study
OL222 pLVX Che-hi3 Rab19b$_{N130I}$	P_{CMV} Rab19b$_{N130I}$		This study
OL223 pLVX Che-hi3 Rab22b/31	P_{CMV} Rab22b/31	NP_006859.2	This study
OL224 pLVX Che-hi3 Rab22b/31$_{N119I}$	P_{CMV} Rab22b/31$_{N119I}$		This study
OL225 pLVX Che-hi3 Rab23	P_{CMV} Rab23	NP_057361.3	This study
OL226 pLVX Che-hi3 Rab23$_{N121I}$	P_{CMV} Rab23$_{N121I}$		This study
OL227 pLVX Che-hi3 Rab26	P_{CMV} Rab26	NP_055168.2	This study
OL228 pLVX Che-hi3 Rab26$_{N177I}$	P_{CMV} Rab26$_{N177I}$		This study

Table 2.1. Plasmids

Construct	Relevant Features	Notes	Source or Reference
OL229 pLVX Che-hi3 Rab27a	P_{CMV} Rab27a	NP_004571.2	This study
OL230 pLVX Che-hi3 Rab27a$_{N133I}$	P_{CMV} Rab27a$_{N133I}$		This study
OL231 pLVX Che-hi3 Rab27b	P_{CMV} Rab27b	NP_004154.2	This study
OL232 pLVX Che-hi3 Rab27b$_{N133I}$	P_{CMV} Rab27b$_{N133I}$		This study
OL233 pLVX Che-hi3 Rab32	P_{CMV} Rab32	NP_006825.1	This study
OL234 pLVX Che-hi3 Rab32$_{N143I}$	P_{CMV} Rab32$_{N143I}$		This study
OL235 pLVX Che-hi3 Rab33a	P_{CMV} Rab33a	NP_004785.1	This study
OL236 pLVX Che-hi3 Rab33a$_{N151I}$	P_{CMV} Rab33a$_{N151I}$		This study
OL237 pLVX Che-hi3 Rab39a	P_{CMV} Rab39a	NP_059986.1	This study
OL238 pLVX Che-hi3 Rab39a$_{H127I}$	P_{CMV} Rab39a$_{H127I}$		This study
OL239 pLVX Che-hi3 Rab40a	P_{CMV} Rab40a	NP_543155.2	This study
OL240 pLVX Che-hi3 Rab40a$_{N126I}$	P_{CMV} Rab40a$_{N126I}$		This study
OL251 pLVX Che-hi3 Rab2b	P_{CMV} Rab2b	NP_116235.2	This study
OL252 pLVX Che-hi3 Rab2b$_{N119I}$	P_{CMV} Rab2b$_{N119I}$		This study
OL253 pLVX Che-hi3 Rab4b	P_{CMV} Rab4b	NP_057238.3	This study
OL254 pLVX Che-hi3 Rab4b$_{N121I}$	P_{CMV} Rab4b$_{N121I}$		This study
OL255 pLVX Che-hi3 Rab5b	P_{CMV} Rab5b	NP_002859.1	This study
OL256 pLVX Che-hi3 Rab5b$_{N133I}$	P_{CMV} Rab5b$_{N133I}$		This study
OL257 pLVX Che-hi3 Rab5c	P_{CMV} Rab5c	NP_004574.2	This study
OL258 pLVX Che-hi3 Rab5c$_{N134I}$	P_{CMV} Rab5c$_{N134I}$		This study
OL259 pLVX Che-hi3 Rab6b	P_{CMV} Rab6b	NP_057661.3	This study

Table 2.1. Plasmids

Construct	Relevant Features	Notes	Source or Reference
OL260 pLVX Che-hi3 Rab6b$_{N126I}$	P_{CMV} Rab6b$_{N126I}$		This study
OL261 pLVX Che-hi3 Rab6c	P_{CMV} Rab6c	NP_115520.2	This study
OL262 pLVX Che-hi3 Rab6c$_{N126I}$	P_{CMV} Rab6c$_{N126I}$		This study
OL263 pLVX Che-hi3 Rab7a	P_{CMV} Rab7a	NP_004628.4	This study
OL264 pLVX Che-hi3 Rab7a$_{N125I}$	P_{CMV} Rab7a$_{N125I}$		This study
OL265 pLVX Che-hi3 Rab9b	P_{CMV} Rab9b	NP_057454.1	This study
OL266 pLVX Che-hi3 Rab9b$_{N124I}$	P_{CMV} Rab9b$_{N124I}$		This study
OL267 pLVX Che-hi3 Rab15	P_{CMV} Rab15	NP_941959.1	This study
OL268 pLVX Che-hi3 Rab15$_{T22N}$	P_{CMV} Rab15$_{T22N}$		This study
OL269 pLVX Che-hi3 Rab17	P_{CMV} Rab17	NP_071894.1	This study
OL270 pLVX Che-hi3 Rab17$_{N132I}$	P_{CMV} Rab17$_{N132I}$		This study
OL271 pLVX Che-hi3 Rab20	P_{CMV} Rab20	NP_060287.1	This study
OL272 pLVX Che-hi3 Rab20$_{N113I}$	P_{CMV} Rab20$_{N113I}$		This study
OL274 pLVX Che-hi3 Rab21	P_{CMV} Rab21	NP_055814.1	This study
OL274 pLVX Che-hi3 Rab21$_{N132I}$	P_{CMV} Rab21$_{N132I}$		This study
OL275 pLVX Che-hi3 Rab22a	P_{CMV} Rab22a	NP_065724.1	This study
OL276 pLVX Che-hi3 Rab22a$_{N118I}$	P_{CMV} Rab22a$_{N118I}$		This study
OL277 pLVX Che-hi3 Rab24	P_{CMV} Rab24	NP_570137.2	This study
OL278 pLVX Che-hi3 Rab24$_{T120I}$	P_{CMV} Rab24$_{T120I}$		This study
OL279 pLVX Che-hi3 Rab28	P_{CMV} Rab28	NP_004240.2	This study
OL280 pLVX Che-hi3 Rab28$_{N129I}$	P_{CMV} Rab28$_{N129I}$		This study

Table 2.1. Plasmids

Construct	Relevant Features	Notes	Source or Reference
OL281 pLVX Che-hi3 Rab29/7L1	P_{CMV} Rab29/7L1	NP_003920.1	This study
OL282 pLVX Che-hi3 Rab29/7L1$_{N125I}$	P_{CMV} Rab29/7L1$_{N125I}$		This study
OL283 pLVX Che-hi3 Rab30	P_{CMV} Rab30	NP_055303.2	This study
OL284 pLVX Che-hi3 Rab30$_{N122I}$	P_{CMV} Rab30$_{N122I}$		This study
OL285 pLVX Che-hi3 Rab33b	P_{CMV} Rab33b	NP_112586.1	This study
OL286 pLVX Che-hi3 Rab33b$_{N148I}$	P_{CMV} Rab33b$_{N148I}$		This study
OL287 pLVX Che-hi3 Rab34	P_{CMV} Rab34	NP_114140.4	This study
OL288 pLVX Che-hi3 Rab34$_{S166I}$	P_{CMV} Rab34$_{S166I}$		This study
OL289 pLVX Che-hi3 Rab36	P_{CMV} Rab36	NP_004905.2	This study
OL290 pLVX Che-hi3 Rab36$_{T237I}$	P_{CMV} Rab36$_{T237I}$		This study
OL291 pLVX Che-hi3 Rab37	P_{CMV} Rab37	NP_001006639.1	This study
OL292 pLVX Che-hi3 Rab37$_{N143I}$	P_{CMV} Rab37$_{N143I}$		This study
OL293 pLVX Che-hi3 Rab38	P_{CMV} Rab38	NP_071732.1	This study
OL294 pLVX Che-hi3 Rab38$_{N127I}$	P_{CMV} Rab38$_{N127I}$		This study
OL295 pLVX Che-hi3 Rab39b	P_{CMV} Rab39b	NP_741995.1	This study
OL296 pLVX Che-hi3 Rab39b$_{H123I}$	P_{CMV} Rab39b$_{H123I}$		This study
OL297 pLVX Che-hi3 Rab40al	P_{CMV} Rab40al	NP_001027004.1	This study
OL298 pLVX Che-hi3 Rab40al$_{N126I}$	P_{CMV} Rab40al$_{N126I}$		This study
OL299 pLVX Che-hi3 Rab40b	P_{CMV} Rab40b	NP_006813.1	This study
OL300 pLVX Che-hi3 Rab40b$_{N126I}$	P_{CMV} Rab40b$_{N126I}$		This study
OL301 pLVX Che-hi3 Rab40c	P_{CMV} Rab40c	NP_066991.3	This study

Table 2.1. Plasmids

Construct	Relevant Features	Notes	Source or Reference
OL302 pLVX Che-hi3 Rab40c$_{N126I}$	P_{CMV} Rab40c$_{N126I}$		This study
OL303 pLVX Che-hi3 Rab41	P_{CMV} Rab41	NP_001027898.2	This study
OL304 pLVX Che-hi3 Rab41$_{N143I}$	P_{CMV} Rab41$_{N143I}$		This study
OL305 pLVX Che-hi3 Rab42	P_{CMV} Rab42	NP_001180461.1	This study
OL306 pLVX Che-hi3 Rab42$_{H129I}$	P_{CMV} Rab42$_{H129I}$		This study
OL307 pLVX Che-hi3 Rab43	P_{CMV} Rab43	NP_940892.1	This study
OL308 pLVX Che-hi3 Rab43$_{N131I}$	P_{CMV} Rab43$_{N131I}$		This study
Lentiviral shRNA plasmids			
pLKO.1			Dharmacon
pLKO.1 shApoE	shApoE, NM_000041	Clone ID TRCN0000010913	Broad Institute
Retroviral plasmids			
LMNI	IRES-BlastR		(Jouvenet et al., 2009)
pLHCX	HygroR		Clontech
pLNCX2	NeoR		Clontech
pRetroX Tet3G	P_{CMV}-TetON3G	Expresses TetON 3G reverse transactivator	Clontech
pRetroX TRE3G	P_{TRE3G}-MCS	For Dox-inducible expression	Clontech
pRetroX TRE3G-FLuc	P_{TRE3G}-FLuc		Clontech
pRetroX TRE3G-mCherry	P_{TRE3G} mCherry		This study
OR161 pRetroX TRE3G mCherry-Rab1b	P_{TRE3G} mCherry-Rab1b		This study
OR162 pRetroX TRE3G mCherry-Rab1b$_{Q67L}$	P_{TRE3G} mCherry-Rab1b$_{Q67L}$		This study
OR163 pRetroX TRE3G mCherry-Rab1b$_{S22N}$	P_{TRE3G} mCherry-Rab1b$_{S22N}$		This study
OR164 pRetroX TRE3G mCherry-Rab1b$_{N121I}$	P_{TRE3G} mCherry-Rab1b$_{N121I}$		This study
OR366 pRetroX TRE3G mEGFP	P_{TRE3G} mEGFP		This study
OR367 pRetroX TRE3G GFP-DrrA$_{61-647}$	P_{TRE3G} GFP-DrrA$_{61-647}$		This study

Table 2.1. Plasmids

Construct	Relevant Features	Notes	Source or Reference
OR332 pRetroX TRE3G mCherry-Rab11a	P_{TRE3G} mCherry-Rab11a		This study
OR333 pRetroX TRE3G mCherry-Rab11a$_{N124I}$	P_{TRE3G} mCherry-Rab11a$_{N124I}$		This study
OR334 pRetroX TRE3G mCherry-Rab11a$_{Q70L}$	P_{TRE3G} mCherry-Rab11a$_{Q70L}$		This study
OR336 pRetroX TRE3G mCherry-Rab11a$_{S25N}$	P_{TRE3G} mCherry-Rab11a$_{S25N}$		This study
OR337 pRetroX TRE3G mCherry-Rab11b	P_{TRE3G} mCherry-Rab11b		This study
OR338 pRetroX TRE3G mCherry-Rab11b$_{N124I}$	P_{TRE3G} mCherry-Rab11b$_{N124I}$		This study
OR340 pRetroX TRE3G mCherry-Rab11b$_{Q70L}$	P_{TRE3G} mCherry-Rab11b$_{Q70L}$		This study
OR341 pRetroX TRE3G mCherry-Rab11b$_{S25N}$	P_{TRE3G} mCherry-Rab11b$_{S25N}$		This study
OR342 pRetroX TRE3G mCherry-Rab8a	P_{TRE3G} mCherry-Rab8a		This study
OR344 pRetroX TRE3G mCherry-Rab8a$_{N121I}$	P_{TRE3G} mCherry-Rab8a$_{N121I}$		This study
OR345 pRetroX TRE3G mCherry-Rab8a$_{Q67L}$	P_{TRE3G} mCherry-Rab8a$_{Q67L}$		This study
OR346 pRetroX TRE3G mCherry-Rab8a$_{T22N}$	P_{TRE3G} mCherry-Rab8a$_{T22N}$		This study
OR348 pRetroX TRE3G mCherry-Rab8b	P_{TRE3G} mCherry-Rab8b		This study
OR349 pRetroX TRE3G mCherry-Rab8b$_{N121I}$	P_{TRE3G} mCherry-Rab8b$_{N121I}$		This study
OR350 pRetroX TRE3G mCherry-Rab8b$_{Q67L}$	P_{TRE3G} mCherry-Rab8b$_{Q67L}$		This study
OR356 pRetroX TRE3G mCherry-Rab8b$_{T22N}$	P_{TRE3G} mCherry-Rab8b$_{T22N}$		This study

Abbreviations: MLV, murine leukemia virus; HIV-1, human immunodeficiency virus 1; P_{CMV}, cytomegalovirus (CMV) promoter; P_{PGK}, phosphoglycerate kinase (PGK) promoter; P_{TRE3G}, third generation tetracycline response element (TRE) promoter; MCS, multicloning site; SP, signal peptide; FLuc, firefly luciferase; BlastR, blasticidin resistance gene, blasticidin S deaminase, *bsd*; HygroR, hygromycin resistance gene, hygromycin B phosphotransferase, *hph*; NeoR, neomycin/kanamycin resistance gene, neomycin phosphotransferase, *npt*; PuroR, puromycin resistance gene, puromycin *N*-acetyl-transferase, *pac*; ZeoR, zeocin/bleomycin/phleomycin resistance gene, *ble*.

2.2. Modified lentivirus expression vectors

To allow for versatile expression of multiple constructs in the same cell, a palette of lentiviral expression vectors was constructed. The vectors are listed in Table 2.1 and some of their relevant features are depicted in Figure 2.1. These vectors were derived from pLVX Puro, and were engineered to carry antibiotic resistance markers that allowed transduced cells to be selected with one of the following antibiotics: puromycin (P), blasticidin (B), hygromycin (H), neomycin or its substitute, G418, (N) , zeocin (Z) or the fluorescent protein reporter mCherry (Che). The multicloning site (MCS) was also expanded in steps. The name of each vector includes all the relevant information about the vector. For example, in the case of pLVX Phi3: ***pLVX*** signifies that the backbone of the vector was derived from Clontech's ***pLVX*** Puro; ***P*** in ***Phi3*** signifies that the resistance/reporter gene is the ***p***uromycin resistance gene; ***hi*** in ***Phi3*** signifies that gene expression from the MCS is controlled by the ***hi***gh expression cytomegalovirus (CMV) promoter; and, lastly, ***3***, in ***Phi3*** signifies that the ***3***rd generation of expanded MCS can be found in this vector. Since all these vectors contain the same MCS, transfer of genes among them can be easily achieved by a simple "cut/paste" reaction: cutting the insert from the donor vector with suitable restriction enzymes followed by ligation between the same sites in the target vector. Here follow the cloning steps that I used to make these vectors. I thank Brenna Flatley and Rachel Belote for performing some of these steps.

pLVX Phi3. An improved MCS DNA, containing sequences cleaved, in order, by the following restriction endonucleases: 5'-ClaI-BlpI-BclI-AgeI-AfeI-HindIII-BglII-XhoI-EcoRI-NotI-BspEI-MluI-SalI-MfeI-PspOMI-ApaI-NsiI-SphI-AvrII-NgoMIV-NaeI-HpaI-AsiSI-SbFI-BamHI-ClaI-3', was custom synthesized into the pUC57-Amp

vector (Genewiz). The improved MCS was excised as a ~100 base-pair (bp) AfeI/BamHI fragment from pUC57-Amp-MCS and ligated into the AfeI/BamHI backbone of pLVX Puro to form pLVX Phi. A modified pSL1180 cloning vector, named pSL1180.1, was obtained by digesting pSL1180 with AfeI and SmaI followed by re-ligation of the purified vector backbone. The ~1.9 kbp XbaI/KpnI fragment of pLVX Puro was ligated into XbaI/KpnI-cut pSL1180.1. In this vector, the BsiWI site within the PuroR gene was mutated by SDM using primers NT430 and NT431. The mutation is silent. The resulting XbaI/KpnI fragment was reinserted into the XbaI/KpnI sites of pLVX Phi. Primers NT454 and NT455 were annealed to each other and then ligated into the XbaI/BamHI sites of the vector to further improve the MCS.

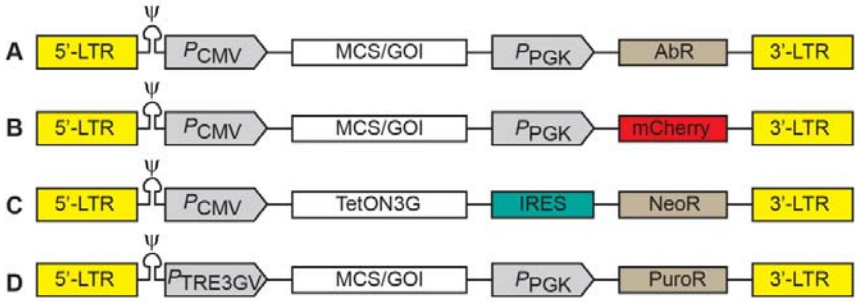

Figure 2.1. Organization of lentiviral and retroviral vectors. (A) pLVX-based vectors expressing an antibiotic selection marker; (B) pLVX Che-hi3 vector expressing an mCherry fluorescent protein reporter in lieu of the antibiotic resistance; (C and D) retroviral vectors used to make inducible expression cell lines. (C) pRetroX Tet3G vector used to generate Huh-7.5 TetON clonal cell lines. It constitutively expresses a TetON3G reverse transactivator. (D) pRetroX TRE3G-based vectors used to transduce the Huh-7.5 TetON clonal cell lines. The TetON3G reverse transactivator binds to the Tetracycline Response Element TRE3G in the presence of doxycycline and induces gene expression. LTR, long terminal repeat; ψ, packaging signal; P_{CMV}, CMV promoter; MCS, multicloning site; GOI, gene of interest; P_{PGK}, phosphoglycerate kinase promoter; AbR, antibiotic resistance marker; IRES, internal ribosome entry site; NeoR, neomycin resistance; P_{TRE3GV}, virus-adapted TRE3G promoter; PuroR, puromycin resistance.

pLVX Bhi3. The PGK promoter sequence of pLVX Puro was amplified using primers NT191 and NT192, then digested with AbsI (Sibenzyme) and XbaI. The woodchuck hepatitis virus posttranscriptional regulatory element (WPRE) sequence was PCR amplified from pLVX Puro using primers NT189 and NT190, then digested with AbsI and KpnI. The Blasticidin resistance gene BlastR was PCR amplified from LMNI using primers NT197 and NT198, then digested with AbsI and XmaI. These three fragments were assembled between the XbaI and KpnI sites of pSL1180.1 to form P_{PGK}-BlastR-WPRE. In this construct, the XhoI site at the 5' end of BlastR was mutated by SDM using primers NT438 and NT439, and the XmaI site at the 3' end of BlastR was mutated by SDM using primers NT440 and NT441. The resulting ~1.7 kilobase-pair (kbp) XbaI/KpnI fragment was ligated into the ~6.3 kbp XbaI/KpnI backbone of pLVX Phi. Primers NT454 and NT455 were annealed to each other and then ligated into the XbaI/BamHI sites of the vector to further improve the MCS.

pLVX Hhi3. The PGK promoter sequence of pLVX Puro was amplified using primers NT191 and NT192, then digested with AbsI (Sibenzyme) and XbaI. The WPRE sequence was PCR amplified from pLVX Puro using primers NT189 and NT190, then digested with AbsI and KpnI. The Hygromycin resistance gene HygroR was PCR amplified from pLHCX using primers NT195 and NT196, then digested with AbsI and XmaI. These three fragments were assembled between the XbaI and KpnI sites of pSL1180.1 to form P_{PGK}-HygroR-WPRE. The EcoRI site within the HygroR gene was mutated by SDM using primers NT432 and NT433. The AsiSI site within the HygroR gene was mutated by SDM using primers NT434 and NT435. The mutations are silent. The XhoI site at the 5' end of the HygroR gene was mutated by SDM using primers

NT442 and NT443. The XmaI site at the 3' end of the HygroR gene of was mutated by SDM using primers NT444 and NT445. The resulting ~2.3 kbp XbaI/KpnI fragment was ligated into the ~6.3 kbp XbaI/KpnI backbone of pLVX Phi. Primers NT454 and NT455 were annealed to each other and then ligated into the XbaI/BamHI sites of the vector to further improve the MCS.

pLVX Nhi3 The PGK promoter sequence of pLVX Puro was amplified using primers NT191 and NT192, then digested with AbsI (Sibenzyme) and XbaI. The WPRE sequence was PCR amplified from pLVX Puro using primers NT189 and NT190, then digested with AbsI and KpnI. The Neomycin resistance gene NeoR was PCR amplified from pLNCX2 using primers NT193 and NT194 and digested with AbsI and XmaI. These three fragments were assembled between the XbaI and KpnI sites of pSL1180.1 to form P_{PGK}-NeoR-WPRE. The XhoI site at the 5' end of the NeoR gene of was mutated by SDM using primers NT446 and NT447. The XmaI site at the 3' end of the NeoR gene was mutated by SDM using primers NT448 and NT449. The resulting ~2.1 kbp XbaI/KpnI fragment was ligated into the ~6.3 kbp XbaI/KpnI backbone of pLVX Phi. Primers NT454 and NT455 were annealed to each other and then ligated into the XbaI/BamHI sites of the vector to further expand the MCS.

pLVX Zhi3. The PGK promoter sequence of pLVX Puro was amplified using primers NT191 and NT192, then digested with AbsI (Sibenzyme) and XbaI. The WPRE sequence was PCR amplified from pLVX Puro using primers NT189 and NT190, then digested with AbsI and KpnI. The Zeocin resistance gene ZeoR of pLenti4/V5-Dest was PCR amplified using primers NT321 and NT322, then digested with AbsI and AgeI. These three fragments were assembled between the XbaI and KpnI sites of pSL1180.1 to

form P_{PGK}-ZeoR-WPRE. The XmaI site within the ZeoR gene was mutated by SDM using primers NT436 and NT437. The mutation is silent. The XhoI site at the 5' end of the ZeoR gene was mutated by SDM using primers NT452 and NT453. The resulting ~1.6 kbp XbaI/KpnI fragment of pSL1180 P_{PGK} -ZeoR-WPRE was ligated into the ~6.3 kbp XbaI/KpnI backbone of pLVX Phi. Primers NT454 and NT455 were annealed to each other and then ligated into the XbaI/BamHI sites of the vector to further expand the MCS.

pLVX Che-hi3. The PGK promoter sequence of pLVX Puro was amplified using primers NT191 and NT192, then digested with AbsI (Sibenzyme) and XbaI. The WPRE sequence was PCR amplified from pLVX Puro using primers NT189 and NT190, then digested with AbsI and KpnI. The two fragments were assembled between the XbaI and KpnI sites of pSL1180.1 to form P_{PGK}-WPRE. Next mCherry was amplified from pmCherry-N1 using primers Inf-For and Inf-Rev and inserted into the XmaI-digested site of the P_{PGK}-WPRE fragment using an InFusion reaction. The ~2.0 kbp XbaI/KpnI resulting fragment was ligated into the ~6.3 kbp XbaI/KpnI backbone of pLVX Phi3.

Table 2.2 DNA oligonucleotide primer sequences

Primer	Nucleotide sequence (5' to 3')
NT117	TATATAGGTACCGCCACCATGGTCAAGGTTCTGTGGGCTGCGTTG
NT189	CCCGGTACCTGAGGTGTGACTGGAAAACCC
NT190	TATATACCTCGAGGCCCGGGTCTGGAACAATCAACCTCTGGATTAC
NT191	TATATACCTCGAGGCAGGTCGAAAGGCCCGGAGATG
NT192	GGGGTCTAGATAATTCTACCGGGTAGGGGAGG
NT193	CACACCTCGAGGATGATTGAACAAGATGGATTGC
NT194	TATACCCGGGTCAGAAGAACTCGTCAAGAAGGCG
NT195	CACACCTCGAGGATGGATAGATCCGGAAAGCC
NT196	TATACCCGGGCTATTCCTTTGCCCTCGGACG
NT197	CACACCTCGAGGATGGCCAAGCCTTTGTCTCAAG
NT198	CACACCCGGGTTAGCCCTCCCACACATAACC
NT321	TATACCTCGAGGATGGCCAAGTTGACCAGTGC
NT322	TATAACCGGTTCAGTCCTGCTCCTCGGCCACG
NT344	TATACGGCCGATGGTGAGCAAGGGCGAGG
NT356	TATATACGCGTGCCACCATGGAAGGGAAGTGGTTGC
NT357	CAGACGGCCGATCATGAGCCTCAACAATAGC
NT358	CGACGCCTAGGCTTGTACAGCTCGTCCATGC

Table 2.2 DNA oligonucleotide primer sequences

Primer	Nucleotide sequence (5' to 3')
NT430	CGACGTCCCCAGGGCAGTACGCACCCTCGCC
NT431	GGCGAGGGTGCGTACTGCCCTGGGGACGTCG
NT432	CTTGACATTGGGGAATTTAGCGAGAGCCTGACC
NT433	GGTCAGGCTCTCGCTAAATTCCCCAATGTCAAG
NT434	GGAGGCCATGGATGCAATCGCTGCGGCCGATC
NT435	GATCGGCCGCAGCGATTGCATCCATGGCCTCC
NT436	GCTCGGGTTCTCCCGAGACTTCGTGGAGGAC
NT437	GTCCTCCACGAAGTCTCGGGAGAACCCGAGC
NT438	GGCCTTTCGACCTGCATCGAGGATGGCCAAG
NT439	CTTGGCCATCCTCGATGCAGGTCGAAAGGCC
NT440	GTGGGAGGGCTAACCCAGGTCTGGAACAATCAACC
NT441	GGTTGATTGTTCCAGACCTGGGTTAGCCCTCCCAC
NT442	GGCCTTTCGACCTGCATCGAGGATGGATAGATC
NT443	GATCTATCCATCCTCGATGCAGGTCGAAAGGCC
NT444	GGCAAAGGAATAGCCTGGGTCTGGAACAATC
NT445	GATTGTTCCAGACCCAGGCTATTCCTTTGCC
NT446	GGCCTTTCGACCTGCATCGAGGATGATTGAAC
NT447	GTTCAATCATCCTCGATGCAGGTCGAAAGGCC
NT448	CGAGTTCTTCTGACCCAGGTCTGGAACAATCAACC
NT449	GGTTGATTGTTCCAGACCTGGGTCAGAAGAACTCG
NT452	CCTTTCGACCTGCCTTGAGGATGGCCAAGTTGACC
NT453	GGTCAACTTGGCCATCCTCAAGGCAGGTCGAAAGG
NT454	GATCCGGCGCGCCCGGGTTCGAATGTACACGTACGTTAATTAAT
NT455	CTAGATTAATTAACGTACGTGTACATTCGAACCCGGGCGCGCCG
NT458	TATACCTAGGTCAGGTGGAGGATCTATGATGGCGAAGACGTACGATTATC
NT459	GATGGATCCTCATCAAAGTAGCGAGCAACGAAAGAAACTGG
NT461	CGACGAGGATCCTCAGCAACACTGGGATTTGTTCTCTGC
NT463	CGAGGATCCTTAGCACCAGCACGTCATTGC
NT465	TATAGGATCCTCAACAGCAGCCGCCCCCAGC
NT466	TATACCTAGGTCAGGTGGAGGATCTATGGCGCAGCCCATCCTGG
NT467	GGCGGAGAATTCGGATCCTCAACAAGGACAGGAAGTTTTACTG
NT468	GAACCTAGGTCAGGTGGAGGATCTATGTTGGAGGAAGATATGG
NT469	CGATGTCGACGGATCCTTAGGGTATGCTACAGCTGC
NT471	CACAGGATCCTCAACAGCCACATGCCCCTTTC
NT472	CACACCTAGGTCAGGTGGAGGATCTATGAACCCCGAATATGACTACC
NT473	TATAGGATCCCTAGCAACAGCCACCGCCAGC
NT475	CACAGGATCCTCAGTTGCTGCAGCACTGGCTCC
NT477	GAGAGGATCCTCAGCCCAGGGAGCACTTGTTGG
NT478	TATACCTAGGTCAGGTGGAGGATCTATGGGGACCCGGGACGACG
NT479	CACAGGATCCTCACAGGTTCTGGCAGCACTGC
NT481	GGAGAGGATCCTCAGTTGCTACAACACTGGCTCTTG
NT483	CCGGTGGATCCTTAGTTACTACAACACTGATTCCTGG
NT484	TATACCTAGGTCAGGTGGAGGATCTATGGGTACCCGCGACGACGAGTACG
NT485	CCGGTGGATCCTTAGATGTTCTGACAGCACTGCACC
NT487	GAGAGGATCCTTAGCAGCAACCTCCACCTGAC
NT489	GAGAGGATCCTCAGCAGCAGCCAGAGTTGG
NT491	GAGAGGATCCTCAGAGGCTGATGCAACAGG
NT493	TATAGGATCCTCAACAGCACCGGCGGCTGG
NT495	GAGAGGATCCCTAGCAGATACATTTCTTCTCTGGTGGC
NT514	CCAACCTCAAAATGTGGATTCAAGAATGCAATGGGCATGC
NT515	GCATGCCCATTGCATTCTTGAATCCACATTTTGAGGTTGG
NT516	CTCAAACAACAAATAGCTGAAGATCCAGAACTAACGCATTCAAG
NT517	CTTGAATGCGTTAGTTCTGGATCTTCAGCTATTTGTTGTTTGAG

Table 2.2 DNA oligonucleotide primer sequences

Primer	Nucleotide sequence (5' to 3')
NT567	TATAGGATCCCTAGCAGCTGCAGCTGCTGGG
NT628	TATAACGCGTGCCACCATGGTCAAGGTTCTGTG
NT635	TATACCTAGGGGAGGAGGTAAGGTGGAGCAAGCGGTGG
NT636	GAGAGGATCCTATTAGTGATTGTCGCTGGGCACAGGG
NT637	ATAGGATCCGCGTGATTGTCGCTGGGCACAGG
NT644	GTGGTATGGCTGATTATGATCTAGAGTCGCGGC
NT653	GGGACACAGCGGGCCTGGAACGGTTCCGGACC
NT654	GGTCCGGAACCGTTCCAGGCCCGCTGTGTCCC
NT667	GGGACACAGCGGGTCTTGAAAGATTCCGAACAATCACG
NT668	CGTGATTGTTCGGAATCTTTCAAGACCCGCTGTGTCCC
NT669	GCACAGATATGGGACACAGCAGGGCTGGAGCGATATCGAGCTATAACATCAGC
NT670	GCTGATGTTATAGCTCGATATCGCTCCAGCCCTGCTGTGTCCCATATCTGTGC
NT671	GCAGATCTGGGACACCGCTGGCCTGGAGCGCTACCGCGCCATCACC
NT672	GGTGATGGCGCGGTAGCGCTCCAGGCCAGCGGTGTCCCAGATCTGC
NT693	TATATACGCGTTGCCACCATGGTGAGCAAGGGCGAGG
NT698	GTCAACAAATTGTTGGTAGGGATTAAATGTGATCTGACCACAAAGAAAG
NT699	CTTTCTTTGTGGTCAGATCACATTTAATCCCTACCAACAATTTGTTGAC
NT700	CGACTCAGGCGTGGGCAAGAACTGCCTGCTCCTGCGGTTTGCTG
NT701	CAGCAAACCGCAGGAGCAGGCAGTTCTTGCCCACGCCTGAGTCG
NT702	CGTCAATAAGCTCCTGGTGGGCATTAAGAGCGACCTCACCACCAAGAAGG
NT703	CCTTCTTGGTGGTGAGGTCGCTCTTAATGCCCACCAGGAGCTTATTGACG
NT729	CGAAGGATCCGCCACCATGGTGAGCAAGGGCG
NT731	TATAGCGGCCGCCTAGCAACAGCCACCGCCAGCCG
NT755	TAGCTTTATCGGGAATTAAGGCCGACCTAGCA
NT756	TGCTAGGTCGGCCTTAATTCCCGATAAAGCTA
NT775	TATACGCGTGCCACCATGGAAGACGCCAAAAACATAAAGAAAGG
NT776	GCGCGGATCCTTACAATTTGGACTTTCCGCCCTTC
NT781	TATACGCGTGCCACCATGTCCAGCATGAATCCCGAATATG
NT782	TATACGCGTGCCACCATGAACCCCGAATATGACTACC
NT783	TATACGCGTGCCACCATGGCCCGGGACTACGACC
NT784	GCGGGATCCTAGCAGCAGCGTTTCTTTCGTTTACTG
NT785	TATACGCGTGCCACCATGGCGTACGCCTATCTCTTCAAG
NT786	TATACGCGTGCCACCATGGCATCCGCCACAGACTCG
NT787	TATGGATCCTTAGCAGGCGCAGTCCTGGTGCGG
NT788	GACGAATTCGCCACCATGGCTTCAGTGACAGATGG
NT789	TATGGATCCTAGCATGAGCAGTTCTGCTGCAGC
NT790	TATACGCGTGCCACCATGAGACACGAAGCGCCCATGC
NT791	TATGGATCCTTAGCAGGCACAGTTGGGCTGCGGTGG
NT792	TATACGCGTGCCACCATGGCATCAGCTGGAGACACC
NT793	TATACGCGTGCCACCATGTCGCAGACGGCCATGTCC
NT794	GAGAGGATCCTTAACAACCACACTCCTGAGCGTTCG
NT795	TATACGCGTGCCACCATGGCTAGTCGAGGCGCAACAAG
NT796	TATACGCGTGCCACCATGTCCACGGGCGGAGACTTCG
NT797	GAGAGGATCCTTAGCAGAACAGCCTCCTTCACTGAC
NT798	TATACGCGTGCCACCATGAATCCCCGGAAGAAGG
NT799	TATGGATCCTAGCAGCATCTGCTCCTTGACTGG
NT800	TATACGCGTGCCACCATGGCGAAGACCTACGATTACC
NT801	GAGAGGATCCTACAGAAGAACACATCGGAAAAAGCTGC
NT802	TATACGCGTGCCACCATGATGGCGAAGACGTACGATTATCTC
NT803	TATACGCGTGCCACCATGGCAGGAAAATCATCAC
NT804	GAGAGGATCCTAACAGCAAGATGAGCTAGGC
NT805	TATACGCGTGCCACCATGGCGAAGAAGACGTACGACC
NT806	GGAGGATCCTAGCAGCATTTGCTCTTCCAGCC

Table 2.2 DNA oligonucleotide primer sequences

Primer	Nucleotide sequence (5' to 3')
NT807	TATACGCGTGCCACCATGGGTACCCGCGACGACG
NT808	TATACGCGTGCCACCATGGGGACCCGGGACGACGAG
NT809	TATACGCGTGCCACCATGGGGAATGGAACTGAGGAAG
NT810	TATACGCGTGCCACCATGGCCAAAGCCTACGACCACC
NT811	TATACGCGTGCCACCATGGCAACTGCACCATACAAC
NT812	TATGGATCCTAGCAGCCACAGCCTTCTCTCTGGGGTTGGGG
NT813	TATACGCGTGCCACCATGGACGAGGACGTGCTAACC
NT814	GCGGGATCCTATAACACAGAGCAATAACCACCACAG
NT815	TATACGCGTGCCACCATGCACTTCTCGAGCTCAGCC
NT816	GAGAGGATCCTAGCAAGTGCAGTGGGTCTTTTCAC
NT817	TATACGCGTGCCACCATGATGGCGATACGGGAGCTC
NT818	TATACGCGTGCCACCATGTTGGAGGAAGATATGGAAG
NT819	TATACGCGTGCCACCATGTCCAGGAAGAAGACCCCCAAG
NT820	TATGGATCCTAAGGGCGGCAGCAGGAGGCCC
NT821	TATACGCGTGCCACCATGTCTGATGGAGATTATGATTACC
NT822	TATACGCGTGCCACCATGACCGATGGAGACTATGATTATCTG
NT823	TATATACGCGTGCCACCATGGCGGGCGGAGGAGCC
NT824	TATACGCGTGCCACCATGGCGCAGCCCATCCTGG
NT825	TATACGCGTGCCACCATGGAGACCATCTGGATCTACC
NT826	GAGAGGATCCTAGCAGAAGCATTCTTTCCTGGGC
NT827	TATATTACGCGTGCCACCATGAGCGCCCCGGGCAGCC
NT828	CGCGCGGATCCTAAGAAATTTTGCAGCTGTTTCTGGTGCAG
NT829	TATAGAATTCGCCACCATGGATCCGGGCGCCGCGC
NT830	GAGCCTAGGCTAACAGCATCGGACATGTGGTCTTGG
NT832	GCCGAATATTAGTGGGTATAAAGAATGACGACCCTGAGC
NT833	GCTCAGGGTCGTCATTCTTTATACCCACTAATATTCGGC
NT834	GGTCATTATGCTTATTGGAATAAAAAGTGATTTAGAATCTAGAAG
NT835	CTTCTAGATTCTAAATCACTTTTTATTCCAATAAGCATAATGACC
NT836	GGTGCTGCTGGTAGGAATTAAGTGTGACATGGAGG
NT837	CCTCCATGTCACACTTAATTCCTACCAGCAGCACC
NT838	GCACAAGTTATTCTGGTGGGGATTAAGTGTGACATGGAGG
NT839	CCTCCATGTCACACTTAATCCCCACCAGAATAACTTGTGC
NT840	CCAAGTTATTCTGGTTGGGATTAAGTGTGACATGGAAGACG
NT841	CGTCTTCCATGTCACACTTAATCCCAACCAGAATAACTTGG
NT842	GGTCATCCTGGTGGGGATTAAGTGTGACCTGGAGG
NT843	CCTCCAGGTCACACTTAATCCCCACCAGGATGACC
NT844	GTGATCATCCTTTGTGGAATTAAGAAGGACCTGGATGC
NT845	GCATCCAGGTCCTTCTTAATTCCACAAAGGATGATCAC
NT846	CATCATGCTAGTAGGAATCAAAACAGATCTTGCTGACAAG
NT847	CTTGTCAGCAAGATCTGTTTTGATTCCTACTAGCATGATG
NT848	CCATGGTGTTGTTGGGGATTAAGATCGATCTGGCAGACC
NT849	GGTCTGCCAGATCGATCTTAATCCCCAACAACACCATGG
NT850	CGAAAAGATGATACTCGGGATTAAGTGTGATGTGAATGACAAG
NT851	CTTGTCATTCACATCACACTTAATCCCGAGTATCATCTTTTCG
NT852	CGAAAGAATGATCCTGGGTATTAAATGTGATATGAATGAC
NT853	GTCATTCATATCACATTTAATACCCAGGATCATTCTTTCG
NT854	CCTTTTGTGATTCTGGGTATTAAGATTGACATAAGCGAACG
NT855	CGTTCGCTTATGTCAATCTTAATACCCAGAATCACAAAAGG
NT856	GGAAAGAATGTTACTAGGAATTAAGTGTGATATGGACGAC
NT857	GTCGTCCATATCACACTTAATTCCTAGTAACATTCTTTCC
NT858	GTTATCATGCTTGTGGGCATCAAGAGTGATCTACGTCATC
NT859	GATGACGTAGATCACTCTTGATGCCCACAAGCATGATAAC
NT860	CGTCATCATGCTGGTGGGCATTAAGAGTGACCTGCGCCACC

Table 2.2 DNA oligonucleotide primer sequences

Primer	Nucleotide sequence (5' to 3')
NT861	GGTGGCGCAGGTCACTCTTAATGCCCACCAGCATGATGACG
NT862	CGTCGTCATGCTCGTGGGTATTAAAAGTGACCTCAGCCAGG
NT863	CCTGGCTGAGGTCACTTTTAATACCCACGAGCATGACGACG
NT866	GAGCTTCTCTTAGTTGGAATCAAGTTGGACTGTGAAACGG
NT867	CCGTTTCACAGTCCAACTTGATTCCAACTAAGAGAAGCTC
NT868	CGCCTCTTGCTGGGGATTAAATGTGACATGGAGG
NT869	CCTCCATGTCACATTTAATCCCCAGCAAGAGGCG
NT870	CTGTAATAATTCTCATAGGAATCAAAGCAGATTTGGAGGCAC
NT871	GTGCCTCCAAATCTGCTTTGATTCCTATGAGAATTATTACAG
NT872	GACATAGTAAACATGCTAGTTGGAATCAAAATCGATAAGGAAAATCGTG
NT873	CACGATTTTCCTTATCGATTTTGATTCCAACTAGCATGTTTACTATGTC
NT874	GGTCATTATGCTGATTGGAATCAAATGTGACCTCTGGG
NT875	CCCAGAGGTCACATTTGATTCCAATCAGCATAATGACC
NT876	GTAATGGCCATCGCTGGAATTAAGTGCGACCTCTCAG
NT877	CTGAGAGGTCGCACTTAATTCCAGCGATGGCCATTAC
NT878	CCAACTGTACTTGTGCAAATTAAGATTGATCTTCTGG
NT879	CCAGAAGATCAATCTTAATTTGCACAAGTACAGTTGG
NT880	GCTCATGCTGCTGGGGATTAAGGTGGACTCTGCCC
NT881	GGGCAGAGTCCACCTTAATCCCCAGCAGCATGAGC
NT882	CCAGATATAGTGCTGTGTGGAATTAAGAGTGATCTGGAGG
NT883	CCTCCAGATCACTCTTAATTCCACACAGCACTATATCTGG
NT884	CCAGATATAGTATTAATTGGCATTAAGGCAGACCTACCAG
NT885	CTGGTAGGTCTGCCTTAATGCCAATTAATACTATATCTGG
NT886	CCTGCTGTCCTCTTGGCTATTAAATGTGACCAGAACAAGG
NT887	CCTTGTTCTGGTCACATTTAATAGCCAAGAGGACAGCAGG
NT888	CCAAAGTGCTTGTGGGCATTAAGTGTGACTTGAGGG
NT889	CCCTCAAGTCACACTTAATGCCCACAAGCACTTTGG
NT890	GGATTGTATTTCTGCTAGTGGGAATAAAATGTGATTTAGCTTCACAACG
NT891	CGTTGTGAAGCTAAATCACATTTTATTCCCACTAGCAGAAATACAATCC
NT892	CCCTAAAATCCTGGTGGGGATACGCCTACATCTGGCATTC
NT893	GAATGCCAGATGTAGGCGTATCCCCACCAGGATTTTAGGG
NT894	GCTCAGCCAGGGCAGCAGATGAGAACTTTGACTATTTGTTCAAG
NT895	CTTGAACAAATAGTCAAAGTTCTCATCTGCTGCCCTGGCTGAGC
NT899	GAGACGCGTGCCACCATGACTTATGCTTATCTCTTCAAG
NT900	TATACGCGTGCCACCATGACTAGCAGAAGCACAGCTAGG
NT901	ATATACGCGTGCCACCATGGCGGGTCGGGGAGGC
NT902	TATACGCGTGCCACCATGGCTGAGGAGATGGAGTCG
NT903	TATGAATTCGCCACCATGGCTGAGACCTACGACTTCC
NT904	TATCCTAGGTTAGCAGCCACACGGCTGAGGGG
NT905	TATACGCGTGCCACCATGTCCGCAGGGGGAGATTTTGG
NT906	TATGGATCCTAGCAGGAGCAGCCGCCCTCG
NT907	TATACGCGTGCCACCATGTCCGCGGGCGGAGACTTCG
NT908	GACGGATCCTACCTCCACGAGACAGGCAGC
NT909	TATACGCGTGCCACCATGACCTCTAGGAAGAAAGTGTTGCT
NT910	TATGGATCCTCAGCAACTGCAGCTTTCTGCCGAGG
NT911	TATACGCGTGCCACCATGAGTGGGAAATCCCTGCTC
NT912	TATGGATCCTAACAGCACGAAGACCCTGCTTTGG
NT913	TATGAATTCGCCACCATGGCGAAGCAGTACGATGTGC
NT914	CGCGGATCCTAGACGCGTGAATGACTCTTTAATG
NT915	TATACGCGTGCCACCATGGCACAGGCACACAGGACC
NT916	GAAGGATCCTAGTGGGCGCAGCATTTGGCCTGC
NT917	TATACGCGTGCCACCATGAGGAAGCCCGACAGCAAG
NT918	CGCGGATCCTAGGCACAACACCCAGATCTGG

Table 2.2 DNA oligonucleotide primer sequences

Primer	Nucleotide sequence (5' to 3')
NT919	TATACGCGTGCCACCATGGCTGCGGCCGGCGG
NT920	GCGCCGGATCCTTATCCAGAAGAACAGCACCCTCC
NT921	TATACGCGTGCCACCATGGCGCTGAGGGAGCTCAAAGTG
NT922	TATGGATCCTCAGCAGCAGCTCCGCTTTGGCTCTG
NT923	TATACGCGTGCCACCATGAGCGGGCAGCGCGTGGACG
NT924	GCGCCGGATCCTCAGTGATGACAACAGCTGTAGAAGTAGG
NT927	TATACGCGTGCCACCATGGGCAGCCGCGACCACC
NT928	GACGGATCCTAGCAGCAGGACCAGCTGGAGGAC
NT929	TATACGCGTGCCACCATGAGTATGGAAGATTATGATTTCC
NT930	GACGGATCCTAGTTGAAATTACAACAAGTCAAATAGC
NT931	TATACGCGTGCCACCATGAACATTCTGGCACCCGTGC
NT932	GACGGATCCTATGGGCAACATGTGGGCTTCTTC
NT933	TATACGCGTGCCACCATGGTGATCGCCGGTGCAAGC
NT934	TATGGATCCTTAGCAGCAGCCCAGGCTGGAGGG
NT935	TATACGCGTGCCACCATGACGGGCACGCCAGGCG
NT936	CACGGATCCTACATGAAGGAGCAGCAGCTGGAGC
NT937	TATACGCGTGCCACCATGCAGGCCCCGCACAAGGAGC
NT938	CGCCGGATCCCTAGGATTTGGCACAGCCAGAGC
NT939	TATACGCGTGCCACCATGGAGGCCATCTGGCTGTACC
NT940	GCCGGATCCTAGCACAAACATCTCCTCTCTG
NT941	TATACGCGTGCCACCATGAGCGCCCCGGGCAGCC
NT942	CGCCGGATCCTAAGAAATTTTGCAGCTGTTTCTGGTGC
NT943	TATACGCGTGCCACCATGAGCGCCCTGGGCAGCCC
NT944	CGCCGGATCCTAAGAAATTTTGCAGCTGTTTCTGGTGC
NT945	TAAGAATTCGCCACCATGGGCTCGCAGGGCAGTCC
NT946	GCCCCTAGGCTAGGAGATCTTGCAGTTACTCC
NT947	TATACGCGTGCCACCATGTCTGCCTTTGGTCACGACG
NT948	CGCCGGATCCTAACAATAGCTTCTGTTGCCTGAC
NT951	TATACGCGTGCCACCATGGCAGGGCCGGGCCCAGG
NT952	GACGGATCCTAGCACCCGCAGCCCCAGCCTTCTCC
NT960	CGTGTGGCTTCTGCCCTTCTTTCCACAAGGACTTCACCTCCACC
NT961	GGTGGAGGTGAAGTCCTTGTGGAAAGAAGGGCAGAAGCCACACG
NT964	GTTACGTTTATTGAAACTAGGGCAAAAGCTGGATACAATGTAAAGCAGC
NT965	GCTGCTTTACATTGTATCCAGCTTTTGCCCTAGTTTCAATAAACGTAAC
NT966	GGATGGCGCGGCCGAGTCCCCGTACGGCCACCCGGCGG
NT967	CCGCCGGGTGGCCGTACGGGGACTCGGCCGCGCCATCC
NT968	GCTGGACGGCCGGCGCGTGAAGCTGGAGCTCTGGGACACG
NT969	CGTGTCCCAGAGCTCCAGCTTCACGCGCCGGCCGTCCAGC
NT972	GGAGATTCTGGTGTTGGAAAGAATAATCTCCTGTCTCGATTTACTCG
NT973	CGAGTAAATCGAGACAGGAGATTATTCTTTCCAACACCAGAATCTCC
NT974	GGACTCAGGCGTGGGCAAGAACAACCTGCTGTCGCGCTTCACC
NT975	GGTGAAGCGCGACAGCAGGTTGTTCTTGCCCACGCCTGAGTCC
NT978	GCAGATATGGGACACAGCCGGTCTGGAACGGTTTCGGACGATC
NT979	GATCGTCCGAAACCGTTCCAGACCGGCTGTGTCCCATATCTGC
NT980	CTCGGGGGTGGGGAAGAACTGTGTCCTGTTCCGC
NT981	GCGGAACAGGACACAGTTCTTCCCCACCCCCGAG
NT982	CTCGGGGGTAGGCAAGAACTGCCTCCTGTTCCGCTTCTC
NT983	GAGAAGCGGAACAGGAGGCAGTTCTTGCCTACCCCCGAG
NT991	TATCCTAGGTCAGGTGGAGGATCTATGGCGAAGACCTACGATTACC
NT996	GGTTATCATGCTCATTGGGATTAAGAGTGACCTAGAGTCCC
NT997	GGGACTCTAGGTCACTCTTAATCCCAATGAGCATGATAACC
NT998	GGTCATCCTCTGTGGCATCAAGAAGGACCTGGACC
NT999	GGTCCAGGTCCTTCTTGATGCCACAGAGGATGACC

Table 2.2 DNA oligonucleotide primer sequences

Primer	Nucleotide sequence (5' to 3')
NT1000	CGTTATTGCCCTGGCAGGGATCAAAGCTGACCTGGCCAAC
NT1001	GTTGGCCAGGTCAGCTTTGATCCCTGCCAGGGCAATAACG
NT1002	CGTCATTGCACTCGCGGGTATCAAGGCAGACCTGGCCAGC
NT1003	GCTGGCCAGGTCTGCCTTGATACCCGCGAGTGCAATGACG
NT1004	CATCATGCTGGTGGGCATCAAGACGGACCTGGCTG
NT1005	CAGCCAGGTCCGTCTTGATGCCCACCAGCATGATG
NT1006	GTTATCATCACGCTAGTAGGAATTAGAACAGATCTTGCTGAC
NT1007	GTCAGCAAGATCTGTTCTAATTCCTACTAGCGTGATGATAAC
NT1008	CCCATTTGTTGTGTTGGGAATCAAGATTGACCTCGAAAACAG
NT1009	CTGTTTTCGAGGTCAATCTTGATTCCCAACACAACAAATGGG
NT1010	CCTTTGTAGTTCTGGGTATCAAGGTAGACAAAGAGG
NT1011	CCTCTTTGTCTACCTTGATACCCAGAACTACAAAGG
NT1012	CCGGGGTGGGCAAGAACTGCCTGCTGTGCCGC
NT1013	GCGGCACAGCAGGCAGTTCTTGCCCACCCCGG
NT1014	CCTGGTGATGCTGGTGGGCATCAAGACGGACCTCAGCCAGG
NT1015	CCTGGCTGAGGTCCGTCTTGATGCCCACCAGCATCACCAGG
NT1016	CTTCGCCATCGTGGGGATCAAAGTGGACCTCACTG
NT1017	CAGTGAGGTCCACTTTGATCCCCACGATGGCGAAG
NT1018	CTGTTTATGTATAGTTGGTATTAAAATAGACTTGGAAAAGG
NT1019	CCTTTTCCAAGTCTATTTTAATACCAACTATACATAAACAG
NT1020	GTAGTTGCCATTGCAGGAATTAAATGTGATCTTATCGATG
NT1021	CATCGATAAGATCACATTTAATTCCTGCAATGGCAACTAC
NT1022	CCAAATCTACTTATGTGGCATCAAGAGTGACCTGCTGGAAG
NT1023	CTTCCAGCAGGTCACTCTTGATGCCACATAAGTAGATTTGG
NT1024	CTGGTTGCCTTGGTAGGCATTAAAATTGATTTGGAGCATATGC
NT1025	GCATATGCTCCAAATCAATTTTAATGCCTACCAAGGCAACCAG
NT1026	CCTGCCTGCTCTTGGCCATCAAGTGTGATCTGTCCCC
NT1027	GGGGACAGATCACACTTGATGGCCAAGAGCAGGCAGG
NT1028	CACTGTGTTAGTGGGCATCAAGATTGACCTGGCTG
NT1029	CAGCCAGGTCAATCTTGATGCCCACTAACACAGTG
NT1030	CCACGGATTCTTGTTGGAATTAAATGTGACTTGAGAAGTGC
NT1031	GCACTTCTCAAGTCACATTTAATTCCAACAAGAATCCGTGG
NT1032	GCTTCTCTTCCTTGTAGGTATCAAGAAGGATCTGAGTACC
NT1033	GGTACTCAGATCCTTCTTGATACCTACAAGGAAGAGAAGC
NT1034	CATCTTCCTCGTGGGAATCAAGAAGGACCTTCTGTC
NT1035	GACAGAAGGTCCTTCTTGATTCCCACGAGGAAGATG
NT1036	GGTGATCATGCTGCTAGGCATCAAGGCGGATATGAGCAGC
NT1037	GCTGCTCATATCCGCCTTGATGCCTAGCAGCATGATCACC
NT1038	CAGTGGTTTTGTTGGCCATCAAATGTGACCAGGGG
NT1039	CCCCTGGTCACATTTGATGGCCAACAAAACCACTG
NT1040	GTATTTGTTCTGGTGGGTATCAAGTGTGACCTGGATACAC
NT1041	GTGTATCCAGGTCACACTTGATACCCACCAGAACAAATAC
NT1042	CCTAAAATCCTGGTGGGGATTCGCCTACATCTGGCATTC
NT1043	GAATGCCAGATGTAGGCGAATCCCCACCAGGATTTTAGG
NT1044	CCAAGATCCTGGTGGGGATTCGCCTGCACCTGGCGTTC
NT1045	GAACGCCAGGTGCAGGCGAATCCCCACCAGGATCTTGG
NT1046	CCGGATCTTGGTTGGAATCCGGCTGCACCTGGCC
NT1047	GGCCAGGTGCAGCCGGATTCCAACCAAGATCCGG
NT1048	GTCATCATGTTGTTGGGTATCAAGATTGATTTGGATAAC
NT1049	GTTATCCAAATCAATCTTGATACCCAACAACATGATGAC
NT1050	CATCTTCCTGCTGGTTGGCATCAAGAGTGACCTGCAGAGC
NT1051	GCTCTGCAGGTCACTCTTGATGCCAACCAGCAGGAAGATG
NT1052	GTGCAGCTGCTGATCGGGATCAAGTCAGACCTCAGCGAGC

Table 2.2 DNA oligonucleotide primer sequences

Primer	Nucleotide sequence (5' to 3')
NT1053	GCTCGCTGAGGTCTGACTTGATCCCGATCAGCAGCTGCAC
NT1054	GCATCAACAGTGATGACAGCAACCTCTACCTAACTGC
NT1055	GCAGTTAGGTAGAGGTTGCTGTCATCACTGTTGATGC
NT1069	GCGCGAATTCTTATTTTATCTTAATGGTTTGTCTTTCTTG
NT1123	TATAGCGGCCGCTAGATGTTCTGACAGCACTGCACC
NT1124	TATAGCGGCCGCTACAGGTTCTGGCAGCACTGCAGC
NT1125	TATAGCGGCCGCTACAGAAGAACACATCGGAAAAAGC
NT1126	TATAGCGGCCGCTAAAGTAGCGAGCAACGAAAGAAACTGG
Inf-For	TGCCTCGAGGCCCGGGCCACCATGGTGAGC
Inf-Rev	TTGTTCCAGACCCGGTTACTTGTACAGCTC

2.3. Lentiviral constructs for constitutive expression

I wish to acknowledge the help that I received in making some of these constructs, primarily from Caroline Gleason, but also from Colin Belanger. Some of the lentiviral vectors listed below and in Table 2.1 were given an identifier starting with the letters "OL". These two letters stand for "**O**rganelle **L**entivirus" and signify that these vectors need to be packaged into lentiviral particles using a human immunodeficiency virus 1 (HIV-1)-based packaging system.

pLVX Phi3 FLuc and **pLVX Bhi3 FLuc** The firefly *(Photinus pyralis)* luciferin 4-monooxygenase (FLuc) was amplified using primers NT775 and NT776 from pRetroX TRE3G-Luc, digested with MluI and BamHI and ligated into the MluI/BamHI sites of pLVX Phi3 or pLVX Bhi3, respectively.

pLVX Phi3 mCherry. The ~0.7 kbp EcoRI/NotI fragment from pmCherry-N1 was ligated into the EcoRI/NotI sites of pLVX Phi3.

OL135 pLVX Phi3 mCherry-Rab1b. Rab1b cDNA was amplified from pCMV-SPORT6 Rab1b using primers NT472 and NT473 and digested with AvrII and BamHI; mCherry was amplified from pmCherry-N1 using primers NT358 and NT693 and digested with MluI and AvrII). The fragments were assembled within the MluI/BamHI

sites of pLVX Phi3. **OL115 pLVX Phi3 mCherry-Rab1b$_{Q67L}$.** Primers NT653 and NT654 were used to introduce the Q67L mutation into the Rab1b sequence by SDM. **OL142 pLVX Phi3 mCherry-Rab1b$_{S22N}$.** Primers NT700 and NT701 were used to introduce the S22N mutation into the Rab1b sequence by SDM. **OL143 pLVX Phi3 mCherry-Rab1b$_{N121I}$.** Primers NT702 and NT703 were used to introduce the N121I mutation into the Rab1b sequence by SDM.

pLVX Hhi3 ApoE3. A DNA sequence encoding an shRNA-resistant version of ApoE3 was chemically synthesized, PCR-amplified using NT628 and NT636, digested with MluI and BamHI and inserted into the MluI/BamHI sites of pLVX Hhi3. The silent mutations present in this ApoE3 cDNA created a mismatch with the shRNA sequence encoded by pLKO.1 shApoE (Clone ID TRCN0000010913, Broad Institute's Genetic Perturbation Platform).

pLVX Hhi3 ApoE3-mEGFP. ApoE3 (shRNAres) was amplified with NT117 and NT637, digested with KpnI and BamHI and inserted into the KpnI/BamHI sites of pmEGFP-N1. ApoE3-mEGFP was then amplified using NT628 and NT644, digested with MluI and XbaI and cloned into the MluI/XbaI sites of pLVX Hhi3.

pLVX Phi3 mEGFP-ApoE3. The following fragments were assembled into the cloning vector pSL1180: a sequence encoding amino acids 1-22 of calnexin (its signal peptide) was amplified using NT356 and NT357 from pCMV6-XL5 Calnexin and digested with MluI and EagI; mEGFP (monomeric enhanced green fluorescent protein) was amplified from pmEGFP-N1 using primers NT344 and NT358 and digested with EagI and AvrII; mature ApoE3 coding sequence (amino acids 1 through 299) was amplified with NT635 and NT636 and digested with AvrII and BamHI. The resulting

signal peptide-mEGFP-ApoE3 was excised using MluI and BamHI and inserted into the MluI/BamHI sites of pLVX Phi3.

OL175 pLVX Che-hi3 Rab1a. Rab1a sequence (obtained from pCMV-Sport6 Rab1a) was PCR amplified using primers NT487 and NT781, digested with MluI and BamHI and cloned into the MluI/BamHI sites of pLVX Che-hi3. **OL 176 pLVX Che-hi3 Rab1a$_{N124I}$.** SDM was performed on OL175 using primers NT698 and NT699.

OL177 pLVX Che-hi3 Rab1b. Rab1b was amplified from OL135 using primers NT473 and NT782, digested with MluI and BamHI and ligated into the MluI/BamHI sites of pLVX Che-hi3. **OL178 pLVX Che-hi3 Rab1b$_{N121I}$.** Rab1b$_{N121I}$ was amplified from OL143 using primers NT473 and NT782, digested with MluI and BamHI and ligated into the MluI/BamHI sites of pLVX Che-hi3. **OL249 pLVX Che-hi3 Rab1b$_{Q67L}$.** Rab1b$_{Q67L}$ was amplified from OL115 using primers NT473 and NT782, digested with MluI and BamHI and ligated into the MluI/BamHI sites of pLVX Che-hi3. **OL250 pLVX Che-hi3 Rab1b$_{S22N}$.** Rab1b$_{S22N}$ was amplified from OL142 using primers NT473 and NT782, digested with MluI and BamHI and ligated into the MluI/BamHI sites of pLVX Che-hi3.

OL179 pLVX Che-hi3 Rab1c/35. Rab1c sequence was PCR amplified from pCMV-Sport6/Rab1c/35 using primers NT783 and NT784, digested with MluI and BamHI and cloned into the MluI/BamHI sites of pLVX Che-hi3. **OL180 pLVX Che-hi3 Rab1c/35$_{N120I}$.** SDM was performed on OL179 using primers NT832 and NT833.

OL181 pLVX Che-hi3 Rab2A. Rab2a sequence (obtained from pOTB7-Rab2a) was PCR amplified using primers NT465 and NT785, digested with MluI and BamHI

and cloned into the MluI/BamHI sites of pLVX Che-hi3. **OL182 pLVX Che-hi3 Rab2a$_{N119I}$.** SDM was performed on OL181 using primers NT834 and NT835.

OL183 pLVX Che-hi3 Rab3a. Rab3a sequence was PCR amplified from pLX304 Rab3a using primers NT786 and NT787, digested with MluI and BamHI and cloned into the MluI/BamHI sites of pLVX Che-hi3. **OL184 pLVX Che-hi3 Rab3a$_{N135I}$.** SDM was performed on OL183 using primers NT836 and NT837.

OL185 pLVX Che-hi3 Rab3b. Rab3b sequence was PCR amplified from pOTB7-Rab3b using primers NT788 and NT789, digested with EcoRI and BamHI and cloned into the EcoRI/BamHI sites of pLVX Che-hi3. **OL186 pLVX Che-hi3 Rab3b$_{N135I}$.** SDM was performed on OL185 using primers NT838 and NT839.

OL187 pLVX Che-hi3 Rab3c. Rab3c sequence was PCR amplified from pLX304 Rab3c using primers NT790 and NT791, digested with MluI and BamHI and cloned into the MluI/BamHI sites of pLVX Che-hi3. **OL188 pLVX Che-hi3 Rab3c$_{N143I}$.** SDM was performed on OL187 using primers NT840 and NT841.

OL189 pLVX Che-hi3 Rab3d/16. Rab3d/16 sequence (from pCMV-Sport6 Rab3d) was PCR amplified using primers NT567 and NT792, digested with MluI and BamHI and cloned into the MluI/BamHI sites of pLVX Che-hi3. **OL190 pLVX Che-hi3 Rab3d/16$_{N135I}$.** SDM was performed on OL189 with primers NT842 and NT843.

OL191 pLVX Che-hi3 Rab4a. Rab4a sequence was PCR amplified from pLX304 Rab4a using primers NT793 and NT794, digested with MluI and BamHI and cloned into the MluI/BamHI sites of pLVX Che-hi3. **OL192 pLVX Che-hi3 Rab4a$_{N126I}$.** SDM was performed on OL191 using primers NT844 and NT845.

OL193 pLVX Che-hi3 Rab5a. Rab5a sequence (obtained from pCDNA5 Flag3-Rab5a) was PCR amplified using primers NT483 and NT795, digested with MluI and BamHI and cloned into the MluI/BamHI sites of pLVX Che-hi3. **OL194 pLVX Che-hi3 Rab5a$_{N133I}$.** SDM was performed on OL193 using primers NT755 and NT756.

OL195 pLVX Che-hi3 Rab6a. Rab6a sequence was PCR amplified from pOTB7-Rab6a using primers NT796 and NT797, digested with MluI and BamHI and cloned into the MluI/BamHI sites of pLVX Che-hi3. **OL196 pLVX Che-hi3 Rab6a$_{N126I}$.** SDM was performed on OL195 using primers NT846 and NT847.

OL197 pLVX Che-hi3 Rab7b. Rab7b sequence was PCR amplified from pLX304 Rab7b using primers NT798 and NT799, digested with MluI and BamHI and cloned into the MluI/BamHI sites of pLVX Che-hi3. **OL198 pLVX Che-hi3 Rab7b$_{N124I}$.** SDM was performed on OL197 using primers NT848 and NT849.

OL199 pLVX Che-hi3 Rab8a. Rab8a sequence was PCR amplified from pOTB7-Rab8a using primers NT800 and NT801, digested with MluI and BamHI and cloned into the MluI/BamHI sites of pLVX Che-hi3. **OL200 pLVX Che-hi3 Rab8a$_{N121I}$.** SDM was performed on OL199 using primers NT850 and NT851. **OL319 pLVX Che-hi3 Rab8a$_{Q67L}$.** SDM was performed on OL199 using primers NT978 and NT979. **OL320 pLVX Che-hi3 Rab8a$_{T22N}$.** SDM was performed on OL199 using primers NT980 and NT981.

OL201 pLVX Che-hi3 Rab8b. Rab8b sequence (obtained from pDNR-LIB-Rab8b) was PCR amplified using primers NT459 and NT802, digested with MluI and BamHI and cloned into the MluI/BamHI sites of pLVX Che-hi3. **OL202 pLVX Che-hi3 Rab8b$_{N121I}$.** SDM was performed on OL201 using primers NT852 and NT853. **OL321**

pLVX Che-hi3 Rab8b$_{Q67L}$. SDM was performed on OL201 using primers NT667 and NT668. **OL322 pLVX Che-hi3 Rab8b$_{T22N}$.** SDM was performed on OL201 using primers NT982 and NT983.

OL203 pLVX Che-hi3 Rab9a. Rab9a sequence was PCR amplified from pLX304 Rab9a using primers NT803 and NT804, digested with MluI and BamHI and cloned into the MluI/BamHI sites of pLVX Che-hi3. **OL204 pLVX Che-hi3 Rab9a$_{N124I}$.** SDM was performed on OL203 using primers NT854 and NT855.

OL205 pLVX Che-hi3 Rab10. Rab10 sequence was PCR amplified from pCMV-XL5/Rab10 using primers NT805 and NT806, digested with MluI and BamHI and cloned into the MluI/BamHI sites of pLVX Che-hi3. **OL206 pLVX Che-hi3 Rab10$_{N122I}$.** SDM was performed on OL205 using primers NT856 and NT857.

OL207 pLVX Che-hi3 Rab11a. Rab11a sequence (obtained from pEGFP-Rab11aWT) was PCR amplified using primers NT485 and NT807, digested with MluI and BamHI and cloned into the MluI/BamHI sites of pLVX Che-hi3. **OL208 pLVX Che-hi3 Rab11a$_{N124I}$.** SDM was performed on OL207 using primers NT858 and NT859. **OL313 pLVX Che-hi3 Rab11a$_{Q70L}$.** SDM was performed on OL207 using primers NT669 and NT670. **OL314 pLVX Che-hi3 Rab11a$_{S25N}$.** SDM was performed on OL207 using primers NT972 and NT973.

OL209 pLVX Che-hi3 Rab11b. Rab11b sequence (obtained from pCR-BluntII-Topo/Rab11b) was PCR amplified using primers NT479 and NT808, digested with MluI and BamHI and cloned into the MluI/BamHI sites of pLVX Che-hi3. **OL210 pLVX Che-hi3 Rab11b$_{N124I}$.** SDM was performed on OL209 using primers NT860 and NT861. **OL315 pLVX Che-hi3 Rab11b$_{Q70L}$.** SDM was performed on OL209 using primers

NT671 and NT672. **OL316 pLVX Che-hi3 Rab11b$_{S25N}$.** SDM was performed on OL209 using primers NT974 and NT975.

OL211 pLVX Che-hi3 Rab11c/25. Rab11c/25 sequence (from pOTB7 Rab11c/25) was amplified using primers NT491 and NT809, digested with MluI and BamHI and cloned into the MluI/BamHI sites of pLVX Che-hi3. **OL212 pLVX Che-hi3 Rab11c/25$_{N125I}$.** SDM was performed on OL211 with primers NT862 and NT863.

OL213 pLVX Che-hi3 Rab12. Rab12 sequence was PCR amplified from pCMV-XL5/Rab12 using primers NT829 and NT830, digested with EcoRI and AvrII and cloned into the EcoRI/AvrII sites of pLVX Che-hi3. **OL214 pLVX Che-hi3 Rab12$_{N155I}$.** SDM was performed on OL213 using primers NT866 and NT867.

OL215 pLVX Che-hi3 Rab13. Rab13 sequence (obtained from pCMV-Sport6/Rab13) was PCR amplified using primers NT477 and NT810, digested with MluI and BamHI and cloned into the MluI/BamHI sites of pLVX Che-hi3. **OL216 pLVX Che-hi3 Rab13$_{N121I}$.** SDM was performed on OL215 using primers NT868 and NT869.

OL217 pLVX Che-hi3 Rab14. Rab14 sequence was PCR amplified from pLX304 Rab14 using primers NT811 and NT812, digested with MluI and BamHI and cloned into the MluI/BamHI sites of pLVX Che-hi3. O**L218 pLVX Che-hi3 Rab14$_{N124I}$.** SDM was performed on OL217 using primers NT870 and NT871.

OL219 pLVX Che-hi3 Rab18. Rab18 sequence was PCR amplified from pEGFP-Rab18 using primers NT813 and NT814, digested with MluI and BamHI and cloned into the MluI/BamHI sites of pLVX Che-hi3. **OL220 pLVX Che-hi3 Rab18$_{N122I}$.** SDM was performed on OL219 using primers NT872 and NT873.

OL221 pLVX Che-hi3 Rab19b. Rab19b sequence was PCR amplified from pLX304 Rab19b using primers NT815 and NT816, digested with MluI and BamHI and cloned into the MluI/BamHI sites of pLVX Che-hi3. The E12STOP mutation from the template was reverted by SDM using primers NT894 and NT895. **OL222 pLVX Che-hi3 Rab19b$_{N130I}$.** SDM was performed on OL221 using primers NT874 and NT875.

OL223 pLVX Che-hi3 Rab22b/31. Rab22b/31 sequence (obtained from pOTB7-Rab22b/31) was amplified using primers NT493 and NT817, digested with MluI and BamHI and cloned into the MluI/BamHI sites of pLVX Che-hi3. **OL224 pLVX Che-hi3 Rab22b/31$_{N119I}$.** SDM was performed on OL223 with primers NT876 and NT877.

OL225 pLVX Che-hi3 Rab23. Rab23 sequence (obtained from pCMV-Sport6 Rab23) was PCR amplified using primers NT468 and NT469, digested with AvrII and SalI and cloned into the AvrII/SalI sites of pSL1180. The BamHI site within the Rab23 coding sequence was mutagenized using primers NT516 and NT517. The resulting mutation is silent. The product was amplified with NT469 and NT818, digested with MluI and BamHI and cloned into the MluI/BamHI sites of pLVX Che-hi3. **OL226 pLVX Che-hi3 Rab23$_{N121I}$.** SDM was performed on OL225 with primers NT878 and NT879.

OL227 pLVX Che-hi3 Rab26. Rab26 sequence was PCR amplified from pLX304 Rab26 using primers NT819 and NT820, digested with MluI and BamHI and cloned into the MluI/BamHI sites of pLVX Che-hi3. **OL228 pLVX Che-hi3 Rab26$_{N177I}$.** SDM was performed on OL227 using primers NT880 and NT881.

OL229 pLVX Che-hi3 Rab27a. Rab27a sequence (obtained from pCMV-Sport6/Rab27a) was PCR amplified using primers NT471 and NT821, digested with

MluI and BamHI and cloned into the MluI/BamHI sites of pLVX Che-hi3. **OL230 pLVX Che-hi3 Rab27a$_{N133I}$.** SDM was performed on OL229 using primers NT882 and NT883.

OL231 pLVX Che-hi3 Rab27b. Rab27b sequence (obtained from pCMV-Sport6/Rab27b) was PCR amplified using primers NT495 and NT822, digested with MluI and BamHI and cloned into the MluI/BamHI sites of pLVX Che-hi3. **OL232 pLVX Che-hi3 Rab27b$_{N133I}$.** SDM was performed on OL231 using primers NT884 and NT885.

OL233 pLVX Che-hi3 Rab32. Rab32 sequence (obtained from pDNR-LIB/Rab32) was PCR amplified using primers NT461 and NT823, digested with MluI and BamHI and cloned into the MluI/BamHI sites of pLVX Che-hi3. **OL234 pLVX Che-hi3 Rab32$_{N143I}$.** SDM was performed on OL233 using primers NT886 and NT887.

OL235 pLVX Che-hi3 Rab33a. Rab33a sequence (from pOTB7-Rab33a) was PCR amplified using primers NT466 and NT467, digested with AvrII and EcoRI and cloned into the AvrII/EcoRI sites of pSL1180. The BamHI site within the Rab33a coding sequence was mutagenized using primers NT514 and NT515. The resulting mutation is silent. The product was amplified using NT467 and NT824, digested with MluI and BamHI and cloned into the MluI/BamHI sites of pLVX Che-hi3. **OL236 pLVX Che-hi3 Rab33a$_{N151I}$.** SDM was performed on OL235 with primers NT888 and NT889.

OL237 pLVX Che-hi3 Rab39a. Rab39a sequence was PCR amplified from pLX304 Rab39a using primers NT825 and NT826, digested with MluI and BamHI and cloned into the MluI/BamHI sites of pLVX Che-hi3. **OL238 pLVX Che-hi3 Rab39a$_{H127I}$.** SDM was performed on OL237 using primers NT890 and NT891.

OL239 pLVX Che-hi3 Rab40a. Rab40a sequence was PCR amplified from pLX304 Rab40a using primers NT827 and NT828, digested with MluI and BamHI and

cloned into the MluI/BamHI sites of pLVX Che-hi3. **OL240 pLVX Che-hi3 Rab40a$_{N126I}$.** SDM was performed on OL239 using primers NT892 and NT893.

OL251 pLVX Che-hi3 Rab2b. Rab2b sequence (obtained from pDNR-LIB/Rab2b) was PCR amplified using primers NT489 and NT899, digested with MluI and BamHI and cloned into the MluI/BamHI sites of pLVX Che-hi3. **OL252 pLVX Che-hi3 Rab2b$_{N119I}$.** SDM was performed on OL251 using primers NT996 and NT997.

OL253 pLVX Che-hi3 Rab4b. Rab4b sequence (obtained from pOTB7-Rab4b) was PCR amplified using primers NT903 and NT904, digested with AvrII and EcoRI and cloned into the AvrII/EcoRI sites of pLVX Che-hi3. **OL254 pLVX Che-hi3 Rab4b$_{N121I}$.** SDM was performed on OL253 using primers NT998 and NT999.

OL255 pLVX Che-hi3 Rab5b. Rab5b sequence (obtained from pCMV-Sport6/Rab5b) was PCR amplified using primers NT481 and NT900, digested with MluI and BamHI and cloned into the MluI/BamHI sites of pLVX Che-hi3. **OL256 pLVX Che-hi3 Rab5b$_{N133I}$.** SDM was performed on OL255 with primers NT1000 and NT1001.

OL257 pLVX Che-hi3 Rab5c. Rab5c sequence (obtained from pCMV-Sport6/Rab5c) was PCR amplified using primers NT475 and NT901, digested with MluI and BamHI and cloned into the MluI/BamHI sites of pLVX Che-hi3. **OL258 pLVX Che-hi3 Rab5c$_{N134I}$.** SDM was performed on OL257 with primers NT1002 and NT1003.

OL259 pLVX Che-hi3 Rab6b. Rab6b sequence was PCR amplified from pLX304 Rab6b using primers NT905 and NT906, digested with MluI and BamHI and cloned into the MluI/BamHI sites of pLVX Che-hi3. **OL260 pLVX Che-hi3 Rab6b$_{N126I}$.** SDM was performed on OL259 using primers NT1004 and NT1005.

OL261 pLVX Che-hi3 Rab6c. Rab6c sequence was PCR amplified from pLX304 Rab6c using primers NT907 and NT908, digested with MluI and BamHI and cloned into the MluI/BamHI sites of pLVX Che-hi3. The A159T mutation from the template was reverted by SDM using primers NT964 and NT965. **OL262 pLVX Che-hi3 Rab6c$_{N126I}$.** SDM was performed on OL261 using primers NT1006 and NT1007.

OL263 pLVX Che-hi3 Rab7a. Rab7a sequence was PCR amplified from pOTB7-Rab7a using primers NT909 and NT910, digested with MluI and BamHI and cloned into the MluI/BamHI sites of pLVX Che-hi3. **OL264 pLVX Che-hi3 Rab7a$_{N125I}$.** SDM was performed on OL263 using primers NT1008 and NT1009.

OL265 pLVX Che-hi3 Rab9b. Rab9b sequence was PCR amplified from pLX304 Rab9b using primers NT911 and NT912, digested with MluI and BamHI and cloned into the MluI/BamHI sites of pLVX Che-hi3. **OL266 pLVX Che-hi3 Rab9b$_{N124I}$.** SDM was performed on OL265 using primers NT1010 and NT1011.

OL267 pLVX Che-hi3 Rab15. Rab15 sequence was PCR amplified from pBlueScriptR-Rab15 using primers NT913 and NT914, digested with EcoRI and BamHI and cloned into the EcoRI/BamHI sites of pLVX Che-hi3. **OL268 pLVX Che-hi3 Rab15$_{T22N}$.** SDM was performed on OL267 using primers NT1012 and NT1013.

OL269 pLVX Che-hi3 Rab17. Rab17 sequence was PCR amplified from pLX304 Rab17 using primers NT915 and NT916, digested with MluI and BamHI and cloned into the MluI/BamHI sites of pLVX Che-hi3. **OL270 pLVX Che-hi3 Rab17$_{N132I}$.** SDM was performed on OL269 using primers NT1014 and NT1015.

OL271 pLVX Che-hi3 Rab20. Rab20 sequence was PCR amplified from pLX304 Rab20 using primers NT917 and NT918, digested with MluI and BamHI and

cloned into the MluI/BamHI sites of pLVX Che-hi3. **OL272 pLVX Che-hi3 Rab20$_{N113I}$.** SDM was performed on OL271 using primers NT1016 and NT1017.

OL273 pLVX Che-hi3 Rab21. Rab21 sequence was PCR amplified from pCMV-Sport6/Rab21 using primers NT919 and NT920, digested with MluI and BamHI and cloned into the MluI/BamHI sites of pLVX Che-hi3. **OL274 pLVX Che-hi3 Rab21$_{N132I}$.** SDM was performed on OL273 using primers NT1018 and NT1019.

OL275 pLVX Che-hi3 Rab22a. Rab22a sequence was PCR amplified from pCMV-Sport6/Rab22a using primers NT921 and NT922, digested with MluI and BamHI and cloned into the MluI/BamHI sites of pLVX Che-hi3. **OL276 pLVX Che-hi3 Rab22a$_{N118I}$.** SDM was performed on OL275 using primers NT1020 and NT1021.

OL277 pLVX Che-hi3 Rab24. Rab24 sequence was PCR amplified from pOTB7-Rab24 using primers NT923 and NT924, digested with MluI and BamHI and cloned into the MluI/BamHI sites of pLVX Che-hi3. **OL278 pLVX Che-hi3 Rab24$_{T120I}$.** SDM was performed on OL277 using primers NT1022 and NT1023.

OL279 pLVX Che-hi3 Rab28. Rab28-coding sequence was synthesized (Genewiz) in the pUC-Kan vector. Rab28 was excised using MluI and BamHI and cloned into the MluI/BamHI sites of pLVX Che-hi3. **OL280 pLVX Che-hi3 Rab28$_{N129I}$.** SDM was performed on OL279 using primers NT1024 and NT1025.

OL281 pLVX Che-hi3 Rab29/7L1. Rab29/7L1 sequence was PCR amplified from pLX304 Rab7L1 using primers NT927 and NT928, digested with MluI and BamHI and cloned into the MluI/BamHI sites of pLVX Che-hi3. **OL282 pLVX Che-hi3 Rab29/7L1$_{N125I}$.** SDM was performed on OL281 using primers NT1026 and NT1027.

OL283 pLVX Che-hi3 Rab30. Rab30 sequence was PCR amplified from pLX304 Rab30 using primers NT929 and NT930, digested with MluI and BamHI and cloned into the MluI/BamHI sites of pLVX Che-hi3. **OL284 pLVX Che-hi3 Rab30$_{N122I}$.** SDM was performed on OL283 using primers NT1028 and NT1029.

OL285 pLVX Che-hi3 Rab33b. Rab33b sequence (obtained from pBlueScriptR-Rab33b) was PCR amplified using primers NT463 and NT902, digested with MluI and BamHI and cloned into the MluI/BamHI sites of pLVX Che-hi3. **OL286 pLVX Che-hi3 Rab33b$_{N148I}$.** SDM was performed on OL285 using primers NT1030 and NT1031.

OL287 pLVX Che-hi3 Rab34. Rab34 sequence was PCR amplified from pLX304 Rab34 using primers NT931 and NT932, digested with MluI and BamHI and cloned into the MluI/BamHI sites of pLVX Che-hi3. The S244N mutation from the template was reverted by SDM using primers NT1054 and NT1055. **OL288 pLVX Che-hi3 Rab34$_{S166I}$.** SDM was performed on OL287 using primers NT1032 and NT1033.

OL289 pLVX Che-hi3 Rab36. Rab36 sequence was PCR amplified from pCR-TOPO/Rab36 using primers NT933 and NT934, digested with MluI and BamHI and cloned into the MluI/BamHI sites of pLVX Che-hi3. **OL290 pLVX Che-hi3 Rab36$_{T237I}$.** SDM was performed on OL289 using primers NT1034 and NT1035.

OL291 pLVX Che-hi3 Rab37. Rab37 sequence was PCR amplified from pLX304 Rab37 using primers NT935 and NT936, digested with MluI and BamHI and cloned into the MluI/BamHI sites of pLVX Che-hi3. **OL292 pLVX Che-hi3 Rab37$_{N143I}$.** SDM was performed on OL291 using primers NT1036 and NT1037.

OL293 pLVX Che-hi3 Rab38. Rab38 sequence was PCR amplified from pCMV-Sport6/Rab38 using primers NT937 and NT938, digested with MluI and BamHI

and cloned into the MluI/BamHI sites of pLVX Che-hi3. **OL294 pLVX Che-hi3 Rab38$_{N127I}$.** SDM was performed on OL293 using primers NT1038 and NT1039.

OL295 pLVX Che-hi3 Rab39b. Rab39b sequence was PCR amplified from pLX304 Rab39b using primers NT939 and NT940, digested with MluI and BamHI and cloned into the MluI/BamHI sites of pLVX Che-hi3. **OL296 pLVX Che-hi3 Rab39b$_{H123I}$.** SDM was performed on OL295 using primers NT1040 and NT1041.

OL297 pLVX Che-hi3 Rab40al. Rab40al sequence was PCR amplified from pLX304 Rab40al using primers NT941 and NT942, digested with MluI and BamHI and cloned into the MluI/BamHI sites of pLVX Che-hi3. **OL298 pLVX Che-hi3 Rab40al$_{N126I}$.** SDM was performed on OL297 using primers NT1042 and NT1043.

OL299 pLVX Che-hi3 Rab40b. Rab40b sequence was PCR amplified from pLX304 Rab40b using primers NT943 and NT944, digested with MluI and BamHI and cloned into the MluI/BamHI sites of pLVX Che-hi3. The P42T mutation from the template was reverted by SDM using primers NT966 and NT967. **OL300 pLVX Che-hi3 Rab40b$_{N126I}$.** SDM was performed on OL299 using primers NT1044 and NT1045.

OL301 pLVX Che-hi3 Rab40c. Rab40c sequence was PCR amplified from pLX304 Rab40c using primers NT945 and NT946, digested with EcoRI and AvrII and cloned into the EcoRI/AvrII sites of pLVX Che-hi3. The K64R mutation from the template was reverted by SDM using primers NT968 and NT969. **OL302 pLVX Che-hi3 Rab40c$_{N126I}$.** SDM was performed on OL301 using primers NT1046 and NT1047.

OL303 pLVX Che-hi3 Rab41. Rab41 sequence was PCR amplified from pLX304 Rab41 using primers NT947 and NT948, digested with MluI and BamHI and cloned into the MluI/BamHI sites of pLVX Che-hi3. The S193P mutation from the

template was reverted by SDM using primers NT960 and NT961. **OL304 pLVX Che-hi3 Rab41$_{N143I}$.** SDM was performed on OL303 using primers NT1048 and NT1049.

OL305 pLVX Che-hi3 Rab42. Rab42-coding sequence was synthesized (Genewiz) in the pUC-Kan vector. Rab42 was excised using MluI and BamHI and cloned into the MluI/BamHI sites of pLVX Che-hi3. **OL306 pLVX Che-hi3 Rab42$_{H129I}$.** SDM was performed on OL305 using primers NT1050 and NT1051.

OL307 pLVX Che-hi3 Rab43. Rab43 sequence was PCR amplified from pOTB7-Rab43 using primers NT951 and NT952, digested with MluI and BamHI and cloned into the MluI/BamHI sites of pLVX Che-hi3. **OL308 pLVX Che-hi3 Rab43$_{N131I}$.** SDM was performed on OL307 using primers NT1052 and NT1053.

2.4. Retroviral constructs for inducible expression

Some of the retroviral vectors listed below and in Table 2.1 were given an identifier starting with the letters "OR". These two letters stand for "**O**rganelle **R**etrovirus" and signify that these vectors need to be packaged into retroviral particles using a murine leukemia virus (MLV)-based packaging system.

pRetroX TRE3G-mCherry. The ~0.7 kbp BamHI/NotI fragment from pmCherry-N1 was ligated into the BamHI/NotI sites of pRetroX TRE3G (Clontech). **OR366 pRetroX TRE3G-mEGFP**. The ~0.7 kbp BamHI/NotI fragment from pmEGFP-N1 was ligated into the BamHI/NotI sites of pRetroX TRE3G.

OR161 pRetroX TRE3G-mCherry-Rab1b. mCherry-Rab1b was amplified from OL135 with primers NT729 and NT731, digested with BamHI/NotI, and ligated into the BamHI/NotI sites of pRetroX TRE3G. **OR162 pRetroX TRE3G-mCherry-Rab1b$_{Q67L}$.** mCherry-Rab1b$_{Q67L}$ was amplified from OL115 with primers NT729 and

NT731, digested with BamHI/NotI, and ligated into the BamHI/NotI sites of pRetroX TRE3G. **OR163 pRetroX TRE3G-mCherry-Rab1b$_{S22N}$.** mCherry-Rab1b$_{S22N}$ was amplified from OL142 with primers NT729 and NT731, digested with BamHI/NotI, and ligated into the BamHI/NotI sites of pRetroX TRE3G. **OR164 pRetroX TRE3G-mCherry-Rab1b$_{N121I}$.** mCherry-Rab1b$_{N121I}$ was amplified from OL143 with primers NT729 and NT731, digested with BamHI/NotI, and ligated into the BamHI/NotI sites of pRetroX TRE3G.

OR332 pRetroX TRE3G mCherry-Rab11a. OR333 pRetroX TRE3G mCherry-Rab11a$_{N124I}$. OR334 pRetroX TRE3G mCherry-Rab11a$_{Q70L}$. OR336 pRetroX TRE3G mCherry-Rab11a$_{S25N}$. mCherry was amplified from pmCherry-N1 using NT358 and NT729 and digested with BamHI and AvrII. Rab11a (WT and mutant) sequences were amplified from OL207, OL208, OL313 or OL314 using NT484 and NT1123, and digested with AvrII and NotI. The resulting mCherry and Rab11a fragments were assembled into the BamHI/NotI sites of pRetroX TRE3G.

OR337 pRetroX TRE3G mCherry-Rab11b. OR338 pRetroX TRE3G mCherry-Rab11b$_{N124I}$. OR340 pRetroX TRE3G mCherry-Rab11b$_{Q70L}$. OR341 pRetroX TRE3G mCherry-Rab11b$_{S25N}$. mCherry was amplified from pmCherry-N1 using NT358 and NT729 and digested with BamHI and AvrII. Rab11b (WT and mutant) sequences were amplified from OL209, OL210, OL315 or OL316 using NT478 and NT1124, and digested with AvrII and NotI. The resulting mCherry and Rab11b fragments were assembled into the BamHI/NotI sites of pRetroX TRE3G.

OR342 pRetroX TRE3G mCherry-Rab8a. OR344 pRetroX TRE3G mCherry-Rab8a$_{N121I}$. OR345 pRetroX TRE3G mCherry-Rab8a$_{Q67L}$. OR346

pRetroX TRE3G mCherry-Rab8a$_{T22N}$. mCherry was amplified from pmCherry-N1 using NT358 and NT729 and digested with BamHI and AvrII. Rab8a (WT and mutant) sequences were amplified from OL199, OL200, OL319 or OL320 using NT991 and NT1125, and digested with AvrII and NotI. The resulting mCherry and Rab8a fragments were assembled into the BamHI/NotI sites of pRetroX TRE3G.

OR348 pRetroX TRE3G mCherry-Rab8b. OR349 pRetroX TRE3G mCherry-Rab8b$_{N121I}$. OR350 pRetroX TRE3G mCherry-Rab8b$_{Q67L}$. OR356 pRetroX TRE3G mCherry-Rab8b$_{T22N}$. mCherry was amplified from pmCherry-N1 using NT358 and NT729 and digested with BamHI and AvrII. Rab8b (WT and mutant) sequences were amplified from OL201, OL202, OL321 or OL322 using NT458 and NT1126, and digested with AvrII and NotI. The resulting mCherry and Rab8b fragments were assembled into the BamHI/NotI sites of pRetroX TRE3G.

OR367 pRetroX TRE3G-GFP-DrrA$_{61-647}$. *L. pneumophila* GFP-DrrA$_{61-647}$ was amplified from pGFP-DrrA$_{61-647}$ using NT729 and NT1069, digested with BamHI/EcoRI and ligated into the BamHI/EcoRI sites of pRetroX TRE3G.

2.5. Mammalian cell lines: derivation, selection and growth

The cell lines used in this work, the retroviral and lentiviral vectors used for their construction and their antibiotic resistances are listed in Table 2.3. Briefly, human hepatocellular carcinoma Huh-7.5 cells (Blight et al., 2002), Huh-7.5-derived cells, human epithelial adenocarcinoma HeLa cells, and human embryonic kidney HEK293T cells were grown in Dulbecco's Modified Eagle's Medium (DMEM, Gibco), supplemented with L-glutamine, sodium pyruvate, 0.1 mM non-essential amino-acids (from here-on referred to as DMEM+) and 10% fetal bovine serum (FBS, Sigma or

HyClone) in humidified incubators at 37°C and in a 5% CO_2 atmosphere. Antibiotic selection of transduced Huh-7.5-derived cell lines employed puromycin (2 μg/mL), G418/geneticin (500 μg/mL), hygromycin (150 μg/mL) or blasticidin (6 μg/mL). HeLa cells were selected using puromycin (1 μg/mL) or hygromycin (250 μg/mL). The antibiotics were from Sigma or Invivogen. Selection was started two days after transduction and was maintained throughout subsequent growth. I wish to thank Caroline Gleason and Jenna Lobby for their help in determining the antibiotic selection conditions employed throughout this work.

Table 2.3. Cell lines

Cell line	Parental Cell Line	Viral vector used for construction	Antibiotic Resistance	Source / Reference
HEK293T	N/A	N/A	G418	P. Bieniasz
Huh-7.5	N/A	N/A	none	(Blight et al., 2002)
Huh-7.5 FLuc	Huh-7.5	pLVX Phi3 FLuc	Puro	This Study
Huh-7.5 TetON (Clone 9, Cl9)	Huh-7.5	pRetroX Tet3G	G418	(Luna et al., 2015)
Huh-7.5 TetON (Clone 1, Cl1)	Huh-7.5	pRetroX Tet3G	G418	This Study
Huh-7.5 TetON (Clone 2, Cl2)	Huh-7.5	pRetroX Tet3G	G418	This Study
Huh-7.5 TetON (Clone 4, Cl4)	Huh-7.5	pRetroX Tet3G	G418	This Study
Huh-7.5 TetON (Clone 12, Cl12)	Huh-7.5	pRetroX Tet3G	G418	This Study
Cl9 FLuc	Cl9	pLVX Bhi3 FLuc	Blast; G418	This Study
Cl9 OR161	Cl9	OR161 pRetroX TRE3G-mCherry-Rab1B	Puro; G418	This Study
Cl9 OR161 FLuc	Cl9 OR161	pLVX Bhi3 FLuc	Puro; G418; Blast	This Study
Cl9 OR162	Cl9	OR162 pRetroX TRE3G-mCherry-Rab1B$_{Q67L}$	Puro; G418	This Study
Cl9 OR162 FLuc	Cl9 OR162	pLVX Bhi3 FLuc	Puro; G418; Blast	This Study

Table 2.3. Cell lines

Cell line	Parental Cell Line	Viral vector used for construction	Antibiotic Resistance	Source / Reference
Cl9 OR163	Cl9	OR163 pRetroX TRE3G-mCherry-Rab1B$_{S22N}$	Puro; G418	This Study
Cl9 OR163 FLuc	Cl9 OR163	pLVX Bhi3 FLuc	Puro; G418; Blast	This Study
Cl9 OR164	Cl9	OR164 pRetroX TRE3G-mCherry-Rab1B$_{N121I}$	Puro; G418	This Study
Cl9 OR164 FLuc	Cl9 OR164	pLVX Bhi3 FLuc	Puro; G418; Blast	This Study
Cl9 OR366 FLuc	Cl9 FLuc	OR366 pRetroX TRE3G-mEGFP	Puro; G418; Blast	This Study
Cl9 OR367 FLuc	Cl9 FLuc	OR367 pRetroX TRE3G-GFP-DrrA$_{61-647}$	Puro; G418; Blast	This Study
Cl9 OR332	Cl9	OR332 pRetroX TRE3G mCherry-Rab11a	Puro; G418	This Study
Cl9 OR333	Cl9	OR333 pRetroX TRE3G mCherry-Rab11a$_{N124I}$	Puro; G418	This Study
Cl9 OR334	Cl9	OR334 pRetroX TRE3G mCherry-Rab11a$_{Q70L}$	Puro; G418	This Study
Cl9 OR336	Cl9	OR336 pRetroX TRE3G mCherry-Rab11a$_{S25N}$	Puro; G418	This Study
Cl9 OR337	Cl9	OR337 pRetroX TRE3G mCherry-Rab11b	Puro; G418	This Study
Cl9 OR338	Cl9	OR338 pRetroX TRE3G mCherry-Rab11b$_{N124I}$	Puro; G418	This Study
Cl9 OR340	Cl9	OR340 pRetroX TRE3G mCherry-Rab11b$_{Q70L}$	Puro; G418	This Study
Cl9 OR341	Cl9	OR341 pRetroX TRE3G mCherry-Rab11b$_{S25N}$	Puro; G418	This Study
Cl9 OR342	Cl9	OR342 pRetroX TRE3G mCherry-Rab8a	Puro; G418	This Study
Cl9 OR344	Cl9	OR344 pRetroX TRE3G mCherry-Rab8a$_{N121I}$	Puro; G418	This Study
Cl9 OR345	Cl9	OR345 pRetroX TRE3G mCherry-Rab8a$_{Q67L}$	Puro; G418	This Study
Cl9 OR346	Cl9	OR346 pRetroX TRE3G mCherry-Rab8a$_{T22N}$	Puro; G418	This Study
Cl9 OR348	Cl9	OR348 pRetroX TRE3G mCherry-Rab8b	Puro; G418	This Study

Table 2.3. Cell lines

Cell line	Parental Cell Line	Viral vector used for construction	Antibiotic Resistance	Source / Reference
Cl9 OR349	Cl9	OR349 pRetroX TRE3G mCherry-Rab8b$_{N121I}$	Puro; G418	This Study
Cl9 OR350	Cl9	OR350 pRetroX TRE3G mCherry-Rab8b$_{Q67L}$	Puro; G418	This Study
Cl9 OR356	Cl9	OR356 pRetroX TRE3G mCherry-Rab8b$_{T22N}$	Puro; G418	This Study
Huh-7.5/EV Hygro	Huh-7.5	pLVX Hhi3	Hygro	This Study
Huh-7.5/ApoE-GFP	Huh-7.5	pLVX Hhi3 ApoE3-mEGFP	Hygro	This Study
EVKD	Huh-7.5	pLKO.1 (EV)	Puro	M. Scull
EVKD/EV Hygro	EVKD	pLVX Hhi3	Puro; Hygro	This Study
EVKD/ApoE-GFP	EVKD	pLVX Hhi3 ApoE3-mEGFP	Puro; Hygro	This Study
EKD1	Huh-7.5	pLKO.1 shApoE	Puro	M. Scull
EKD1/EV Hygro	EKD1	pLVX Hhi3	Puro; Hygro	This Study
EKD1/ApoE	EKD1	pLVX Hhi3 ApoE3	Puro; Hygro	This Study
EKD1/ApoE-GFP	EKD1	pLVX Hhi3 ApoE3-mEGFP	Puro; Hygro	This Study
EKD2	Huh-7.5	pLKO.1 shApoE	Puro	M. Scull
EKD2/EV Hygro	EKD2	pLVX Hhi3	Puro; Hygro	This Study
EKD2/ApoE	EKD2	pLVX Hhi3 ApoE3	Puro; Hygro	This Study
EKD2/ApoE-GFP	EKD2	pLVX Hhi3 ApoE3-mEGFP	Puro; Hygro	This Study
HeLa	N/A	N/A	None	P. Bieniasz
HeLa/ApoE-GFP	HeLa	pLVX Hhi3 ApoE3-mEGFP	Hygro	This Study
HeLa/GFP-ApoE	HeLa	pLVX Phi3 mEGFP-ApoE3	Puro	This Study

Abbreviations: Blast, blasticidin S; Puro, puromycin; Hygro, hygromycin B; EV, empty vector.

Huh-7.5 TetON clonal cell lines. HCV-permissive Huh-7.5-derived clonal cell lines were engineered to constitutively express the TetON3G transactivator protein via transduction with retroviral particles generated using pRetroX Tet3G. Transduced cells were selected with G418, then clonal cell lines were obtained by plating the selected population in 96-well plates at 0.5-0.8 cells/well. Six weeks later, 12 Huh-7.5 TetON single-clone-containing wells were expanded and characterized. The Huh-7.5 TetON clones were tested for permissivity to HCV infection and spread using the reporter virus Jc1 378-1-TagRFP (Christopher Jones). This HCV reporter is similar to Jc1 378-1-YPet (Horwitz et al., 2013), but expresses a NS5A-TagRFP fusion instead of a NS5A-YPet fusion. TagRFP is a red fluorescent protein (RFP) variant (Merzlyak et al., 2007), while YPet is a yellow fluorescent protein variant (Nguyen and Daugherty, 2005). The clones, alongside the parental Huh-7.5 cells, were infected with the RFP reporter HCV at a multiplicity of infection (MOI) of 0.1 tissue culture infectious dose 50 (TCID50) per cell. The cells were harvested at 30 h or at 72 h post infection, fixed, and the percentage of infected (RFP-positive) cells was determined by flow cytometry. Clones 1, 2, 4, 9 and 12 were infected at levels comparable to the parental Huh-7.5 at both time points and were chosen for further characterization. To determine expression induction properties, each clone was transduced with retroviral particles made using pRetroX TRE3G-mCherry. Transduced populations were selected with G418 and Puromycin. To determine a dose-response induction curve for each TRE3G-mCherry-transduced TetON clone, decreasing 3-fold serial dilutions of doxycycline (Clontech) were used, starting from a high dose of 10 μg/mL. The cells were treated for 48 h then the mCherry fluorescence was quantified by flow cytometry (Figure 2.2A). Since induction of mCherry expression in all the clones

was found to near a plateau at about 3 μg/mL, this dose was used in all subsequent experiments. To determine the time-course of induction, the reporter-transduced clones were incubated with 3 μg/mL doxycycline for 0, 6, 12, 24, 36 or 48 h, and then the mCherry fluorescence was quantified by flow cytometry (Figure 2.2A-B). Growth rates were quantified using CyQuant NF Cell Proliferation Assay (Molecular Probes) for several days after plating 15,000 or 5,000 cells/well in 96-well plates. All clones had indistinguishable growth rates compared to the parental Huh-7.5, except for Clone 4, which had a 30% lower growth rate as measured at 96 h after plating. Based on these tests, Clone 9 was deemed to have the best properties in terms of permissivity to HCV infection, tightness and magnitude of induction in response to doxycycline, was therefore used in future studies, and was designated as Huh-7.5 TetON.

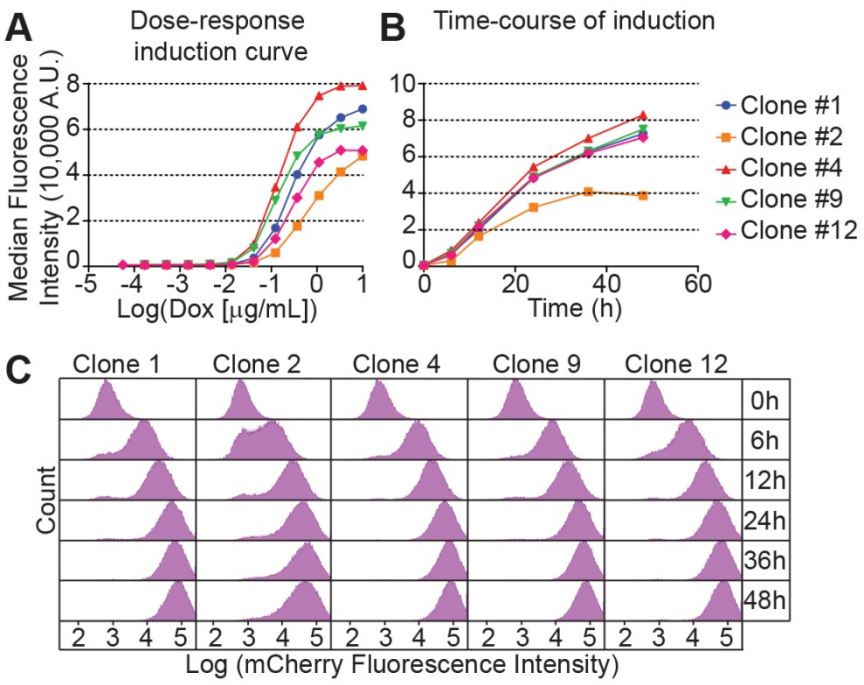

Figure 2.2. Characterization of Huh-7.5 TetON clonal cell lines. The Huh-7.5 TetON clones were transduced with a retrovirus expressing a doxycycline-inducible mCherry fluorescent protein reporter and the induction of gene expression was characterized by flow cytometry. (A) Doxycycline dose-response curve. Median fluorescence intensity values of populations of cells treated for 48 h with the indicated concentrations of doxycycline. A.U., arbitrary units. (B and C). Time course of induction. The cells were treated with 3 μg/mL doxycycline for the indicated amounts of time, then the mCherry fluorescence levels were quantified in single live cells by flow cytometry. (B) Data points represent the median single-cell mCherry fluorescence intensity levels in each sample. (C) Histograms of single cell mCherry fluorescence levels corresponding to the data points from panel B.

Huh-7.5 ApoE knockdown cell clones. Stable clonal control knockdown and ApoE knockdown Huh-7.5 cell lines were generated by Dr. Margaret A. Scull. I am grateful to her for allowing me to use these cell lines. Huh-7.5 cells were transduced with lentivirus particles generated using empty vector pLKO.1, or pLKO.1 shApoE, which expresses an ApoE-targeting shRNA (clone ID=TRCN0000010913, Broad Institute's

Genetic Perturbation Platform). The cells were selected using puromycin before undergoing single cell sorting into 96-well plates on a BD Aria2 Sorter at the Rockefeller University Flow Cytometry Core Facility. Individual cell clones were expanded in DMEM+ supplemented with 10% FBS and 10 units/mL penicillin and 10 μg/mL streptomycin (Gibco) and screened for HCV pseudoparticle entry and HCV replication competence as well as ApoE knockdown by quantitative reverse transcription PCR (qRT-PCR) and Western blotting. The empty vector-transduced clone was designated Huh-7.5 EV KD, while the two ApoE knockdown clones were designated Huh-7.5 EKD1 and Huh-7.5 EKD2, respectively.

2.6. Plasmid transfections

Plasmid transfection of HEK293T cells was done by quickly vortexing plasmid DNA and polyethyleneimine (Polysciences Inc, stock at 1 mg/mL in water) at a ratio of 1:4 in Optimem-I (Gibco, 10% of total media volume in the plate). The transfection mix was kept at room temperature for 10 min, then the media on the cells was changed to fresh media and the transfection mix was added. The media was again changed at 4-6 h. Huh-7.5 cells were transfected with Lipofectamine-3000 (Invitrogen) according to the manufacturer's instructions.

2.7. Lentivirus and retrovirus particle production

Low-passage HEK293T cells (60-80% confluent) were co-transfected using polyethyleneimine and a 5:5:1 ratio of a retroviral or lentiviral plasmid, a suitable GagPol plasmid, and a VSVg plasmid, respectively. To obtain virus for routine transductions, 11 μg of total DNA were used to transfect a 100-mm dish, in a total of 10 mL of media. To produce high titer virus stocks, 88 μg of total DNA were used to transfect a 150-mm dish

in a total of 20 mL of media. Virus-producing HEK293Ts were maintained in DMEM+ supplemented with 3% FBS. Virus-containing media was collected at 24 h, (and 48 h and 72 h, as needed) post transfection, filtered through a 0.45 μm filter, and used to transduce target cells immediately, after short storage at 4°C, or frozen at -80°C with added 20 mM 4-(2-hydroxyethyl)-1-piperazineethanesulfonic acid (HEPES, Gibco) and 4 μg/mL Polybrene (Millipore). Fresh media was added to cells after each harvest, if further collections were needed. For virus concentration, pooled virus-containing media was mixed at a ratio of 3:1 with LentiX Concentrator (Clontech), cooled at 4°C, then centrifuged for 45 min at 4°C and 1,500 x g. The viral pellet was resuspended into DMEM+ supplemented with 3% FBS, 20 mM HEPES and 4 μg/mL Polybrene, to achieve a 50 to 100-fold concentration, then aliquoted and stored at -80°C until used. Infections of Huh-7.5-derived cell lines were done in DMEM+ supplemented with 3% FBS, and 4 μg/mL Polybrene, for between 6 and 16 h, after which the media was changed to DMEM+ containing 10% FBS.

2.8. Lentivirus titer determinations

Titers of lentiviruses expressing fluorescent protein (FP) markers were determined using a flow cytometry-based assay as previously described (Sastry et al., 2002). Briefly, Huh-7.5 cells were plated in 12-well plates at 10^5 cells/well. The following morning, serial dilutions of lentivirus stocks were made in DMEM+ (supplemented with 3% FBS and 4 μg/mL Polybrene) and 1 mL of each dilution was used to infect individual wells. The media was changed at 6-8 h to 1 mL DMEM+ supplemented with 10% FBS. At 48 h post infection, the cells were processed and analyzed live by flow cytometry. Mock-transduced Huh-7.5 cells were used for gating.

The percent of fluorescent protein-positive, single live cells was recorded. Dilutions yielding a percent of fluorescent protein-positive cells between 1 and 20% were used to calculate the titer of the original stock using the formula:

$$Titer = \frac{(number\ cells\ plated) \times (\%\ positive\ cells) \times (dilution\ factor)}{(volume\ of\ inoculum)}$$

2.9. Flow cytometry

Cells were washed with phosphate-buffered saline (PBS) and trypsinized; trypsin was inactivated using cold DMEM+ containing 10% FBS. The cells were then pelleted for 2-3 min at 1,500 x g and 4°C, washed once with cold FACS buffer (PBS, 25 mM HEPES, pH 7.4, 1% bovine serum albumin), resuspended in FACS buffer containing 50 ng/mL 4',6-diamidino-2-phenylindole (DAPI, Molecular Probes), and kept on ice until analyzed on a BD-LSRII flow cytometer equipped with 405, 488, 561 and 640 nm lasers. Gating and analysis was performed using BD FACSDiva and FlowJo software.

2.10. HCV

RNA transcripts of the infectious HCV clone J6/JFH1 were generated from plasmids as previously described (Lindenbach et al., 2005). Briefly, plasmid DNA was linearized by digestion with XbaI, templates were purified by Minelute column (Qiagen), and 1 µg DNA was transcribed using the T7 RiboMAX™ Express Large Scale RNA Production System (Promega). Template DNA was removed by digestion with 1 U DNase I and RNA was cleaned up by RNeasy kit (Qiagen) with an additional on-column DNase I digestion step (Qiagen). RNA was quantified by absorbance at 260 nm, its integrity was verified by agarose gel electrophoresis, and 5 µg aliquots were stored at -80°C.

HCV RNA was transfected into Huh-7.5 cells by electroporation as described previously (Lindenbach et al., 2005). Briefly, Huh-7.5 cells were trypsinized, washed twice with ice-cold Hanks' Balanced Salt Solution (HBSS, Ca^{2+}/Mg^{2+}-free, Gibco), and resuspended to 1.5 x 10^7 cells/mL in cold PBS. For each electroporation, 5 μg of HCV RNA were mixed with 6 x 10^6 cells and immediately pulsed using an ElectroSquare Porator ECM 830 (BTX, Holliston, MA; 860 V, 99 μsec, five pulses). Electroporated cells were diluted in 30 mL of DMEM+ supplemented with 10% FBS, and plated in 24-well plates. Media was changed at 4-6 h, when a set of wells was further washed in cold PBS and harvested in RLT buffer (Qiagen) containing 0.14 M 2-mercaptoethanol for quantification of HCV RNA by qRT-PCR. When needed, cell supernatants were harvested, clarified through a 0.45 μm filter and frozen at -80°C for assay of infectious virus production by limiting dilution assay and tissue culture infectious dose 50 calculation by the method of Reed and Muench, as previously described (Lindenbach et al., 2005). For quantification of intracellular infectious virus levels (Gastaminza et al., 2006), the cells were trypsinized and pelleted at 1,500 x g for 3 min. Pellets were washed and resuspended in DMEM+ supplemented with 10% FBS. The cells were lysed by four freeze-thaw cycles, and the debris pelleted by twice centrifuging at 1,500 x g for 5 min. The supernatant was collected and viral infectivity was quantified as described above.

2.11. Luciferase assay

For luciferase activity measurements in the cell lysates, cells expressing the firefly luciferase were washed once in cold PBS, then 1 x Cell culture lysis reagent (Promega) was added. The plates were immediately sealed with adhesive aluminum foil, and stored at -80°C. On the day of the assay, the plates were thawed at 4°C and the cell lysates were

transferred to 96-well plates. Protein concentration in the samples was determined when needed using the Microplate BCA Protein Assay Kit, Reducing Agent Compatible (Thermo Scientific). Activity (luminescence) in 20 μL of lysate was measured immediately following injection of 50 μL of firefly luciferase assay buffer + substrate (Promega) using a Synergy Neo plate reader (Bio-Tek).

2.12. Microscopy

Cells were imaged live in growth medium or in cell imaging media (Hanks' balanced salts [Sigma], supplemented with 5% FBS, 0.1 mM non-essential amino acids, 10 mM HEPES, pH 7.5) or after fixation with 4% paraformaldehyde (Electron Microscopy Sciences) solution in PBS and further PBS washes. Images were acquired on the following systems: Olympus IX70/IX81 inverted microscopes equipped with 10X UplanFL 0.3 numerical aperture air or 60X UPlanApo 1.2 numerical aperture water objectives and Hamamatsu ORCA-ER cameras and Metamorph software (Molecular Devices), or a Deltavision system (Applied Precision) equipped with a 60X 1.42 numerical aperture oil objective and SoftWoRx software (Applied Precision). Deconvolution of fluorescence images using measured point-spread function was done in the SoftWoRx software, Pearson's coefficient measurements were done in Imaris (Bitplane), and final images were processed using FiJi (Schindelin et al., 2012) or Metamorph software.

2.13. Transferrin uptake

The protocol to measure the uptake of transferrin was adapted from (Fielding et al., 2012). Huh-7.5 cells were grown in 6-well plates. They were incubated for 1 h at 37°C in serum-free DMEM+, then washed with PBS and incubated in CellStripper

(Corning) at room temperature until they became detached. The cells were immediately moved into microcentrifuge tubes, cooled and subsequently processed on ice. The cells were pelleted for 2 min at 1,500 x g and 4°C and resuspended in 250 µL cold serum-free DMEM+, then 250 µL serum-free DMEM+ containing 100 µg/mL transferrin-Alexa Fluor 647 (Molecular Probes) were added, mixed with the cells, and the entire volume was split into two tubes and incubated for 5 min on ice to allow binding to the cell surface, then pelleted as above. The cells from one set of tubes were washed twice each with 1 mL ice-cold acid buffer (PBS, 1% bovine serum albumin, pH 5.0), then resuspended in 100 µL FACS buffer, supplemented with 50 ng/mL DAPI as dead cell exclusion stain and analyzed by flow cytometry to quantify the amount of transferrin bound at 4°C. The cells from the second set of tubes were resuspended in serum-free DMEM+, incubated at 37°C for 10 min to allow uptake, then cooled on ice for 5 min and further acid-washed and analyzed as described above.

2.14. VSVg transport assays

VSVg transport was monitored biochemically by co-transfection of (per well of a 6-well plate) 2 µg of pVSVg$_{tsO45}$-GFP (Presley et al., 1997) and 0.5 µg of a pLVX plasmid expressing mCherry or mCherry-Rab1b constructs. The plates were placed in an incubator set at 39.5°C. The media was changed at 4-6 h and the cells were returned to 39.5°C. At 24 h post-transfection, a plate containing one set of transfections was moved to a 32°C incubator for 3 h. The plates were then rapidly cooled on ice, washed once with cold PBS, scraped into PBS and moved into microcentrifuge tubes, on ice. The cells were pelleted at 1,500 x g for 3 min at 4°C. The pellet was resuspended in 100 µL RIPA buffer (Sigma) supplemented with Complete protease inhibitors (Roche), lysed on ice for 15

min, then centrifuged at 20,000 x g for 15 min at 4°C. The lysates were moved to a new tube and stored at -20°C. For endoglycosidase digestion, the lysates were thawed on ice and divided into 3 aliquots. One aliquot was digested with EndoH, one with PNGase F, and one was left untreated. Digestions were done for 2 h at 37°C according to New England Biolabs instructions, and were stopped by boiling the samples in 2X sodium dodecyl sulfate (SDS) sample buffer (containing protease inhibitors and 0.3 M 2-mercaptoethanol) and followed by processing for SDS Polyacrylamide gel electrophoresis (SDS-PAGE) and Western blotting experiments.

Huh-7.5 cells were plated in 35-mm glass-bottom MatTek dishes. The next day, each dish was co-transfected with 1 µg of pVSVg_{tsO45}-GFP and 0.5 µg of pLVX Phi-derived plasmid expressing mCherry or mCherry-Rab1b constructs. The dishes were immediately placed in an incubator set at 39.5°C. The media was changed at 4 h and the cells were returned to 39.5°C. At 24 h post-transfection, one set of dishes was moved to a 32°C incubator for 3.5 h, while a second set was kept at 39.5°C, before all were fixed with 4% paraformaldehyde in PBS for 15 min at room temperature, then washed with PBS and imaged.

2.15. SDS-PAGE and Western blotting

Cells were lysed and boiled in reducing SDS sample buffer. The proteins were separated on 4-12% Bis-Tris SDS-PAGE gels (Invitrogen), then transferred onto nitrocellulose membranes using the iBlot system (Invitrogen). The membranes were blocked in 5% non-fat milk in Tris-buffered saline supplemented with 0.1 % Tween-20) for 1 h at room temperature, immunoblotted with primary antibodies (overnight at 4°C) and matched horseradish peroxidase-conjugated secondary antibodies (1 h at room

temperature), treated with chemiluminescence substrates (ECL Prime, Amersham or West Pico or West Femto, Pierce), before being exposed to Amersham Hyperfilm MP autoradiography film and developed.

2.16. Antibodies

The antibodies used throughout this work are listed in Table 2.4, alongside the dilutions they were used at in each application. For immunoprecipitation, the amounts of antibody used are described in the respective specific sections.

Table 2.4 Antibodies and usage conditions

Antibody	Type	Conjugation	Usage	Source/Reference	Catalog or clone no.
α-GFP	mouse mAb		WB 1:2000 IF 1:250	Clontech	632381 Clone JL-8
α-GFP	rabbit mAb		IP	(Cristea et al., 2006)	N/A
α-dsRed	rabbit pAb		WB 1:1000	Clontech	632496
α-(β)actin	mouse mAb		WB 1:2000	Sigma	A5316 Clone AC-74
α-ApoB	goat pAb		IP	Calbiochem	178467
α-ApoB	goat pAb		WB 1:1000	Millipore	AB742
α-ApoB	rabbit pAb		IP	Abcam	50069
α-ApoE	rabbit mAb		WB 1:1000 IF 1:250	Abcam	52607 Clone EP1374Y
α-ApoE	goat pAb		WB 1:1000 IP	Millipore	AB947
α-albumin	goat pAb		IP	Midland Bioproducts	71907
α-NS5A	mouse mAb		IHC 1:25000	????	Clone 9E10
α-mouse IgG	goat pAb	HRP	WB 1:80000 - 1:150000	Sigma	A9917
α-rabbit IgG	goat pAb	HRP	WB 1:80000 - 1:150000	Sigma	A0545
α-goat IgG	rabbit pAb	HRP	WB 1:80000 - 1:150000	Sigma	A5420

Table 2.4 Antibodies and usage conditions

Antibody	Type	Conjugation	Usage	Source/Reference	Catalog or clone no.
α-mouse IgG	goat pAb	HRP	IHC 1:200	Jackson Immunoresearch	115-035-146
normal IgG	rabbit		IP	Jackson Immunoresearch	011-000-002
α-mouse IgG	goat pAb	AF488	IF 1:1000	Molecular Probes	A-11029
α-rabbit IgG	goat pAb	AF594	IF 1:1000	Molecular Probes	A-11037

Abbreviations: IgG, immunoglobulin G; mAb, monoclonal antibody; pAb, polyclonal antibody; IP, immunoprecipitation; IF, immunofluorescence; WB, Western blotting; IHC, immunohistochemistry; HRP, horseradish peroxidase; AF, Alexa Fluor.

2.17. Secretion assays and cargo quantification

Cells were washed once with DMEM+ containing 1% FBS, and then were allowed to secrete cargo in the same media for the indicated amounts of time (usually 6 h for samples analyzed by ELISA, 5 h for samples subjected to lipoprotein immuno-precipitation, and 6 or 24 h for HCV infectivity assays, respectively, or otherwise as indicated in the text or on the figures). For HCV secretion experiments, secretion was performed in media containing 10% FBS. At the end of the secretion period, media and cells were harvested and stored at -80°C until processed. If needed, cell lysates were harvested at this time for luciferase activity assays. For ELISA-based quantification of cell-associated cargo, cells were grown in 6-well plates, washed once in cold PBS supplemented with 50 mM ethylenediaminotetraacetic acid (EDTA), then scraped on ice in PBS supplemented with 50 mM EDTA. The cells were then pelleted and resuspended in 500 μL RIPA buffer supplemented with protease inhibitors and lysed on ice for 15 min, then stored at -80°C. Cargo amounts in cell lysates and supernatants were quantified using human-specific ELISA kits (Abcam: ApoE, ab108813; ApoB100, ab108807;

albumin, ab108788). Unconditioned media containing 1% or 10% FBS contained undetectable amounts of human albumin, ApoE, or ApoB100.

2.18. DN Rab GTPase screen

Huh-7.5 FLuc cells were plated at 42,000 cells/well in 12-well plates. After 7 h, the cells were infected with pLVX Che-hi3-derived viruses expressing WT or DN untagged Rab GTPases. The viruses, previously concentrated and titrated, were diluted in DMEM+ supplemented with 3% FBS and 4 μg/mL Polybrene such that the final dose in each target well was either 25 or 100 I.U./cell, and was contained in a total volume of 300 μL/well. The media was changed after 12 h to 500 μL/well of DMEM+ supplemented with 10% FBS. At 48 h post transduction, the cells were washed with 250 μL/well of DMEM+ containing 1% FBS, and then were incubated in the same media for 6 h at 37°C. Finally, the media was harvested and stored at -80°C until ELISA assays were performed. The cells were lysed on the plate in 100 μL/well of 1X cell culture lysis reagents, and stored at -80°C until a luciferase assay was performed. Transductions and secretion assays, ELISA assays and luciferase assays for paired WT-DN Rab samples were always performed on the same plate to minimize technical variations.

2.19. Polarized induced hepatocyte-like cells

The yet unpublished differentiation protocol for human induced hepatocyte-like cells (iHeps) from human embryonic stem cells has been developed by Dr. Xianfang Wu. The conditions in which the iHeps may be differentiated and polarized in a monolayer culture on trans-well filters has been developed by Dr. Wu and Dr. Viet Loan Dao Thi. The details of these protocols will be described by Dr. Wu and Dr. Dao Thi in an article currently in preparation. For the experiments presented in Chapter 4, trans-well filter-

grown iHep monolayers were washed twice with HBM basal medium (Lonza) and exposed to fresh media in both the apical and basolateral chambers for 6 h. The medium added to the apical chamber (within the trans-well insert) was the HBM basal medium. The medium added to the basolateral chamber (outside the trans-well insert) was the same HBM medium supplemented with all the components of the HCM Bullet Kit (Lonza) with the exception of the epidermal growth factor, EGF. The media was also supplemented with 10 U/mL penicillin, 10 μg/mL streptomycin and 20 ng/mL Oncostatin-M. At the end of the 6 h secretion assay, the media were harvested and stored at -80°C. The cells were washed in cold PBS and then lysed at 4°C on the filter in 300 μL cold RIPA buffer supplemented with protease inhibitors. The lysate was also stored at -80°C and the cargo amounts were measured in the media and in the lysates by ELISA Unconditioned media did not yield an ELISA signal for either human albumin, ApoE or ApoB100.

2.20. Co-immunoprecipitation of lipoproteins

Huh-7.5/EV Hygro or Huh-7.5/ApoE-GFP cells were washed once with DMEM+ containing 1% FBS, allowed to secrete cargo in the same media for 5 h, then media and cells were harvested. Media was cleared by a 3 min, 500 x g spin, then an aliquot of the media was mixed with SDS sample buffer, denatured, and stored at -20°C. Immunoprecipitation of 1.8 mL of cleared media was done as follows. All tubes were pre-coated with 1% bovine serum albumin, 0.1% Tween-20, PBS for 1 h, then washed 3 times with PBS. Media was incubated with 29 μg of rabbit α-GFP, rabbit α-ApoB100, or normal rabbit IgG, overnight at 4°C. Protein G Dynabeads (50 μL, pre-washed with PBS) were added and incubated 1 h at room temperature, then washed 4 times with PBS, then

denatured in SDS sample buffer. Samples were then processed by SDS-PAGE and Western blotting.

2.21. Radioactivity pulse-chases

This procedure was adapted from a previous study (Wang et al., 1993) as follows. Huh-7.5/EV Hygro and Huh-7.5/ApoE-GFP cells were plated at 3 x 10^5 cells/well in 6-well plates once day prior to the pulse chase assay. Clone 9 OR164 FLuc cells (inducibly expressing mCherry-Rab1b$_{N121I}$) were plated at 2.5 x 10^5 cells/well in 6-well plates 2 days before the pulse chase assay; the next day, half of the wells in each plate were induced with 3 μg/mL doxycycline, and the rest were left uninduced. On the day of the pulse chase assay, the cells were washed in PBS and then pulse labeled with ^{35}S-cysteine and ^{35}S-methionine (120 μCi/well) in DMEM containing no cold cysteine or methionine, and supplemented with 1% FBS and 0.1 mM non-essential amino acids for 20 min. The cells were then washed twice in PBS and chased in DMEM containing cycloheximide (Millipore, 50 μM) and excess of methionine (1.5 mg/mL) and cysteine (0.5 mg/mL). At each time point, the media was removed and the cells were washed once with PBS. The cells were lysed by rocking at 4°C for 30 min in 1 mL of Lysis buffer: 6.1 mM Na_2HPO_4, 4.5 mM NaH_2PO_4, 88.4 mM NaCl, 36.58 mM LiCl, 24.1 mM sodium deoxycholate, 1% Triton X100, 1% SDS, pH 7.4, supplemented with 4 μL/mL phenylmethane-sulfonylfluoride (Sigma, 0.1 M in ethanol) and Complete protease inhibitors. Total protein-incorporated radioactivity in the samples collected at each time point was determined after trichloroacetic acid precipitation, using scintillation fluid. Immunoprecipitation of ApoE, ApoB100 and albumin from media and cell lysates was performed by incubation with 5 μL each of the anti-ApoE, anti-ApoB100 and anti-

albumin antibodies and 50 µL protein A sepharose 4B beads (Invitrogen) in 1X NET buffer (0.15 M NaCl, 5 mM EDTA, 50 mM Tris, pH 7.5) supplemented with 1% Triton X100, overnight at 4°C. The beads were then washed 3 times in 1X NET buffer supplemented with 1% Triton X100 and 1% SDS, then the bound protein was eluted in 1X NET buffer containing 1% SDS. Samples were resuspended in denaturing buffer: 125 mM Tris-HCl, pH 6.8, 6 M urea, 1 mM EDTA, 10 mM dithiothreitol, 4% SDS, 25 mM 2-mercaptoethanol, and separated by SDS-PAGE on 4-12% Bis-Tris gels. The gels were fixed for 15 min with a 50% methanol, 7% acetic acid aqueous solution, incubated with Autofluor (National Diagnostic) for 15 min, and exposed in a Typhon 9400 phosphorimager. The intensity of each band was quantified and the background was subtracted in the Fiji software (Schindelin et al., 2012). Relative amounts of radiolabeled amino acid incorporation were calculated by dividing the intensity of the protein-specific band at the end of the pulse period by the measured total protein-contained radioactivity in the corresponding sample. Secretion of newly synthesized proteins was assessed by expressing the amount of radioactively labeled protein present in the media at a given time point as a percent of the total (secreted + cell-associated) radioactively labeled protein measured at the same time point.

2.22. qRT-PCR

To harvest RNA, cells were lysed in RLT buffer (350 µL/well, supplemented with 0.14 M 2-mercaptoethanol), processed using Qiashredder (Qiagen) and the lysates stored at -80°C. RNA was isolated using the RNeasy kit (Qiagen) with the additional on column DNase I digestion, and stored again at -80°C. qRT-PCR was performed on 10 or 50 ng total RNA using the QuantiFast SYBR Green RT-PCR kit (Qiagen) and QuantiTect

Primer Assay kits (Qiagen) specific for human *GAPDH* (QT00079247), *RAB1B* (QT00046396), *APOE* (QT00087297), *APOB* (QT00020139) and *ALB* (QT00063693), respectively. Fold changes in mRNA expression levels were determined using the $\Delta\Delta C_t$ method (Livak and Schmittgen, 2001), using *GAPDH* as reference housekeeping gene. HCV RNA levels were quantified against a standard curve using a one-step qRT-PCR assay (Multicode-RTx HCV RNA kit, Luminex Corp.) targeting the 3' UTR of the viral genome. Cycling was performed on a Roche Light Cycler 480 (Roche). Data analysis was performed on the Light Cycler 480 Software (Roche) and on the MultiCode-RTx Analysis Software (EraGen Biosciences).

2.23. Transcript expression levels by RNA sequencing

Huh-7.5 RNA sequencing (RNAseq) expression data for members of the Rab GTPase family, as well as for several other selected genes were extracted from datasets previously generated (Luna et al., 2015). The genes were ranked in ascending order of their expression levels. Genes to which no reads mapped were nonetheless assigned a score of -10 Log_2CPM, to allow them to be included in the graph. Unpublished RNAseq data from human fetal liver cultures, or HFLCs (Andrus et al., 2011) was kindly provided by Drs. William Schneider, Joseph Luna and Linda Andrus.

2.24. Statistical analyses

Unpaired two-tailed Student's *t*-test was performed in most cases. For analysis of the DN Rab screen data, the unpaired two-tailed Student's *t*-test with Bonferroni correction was performed. For HCV experiments, a two-way ANOVA test was performed. *P*-values were calculated in Microsoft Excel or in GraphPad Prism. I am

grateful to Dr. Michelle Itano for expert advice and help on performing statistical analyses.

2.25. Miscellaneous methods

Rab protein amino acid sequences were aligned using the ClustalW function of the Megalign program of DNAStar Lasergene. Rab1b crystal structure, Protein Data Bank structure 3NKV (Muller et al., 2010) was manipulated using PyMOL (Schrödinger Inc.).

Chapter 3

A Dominant Negative Rab GTPase Screen

Identifies Regulators of Hepatic Cargo Secretion

3.1. The concept

While progress has been achieved in characterizing the transport pathways mediating the secretion of hepatic lipoproteins (Sundaram and Yao, 2012; Tiwari and Siddiqi, 2012) and of HCV (Lindenbach, 2013; Lindenbach and Rice, 2013), further elucidation is required to improve our understanding of these processes. To investigate hepatic cargo secretion, I relied on the knowledge that Rab GTPases control relatively specific steps of intracellular vesicular transport (Hutagalung and Novick, 2011; Stenmark, 2009). For example, the Rab1, Rab2, and Rab6 subfamilies control traffic between the ER and the Golgi compartment, and within the Golgi (Chavrier et al., 1990a; Goud et al., 1990; Martinez et al., 1994; Plutner et al., 1991; Segev et al., 1988; Tisdale and Balch, 1996; Tisdale et al., 1992); the Rab3 and Rab8 subfamilies control post Golgi exocytosis (Fischer von Mollard et al., 1990; Fischer von Mollard et al., 1991; Huber et al., 1993a; Huber et al., 1993b); the Rab5 subfamily controls early steps of endocytosis (Bucci et al., 1992; Gorvel et al., 1991); and the Rab11 subfamily controls recycling of endocytosed proteins (Ren et al., 1998; Ullrich et al., 1996). Indeed, Rabs are considered a class - although not the only one - of identity markers that define the nature of a particular membrane-bound compartment (Barr, 2013; Pfeffer, 2013). I thus hypothesized that by inhibiting the function of individual Rab proteins and by measuring the effects

this inhibition had on the efficiency of cargo secretion, I may well be able to identify the Rabs, and therefore the vesicular transport pathways involved in the secretion of hepatic cargoes.

This is not the first screen of this nature. Previous studies have utilized overexpression of proteins regulating the Rab functional cycle, such as GAPs and GEFs, and/or knockdown experiments to attain similar goals (Fuchs et al., 2007; Pilli et al., 2012; Udayar et al., 2013; Yoshimura et al., 2010). Their success cemented my belief that this idea was sound. Furthermore, the wealth of knowledge accumulated over the past three decades of investigation of the regulation of intracellular transport by the Rab proteins (Hutagalung and Novick, 2011) allowed me to design an experimental approach whose implementation relied on the use of many previously described molecular tools. These include well characterized DN mutants, functional fusions of fluorescent proteins to the Rabs, activators and repressors of endogenous Rab function (Barr and Lambright, 2010), and an ever-growing list of known Rab effectors (Hutagalung and Novick, 2011).

3.2. DN Rab screen outline

The outline of the screen is depicted in Figure 3.1. Since expression of DN Rab mutants is a well established method of inhibition of Rab function, I expressed a panel of such mutants in a liver-derived cell line (Figure 3.1A). For each DN Rab (red text and cartoons), I used expression of the WT Rab (blue text and cartoons) as the control condition (Figure 3.1B). I did so in an attempt to distinguish between effects due to mere overexpression of the Rabs and the effects due to functional differences between the WT and the DN versions of a given Rab. Following expression of WT-DN Rab pairs, I washed the cells to remove cargo loosely attached to the cell surface or to the plate, and

then performed a secretion assay. At the end of the secretion assay, I quantified the amount of cargo released into the media, and also estimated the cellular mass present in the well and thus responsible for secretion (Figure 3.1C). By dividing the secreted cargo amounts by the cell mass measurement (Figure 3.1D), I calculated a normalized level of secretion in each well. I then compared these normalized secretion values obtained in the presence of WT and DN Rab expression (Figure 3.1E). I interpreted significant differences between the two values to signify that the Rabs causing them were likely to be involved in regulating secretion of the tested cargo. To elucidate the fine details of the control of secretion by any given Rab would of course require further analysis.

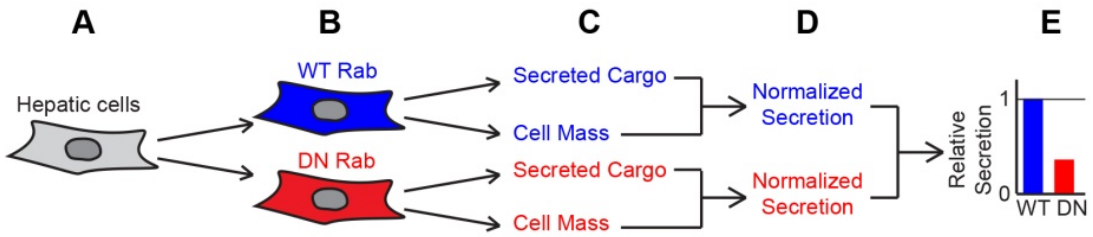

Figure 3.1. Outline of the DN Rab GTPase screen. Hepatic cells (A) were made to express WT (blue) or DN (red) Rab GTPases (B). Secretion assays were performed and secreted cargo amounts and cell masses were measured (C). The amounts of cargo secreted were divided by the corresponding well's cell mass measurement to obtain normalized secretion values (D). The normalized secretion values obtained in the presence of DN Rab expression were compared to those obtained in the presence of the WT Rab (E).

3.3. The experimental system

I performed the DN Rab GTPase screen in the Huh-7.5 human hepatoma cell line (Blight et al., 2002). I chose this cell line since I wanted to be able to directly contrast the effects of inactivation of the hits of the Rab screen on lipoprotein secretion to their effects on HCV egress. The Huh-7.5 cells (Blight et al., 2002; Lindenbach et al., 2005) possess the ability to support the entire HCV lifecycle, which includes permitting high levels of HCV RNA genome replication and infectious HCV particle release. I remain aware that the parental Huh-7 cells (Meex et al., 2011), as well as the Huh-7.5 cells themselves (Ursula Andreo, personal communication), remain defective in secreting ApoB100 in the appropriate VLDL density fraction, and instead preponderantly secrete IDL/LDL-like ApoB100-containing particles. Confirmation that a certain Rab GTPase is involved in the secretion of HCV and/or lipoproteins in a more physiologic setting would require further testing in more informative, but also more expensive, and potentially less easily tractable or readily available primary cell or *in vivo* system(s).

A final requirement of this experimental design was that I be able to estimate the mass of cells present at the time of the measurement of cargo secretion. Therefore, I transduced the Huh-7.5 cells with a lentivirus expressing firefly luciferase (FLuc). I confirmed that in the resulting Huh-7.5 FLuc cell line, the measured luciferase activity correlated linearly with the number of cells present in the culture (Figure 3.2A). Furthermore, this tight correlation, together with the simplicity of the luciferase activity assay, its large dynamic range and its high sensitivity made this a more suitable cell-mass estimation method than total protein concentration measurements (Figure 3.2B).

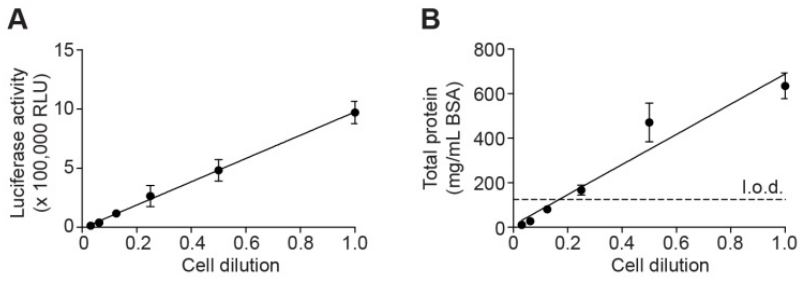

Figure 3.2. Characterization of luciferase-expressing Huh-7.5 FLuc cells. Two-fold serial dilutions of Huh-7.5 FLuc cells were plated each in 4 wells of a 24-well plate and the cell lysates were harvested the next day. Luciferase activity (A) and total protein concentration (B) were measured in each sample and were plotted against the dilution factor. Values are means ± standard deviation (s.d.) of the values obtained in 4 replicate wells. RLU, relative light units; BSA, bovine serum albumin; l.o.d. limit of detection of the protein concentration assay.

3.4. Expression of WT and DN Rab GTPase constructs

To ensure relatively uniform construct expression in an overwhelming majority of the cells in culture, I utilized lentivirus transduction as the preferred method of Rab expression. In preliminary experiments, I had noticed that the transduction efficiencies of lentiviruses expressing DN Rab1 constructs were regularly lower than those of the lentiviruses expressing WT Rab1 or irrelevant proteins, despite the fact that the lentiviral vectors had been packaged into lentiviral particles in parallel, using the same protocol. This observation was not surprising since I pseudotyped the lentiviral particles using VSVg. Loading of VSVg onto the budding lentiviral particle requires transport of VSVg to the plasma membrane, the site of HIV-1 lentivirus assembly (Jouvenet et al., 2006). Since Rab expression was driven by the constitutively-active CMV promoter, DN Rabs expressed in the lentivirus particle-packaging HEK293T cells could interfere with lentivirus particle infectivity by affecting the exocytic transport of VSVg (Tisdale et al.,

1992). It thus became important for me to ensure that equal doses of infectious WT and DN Rab-expressing lentiviruses were delivered to the target cells. I therefore established a method for relatively large-scale lentivirus production, followed by concentration of the virus stock and determination of its infectivity. To measure lentivirus titers, I utilized a flow cytometry-based protocol which used as readout the fluorescence of the mCherry protein expressed from the lentiviral vector pLVX Che-hi3 (Figure 2.1B) in which I cloned the WT and mutant Rabs. Using this protocol I routinely prepared concentrated Rab-expressing lentivirus stocks with titers in the range of $2x10^7$ to $5x10^8$ infectious units (I.U.)/mL, which were measured on Huh-7.5 cells, the same cell type that I used in most of the experiments.

I also confirmed that the fluorescence measured in the transduced cells and used to determine lentivirus titers was due to infection by the viral particles themselves, and not by unspecific staining of the target cells by the lentivirus particle inoculum. This was a concern since I used a proprietary commercial reagent to concentrate the lentivirus stocks, and I had no information on whether the concentration protocol could also enrich exosomes, which are expected to be produced alongside the lentivirus particles (Cantin et al., 2008) and could deliver mRNAs from the lentivirus producing cells (Valadi et al., 2007). Carryover of the DNA that had been used to launch lentivirus production could also, in principle, cause mCherry expression in the transduced cells. I thus produced lentiviral particles using an mCherry-expressing lentiviral vector, VSVg, and either the packaging system encoded by pCR/V1 NL GagPol (Zennou et al., 2004), or a plasmid encoding only HIV-1 Gag (Graf et al., 2000). Although HIV-I Gag retains the ability to form lentivirus-like particles (Zennou et al., 2004), it nevertheless cannot support particle

infectivity since it lacks essential enzymatic activities such as protease, reverse transcriptase and integrase, all of which are contained in HIV-1 Pol and required for productive infection (Freed, 2015). Indeed, when I titrated the lentivirus stock produced using HIV-1 Gag, I detected roughly 100- to 1000-fold fewer positive cells in the transduced population than I did when I titrated the lentivirus stock produced using GagPol (Figure 3.3A). The positive cells obtained by transduction with HIV-1 Gag-packaged particles also had lower fluorescence levels than the positive cells obtained by transduction with GagPol-packaged particles (Figure 3.3B). This difference was not due to production of fewer particles in the presence of HIV-1 Gag, since both virus stocks contained comparable amounts of material that was recognized by an α-capsid (CA) antibody (Figure 3.3C). Capsid is one of the domains of HIV-1 Gag (Bieniasz, 2009). As expected, HIV-Gag (p55) did not undergo proteolytic processing in the absence of the Pol-encoded protease activity (Figure 3.3C, left lane), but was cleaved in the presence of Pol (Figure 3.3C, right lane). This test therefore confirmed that the readout from the titration assay was primarily due to lentivirus infection-dependent gene expression.

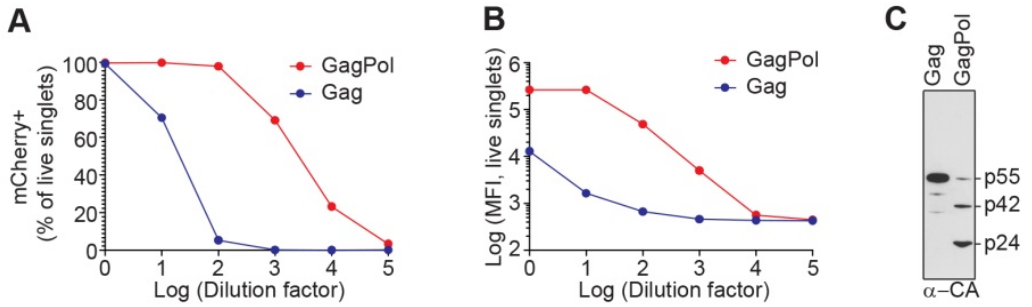

Figure 3.3. Specificity of lentivirus transduction. Concentrated lentivirus particle stocks were made using an mCherry-expressing lentiviral vector and either an HIV-1 GagPol-expressing packaging plasmid (red) or a control HIV-1 Gag-expressing plasmid (blue). Huh-7.5 cells were transduced with serial dilutions of each of the stocks. The abundance of mCherry-positive cells (A) and their associated mCherry fluorescence amounts (B) are plotted. MFI, median fluorescence intensity. (C) lentiviral particles from each of the stocks were concentrated and analyzed by Western blotting using an α-HIV-1 capsid (CA) antibody. Molecular weights (kDa) of the major bands are listed at the right. Cleavage of full length Gag (p55) is indicated by the appearance of the p42 and p24 bands.

Having established a method to produce high titer lentivirus stocks, I next tested the efficiency of target cell transduction using these viruses. Previous reports have overexpressed Rab1 constructs by infecting target cells with adenoviruses or lentiviruses at a MOI of 5-100 I.U./cell (Filipeanu et al., 2004; Filipeanu et al., 2006; Li et al., 2010; Yin et al., 2011). I tested two doses of lentivirus within this range, namely 25 and 100 I.U./cell. Both doses were sufficient to transduce the overwhelming majority of the target cell population (Figure 3.4A) and to yield a fluorescent signal easily detectable by fluorescence microscopy (Figure 3.4B). Therefore, I planned to express the Rab constructs under the control of a CMV promoter using a lentivirus vector which also expressed the fluorescent protein reporter mCherry from a PGK promoter (Figure 2.1D).

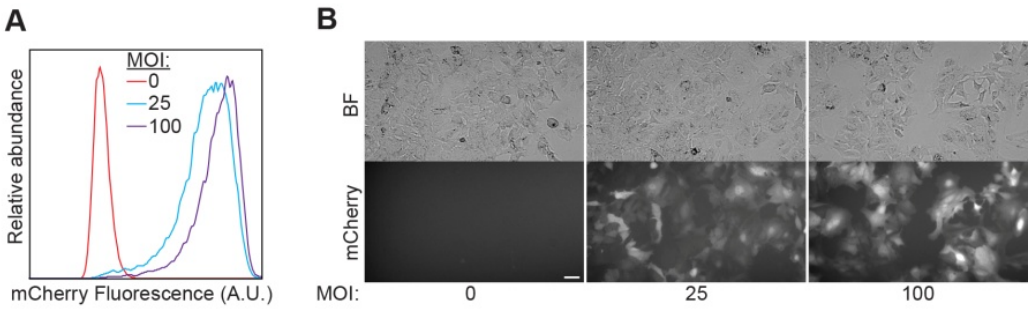

Figure 3.4. Lentivirus transduction efficiency in Huh-7.5 cells. Cells were left uninfected or were infected with an mCherry-expressing lentivirus stock at a MOI of 25 or 100 I.U./cell, and were then analyzed 48 h later by flow cytometry (A) or fluorescence microscopy (B). A.U., arbitrary units; BF, brightfield. Scale bar, 50 μm.

3.5 The Rabs

I chose to test the involvement of 62 human Rab GTPases in regulating hepatic cargo secretion (listed in the Table 2.1; the NCBI reference sequence identifiers for their amino acid sequences are listed in the table as well). Amino acid sequences were numbered by assigning position 1 to the predicted START methionine residue. Alignment of these sequences revealed, as expected (Diekmann et al., 2011; Gurkan et al., 2005; Wittinghofer and Vetter, 2011), a high degree of sequence similarity, particularly in the regions predicted to participate in the formation of the conserved Rab GTPase domain (Figure 3.5). These amino acid stretches contained two conserved phosphoryl binding sites and a guanine ring binding site, respectively, as identified in a previous study (Tisdale et al., 1992) and highlighted in blue in the consensus sequence listed at the top of the alignment (Figure 3.5).

Several mutations that interfere with various aspects of the Rab functional cycle exist; these include mutations that target conserved residues that affect the Rab guanine nucleotide binding and hydrolysis cycle (Table 1.1, and highlighted in red ink Figure 3.5)

and have been widely used to inhibit Rab function. One mutation targets the conserved serine/threonine residue involved in phosphoryl binding, equivalent to $Rab1a_{S25}$. This serine/threonine residue is conserved in all the Rab sequences in the list except for Rab40b and 40c, where it is replaced by glycine. Mutation of this residue to asparagine yields proteins that cannot stably bind GTP, and thus remains locked in the inactive GDP-bound form (Nuoffer et al., 1994). Another mutation targets the conserved glutamine residue involved in (basal or stimulated) GTP hydrolysis and equivalent to $Rab1a_{Q70}$. Mutation of this residue may yield proteins defective in GTP-hydrolysis which causes them to be locked in the GTP-bound active state (Mishra et al., 2013). This residue is not conserved in 4 Rabs: Rab11c (replaced by leucine), Rab20 (replaced by arginine), Rab24 (replaced by serine) and Rab42 (replaced by histidine). A third mutation targets the conserved asparagine residue involved in guanine ring binding. Mutation of this residue to isoleucine may prevent the Rab from stably binding the GDP or GTP nucleotides (Pind et al., 1994). Rabs 24, 34, and 36 carry a serine or threonine at this site, while Rabs 39a, 39b and 42 carry a histidine. The sequence of Rab15, however, did not align well in this region with the rest of the Rab sequences (depicted in orange in Figure 3.5).

Figure 3.5. Alignment of Rab protein sequences (next page). The amino acid sequences of 62 Rab proteins were aligned to one another, and the alignment within selected conserved sequences is shown. The consensus sequence is listed at the top. The two phosphoryl binding sites and the guanine ring binding site, as defined in (Tisdale et al., 1992), are highlighted in blue within the consensus sequence. Conserved, functionally important amino acids, as defined in the text, are highlighted in red. The position of the first amino acid in each set of sequences is listed in purple at the left of the alignment. The divergent Rab15 sequence within the guanine ring binding site is highlighted in orange.

		phosphoryl binding site I		phosphoryl binding site II		guanine ring contact site
Rab		LFKLLLIGDSGVGKTSLLLRF		QIWDTAGQERFR		MLVGNKCDLXDK
1A	11	LFKLLLIGDSGVGKSCLLLRF	63	QIWDTAGQERFR	120	LLVGNKCDLTTK
1B	8	LFKLLLIGDSGVGKSCLLLRF	60	QIWDTAGQERFR	117	LLVGNKSDLTTK
1C	8	LFKLLIIGDSGVGKSSLLLRF	60	QIWDTAGQERFR	116	ILVGNKNDDPER
2A	6	LFKYIIIGDTGVGKSCLLLQF	58	QIWDTAGQESFR	115	MLIGNKSDLESR
2B	6	LFKYIIIGDTGVGKSCLLLQF	58	QIWDTAGQESFR	115	MLIGNKSDLESR
3A	22	MFKILIIGNSSVGKTSFLFRY	74	QIWDTAGQERYR	131	LLVGNKCDMEDE
3B	22	MFKLLIIGNSSVGKTSFLFRY	74	QIWDTAGQERYR	131	ILVGNKCDMEEE
3C	30	MFKLLIIGNSSVGKTSFLFRY	82	QIWDTAGQERYR	139	ILVGNKCDMEDE
3D	22	MFKLLLIGNSSVGKTSFLFRY	74	QIWDTAGQERYR	131	ILVGNKCDLEDE
4A	13	LFKFLVIGNAGTGKSCLLHQF	65	QIWDTAGQERFR	122	ILCGNKKDLDAD
4B	8	LFKFLVIGSAGTGKSCLLHQF	60	QIWDTAGQERFR	117	ILCGNKKDLDPE
5A	20	QFKLVLLGESAVGKSSLVLRF	72	EIWDTAGQERYH	129	ALSGNKADLANK
5B	20	QFKLVLLGESAVGKSSLVLRF	72	EIWDTAGQERYH	129	ALAGNKADLANK
5C	21	QFKLVLLGESAVGKSSLVLRF	73	EIWDTAGQERYH	130	ALAGNKADLASK
6A	13	KFKLVFLGEQSVGKTSLITRF	65	QLWDTAGQERFR	122	MLVGNKTDLADK
6B	13	KFKLVFLGEQSVGKTSLITRF	65	QLWDTAGQERFR	122	MLVGNKTDLADK
6C	13	KFKLVFLGEQSVAKTSLITRF	65	RLWDTAGQERLR	122	TLVGNRTDLADK
7A	8	LLKVIILGDSGVGKTSLMNQY	60	QIWDTAGQERFQ	121	VVLGNKIDLENR
7B	8	DLKLIIVGAIGVGKTSLLHQY	60	QIWDTGGQERFR	120	VLLGNKIDLADR
8A	8	LFKLLLIGDSGVGKTCVLFRF	60	QIWDTAGQERFR	117	MILGNKCDVNDK
8B	8	LFKLLLIGDSGVGKTCLLFRF	60	QIWDTAGQERFR	117	MILGNKCDMNDK
9A	7	LFKVILLGDGGVGKSSLMNRY	59	QIWDTAGQERFR	120	VILGNKIDISER
9B	7	LLKVILLGDGGVGKSSLMNRY	59	QIWDTAGQERFK	120	VVLGNKVDKEDR
10	9	LFKLLLIGDSGVGKTCVLFRF	61	QIWDTAGQERFH	118	MLLGNKCDMDDK
11A	11	LFKVVLIGDSGVGKSNLLSRF	63	QIWDTAGQERYR	120	MLVGNKSDLRHL
11B	11	LFKVVLIGDSGVGKSNLLSRF	63	QIWDTAGQERYR	120	MLVGNKSDLRHL
11C	12	VFKVVLIGESGVGKTNLLSRF	64	QIWDTAGLERYR	121	MLVGNKSDLSQA
12	42	KLQVIIIGSRGVGKTSLMERF	94	QIWDTAGQERFN	151	LLVGNKLDCETD
13	8	LFKLLLIGDSGVGKTCLIIRF	60	QVWDTAGQERFK	117	LLLGNKCDMEAK
14	11	IFKYIIIGDMGVGKSCLLHQF	63	QIWDTAGQERFR	120	ILIGNKADLEAQ
15	8	LFRLLLIGDSGVGKTCLLCRF	60	QIWDTAGQERYQ	116	PGCGEGASPGKA
17	19	VFKLVLLGSGSVGKSSLALRY	70	EIWDTAGQEKYH	128	MLVGNKTDLSQE
18	8	TLKILIIGESGVGKSSLLLRF	60	AIWDTAGQERFR	118	MLVGNKID-KEN
19B	17	LFKIILIGDSNVGKTCVVQHF	69	QVWDTAGQERFR	126	MLIGNKCDLWEK
20	5	DSKIVLLGDMNVGKTSLLQRY	52	SIWDTAGREQFH	109	AIVGNKVDLTEE
21	19	SFKVVLLGEGCVGKTSLVLRY	71	AIWDTAGQERFH	128	CIVGNKIDLEKE
22A	5	ELKVCLLGDTGVGKSSIVWRF	57	LIWDTAGQERFR	114	AIAGNKCDLIDV
22B	6	ELKVCLLGDTGVGKSSIVCRF	58	LIWDTAGQERFH	115	AIAGNKCDLSDI
23	9	AIKMVVVGNGAVGKSSMIQRY	61	MLWDTAGQEEFD	117	VLVQNKIDLLDD
24	7	DVKVVMLGKEYVGKTSLVERY	60	GIWDTAGSERYE	116	YLCGTKSDLLEE
26	63	AFKVMLVGDSGVGKTCLLVRF	116	QMWDTAGQERFR	173	MLLGNKVDSAHE
27A	9	LIKFLALGDSGVGKTSVLYQY	71	QLWDTAGQERFR	129	VLCGNKSDLEDQ
27B	9	LIKLLALGDSGVGKTTFLYRY	71	QLWDTAGQERFR	129	VLIGNKADLPDQ
28	12	QLKIVVLGDGASGKTSLTTCF	65	QIWDIGGQTIGG	125	ALVGNKIDLEHM
29	7	LFKVLVVGDAAVGKTSLVQRY	60	QLWDIAGQERFT	121	LLLANKCDLSPW
30	9	LFKIVLIGNAGVGKTCLVRRF	61	QIWDTAGQERFR	118	VLVGNKIDLAER
32	25	LFKVLVIGELGVGKTSIIKRY	78	QLWDIAGQERFG	139	VLLANKCDQNKD
33A	36	IFKIIVIGDSNVGKTCLTFRF	88	QVWDTAGQERFR	147	VLVGNKCDLREQ
33B	33	IFKIIVIGDSNVGKTCLTYRF	85	QLWDTAGQERFR	144	ILVGNKCDLRSA
34	52	ISKVIVVGDLSVGKTCLINRF	104	QLWDTAGQERFK	162	FLVGSKKDLSTP
36	123	LSKVVVVGDLYVGKTSLIHRF	175	QIWDTAGQEKFK	233	FLVGTKKDLLSG
37	29	TGKVMLLGDTGVGKTCFLIQF	82	QIWDTAGQERFR	139	MLLGNKADMSSE
38	9	LYKLLVIGDLGVGKTSIIKRY	62	QLWDIAGQERFG	123	VLLANKCDQGKD
39A	8	QFRLIVIGDSTVGKSCLLHRF	65	QLWDTAGQERFR	123	LLVGHKCDLASQ
39B	8	QFRLIVIGDSTVGKSCLIRRF	61	QIWDTAGQERFR	119	VLVGHKCDLDTQ
40A	14	LLKFLLVGDRDVGKSEILESL	66	KLWDTSGQGRFC	122	ILVGNRLHLAFK
40AL	14	LLKFLLVGDRDVGKSEILESL	66	KLWDTSGQGRFC	122	ILVGNRLHLAFK
40B	14	LLKFLLVGDSDVGKGEILASL	66	QLWDTSGQGRFC	122	ILVGNRLHLAFK
40C	14	LLKFLLVGDSDVGKGEILESL	66	ELWDTSGQGRFC	122	ILVGNRLHLAFK
41	31	KSKLLFLGEQS-GKTSIISRF	82	QLWDTAGQERFH	139	MLLGNKIDLDNK
42	9	QFRVALLGDAAVGKTSLLRSY	67	QLWDTAGHERFR	125	LLVGHKSDLQST
43	18	LFKLVLVGDASVGKTCVVQRF	70	QIWDTAGQERFR	127	LLIGNKSDLSEL

Since introduction of the GTPase inactivating mutation does not always yield a DN Rab (Tisdale et al., 1992), and since in preliminary experiments the nucleotide binding mutant Rab1b$_{N121I}$ caused a stronger Rab1b inactivation phenotype than the GDP-locked mutant Rab1b$_{S22N}$, I chose to substitute isoleucine for the asparagine residue equivalent to Rab1b's N121 to create a panel of DN Rab mutants. The only exception was Rab15, for which I used the GDP-locked T22N mutant instead. Therefore, for all of the Rabs listed in Figure 3.5, I cloned sequences encoding the WT and the indicated mutant protein into the reporter lentiviral vector pLVX Che-hi3 (Figure 2.1B). I, then, used these constructs to make lentiviral particles, which I concentrated and whose titers I determined before using them in the DN Rab screen.

3.6. DN Rab screen: technical considerations

While the technical details involved in performing the DN Rab screen experiments are described in detail in Chapter 2, I wish to underline some technical aspects which I find informative in ensuring a proper interpretation of the results. First, the screen was performed in Huh-7.5 FLuc (Figure 4.2) cells which allowed me to easily quantify changes in the cell mass by measuring luciferase activities in the cell lysates.

Second, I infected these cells with two doses of infectious virus, MOI 25 and 100 I.U./cell, respectively (Figure 4.4). Since the effectiveness of the DN Rabs in inhibiting Rab function is likely correlated with the ratio between the expressed mutant and the natively expressed WT Rab (Nuoffer et al., 1994), by using two doses of Rab-expressing vectors I hoped to enhance the likelihood that I would express just the right amount of DN Rab constructs, which would then allow me to detect DN Rab-mediated changes in cargo secretion.

Third, all infections with a given WT-DN pair of Rabs were done in wells of a single plate to ensure that the wells were exposed to very similar environmental conditions and that any variations among the time lengths needed to process the samples belonging to each WT-DN Rab pair were small. Similarly, luciferase activity and ELISA assays for all paired samples for each of the Rabs were performed on a single plate.

Fourth, the amount of each of the three cargoes tested: albumin, ApoE and ApoB100 was measured in each biological sample. I reasoned that this procedure would help minimize technical and/or biological variations which could cause cargo-related differences in the effects exerted by the inhibition of a given Rab.

3.7. Effects of DN Rab expression on cellular luciferase activity

By comparing the luciferase activities of lysates from cells transduced with DN Rabs with those of the lysates from cells transduced with the corresponding WT Rabs, I found that for most Rabs expression of the DN form did not significantly change the luciferase activity values (Figure 3.6A-B). For roughly one third of the comparisons where luciferase activity significantly differed between the WT and the DN-transduced conditions, the differences were within one Log_2 distance from the reference value. I was encouraged by the lack of any larger differences in luciferase activities. I cannot, based on this data alone, discount the possibility that, under these experimental conditions, DN (or WT) Rab expression was accompanied by any number of toxic effects on cell physiology. However, the magnitude of the differences observed suggests that if any toxic effects accompanied Rab expression, they likely were of a limited nature in this experimental setting.

Figure 3.6. Effects of DN Rab expression on cell mass (next page). Huh-7.5 FLuc cells were transduced with WT (blue) or DN (red) Rab-expressing lentiviruses at MOI of 25 (A) or 100 (B) I.U./cell. A secretion assay was performed at 48 h. Mean luciferase activity values in WT Rab-transduced cells were set to 1. The resulting relative luciferase activities were plotted on a Log_2 scale. Shown are means ± s.d. from n=3 parallel wells. Significant changes in activity (Student's *t*-test, $p<0.05$) are highlighted in gray.

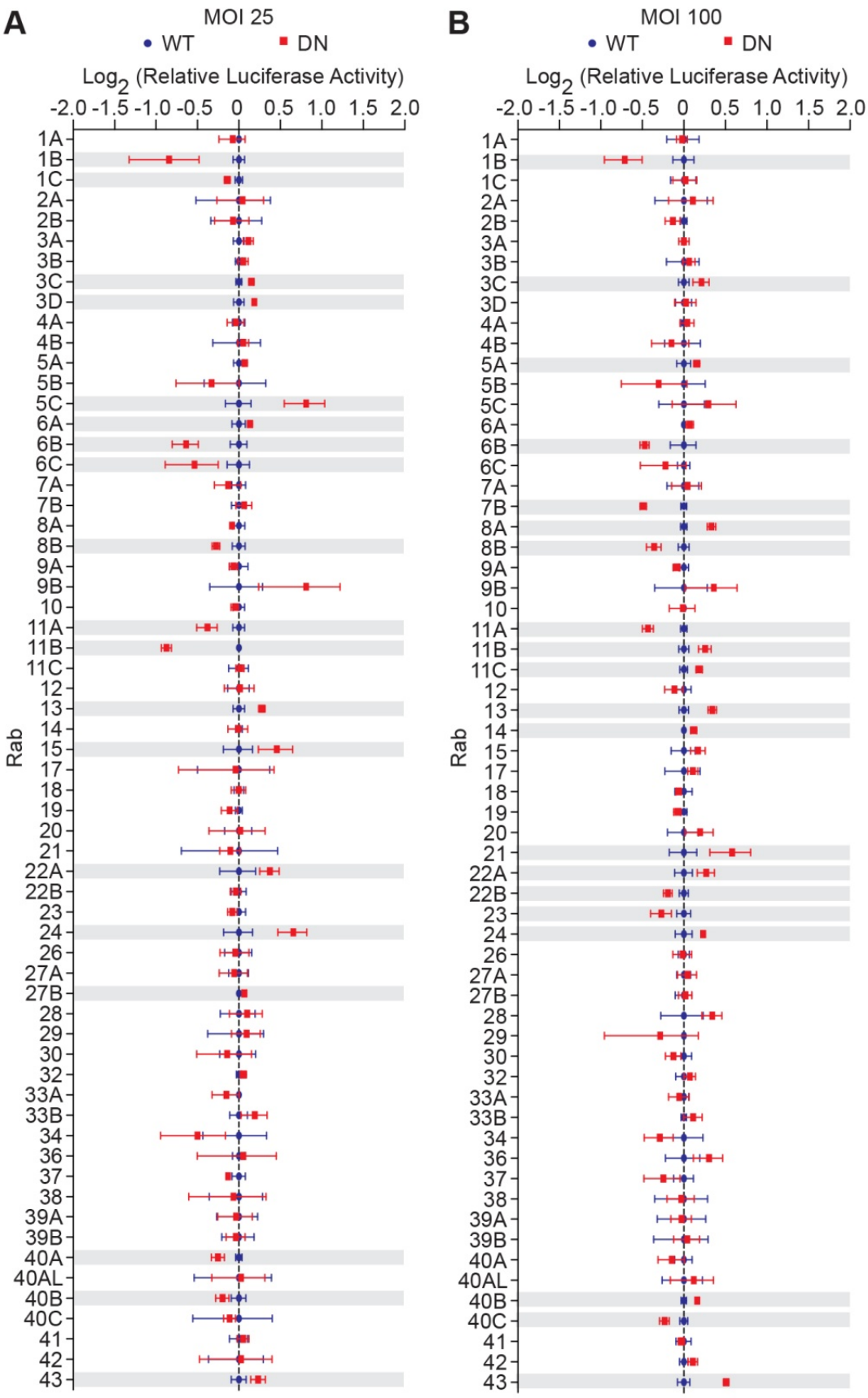
A
MOI 25
WT
DN
Log2 (Relative Luciferase Activity)
-2.0 -1.5 -1.0 -0.5 0 0.5 1.0 1.5 2.0
Rab
1A
1B
1C
2A
2B
3A
3B
3C
3D
4A
4B
5A
5B
5C
6A
6B
6C
7A
7B
8A
8B
9A
9B
10
11A
11B
11C
12
13
14
15
17
18
19
20
21
22A
22B
23
24
26
27A
27B
28
29
30
32
33A
33B
34
36
37
38
39A
39B
40A
40AL
40B
40C
41
42
43
B
MOI 100
WT
DN
Log2 (Relative Luciferase Activity)
-2.0 -1.5 -1.0 -0.5 0 0.5 1.0 1.5 2.0
Rab
1A
1B
1C
2A
2B
3A
3B
3C
3D
4A
4B
5A
5B
5C
6A
6B
6C
7A
7B
8A
8B
9A
9B
10
11A
11B
11C
12
13
14
15
17
18
19
20
21
22A
22B
23
24
26
27A
27B
28
29
30
32
33A
33B
34
36
37
38
39A
39B
40A
40AL
40B
40C
41
42
43

3.8. Effects of DN Rab expression on cargo secretion

For each WT-DN Rab pair tested, for each of the cargoes tested, namely albumin, ApoE and ApoB100, and for each of the two doses of lentivirus particles that I used, I compared the normalized secretion measured in the presence of DN Rab expression to the normalized secretion measured in the presence of the WT Rab expression (Figure 3.1). The results are presented in Figure 3.7A-C for the MOI = 25 I.U./cell condition and in Figure 3.8A-C for the MOI = 100 I.U./cell condition. Each Rab for which I identified a significant difference between the secretion of cargo measured in the presence of the WT form and that measured in the presence of the DN form is highlighted by a gray background bar. In some cases, DN Rab expression caused a decrease in secretion, when compared to WT expression (i.e. DN Rab1c/35 at MOI 100 caused a decrease in the secretion of albumin, ApoE and ApoB100, although the ApoE change was not significant). In other cases, DN Rab expression caused an increase in secretion (i.e. DN Rab11b expression increased the secretion of all three cargoes, and at both doses).

Figure 3.7. Effects of DN Rabs on cargo secretion at MOI 25 I.U./cell (next page). Huh-7.5 FLuc cells were transduced with WT (blue) or DN (red) Rab-expressing lentiviruses at MOI 25 I.U./cell. A secretion assay was performed at 48 h post transduction. Secreted cargo amounts were measured by ELISA and divided by the corresponding well's luciferase activity. The mean secretion values of WT Rab-transduced cells were set to 1. The relative secretion values of albumin (A), ApoE (B) and ApoB100 (C) are plotted on a Log_2 scale. Shown are means ± s.d. from n=3 parallel wells. Significant changes in cargo secretion values (Student's *t*-test with Bonferroni correction, $p<0.0167$) are in gray.

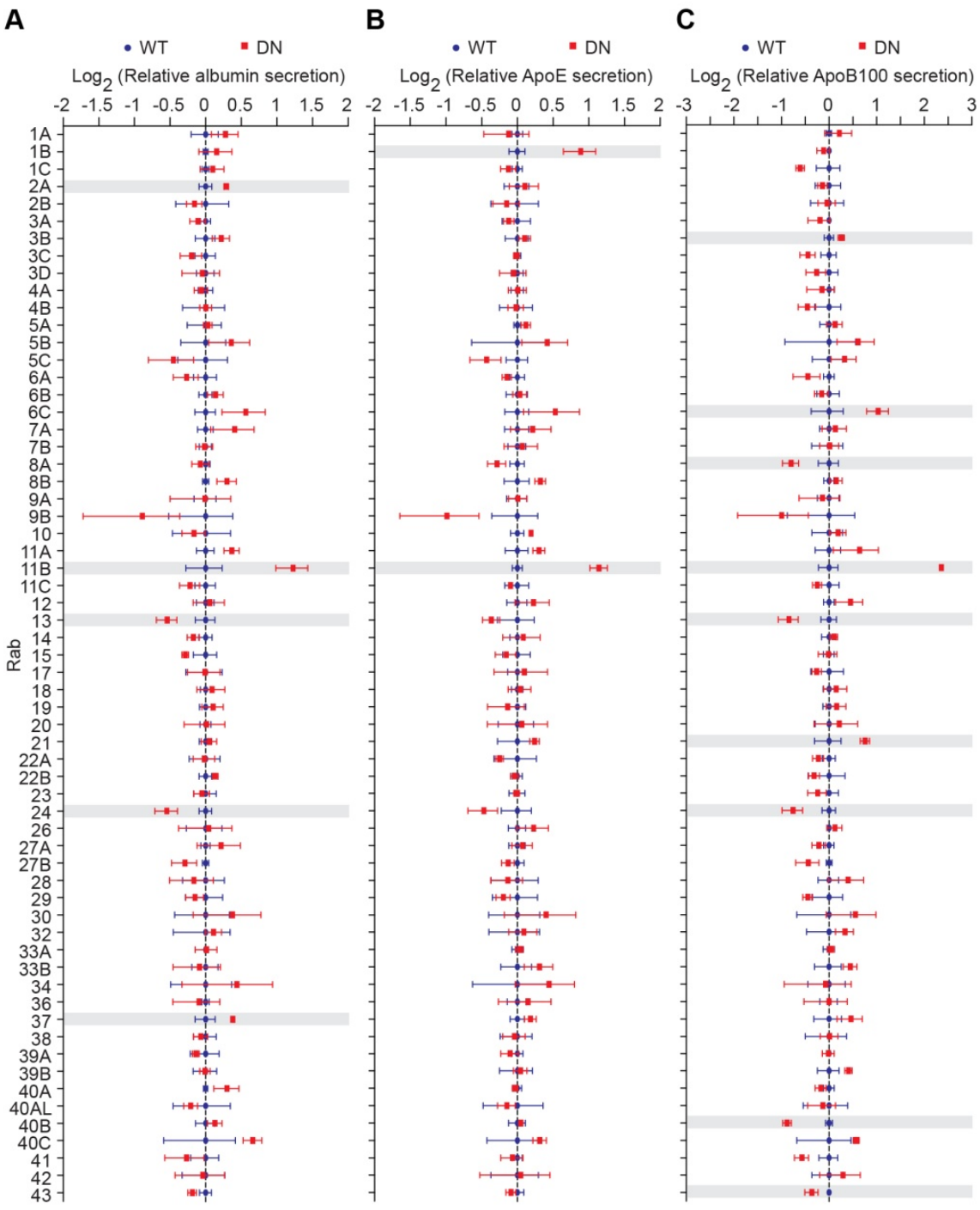
A
B
C
WT
DN
Log2 (Relative albumin secretion)
Log2 (Relative ApoE secretion)
Log2 (Relative ApoB100 secretion)
-2 -1.5 -1 -0.5 0 0.5 1 1.5 2
-3 -2 -1 0 1 2 3
Rab
1A
1B
1C
2A
2B
3A
3B
3C
3D
4A
4B
5A
5B
5C
6A
6B
6C
7A
7B
8A
8B
9A
9B
10
11A
11B
11C
12
13
14
15
17
18
19
20
21
22A
22B
23
24
26
27A
27B
28
29
30
32
33A
33B
34
36
37
38
39A
39B
40A
40AL
40B
40C
41
42
43

Figure 3.8. Effects of DN Rabs on cargo secretion at MOI 100 I.U./cell (next page). Huh-7.5 FLuc cells were transduced with WT (blue) or DN (red) Rab-expressing lentiviruses at MOI 100 I.U./cell. A secretion assay was performed at 48 h post transduction. Secreted cargo amounts were measured by ELISA and divided by the corresponding well's luciferase activity. The mean secretion values of WT Rab-transduced cells were set to 1. The relative secretion values of albumin (A), ApoE (B) and ApoB100 (C) are plotted on a Log_2 scale. Shown are means ± s.d. from n=3 parallel wells. Significant changes in cargo secretion values (Student's *t*-test with Bonferroni correction, $p<0.0167$) are in gray.

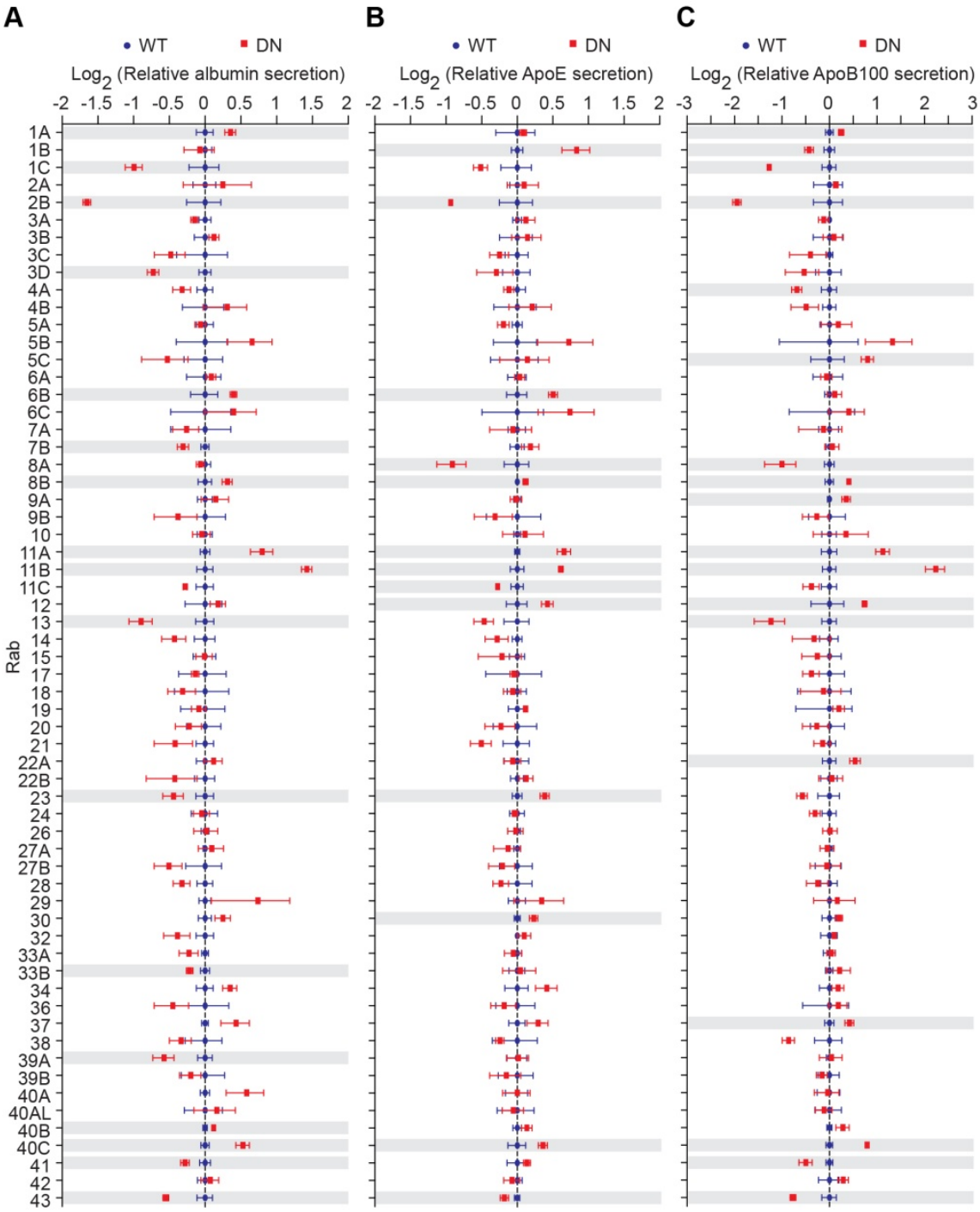
A
B
C
WT
DN
Log2 (Relative albumin secretion)
Log2 (Relative ApoE secretion)
Log2 (Relative ApoB100 secretion)
-2 -1.5 -1 -0.5 0 0.5 1 1.5 2
-2 -1.5 -1 -0.5 0 0.5 1 1.5 2
-3 -2 -1 0 1 2 3
Rab
1A
1B
1C
2A
2B
3A
3B
3C
3D
4A
4B
5A
5B
5C
6A
6B
6C
7A
7B
8A
8B
9A
9B
10
11A
11B
11C
12
13
14
15
17
18
19
20
21
22A
22B
23
24
26
27A
27B
28
29
30
32
33A
33B
34
36
37
38
39A
39B
40A
40AL
40B
40C
41
42
43

To more easily organize and interpret these results, I defined a DN Rab effect score as follows. For each Rab, every instance in which secretion of a cargo was affected was assigned a score of 1. Thus, the maximum score for any given Rab was 6 (2 Rab lentivirus doses tested x 3 cargoes). For the purposes of this analysis, I did not distinguish between a case when cargo secretion was increased and a case when cargo secretion was decreased. I only asked whether the difference between the effect on secretion of the DN Rab was significantly different from the effect of its WT control. Then, I ranked the Rabs in descending order based on their total effect scores (Figure 3.9). For the Rabs which had the same total score, I ranked them in descending order of the sub-score obtained using the higher dose of Rab-expressing lentivirus (Figure 3.9, filled bars). The hits were also organized by known protein function (Table 3.1), following the information summarized in a recent comprehensive review (Hutagalung and Novick, 2011). Of note, most significant effects were caused by WT-DN Rab pairs previously implicated in exocytic (including ER to Golgi transport, intra-Golgi transport, Golgi structure maintenance; post-Golgi exocytosis) or recycling processes (Table 3.1). Conversely, Rabs involved in endocytic trafficking had either a low effect on secretion, or none at all (Figure 3.9 and Table 3.1). Similarly, the Rab3 subfamily, whose major function is to control regulated exocytosis (Fukuda, 2008), such as that of neurotransmitters in the nervous system, was underrepresented among the hits of this DN Rab screen. The functional clustering of the hits was thus consistent with albumin and the lipoproteins being constitutively secreted cargoes (Dashti et al., 1980), and attests to the usefulness of the methodology that we developed to identify likely regulators of cargo secretion.

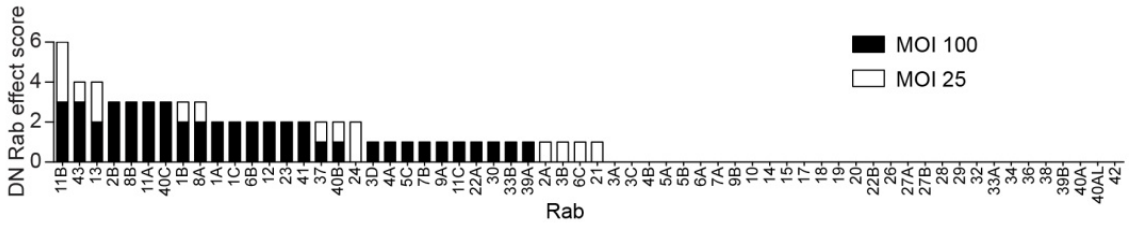

Figure 3.9 Ranking of Rab effects on cargo secretion. To each Rab, for each cargo whose secretion the DN Rab expression significantly changed, an effect score of 1 was awarded. Scores accumulated at MOI 25 I.U./cell are marked with open bars; scores accumulated at MOI 100 I.U. /cell are marked with filled bars. The Rabs are ranked first in descending order of the total score, and then in descending order of the score obtained at MOI 100 I.U./cell.

3.9. Rab expression profiles in hepatic cells

I next inquired whether the Rabs that I identified as likely regulators of hepatic cargo secretion were expressed in the cells in which I performed the screen. If a DN effect was detected but the endogenous Rab was not expressed, I was concerned that the effect may have been unspecific. I thank Dr. Joseph Luna for providing RNAseq data (Luna et al., 2015) for Rab gene expression in Huh-7.5 cells (Figure 3.10A). I furthermore thank Drs. Joseph Luna, William Schneider and Linda Andrus for providing unpublished RNAseq expression data from human fetal liver cultures (HFLC, Figure 3.10B). HFLCs represent a primary hepatocyte cell culture system (Andrus et al., 2011; Marukian et al., 2011). I ranked the Rabs in ascending order of their expression level in each of the two hepatocyte cell culture systems. I also included in this analysis several genes known to be ubiquitously expressed (such as those encoding β-actin and β-tubulin), genes expressed in hepatocytes (such as those encoding ApoE, ApoB100, albumin, and the tight junction proteins claudin-1 and occludin), and genes whose expression is

expected to be confined to other cell types (such as those encoding the T-cell receptor subunits α and β, and the photoreceptor rhodopsin). Unsurprisingly, the housekeeping genes and the hepatocyte-specific genes were amongst the highest expressed genes, while the non-hepatocyte genes had undetectable expression levels (I graphed these nonetheless by assigning them an expression level of -10 Log_2CPM. Of the Rabs which I identified as hits in the DN screen (Figure 3.9), Rabs 40b and 40c had expression levels amongst the lowest of all the Rabs in the Huh-7.5 cells. Rab41, similarly, had a very low expression level in the Huh-7.5 cells, while its expression was not detected in HFLCs. Rab11c/25 transcripts were not detected in the Huh-7.5 cells, and their expression level was also very low in HFLCs. Due to their low or even undetectable expression levels, Rabs 11c, 40b, 40c and 41 were not considered for further analysis.

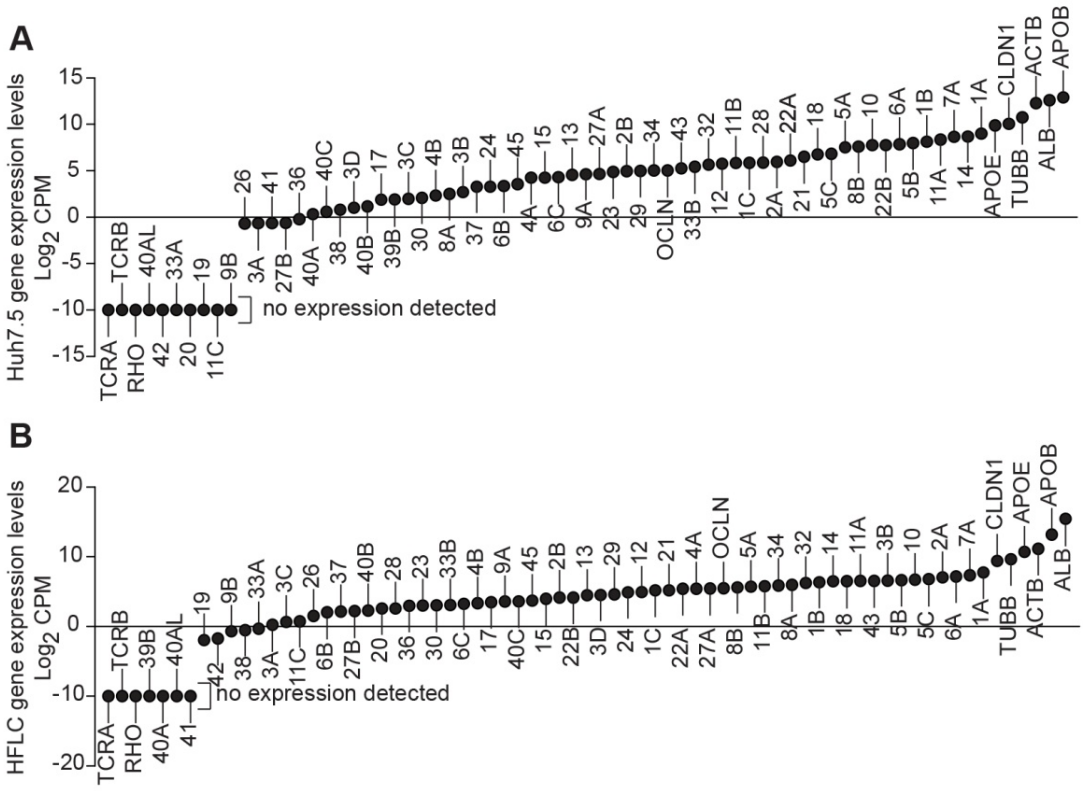

Figure 3.10. Rab expression levels in hepatic cultures. Rab-specific transcript expression levels (Log_2CPM) from RNAseq analysis of Huh-7.5 (A) and HFLC (B) cultures were ranked in ascending order. The Rabs are listed by their numbers. Included were expression levels of genes encoding the T cell receptor subunits α and β, (*TCRA*, and *TCRB*, respectively), rhodopsin (*RHO*), β-actin (*ACTB*), β-tubulin (*TUBB*), occludin (*OCLN*), claudin1 (*CLDN1*), albumin (*ALB*), ApoE (*APOE*) and ApoB100 (*APOB*). When no reads mapping to the transcript were detected, an artificially low -10 Log_2CPM was assigned to the respective constructs.

3.10. On the interpretability and meaning of the results

For the remaining Rab hits, further investigation is required to confirm their involvement in cargo secretion. The screen only identified whether there was a difference between the effect that a WT Rab had on secretion and the effect of its DN mutant. The screen did not distinguish between an effect on secretion mediated by changes in the expression of cargo mRNAs, in the rate of their translation or translocation into the ER, or in the rate of protein transport along the secretory pathway. Furthermore, it is important to bear in mind that if a DN Rab caused a relative decrease in cargo secretion, this effect may have been mediated through inhibition of secretion by the DN Rab, through stimulation of secretion by the corresponding WT Rab, or through a combination of these two scenarios. Conversely, if a DN Rab caused a relative increase in cargo secretion, this may have been mediated through stimulation of secretion by the DN Rab, through inhibition of secretion by the corresponding WT Rab, or through a combination of these two scenarios. Lastly, some DN Rabs affected the secretion of more than one cargo. In some cases, such as those of Rab11A and Rab11B, the secretion of all cargoes was affected in the same direction (Figures 3.7 and 3.8). A possible explanation of such a phenotype is that the examined Rab controls the transport of all the cargoes whose secretion was affected. In other cases, a DN Rab caused a relative increase in the secretion of one cargo, while, in the same sample, causing a relative decrease in the secretion of another cargo. For example, Rab1b appeared to stimulate ApoE secretion but at the same time to inhibit ApoB secretion (Figure 3.8 and Chapter 5). A possible explanation of such a phenotype is that the Rab differentially controls the transport of the

several cargoes tested; which would make the Rab an interesting candidate for further investigation.

3.11. Overview of the hits

The Rabs which were determined to be expressed in the Huh-7.5 cells and in the HFLCs, and whose DN mutants significantly altered the secretion of one or several of the hepatic cargoes tested, were considered for further analysis. Ongoing efforts to elucidate the involvement of Rabs 11a, 11b, 8a, and 8b in hepatic cargo secretion are presented in greater detail in Chapter 4. The characterization of the differential control of hepatic cargo egress by Rab1b is presented in Chapter 5. I summarize herein some possibly interesting notes that I have gathered on documented functions of some of the other Rab hits. I also suggest potential means by which these Rabs may control cargo secretion in general, and secretion of the hepatic cargoes albumin, the lipoproteins, and HCV, in particular. Some of these functions are selectively summarized in Table 3.1.

Rab1c (more widely known as Rab35) controls various aspects of endocytic recycling and endosome function, including delivery of membrane vesicles to the cytokinesis furrow of dividing cells (Kouranti et al., 2006). Since Rab1c/35 inactivation impaired the secretion of all the cargoes tested, it would be interesting to analyze the extent to which, if any, it mediates transport of vesicles containing these cargoes. The experiments would need to carefully rule out domino effects on secretion caused downstream of inhibition of cell division, which would be a major general concern in all experiments inhibiting Rab1c/35 function.

Table 3.1. Selected known functions of the DN Rab screen hits.

Function	Rab	References
ER to Golgi traffic; intra Golgi traffic; Golgi structure maintenance	Rab1a, Rab1b	(Plutner et al., 1991; Segev et al., 1988; Tisdale et al., 1992)
	Rab2a, Rab2b	(Chavrier et al., 1990a; Tisdale and Balch, 1996; Tisdale et al., 1992)
	Rab6b, Rab6c	(Goud et al., 1990; Martinez et al., 1994)
	Rab30	(Thomas et al., 2009)
	Rab33b	(Zheng et al., 1998)
	Rab43	(Dejgaard et al., 2008; Fuchs et al., 2007; Haas et al., 2007)
Post-Golgi secretion and recycling	Rab1c/35	(Allaire et al., 2010; Hsu et al., 2010; Patino-Lopez et al., 2008)
	Rab3b Rab3d/16	(Fischer von Mollard et al., 1990)
	Rab8a Rab8b	(Huber et al., 1993b)
	Rab11a Rab11b Rab11c/25	(Casanova et al., 1999; Ren et al., 1998; Ullrich et al., 1996)
	Rab13	(Nokes et al., 2008; Zahraoui et al., 1994)
Autophagy	Rab1a Rab1b	(Winslow et al., 2010; Zoppino et al., 2010)
	Rab24	(Munafo and Colombo, 2002)
	Rab33b	(Itoh et al., 2008)
Endocytic transport and endolysosomal functions	Rab1c/35	(Kouranti et al., 2006)
	Rab4a	(van der Sluijs et al., 1992; Van Der Sluijs et al., 1991)
	Rab5c	(Chavrier et al., 1990a)
	Rab7b	(Chavrier et al., 1990a)
	Rab9a	(Lombardi et al., 1993)
	Rab12	(Matsui et al., 2011)
	Rab21	(Simpson et al., 2004)
	Rab22a	(Mesa et al., 2001)
	Rab23	(Eggenschwiler et al., 2001; Evans et al., 2003)
	Rab39a	(Chen et al., 2003)

Rab3d/16 inactivation affected albumin secretion in our assays, and Rab3d has previously been implicated in HCV release (Coller et al., 2012). It may well be one of the Rabs which controls the final stages of cargo release. From the same functional group of Rabs associated with regulated secretion, the Rabs 3b and 37 also exhibited phenotypes in our assays and may also be involved in hepatic cargo secretion (Fukuda, 2008).

Rab12 inactivation stimulated ApoE and ApoB100 release, but not albumin release. A previous study has implicated Rab12 in regulating transport of cargo destined for degradation from a recycling compartment to an endolysosomal compartment (Matsui et al., 2011). Since hepatocytes control lipoprotein release by in part regulating their intracellular degradation, including from post-Golgi compartments (Pan et al., 2008a), and since Rab12 mediates such a process, then the observed selective stimulation of cargo secretion could be easily explained. The lipoprotein cargo that would no longer be targeted for degradation in the presence of DN Rab12 could instead find its way out of the cells. It would be interesting to evaluate if the density distribution profile of secreted ApoB100-containing lipoproteins changes in response to Rab12 inactivation.

Rab13 inactivation impaired the release of all three cargoes I tested. An inquiry into Rab13 function could tease out whether Golgi to TGN traffic inhibition by expression of DN Rab13 (Nokes et al., 2008) is the only cause or the main cause of the observed phenotype, or whether other Rab13 secretory functions may also play a part (Sun et al., 2014). For experiments also focusing on HCV release, care should be taken to avoid inhibition of early events in the HCV life cycle by inactivation of Rab13 function in tight junction formation and maintenance. Such a concern is valid since HCV uses the tight junction proteins claudin-1 and occludin as essential entry co-receptors (Evans et al.,

2007; Ploss et al., 2009), while the same tight junction proteins are known Rab13 cargoes (Marzesco et al., 2002; Morimoto et al., 2005; Terai et al., 2006; Yamamura et al., 2008; Zahraoui et al., 1994). Tight junction disruption could thus interfere with HCV infection and may skew interpretation of any HCV release experiments where the HCV was introduced into the cells via infection.

Rab23 also exhibited an interesting phenotype, since its DN mutant decreased albumin secretion while simultaneously increasing ApoE secretion. Rab23 regulates Sonic hedgehog signaling and has been implicated in the developmental disease Carpenter syndrome (Eggenschwiler et al., 2001; Evans et al., 2003; Jenkins et al., 2007; Wang et al., 2006). Future experiments would need to carefully account for any change in the activation state of the cells that may result from interference with Rab23 function.

Autophagy has also been implicated in the regulation of the secretion of hepatic lipoproteins, HCV and other viruses (Chen et al., 2015; Pan et al., 2008a; Shrivastava et al., 2015). That several Rabs associated with autophagosome formation, namely Rabs 1, 24, and 33B (Itoh et al., 2008; Munafo and Colombo, 2002; Winslow et al., 2010; Zoppino et al., 2010) were identified as hits in the secretion screen attests to the importance of this process for cell physiology and potentially for the secretion or the quality control of these cargoes.

Finally, several other Rabs (4a, 5c, 7b, 9a, 21, 22a and 39a) involved in endocytic and degradative processes were hits of the DN Rab screen, but their cumulative score was relatively small (Figure 3.9 and Table 3.1). It is possible that these effects were indirect.

3.12. Discussion: On the future the DN Rab screen

As I hope I have shown in this chapter, and as I will describe in further detail in the following two chapters, expression of a collection of 62 DN Rab GTPases has proven to be an effective and unbiased method that I used to inhibit secretion events from cells, and to identify transport pathways utilized by the tested secretory cargoes. The experiments that I described above outline a succession of inquiry steps that can be easily applied to other cellular systems and other cargoes. Indeed, since the Rab constructs were expressed using VSVg-pseudotyped lentiviruses, they could be easily and efficiently delivered to a great number of other cell types, including hard to transfect ones. I suspect that the facility with which I was able to transduce the overwhelming majority (Figure 3.4) of the cells in culture may well have been instrumental in ensuring the success of the approach. While preparation of the virus stocks was not trivial, it did not necessitate large scale operations or specialized equipment. It was particularly advantageous that ultracentrifugation was not required to concentrate the virus stocks. Furthermore, the titer determination method was sufficiently easy and amenable to multiplexing, even though I did all the steps manually. All of these methods can easily be transferred to an averagely equipped laboratory that also had access to a flow cytometer.

The methodology of the screen could nevertheless be further improved. For example, the lentiviral vectors could be modified to express *Renilla* luciferase from an IRES downstream of the Rab protein. In this setting, the efficiency of target cell transduction could be easily monitored biochemically, while continuing to estimate cell mass by the FLuc measurements (Figure 3.2). Alternatively, a cargo of interest could be modified by tagging it with an enzymatic reporter, such as a luciferase domain. Of

course, functional assays would need to be first performed to confirm that the tagged cargo molecule reproduced the secretory behavior of the endogenous protein, as outlined for ApoE-GFP in Chapter 6. If the tagged cargo proved functional, however, fast, easy and inexpensive enzymatic assays of the media and of the cell lysates may replace the somewhat cumbersome and expensive ELISA assays that I employed, and would therefore mitigate the effort and cost associated with developing and characterizing such a cargo reporter.

Chapter 4

Ongoing Characterization of the Involvement of Rab11 and Rab8 in Hepatic Cargo Secretion

The DN Rab screen (discussed in the previous chapter) identified several potential regulators of hepatic cargo egress. For reasons described throughout this chapter, the Rabs 11a, 11b, 8a, and 8b were particularly interesting hits. Efforts are underway to understand how are these Rabs, as well as the transport pathways that they regulate, involved in lipoprotein, albumin, and HCV secretion. Since this work is not yet complete, I present only the preliminary experiments that I have set up to advance this inquiry. I also outline some immediately obvious experiments that I am performing in order to gain a better understanding of the process that I am studying. Experiments further down the line will need to be decided based on results that have not yet been generated, so I shall not subject the reader to an exercise in long-term experimental planning. I do discuss however the implications of some possible findings, while being fully aware that, in the large scheme of scientific inquiry, experiments may provide unexpected results.

4.1. Overview: Rab11 and Rab8 functions in cargo secretion

Rab11a and Rab11b were interesting hits of the DN Rab screen (Chapter 3), since expression of their DN mutants caused some of the largest phenotypes measured. The major known functions of the Rab11 subfamily members Rab11a, Rab11b and Rab11c (also known as Rab25), have been recently reviewed (Kelly et al., 2012; Welz et al., 2014) and are summarized in Table 4.1. In non-polarized cells, Rab11 localizes at and controls the function of the recycling endosome, including recycling and secretory

activities associated with it. For example, Rab11 mediates transferrin recycling and post-Golgi exocytosis of VSVg in non-polarized cells (Chen et al., 1998). In contrast, in polarized cells, Rab11 functions primarily at the apical pole, where it localizes at the apical recycling endosome (Casanova et al., 1999; Goldenring et al., 1996). There, Rab11 primarily controls secretory and recycling activities of apical cargoes, with little or no involvement in basolateral secretion and recycling (Brown et al., 2000; Casanova et al., 1999; Cresawn et al., 2007; Hoekstra et al., 2004; Leung et al., 2000; Sheff et al., 1999; Thompson et al., 2007; Wang et al., 2000).

Table 4.1 Summary of known Rab11 functions

Rab11 cargoes or functions	Reference
Plasma membrane receptor transport or recycling	
Transferrin and the transferrin receptor in non-polarized cells	(Ren et al., 1998; Ullrich et al., 1996; Wilcke et al., 2000)
Fc receptor FcRn	(Tzaban et al., 2009; Ward et al., 2005)
Glucose transporter GLUT4	(Uhlig et al., 2005)
Chemokine scavenging decoy receptor D6	(Bonecchi et al., 2008)
Langerin and CD1α in Langerhans cells	(Gidon et al., 2012; Salamero et al., 2001; Uzan-Gafsou et al., 2007)
Transforming growth factor-β (TGF-β) receptor	(Mitchell et al., 2004)
Fibroblast growth factor receptor 4, FGFR4	(Haugsten et al., 2014)
Protease-activated receptor 2, PAR2	(Roosterman et al., 2003)
CXCR2	(Fan et al., 2003; Fan et al., 2004)
Low-affinity formyl peptide receptor FPRL1	(Ernst et al., 2004)
Angiotensin II type 1 receptor AT_1R	(Dale et al., 2004; Hunyady et al., 2002)
Thromboxane A_2 receptor TPβ	(Hamelin et al., 2005; Theriault et al., 2004)
β1-adrenergic receptor β1AR	(Gardner et al., 2011)
β2-adrenergic receptors β2AR	(Moore et al., 2004)
M_4 muscarinic acetylcholine receptor	(Volpicelli et al., 2002)
μ-opioid receptor	(Wang et al., 2008)
V2 vasopressin receptor	(Innamorati et al., 2001)
E-cadherin	(Lock and Stow, 2005)

Table 4.1 Summary of known Rab11 functions

Rab11 cargoes or functions	Reference
Channel and transporter recycling	
H^+-K^+-ATPase of gastric parietal cells	(Calhoun and Goldenring, 1997; Calhoun et al., 1998; Duman et al., 1999; Goldenring et al., 1994)
V-ATPase in salivary duct cells	(Oehlke et al., 2011)
Bile salt export pump, BSEP or ABCB11	(Wakabayashi et al., 2005; Wakabayashi et al., 2004)
Hepatic multidrug resistance-associated protein 2, MRP2	(Park et al., 2014)
Cystic fibrosis transmembrane conductance regulator, CFTR	(Gentzsch et al., 2004; Silvis et al., 2009; Swiatecka-Urban et al., 2005; Swiatecka-Urban et al., 2007)
Dopamine transporter	(Furman et al., 2009)
Various cation channels: HCN2, HCN4, KCNA5, KCNQ1, KCNE1, TRPV5, TRPV6, $Ca_v1.2$, ENaC	(Best et al., 2011; Butterworth et al., 2012; Hardel et al., 2008; McEwen et al., 2007; Seebohm et al., 2007; van de Graaf et al., 2006)
Secreted cargo transport	
Insulin	(Sugawara et al., 2009)
Human growth hormone	(Khvotchev et al., 2003)
Interferon-γ and tumor necrosis factor α	(Reefman et al., 2010)
Soluble vascular endothelial growth factor	(Jung et al., 2012);
Matrix metalloproteinase secretion	(Yu et al., 2014)
Other Rab11 functions	
Ciliogenesis and transport to the primary cilium membrane	(Deretic et al., 1996; Knodler et al., 2010; Li et al., 2007; Mazelova et al., 2009a; Satoh et al., 2005; Thuenauer et al., 2014; Ward et al., 2011; Westlake et al., 2011)
Intestinal and hepatic apical transport defects associated with microvillus inclusion disease	(Girard et al., 2014; Knowles et al., 2014; Knowles et al., 2015)
Exosome production and multivesicular body-plasma membrane fusion	(Savina et al., 2005; Savina et al., 2002)
β-amyloid production	(Udayar et al., 2013)
Stretch-regulated exocytosis of discoidal-fusiform vesicles in bladder umbrella cells	(Khandelwal et al., 2013; Khandelwal et al., 2008)
Colocalization with epidermal lamellar granules in keratinocytes	(Ishida-Yamamoto et al., 2007)
Melanin transfer between melanocytes and keratinocytes	(Tarafder et al., 2014)
Macrophage phagocytosis	(Cox et al., 2000)
Sorting activities in the renal proximal tubule	(Mattila et al., 2014)

Table 4.1 Summary of known Rab11 functions

Rab11 cargoes or functions	Reference
Membrane recycling during cell migration	(Assaker et al., 2010; Jones et al., 2006; Kessler et al., 2012; Prigozhina and Waterman-Storer, 2006)
Membrane delivery during cytokinesis	(Fielding et al., 2005; Neto et al., 2013; Wilson et al., 2005)
Neuronal dendrite and axon growth	(Takano et al., 2012; Takano et al., 2014)
Developmental signaling	(Emery et al., 2005; Jafar-Nejad et al., 2005; Ossipova et al., 2015; Ossipova et al., 2014)
General apical lumen formation	(Alvers et al., 2014; Bryant et al., 2010)
Bile canaliculus formation	(Wakabayashi et al., 2005)
IgA transcytosis	(Casanova et al., 1999; Sheff et al., 1999; Xu et al., 2011; Xu et al., 2013)
VSVg post-Golgi transport in non-polarized cells	(Chen et al., 1998; de Graaf et al., 2004)
Functions in host cell-pathogen interactions	
HIV-1 Vpu function	(Varthakavi et al., 2006)
Influenza A virus particle formation	(Amorim et al., 2011; Bruce et al., 2010; Chou et al., 2013; Eisfeld et al., 2011; Momose et al., 2011)
Hantavirus (Andes virus) release	(Rowe et al., 2008)
HCV release	(Coller et al., 2012)
Porphyromonas gingivalis exit from recycling endosomes	(Takeuchi et al., 2011)

Functionally associated with Rab11 are two other hits of our screen, the Rab8 isoforms Rab8a (Chavrier et al., 1990b; Chen et al., 1993) and Rab8b (Armstrong et al., 1996). They localize to the cell periphery (Chen et al., 1993) and have been involved in cargo secretion (Huber et al., 1993a; Huber et al., 1993b), cell shape regulation (Peranen, 2011), and primary cilium formation and function (Das and Guo, 2011; Nachury et al., 2007). These known functions are summarized in Table 4.2. As with Rab11, Rab8 involvement in both basolateral (Huber et al., 1993a; Huber et al., 1993b) and apical (Nachury et al., 2007; Sato et al., 2014; Sato et al., 2007) cargo transport has been

described. The functional coordination between Rab11 and Rab8 (Khandelwal et al., 2013; Knodler et al., 2010; Wang et al., 2012; Westlake et al., 2011) is likely due to a well described axis of control that involves these two GTPases: GTP-loaded Rab11 recruits Rabin8, a Rab8-specific GEF, which in turn recruits and activates Rab8 (Knodler et al., 2010; Westlake et al., 2011). Unsurprisingly therefore, in our assays, the phenotype associated with DN Rab11a or Rab11b expression, namely an increased relative secretion, was mirrored by that associated with DN Rab8b expression, which also caused a significant increase in relative cargo secretion (Figures 3.7 and 3.8). Expression of DN Rab8a, in contrast, impaired the relative cargo secretion (Figures 3.7 and 3.8). That inactivation of three Rabs that are expected to function in tandem (Rabs 11a, 11b, and 8b) caused similar effects on cargo secretion strongly supports the conclusion that these Rabs are likely involved in the same secretion pathway(s).

Table 4.2 Summary of known Rab8 functions

Rab8 cargoes or functions	References
VSVg	(Ang et al., 2003; Ang et al., 2004; Huber et al., 1993b; Schuck et al., 2007)
Semliki Forest virus E2 glycoprotein transport	(Huber et al., 1993a)
Intestinal and hepatic apical transport defects associated with microvillus inclusion disease	(Knowles et al., 2014; Sato et al., 2014; Sato et al., 2007)
Primary ciliogenesis and transport	(Feng et al., 2012; Knodler et al., 2010; Nachury et al., 2007; Omori et al., 2008; Sato et al., 2014; Westlake et al., 2011) (Deretic et al., 1995; Moritz et al., 2001; Wang et al., 2012; Ward et al., 2011)
Cell membrane protrusion formation and actin reorganization	(Hattula et al., 2002; Hattula et al., 2006; Huber et al., 1993a; Huber et al., 1995; Peranen et al., 1996; Powell and Temesvari, 2004; Simons et al., 1999)
Wnt signaling	(Demir et al., 2013)
Stretch-regulaterd exocytosis of discoidal-fusiform vesicles in bladder umbrella cells	(Khandelwal et al., 2013)

Table 4.2 Summary of known Rab8 functions

Rab8 cargoes or functions	References
Vesicle delivery during cytokinesis	(Kaplan and Reiner, 2011)
Melanosome movement	(Chabrillat et al., 2005; Chakraborty et al., 2003)
Glucose transporter GLUT4 vesicle translocation	(Ishikura and Klip, 2008; Randhawa et al., 2008; Sun et al., 2010b)
Zymogen granule formation in pancreatic acinar cells	(Faust et al., 2008)
Cryptococcus neoformans capsular polysaccharide secretion	(Yoneda and Doering, 2006)
E-cadherin transport	(Yamamura et al., 2008)
Membrane Type-1 matrix metalloproteinase secretion	(Bravo-Cordero et al., 2007)
Adenocorticotropic hormone secretion	(Chen et al., 2001)
AMPA glutamate receptor recycling	(Brown et al., 2007; Gerges et al., 2004)
Anti-mycobacterial autophagy	(Pilli et al., 2012)
Transferrin receptor traffic	(Vaibhava et al., 2012)
Apical lumen formation	(Galvez-Santisteban et al., 2012)
Metabotropic glutamate receptor subtype 1 traffic	(Esseltine et al., 2012)
Dense granule release in platelets	(Hampson et al., 2013)
Endospanin interaction	(Hirvonen et al., 2013)
KCNN4 potassium channel trafficking	(Bertuccio et al., 2014)
Cytotoxic T-lymphocyte-associated protein 4	(Banton et al., 2014)
α_{2B}- and β_2-Adrenergic receptors	(Dong et al., 2010)
Dengue virus 2	(Xu et al., 2009; Xu et al., 2008)
ABCA1 function and cholesterol efflux	(Linder et al., 2009; Linder et al., 2007)
Sucrase-isomaltase and lactase-phlorizin hydrolase	(Cramm-Behrens et al., 2008)

How do Rab11 and Rab8 GTPases control hepatic cargo secretion? In my hands, Rab11a, 11b and 8b inactivation by expression of DN mutants resulted in significant stimulation of the secretion of albumin, ApoE and ApoB100, while DN Rab8a expression inhibited cargo secretion (Figures 3.7 and 3.8). Albumin, ApoE and ApoB100 are expected to be secreted basolaterally, since all are secreted into the bloodstream. It is not surprising therefore that inactivation of a basolateral secretion factor, Rab8a (Huber et al.,

1993a; Huber et al., 1993b), would result in decreased secretion of these cargoes. That inactivation of Rabs primarily involved with apical transport (Rabs 11a, 11b, and 8b) would result in stimulation of basolateral cargo secretion could be easily explained if competition existed between apical and basolateral secretion activities. Common factors utilized by both apical and basolateral secretion processes (recycling endosome membranes come to mind as obvious candidates, although Rab effectors or other vesicular traffic regulators may also be involved) could be limiting. In such a scenario, if apical secretion is stimulated (by WT Rab11 or 8b overexpression), then basolateral secretion is expected to become inhibited. Conversely, if apical secretion is impaired (by DN Rab11 or 8b overexpression), then basolateral secretion is expected to become stimulated. If either or both of the above scenarios is true, then the overall effect of paired WT-DN Rab expression would be a relative stimulation of basolateral cargo secretion, similar to what I observed. Of course, other plausible transport regulation scenarios could be invoked to explain the observed phenotype.

The pattern of Rab11 and Rab8 potential involvement in polarized hepatic cargo secretion that I proposed above is corroborated by the findings of a study testing the function of these Rabs in the release of Andes virus, a New World hantavirus (Rowe et al., 2008). Several hantaviruses, the etiologic agents of the often lethal hantavirus pulmonary syndrome, have been shown to be released primarily at the apical side of polarized cell cultures (Krautkramer et al., 2012; Ravkov et al., 1997; Rowe and Pekosz, 2006), with roughly 1,000-fold higher viral titers being shed apically compared to basolaterally (Ravkov et al., 1997; Rowe and Pekosz, 2006). This preference for polarized apical release is consistent with a predominantly respiratory mode of Andes

virus transmission (Padula et al., 2004). Andes virus release was severely inhibited by Rab11a, 11a and 11b, or 8a and 8b knockdown, but not by Rab8a knockdown alone (Rowe et al., 2008). While these experiments were done in sparsely-plated monolayer-grown African green monkey kidney cells Vero E6/C1008 (Rowe et al., 2008), I wish to emphasize that these cells do possess the capacity to form polarized monolayers and to support polarized cargo transport (Srinivas et al., 1986; Zhou et al., 2011). In this context, the similarity between my findings and those of (Rowe et al., 2008) lie in the functional grouping of the Rab effects. Rab11a, 11b and 8b inhibition apparently stimulated basolateral cargo secretion (Figures 3.7 and 3.8), while Rab11a and 8b inhibition impaired apical cargo secretion (Rowe et al., 2008). In contrast Rab8a inhibition apparently impaired basolateral cargo secretion (figures 3.7 and 3.8), while not affecting (or even slightly stimulating) apical cargo secretion (Rowe et al., 2008). These correlated observations, therefore, together with the cumulative knowledge of Rab11 and Rab8 involvement in polarized cargo secretion (Tables 4.1 and 4.2), identify these Rabs as interesting targets more in-depth investigations.

4.2. Experiments investigating Rab11 and Rab8 involvement in secretion

The approach that I am using to investigate the involvement of Rab11 and Rab8 in hepatic cargo secretion parallels to some extent the line of inquiry that I pursued to investigate the involvement of Rab1b in hepatic cargo secretion and which I present in detail in the next chapter. Briefly, the following steps are part of my immediate experimental plan:

1. Repeat the experiments detailed in the DN Rab screen to confirm the reproducibility of the observed phenotype. Also include in this assay the GTPase-

deficient and the GDP-restricted DN Rab mutants, besides the already used nucleotide-binding mutants.

2. Quantify cargo expression levels in the presence of DN Rab expression to determine whether any DN Rab-associated changes in expression levels may need to be accounted for when interpreting the observed changes in cargo secretion.
3. Inducibly express DN and WT Rab11 and Rab8 constructs and quantify cargo secretion. As explained in more detail below and in Chapter 5, inducible DN Rab expression is preferable to lentivirus-mediated transient expression, since potentially confounding experimental variations associated with lentivirus transduction may be easily avoided.
4. Perform colocalization analyses between the Rabs and the cargo. I show in Chapter 6 that an ApoE-GFP fusion protein is functional with respect to lipoprotein egress, which will facilitate such colocalization experiments.
5. Assess the effect of inhibition of Rab11 and Rab8 on cargo egress from a polarized, primary hepatocyte-like cell culture system.
6. Assess the effects of DN Rab11 and Rab8 expression on HCV egress.

Some of the experiments outlined above have been performed, and I present my findings below.

4.3. Effects of expression of a panel of DN Rab11 and Rab8 mutants on hepatic cargo secretion

To confirm the secretion phenotypes that I observed when I overexpressed the nucleotide-binding DN mutants of Rab11 and Rab8, I repeated the lentivirus infection experiment. This time, besides the WT and the nucleotide-binding DN Rab mutants, I included both the GDP-restricted and GTPase mutants of Rabs 11a, 11b, 8a, and 8b. I reasoned that if one of a given Rab's mutants specifically affected cargo secretion, then the other mutants are also likely to do so, since they likely inhibit the same process, albeit at a different stage. In a parallel experiment, I also quantified cargo mRNA levels in the transduced cells to determine whether Rab expression was associated with changes in cargo expression that may account, at least in part, for the secretion phenotype observed (Figure 4.1).

Figure 4.1. Confirmation of the effects of DN Rab11 and Rab8 expression on cargo secretion (next page). (A) Huh-7.5 FLuc cells were transduced with 100 I.U./cell of lentiviruses expressing the indicated constructs. At 48 h, a secretion assay was performed. Secreted cargo amounts and lysate luciferase activities were measured. Normalized secreted cargo amounts are shown relative to the WT values, on a Log_2 scale. (B) Huh-7.5 cells were transduced as in (A), RNA was extracted at 48 h post transduction, and cargo mRNA levels were measured. Shown are relative cargo expression levels, on a Log_2 scale. (A and B). Shown are means ± s.d. from n=3 parallel wells. Statistical significance (Student's *t* test): *, $p<0.05$; **, $p<0.01$; ***, $p<0.001$: ****, $p<0.0001$.

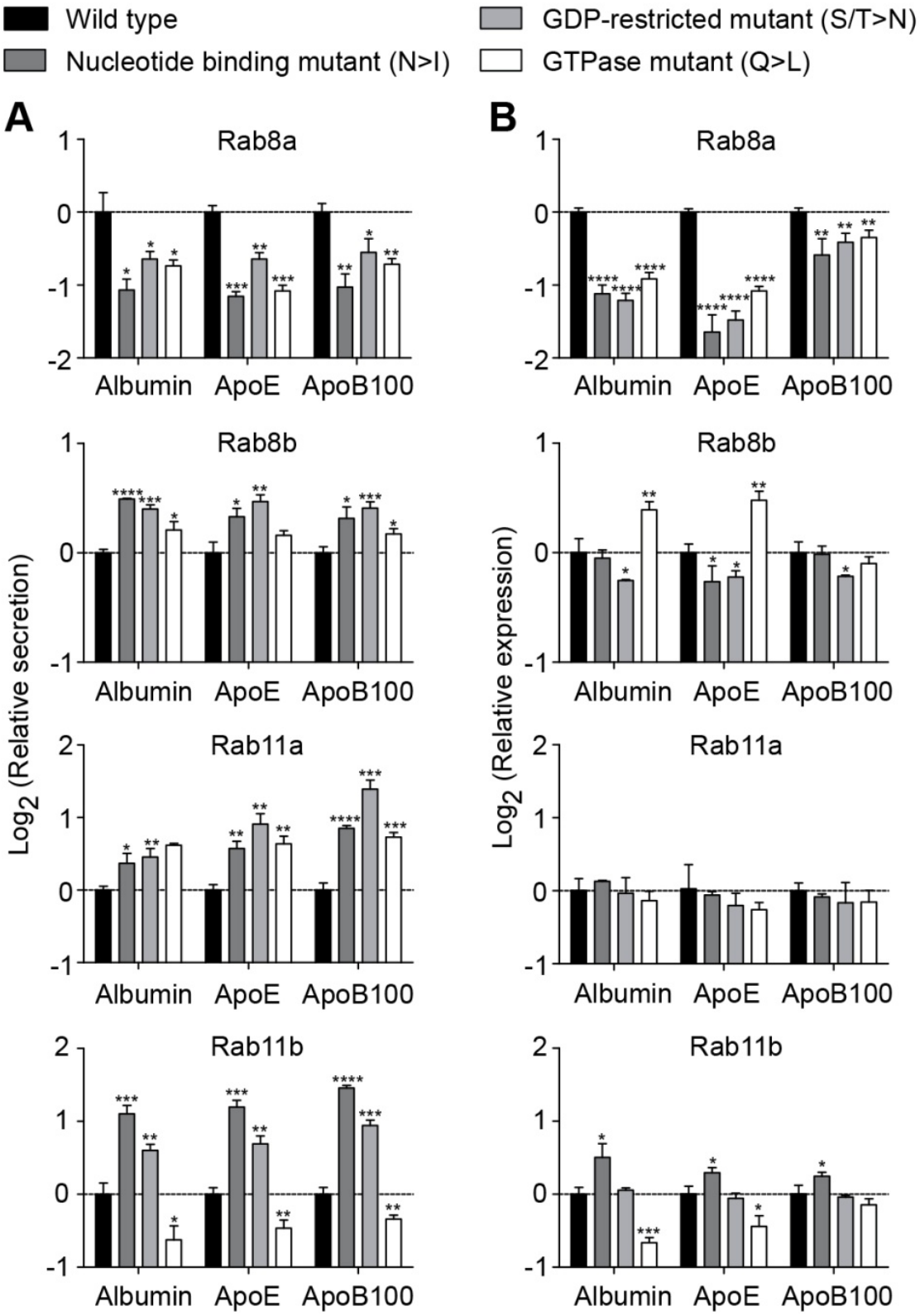
Wild type
Nucleotide binding mutant (N>I)
GDP-restricted mutant (S/T>N)
GTPase mutant (Q>L)
A
B
Rab8a
Rab8b
Rab11a
Rab11b
Albumin
ApoE
ApoB100
Log2 (Relative secretion)
Log2 (Relative expression)

Expression of all three Rab8a mutants caused a significant decrease in the secretion of all three cargoes tested (Figure 4.1A), consistent with previous observations (Figure 3.8). Cargo mRNA levels, however, were also decreased in the presence of DN Rab8a expression (Figure 4.1B), raising the possibility that some or all of the observed decrease in secretion could have been due to downregulation of cargo expression. Further tests are needed to distinguish the change in secretion levels due to downregulation of cargo expression and any possible direct effects of DN Rab8a construct expression on cargo transport.

In contrast to Rab8a, expression of the Rab8b and Rab11a mutants resulted in increased secretion levels for all three cargoes tested. Expression of the nucleotide-binding (N124I) and of the GDP-restricted (S25N) DN Rab11b also stimulated cargo secretion, while expression of the GTPase mutant (Q70L) of Rab11b resulted in impaired cargo secretion. The later result correlated with a downregulation of cargo expression levels by $Rab11b_{Q70L}$. Similarly, increased secretion caused by $Rab8b_{Q67L}$ or $Rab11b_{N124I}$ partly correlated with increased cargo expression. For all the other mutants, namely $Rab8b_{N121I}$, $Rab8b_{T22N}$, $Rab11a_{N124I}$, $Rab11a_{S25N}$, $Rab11a_{Q70L}$, and $Rab11b_{S25N}$, the increased secretion associated with DN Rab expression did not correlate with increased cargo mRNA levels in the transduced cells, suggesting that the observed secretion phenotypes may be primarily due to effects of the DN Rabs on the vesicular transport of these cargoes. Nonetheless, additional experimentation is required to further parse these reproducible secretion phenotypes.

4.4. Cell lines inducibly expressing DN Rab11 and Rab8

A drawback of using concentrated lentivirus particles to express the DN Rabs in the short term expression experiments described above and in Chapter 3 is that other material besides the lentivirus particles may be present in the virus stock. Such contaminants may include cell debris from the lentivirus producing HEK293T cells, exosomes, or the DNA transfected into these cells to make the lentivirus particles. To exclude confounding and likely unaccountable effects of non-lentivirus components of the lentivirus preparation, I created cell lines that can be induced to express mCherry-tagged Rabs. To do so, I transduced the Huh-7.5 TetON cell line with retroviruses expressing the mCherry-tagged WT and mutant Rabs from a tetracycline response element (Figure 2.1D), then selected stably transduced cell populations. I used mCherry expression as a marker that allowed me to easily identify and quantify Rab construct expression. I preferred this inducible expression approach to long-term constitutive expression of the DN Rab constructs, in part because Rab11a (Sobajima et al., 2014; Yu et al., 2014) and Rab8a (Sato et al., 2014; Sato et al., 2007) knockouts are lethal in mice.

These cell lines are in the process of being characterized. They robustly induced Rab construct expression after exposure to doxycycline (Figure 4.2A), and the mCherry-Rab fusions were easily detected by Western blotting in the lysates of the induced cells (Figure 4.2B). Ongoing experiments in these inducible expression cell lines are designed to quantify the effects of DN Rab11 or Rab8 expression on cargo mRNA levels, and on cargo secretion as determined by quantifying both the cell-associated and secreted cargo amounts, as described in detail for Rab1b in the next chapter.

Figure 4.2. Cell lines for inducible expression of Rab11 and Rab8 constructs (next page). Huh-7.5 TetON cells were transduced with retroviruses expressing the indicated constructs under the control of a tetracycline response element, and were then selected. (A) Induction of mCherry-Rab expression after 2 days of treatment with 3 μg/mL of doxycycline was characterized by flow cytometry. Red traces, non-induced cells; blue traces, induced cells. (B) Cell lysates from cells treated as in (A) were harvested and immunoblotted with an α-dsRed antibody (recognizes mCherry) and an α-actin antibody.

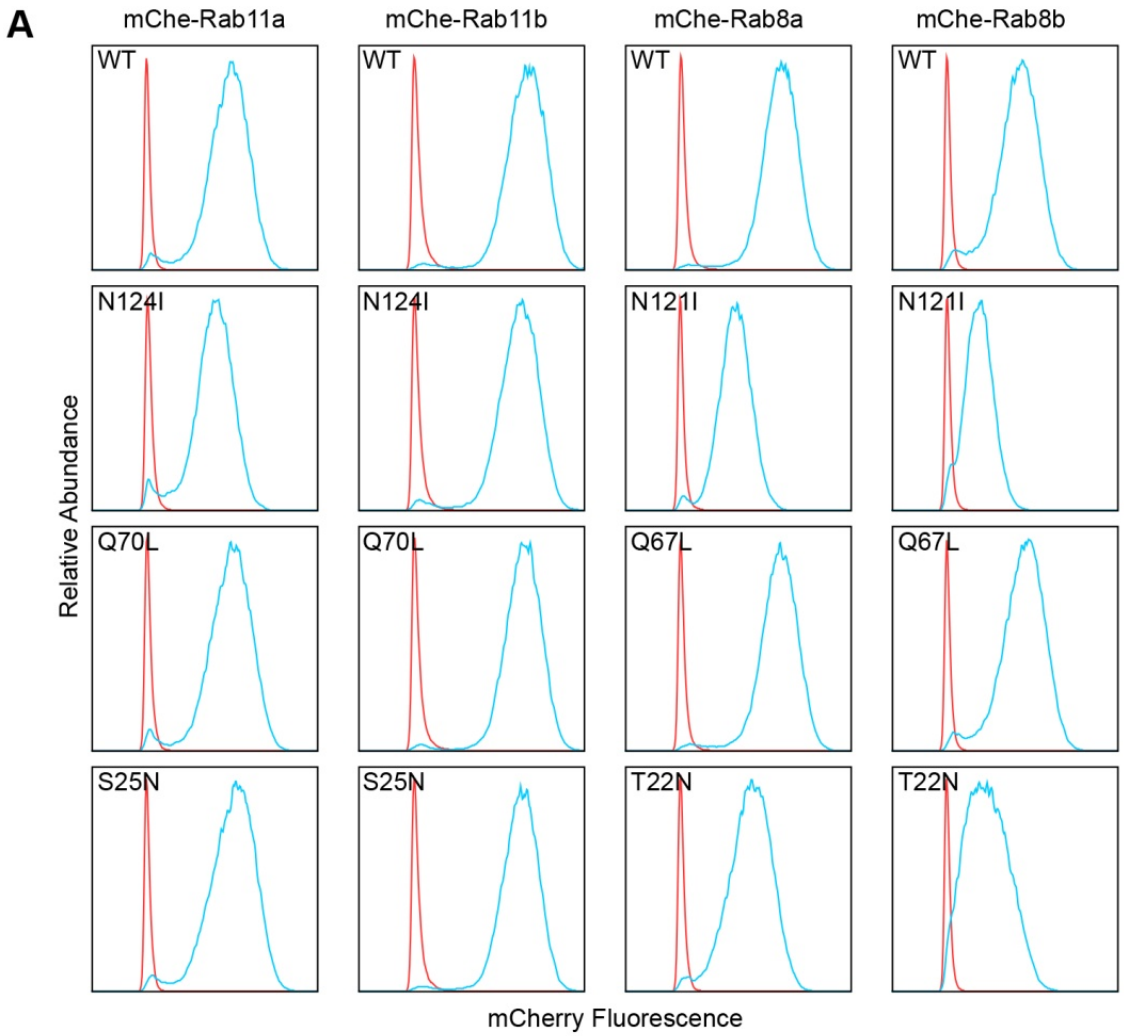
A
mChe-Rab11a
mChe-Rab11b
mChe-Rab8a
mChe-Rab8b
WT
N124I
N121I
Q70L
Q67L
S25N
T22N
Relative Abundance
mCherry Fluorescence
B
mCherry-Rab11a
mCherry-Rab8a
mCherry-Rab11b
mCherry-Rab8b
WT N124I Q70L S25N
WT N121I Q67L T22N
0 3 0 3 0 3 0 3
μg/mL Doxycycline
α-dsRed
α-actin

4.5. A polarized, primary hepatocyte-like cell culture system

As discussed at the beginning of this chapter, the increase in cargo secretion observed in the DN Rab screen and in the confirmatory experiments described above was puzzling, since Rab11 (and Rab8 acting downstream) have overwhelmingly been shown to control the secretion or recycling of apically-targeted secretory or membrane-associated cargoes (Tables 4.1 and 4.2). Albumin, ApoE (Lee et al., 2003; Traber et al., 1987), and ApoB (Traber et al., 1987) are basolateral secretory cargoes. Is the phenotype that I observed a manifestation of defective polarized transport that might occur in the Huh-7.5 cell line, or is it revealing of a potentially interesting regulation of hepatic basolateral secretion by Rab11?

Historically, hepatocyte cell culture systems have been difficult to use for the study of at least some polarity-associated processes (Treyer and Musch, 2013). Even in cases where the cells retained a polar phenotype, this phenotype has manifested in formation of bile canaliculi-like structures between adjacent cells (Andrus et al., 2011; Chiu et al., 1990; Ploss et al., 2010; Treyer and Musch, 2013). A separation of basolateral and apical compartments easily amenable to biochemical investigations, such as that obtained by growing the epithelial cell lines MDCK or Caco-2 on trans-well filters has not been achieved for hepatocyte cell culture models. I am fortunate that Dr. Viet Loan Dao Thi and Dr. Xianfang Wu of the Rice lab are currently leading an effort to develop and characterize a promisingly useful hepatocyte polarity model. I am very thankful to Dr. Dao Thi, Dr. Wu, Dr. Ursula Andreo, and soon-to-be-Dr. Rachel Belote for their wonderful collaboration on this project. The system is still being characterized, and I only

mention here some preliminary findings that informed us that this system may aid in the analysis of polarized secretory transport by hepatocytes.

Briefly, the system is based on *in vitro* differentiation of human embryonic stem cells along the endoderm/hepatocyte lineage. The resulting cells were called iHeps (induced hepatocyte-like cells). During differentiation, the iHeps were plated on trans-well filters, where they were allowed to complete their differentiation. The resulting filter-grown iHep monolayer (Figure 4.3A) had the following properties (Viet Loan Dao Thi, Xianfang Wu, Ursula Andreo and Rachel Belote, personal communications): (i) the cells expressed hepatocyte-specific genes; (ii) the monolayer formed a tight diffusion barrier, as evidenced by measurement of high trans-epithelial resistance values and by impermeability of the monolayer to diffusion of fluorescent dextrans; (iii) the monolayer secreted bile acids exclusively in the inner chamber of the trans-well filter (Figure 4.3A), which I will refer to from here on as the "apical chamber"; (iv) the iHeps secreted ApoB100-containing lipoproteins which floated in a density gradient at density fractions consistent with those of properly lipidated VLDL particles; and (v) the cells formed a continuous tight junction network and displayed some polarized protein localization patterns.

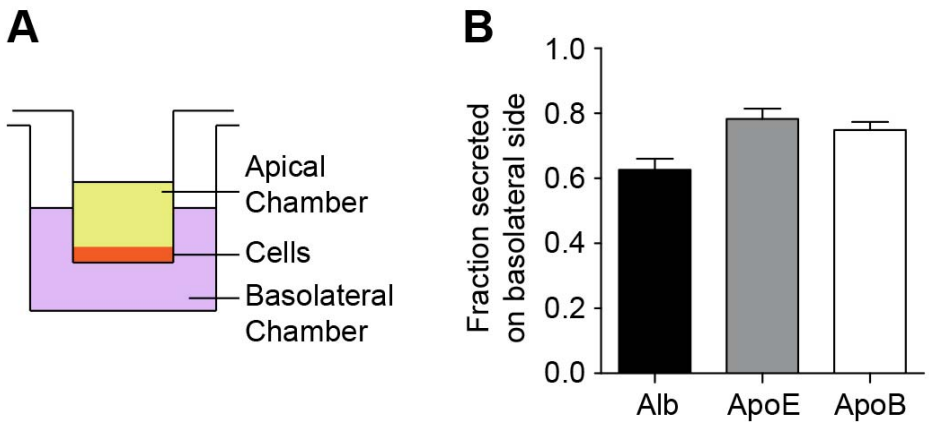

Figure 4.3. Hepatic cargo secretion by polarized iHeps (A) Schematic representation of the polarized iHeps growth setup. Cells were grown on a trans-well filter with media on both sides. The chamber within the insert was designated as "apical" compartment, while the chamber surrounding the insert was designated as "basolateral" compartment. (B) Preponderantly basolateral secretion of albumin and apolipoproteins by the polarized iHeps. Media from both apical and basolateral chambers was collected after a 6 h secretion assay and its cargo content was quantified by ELISA. The amount secreted in the basolateral chamber was expressed as fraction of the total (apical + basolateral) secreted cargo amount. Shown are means ± s.d. from n=3 trans-wells.

The focus of this work is to investigate the regulation of the secretion of basolaterally-targeted hepatocyte cargoes. I therefore measured the amounts of albumin, ApoE, and ApoB100 that were released by trans-well-grown iHeps in both the apical and basolateral chambers of the growth set-up (Figure 4.3A). I expressed the cargo amounts secreted on the basolateral side as percentages of the total (basolateral + apical) secreted cargo amounts. The results of one such experiment are shown in Figure 4.3B. All cargoes were reproducibly secreted primarily on the basolateral side of the trans-well filter, as expected by the site of secretion of these cargoes *in vivo*. Furthermore, the percentages of cargo amounts secreted by the iHeps in the basolateral chamber (63% for albumin, 78%

for ApoE, and 75% for ApoB100, Figure 4.3B) were similar to the percentages of triglycerides (60-80%) or apolipoproteins (75-100%) shown to be secreted basolaterally by the polarized intestinal cell line Caco-2 (Traber et al., 1987). That the basolaterally-secreted albumin fraction was slightly smaller than the fractions of the basolaterally-secreted ApoE or ApoB100 (Figure 4.3B) was not surprising, since albumin may be transcytosed across epithelial barriers (Monks and Neville, 2004). This result, together with the totality of the data obtained by my collaborators, indicated that the likely polarized filter-grown iHeps may become a useful cell culture model for the study of polarized hepatic secretion.

To investigate the involvement of Rab11 and Rab8 in polarized hepatic cargo secretion from these iHeps, we are modifying the parental embryonic stem cells to allow for inducible expression of WT or DN Rab constructs. We will then differentiate these cells into filter-grown iHeps, induce the expression of the Rab constructs, and then quantify the amounts of cargoes released in the apical and basolateral chambers of the trans-well culture system. The effects of DN Rab11 or Rab8 constructs on total and chamber-specific albumin and lipoprotein secretion will be therefore measured. They will be contrasted to any changes in apical bile salt secretion that we will measure in the apical chamber. Since bile salt transporters are recycled through the Rab11-positive apical recycling endosome (Wakabayashi et al., 2005; Wakabayashi et al., 2004), I expect that Rab11 inhibition will decrease the amounts of bile salt secretion secondary to intracellular endosomal retention of the bile salt transporters. The apical bile salt measurements will therefore serve as a positive control for Rab11 inactivation. Barring of course any unexpected experimental difficulties, we are poised to determine to what

extent these basolaterally-secreted hepatic cargo transport processes are dependent on Rab11 or Rab8 function.

4.6. Rab11 involvement in HCV secretion

My interest in defining the involvement of Rab11 and Rab8 in hepatic cargo egress was also in part prompted by a recent report which proposed that Rab11a controls infectious HCV secretion (Coller et al., 2012). This conclusion was based on two main findings. First, the authors showed that treatment of Huh7.5 cells with a cocktail of 4 small interfering RNAs (siRNAs) or with any of two individual siRNAs directed against the Rab11a message resulted in decreased release of infectious HCV, and concurrent accumulation of intracellular infectious virus (Coller et al., 2012). While the authors detected a substantial decrease in Rab11a message levels in siRNA-treated cells, they did not investigate whether Rab11a protein levels had decreased as well (Coller et al., 2012). Furthermore, the authors did not exclude the possibility that the observed phenotype was due to off-target effects of the two active siRNA molecules (Coller et al., 2012). Such off-target effects have been documented in other settings (Chung et al., 2014) and would need to be ruled out in order to better interpret the results of knockdown experiments. Indeed, an experiment attempting to rescue HCV infectivity release by expressing an siRNA-resistant Rab11a construct was not performed (Coller et al., 2012). The authors do however perform colocalization experiments showing that HCV Core, labeled using a tetracysteine-tagged HCV Core protein expressed from the viral genome and FlAsH/ReAsH staining (Griffin et al., 1998), colocalized with GFP-Rab11a (Coller et al., 2012). The authors interpreted this observation to mean that HCV particles were secreted through Rab11a-positive recycling endosomes. Unfortunately, this conclusion is also

insufficiently supported for the following reasons. First, the FlAsH/ReAsH labeling involved treatment of the cells with 500 μM of the reducing agent 1,2-ethanedithiol (Coller et al., 2012). Significantly lower concentrations of a very similar reducing agent, dithiothreitol can be used to induce the unfolded protein stress response: 0.025-25.6 μM (Carpio et al., 2015) or 0.1-10 mM (Cox et al., 2011). As such, the possibility that the cells behaved aberrantly due to physiological stress was not excluded. Second, the labeled tetracysteine-Core puncta observed in these cells could have undergone non-productive transport, by having become diverted from productive secretion routes into Rab11a-positive recycling endosomes and from there potentially into degradative compartments. Third, the cell line used in this study, Huh-7.5, expresses the full complement of HCV entry receptors and supports HCV entry (Evans et al., 2007; Lindenbach et al., 2005; Ploss et al., 2009). As a result, tetracysteine-Core could have made its way into Rab11a-positive recycling endosomes after first being secreted through Rab11a-independent pathway(s), followed by internalization and endocytic recycling transport. For these reasons, while the results of these experiments are consistent with the authors' conclusion that Rab11a controls HCV egress through the recycling endosome, the same experimental results may not add up to sufficiently strong evidence to rule out alternative scenarios.

When considering the implications of HCV secretion through a Rab11-positive endosome, one must view this model in the larger context of the intra-host and inter-host virus transmission dynamics and evolutionary history. Studies of other viruses, such as influenza A virus (Amorim et al., 2011; Bruce et al., 2010; Chou et al., 2013; Eisfeld et al., 2011; Momose et al., 2011), HIV-I (Varthakavi et al., 2006), and Andes virus (Rowe

et al., 2008), have implicated Rab11a in virus release. Both influenza A virus (Rodriguez Boulan and Pendergast, 1980; Rodriguez Boulan and Sabatini, 1978) and Andes virus (Rowe and Pekosz, 2006) are released at the apical pole of infected cells, therefore Rab11 involvement in the biogenesis of these viruses is not surprising. HCV epidemiological history suggests however that the primary (or at least the recent primary) route of virus transmission is through the blood or blood products, secondary to medical procedures, injection drug use, or risky sexual practices (Thomas, 2013). A potential implication of this mode of transmission is that HCV may be a virus that is primarily released at the basolateral sides of the hepatocytes. Therefore, Rab11 should not be involved in HCV release. Release of the virus at the apical side would also be problematic since HCV is an enveloped virus. HCV, unlike the non-enveloped hepatitis A and E viruses, which are primarily transmitted between hosts by a fecal-to-oral route (Protzer et al., 2012), might not survive the digestive environment of the duodenum where the bile products - and the apically released hepatotropic viruses - would access the digestive tube. Several questions arise then. Was Rab11 implicated in HCV release as a result of over interpretation of experimental findings, or as the manifestation of an *in vitro* phenotype with little significance for how HCV egress is regulated in the infected liver (Coller et al., 2012)? Does Rab11 carry an unexpected function in the transport of a presumably basolateral cargo, HCV, in the native hepatocyte? Or is the Rab11-HCV association an indication that HCV may indeed be released apically? If yes, how would such a finding fit into the larger picture of hepacivirus transmission and evolution? There is little information at the moment as to how HCV was transmitted before its modern efficient spread facilitated by advances in medical practice, or as to how the HCV-related hepaciviruses have evolved

and crossed species barriers (Pybus and Theze, 2015). The entire family could have been spread through blood-to-blood routes, perhaps mediated by tabanids such as horse flies (Pybus et al., 2007), similar to how the more distantly related flaviviruses use ticks and mosquitoes for transmission. If the hypothesized insect-mediated transmission was purely passive, with the insects simply carrying infected blood from one host to the other, there would be no need for the virus to possess capacity of being secreted apically. The virus could have nonetheless retained apical secretion capabilities from a distant ancestor which had been in fact released on the apical side of a producing cell. The virus may also require apical secretion capabilities if insect-mediated transmission involved virus replication in the vector's gut. Alternatively, vector-free transmission could have occurred through secretions (respiratory secretions, saliva) (Pybus and Theze, 2015), in which case apical secretion capabilities of the virus could be directly relevant. It is worth noting that hepacivirus RNA has been detected in respiratory secretions of likely infected animals (Kapoor et al., 2011), although it is unknown whether the presence of viral genetic material at that site was due to passive processes, such as leakage-mediated contamination of respiratory secretions by serum products in the context of an inflamed mucosa, or active processes, such as replication and assembly of the virus in cells of the lining of the upper respiratory tract.

4.7. Conclusion

The nature of Rab11 (and Rab8) involvement in hepatic cargo secretion, be that of the basolaterally targeted albumin and lipoproteins, or of HCV, remains at this time a mystery. Obviously, much work is needed to generate answers to the questions that I identified in this chapter, and my investigation into the regulation of these processes remains in its infancy. I hope nonetheless that the discussion of the possible involvement of Rab8 and Rab11 in cargo secretion, in both non-polarized Huh-7.5 cells or in polarized hepatocyte-like cells, highlights some exciting, interesting and important avenues of investigation.

Chapter 5

Involvement of Rab1 in Hepatic Cargo Transport

5.1. Rab1 and ER-to-Golgi transport

Of the hits of the DN Rab screen (Chapter 3), Rab1b presented a peculiar phenotype. Compared to WT Rab1b expression, expression of $Rab1b_{N121I}$ apparently stimulated ApoE secretion when administered at an MOI dose of 25 (Figure 3.7) or 100 (Figure 3.8) I.U./cell, and apparently impaired ApoB100 secretion when used at 100 I.U./cell (Figure 3.8). This indicated that ApoE and ApoB100 secretion may respond differently to Rab1 inhibition. I have therefore proceeded to analyze Rab1b's involvement in cargo secretion in greater detail.

The partially redundant Rab GTPases, Rab1a and Rab1b (Nuoffer et al., 1994), regulate anterograde vesicular transport from the ER to the Golgi system, and inhibition of their function impairs early anterograde transport of many secretory cargoes, the most extensively characterized being VSVg (Plutner et al., 1991; Tisdale et al., 1992). Other cargoes include the viral envelope glycoproteins of HIV-1 (Nachmias et al., 2012) and human herpes simplex-1 (Zenner et al., 2011); the Ebola virus VP40 capsid protein (Yamayoshi et al., 2010); the G-protein coupled receptors (GPCRs) rhodopsin (Satoh et al., 1997), angiotensin and adrenergic receptors (Filipeanu et al., 2004; Filipeanu et al., 2006; Wu et al., 2001; Wu et al., 2003) and the calcium-sensing receptor (Zhuang et al., 2010); ion channels (Flowerdew and Burgoyne, 2009; Robitaille et al., 2009); the β-amyloid precursor protein (Dugan et al., 1995), and the secreted proteins human growth

hormone, interleukin-8 (Dong et al., 2012) and alkaline phosphatase (Ingmundson et al., 2007).

Rab1 localizes at the ER, at the Golgi, ERGIC, and on vesicles that transport cargo from the ER to the Golgi (Alvarez et al., 2003; Moyer et al., 2001b; Plutner et al., 1991; Saraste et al., 1995). Rab1's function in early anterograde transport is underscored by the list of its known effectors. These include several Golgi tethers or Golgi structural proteins: p115 (Allan et al., 2000), GM130 (Moyer et al., 2001a; Weide et al., 2001), golgin-84 (Diao et al., 2003; Satoh et al., 2003) and giantin (Beard et al., 2005). Through these vesicle- and Golgi-associated proteins, Rab1 controls the delivery of secretory cargo into the Golgi compartment. Other effectors are: MICAL-1 (Weide et al., 2003), Iporin (Bayer et al., 2005), and GBF1 (Monetta et al., 2007). GBF1 is an Arf1 GEF that activates Arf1 on the surface of Golgi compartments and by doing so initiates COPI recruitment and therefore COPI-dependent vesicular transport (Alvarez et al., 2003; Claude et al., 1999; Garcia-Mata et al., 2003; Kawamoto et al., 2002; Monetta et al., 2007; Niu et al., 2005; Szul et al., 2005; Zhao et al., 2002).

Given that Rab1b inactivation as a consequence of expression of $Rab1b_{N121I}$ differentially affected the secretion of the several hepatic cargoes tested (Figure 3.8), and given that Rab1 controls anterograde transport from the ER to the Golgi, I inquired whether transport of albumin, ApoE and ApoB100 between these compartments may be differentially regulated. This idea was not unprecedented, since *in vitro* biochemical assays had already documented that ApoB and ApoE (Gusarova et al., 2007), or ApoB and albumin (Siddiqi, 2008), were packaged into distinct ER-derived vesicles. These findings, combined with my own observations, raised the possibility that Rab1b may

differentially control secretion of the cargoes that I investigated. I therefore set out to investigate in greater detail the function of Rab1 in hepatic cargo secretion.

The main experimental approach that I utilized relied on inactivation of Rab1 function by expression of DN Rab1 mutants. DN Rab1a or Rab1b mutants have been shown to inactivate Rab1 function (Nuoffer et al., 1994; Pind et al., 1994; Tisdale et al., 1992). When VSVg anterograde transport was investigated, the GDP-restricted mutants (i.e. $Rab1b_{S22N}$) and the nucleotide binding mutants (i.e. $Rab1b_{N121I}$) blocked VSVg transport from the ER to the Golgi, while the WT versions and the GTPase-inactivating mutants (i.e. $Rab1b_{Q67L}$) did not interfere with this process (Nuoffer et al., 1994; Pind et al., 1994; Tisdale et al., 1992). Furthermore, the transport stages at which the GDP-restricted and the nucleotide binding mutants blocked VSVg progression were distinct. The GDP-restricted mutant blocked VSVg exit from the ER (Nuoffer et al., 1994), while the nucleotide binding mutant caused accumulation of VSVg in an ERGIC-like compartment (Pind et al., 1994). I therefore used this knowledge, and these Rab1 mutants to investigate the secretion of hepatic cargoes in greater detail.

Before going onto describing the results, I wish to caution the reader that throughout this chapter I have used two methods to quantify cargo egress. In both methods, the amount of cargo that accumulated in the cell culture media was quantified by ELISA, but these measurements of secreted cargo by themselves were not sufficient to assess secretion. I needed to also control for the possibility - the fact even - that the various treatment conditions resulted in different amounts of cells being present in the culture at the time of the secretion assay, and therefore being responsible for the secretion activities measured. I utilized two methods to account for variation in cell mass. One took

advantage of luciferase activity measurements that I performed on cell lysates at the end of the secretion assay, the other used cell-associated cargo amounts measured in similar lysates. As I will explain throughout this chapter, the two methods estimated different aspects of secretion. While the overall results are facially different, I hope to convince the reader by the end of this chapter that the findings obtained using each of the methods do indeed agree with each other.

5.2. Confirmation of DN Rab screen results

I began my inquiry into how Rab1 controls hepatic cargo egress by repeating the type of secretion assays I performed as part of the DN Rab screen. I transduced Huh-7.5 FLuc cells with lentiviruses expressing Rab1b or Rab1b$_{N121I}$. In parallel, I also tested mCherry-tagged Rab1b constructs, both the WT form and the N121I mutant. I performed secretion assays and normalized the secreted cargo amounts by the luciferase activity of the cell lysates. The results were consistent with the previous observations (Figures 3.7 and 3.8). Thus, untagged Rab1b$_{N121I}$ expression had only a small effect on albumin secretion (Figure 5.1A) while mCherry-Rab1b$_{N121I}$ had no detectable effect (Figure 5.1B). In contrast, ApoE secretion was stimulated by tagged or mCherry-tagged Rab1b$_{N121I}$ expression, while ApoB secretion was inhibited, by the same constructs (Figure 5.1A and B). As before, Rab1b$_{N121I}$ construct expression was associated with decreased luciferase activity in the cell lysates (Figure 5.1C).

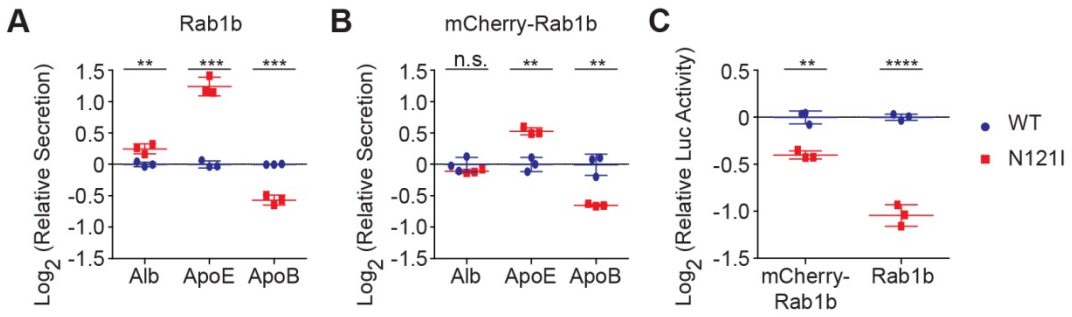

Figure 5.1. Confirmation of Rab1b$_{N121I}$ effect on hepatic cargo secretion. Huh-7.5 FLuc cells were infected with lentiviruses expressing WT (blue circles) or N121I mutant (red squares) versions of untagged Rab1b (A) or mCherry-Rab1b (B), respectively, all at an MOI of 100 I.U./cell. At 48 h post transduction, a 6 h secretion assay was performed. Albumin, ApoE, and ApoB100 amounts in the media were measured by ELISA, and the results were normalized by the luciferase activity in the cell lysates of the corresponding wells. Cargo secretion levels in the presence of the DN Rab1b constructs were plotted as relative to the secretion levels in the presence of WT Rab1b constructs, on a Log_2 scale. (C) Relative luciferase (Luc) activities (Log_2 scale) in the cell lysates from the experiments presented in panels (A) and (B), respectively. For each condition, means ± s.d. of values obtained in 3 parallel wells are presented. Significant differences (Student's *t*-test): n.s., non-significant; **, $p<0.01$; ***, $p<0.001$; ****, $p<0.0001$.

5.3. Functional characterization of the mCherry-tagged Rab1b constructs

Since mCherry-Rab1b$_{N121I}$ caused a secretion phenotype similar to the one caused by the untagged Rab1b mutant (Figure 5.1A-B), it was likely that mCherry tagging of Rab1b did not impair its activity. Indeed, GFP-Rab1 constructs have been shown to successfully carry out Rab1 functions (Alvarez et al., 2003; Moyer et al., 2001b). Since using mCherry-tagged Rab1b constructs in experiments would facilitate direct measurement of Rab construct expression levels and since the fusion proteins could be used in imaging experiments, I set out to more comprehensively characterize the functionality of these constructs.

Expression and localization of mCherry-Rab1b fusion proteins. I created constructs that encoded mCherry at the amino terminus of WT, N121I, S22N and Q67L Rab1b. When expressed in cells, these fusion proteins migrated on SDS-PAGE gels as single polypeptides of the expected ~ 49 kDa molecular weight (Figure 5.2A). Furthermore, the constructs displayed subcellular localizations (Figure 5.2B) similar to those previously described for GFP- and epitope-tagged Rab1 (Alvarez et al., 2003; Moyer et al., 2001b). These patterns of localization were: reticulate ER-like, perinuclear Golgi-like, and punctate vesicle-like signals for the WT and Q67L forms; ER-like and cytosolic for the S22N form; and largely cytosolic and nuclear for the N121I form (Figure 5.2B).

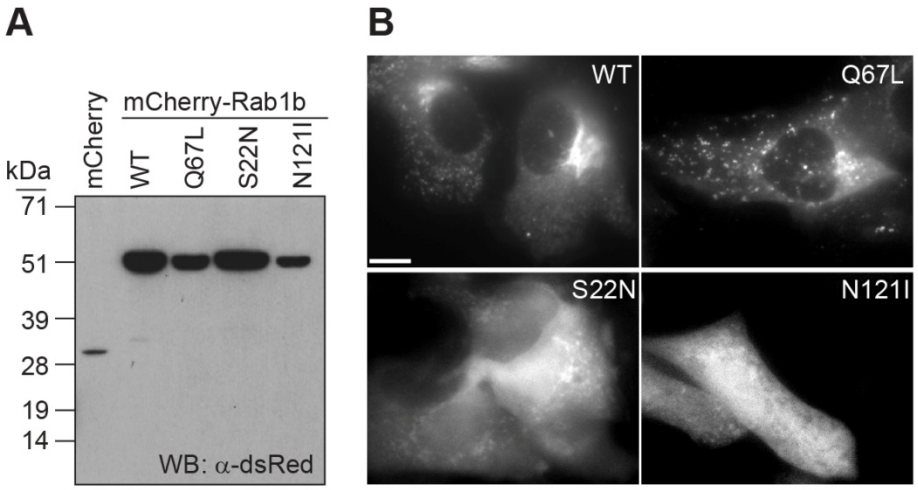

Figure 5.2. Expression and characterization of mCherry-Rab1b constructs. (A) Western blot of lysates of HEK293T cells transfected with mCherry- or mCherry-Rab1b expressing plasmids. mCherry was detected using an α-dsRed antibody. (B) Subcellular localization of mCherry-Rab1b constructs in Huh-7.5 cells. The cells were transduced with lentiviral particles expressing the indicated WT or mutant forms of mCherry-Rab1b and imaged by epifluorescence microscopy at 48 h post transduction. Scale bar, 10 μm.

Functionality of mCherry-Rab1b constructs. I next confirmed that the mCherry-Rab1b constructs could functionally interfere with VSVg anterograde transport. VSVg is amongst the best characterized Rab1 cargoes, and its tsO45 mutant allows for synchronized analysis of cargo egress (Bergmann et al., 1981). I co-transfected cells with a plasmid encoding mCherry or mCherry-Rab1b constructs and a plasmid encoding $VSVg_{tsO45}$-GFP (Presley et al., 1997). I then allowed expression of the proteins at 39.5°C, under which conditions $VSVg_{tsO45}$-GFP is retained in the ER (Kreis and Lodish, 1986; Presley et al., 1997) and its *N*-linked glycan chains are sensitive to digestion with both endoglycosidase H (Endo H) and peptide-*N*-glycosidase F (PNGase F). Next, I switched a set of the transfected cells to 32°C, a temperature which allows transport of this VSVg mutant out of the ER, through the Golgi system, to the plasma membrane (Bergmann et al., 1981). Transport of VSVg through the Golgi is accompanied by modification of its glycan chains by Golgi-resident enzymes, resulting in an Endo H-resistant, but PNGase F-sensitive form (Schwaninger et al., 1991). The cartoon in Figure 5.3A depicts the expected SDS-PAGE migration patterns of glycosidase-digested (Endo H- and PNGase F-sensitive) VSVg that has been retained in the ER either by the 39.5°C temperature block or by the lack of Rab1 activity (Figure 5.3A, the three bands at the left). The same cartoon also depicts the expected migration patterns of glycosidase-digested (Endo H-resistant but PNGase F-sensitive) VSVg that has been transported out of the ER at the permissive temperature and in the presence of active Rab1 (Figure 5.3A, the three bands at the right).

In my hands, regardless of the construct expressed from the co-transfected plasmid, VSVg-transfected cells that had been incubated solely at 39.5°C displayed

VSVg migration patterns on the SDS-PAGE gel that were expected of ER-retained VSVg. In these conditions, VSVg was sensitive to both Endo H and PNGase F digestion (Figure 5.3B, left three columns of bands). After release from the 39.5°C block, and as predicted by previous studies (Tisdale et al., 1992), mCherry, or WT or Q67L mCherry-Rab1b allowed processing of a significant fraction of the VSVg protein to an Endo H-resistant form (Figure 5.3B, top three sets of bands). Some VSVg protein remained unprocessed in the presence of WT or Q67L mCherry-Rab1b, but not in the presence of mCherry, presumably due to DN-like effects of the high overexpression of otherwise functional mCherry-Rab1b constructs that can be achieved in some of the transfected cells. In contrast to the WT and Q67L constructs, overexpression of S22N or N121I mCherry-Rab1b potently inhibited VSVg processing to the Endo H-resistant form (Figure 5.3B, bottom two sets of bands).

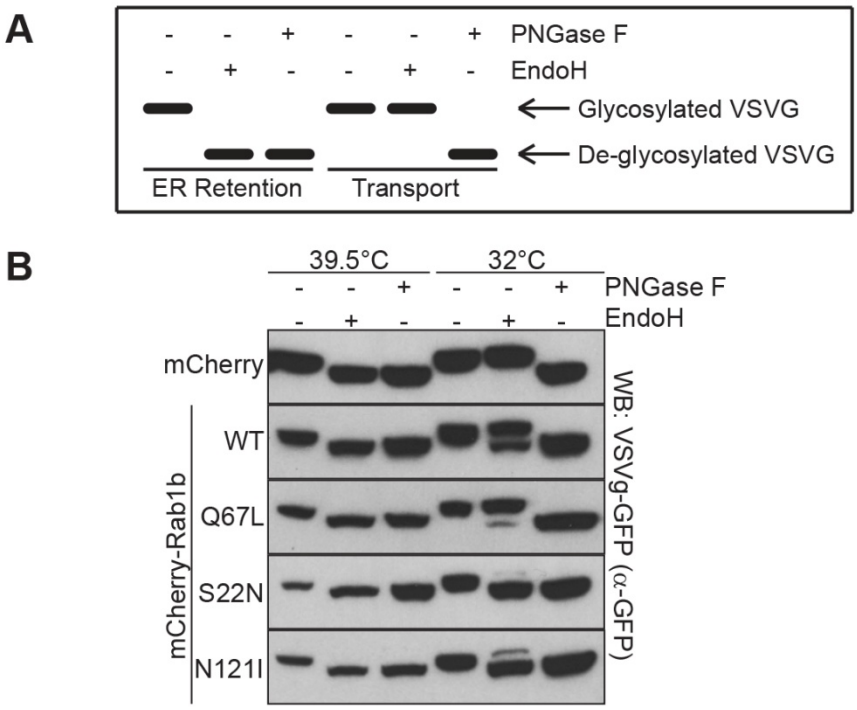

Figure 5.3. Effects of mCherry-Rab1b constructs on VSVg glycan chain processing. (A) Schematic depiction of expected ER-retained or ER-exported VSVg mobilities on SDS-PAGE gels. ER-retained VSVg is expected to be sensitive to deglycosylation by both Endo H and PNGase F and therefore to gain a higher mobility after digestion with either enzyme. VSVg that had been transported out of the ER is expected to become resistant to Endo H digestion, but to remain sensitive to PNGase F digestion. (B) $VSVg_{tsO45}$-GFP and the noted mCherry or mCherry-Rab1b constructs were co-transfected into HEK293T cells maintained at 39.5°C. After 24 h, one set of plates was transferred to 32°C to allow VSVg transport out of the ER and processing of its glycan chains. Next all cell lysates were harvested, digested with PNGase F, Endo H, or left undigested, and finally processed by Western blotting with an α-GFP antibody that recognized both the lower mobility glycosylated and higher mobility deglycosylated forms of VSVg-GFP.

I also confirmed, in the Huh-7.5 cell line, that VSVg-GFP was able to reach the plasma membrane in the presence of mCherry, or of WT or Q67L mCherry-Rab1b expression, where it decorated the contours of the cells, while it was retained intracellularly in the presence of continued 39.5°C temperature block, or of S22N or N121I mCherry-Rab1b construct expression (Figure 5.4A-B). These biochemical and localization results document that the mCherry-Rab1b constructs affected the anterograde transport of VSVg as predicted by previous studies (Alvarez et al., 2003; Tisdale et al., 1992). These findings further supported using WT and DN mCherry-Rab1 constructs to investigate the role of Rab1 function in hepatic cargo egress.

Figure 5.4. Effects of mCherry-Rab1b constructs on VSVg transport to the plasma membrane (next page). (A) Huh-7.5 cells were transfected with $VSVg_{tsO45}$-GFP and the indicated mCherry, or mCherry-Rab1b constructs, and maintained at 39.5°C before being switched to the indicated temperatures and then fixed and imaged. Representative single deconvolved planes in the GFP (left column), mCherry (middle column) and overlayed (right column) fluorescent channels are presented. Signal intensities along the white lines depicted on the overlay images were quantified and are shown in panel B. Scale bar, 10 μm. (B) Line scan quantification of signal intensities in the GFP channel (green trace) and mCherry channel (red trace) along the white lines depicted in panel A. The mCherry or mCherry-Rab1b construct expressed in each of the cells is listed at the top of each graph, along with the temperature that the cells were exposed to before fixation. The left column of graphs shows examples where the VSVg-GFP signal was transported to the plasma membrane as denoted by the clear GFP signal peaks (black arrows) that encase the mCherry signal. Right column of graphs shows examples where the VSVg-GFP signal was retained intracellularly, as depicted by the absence of clear GFP signal peaks at the periphery of the mCherry and GFP signal traces, indicated by black arrowheads. A.U., arbitrary units.

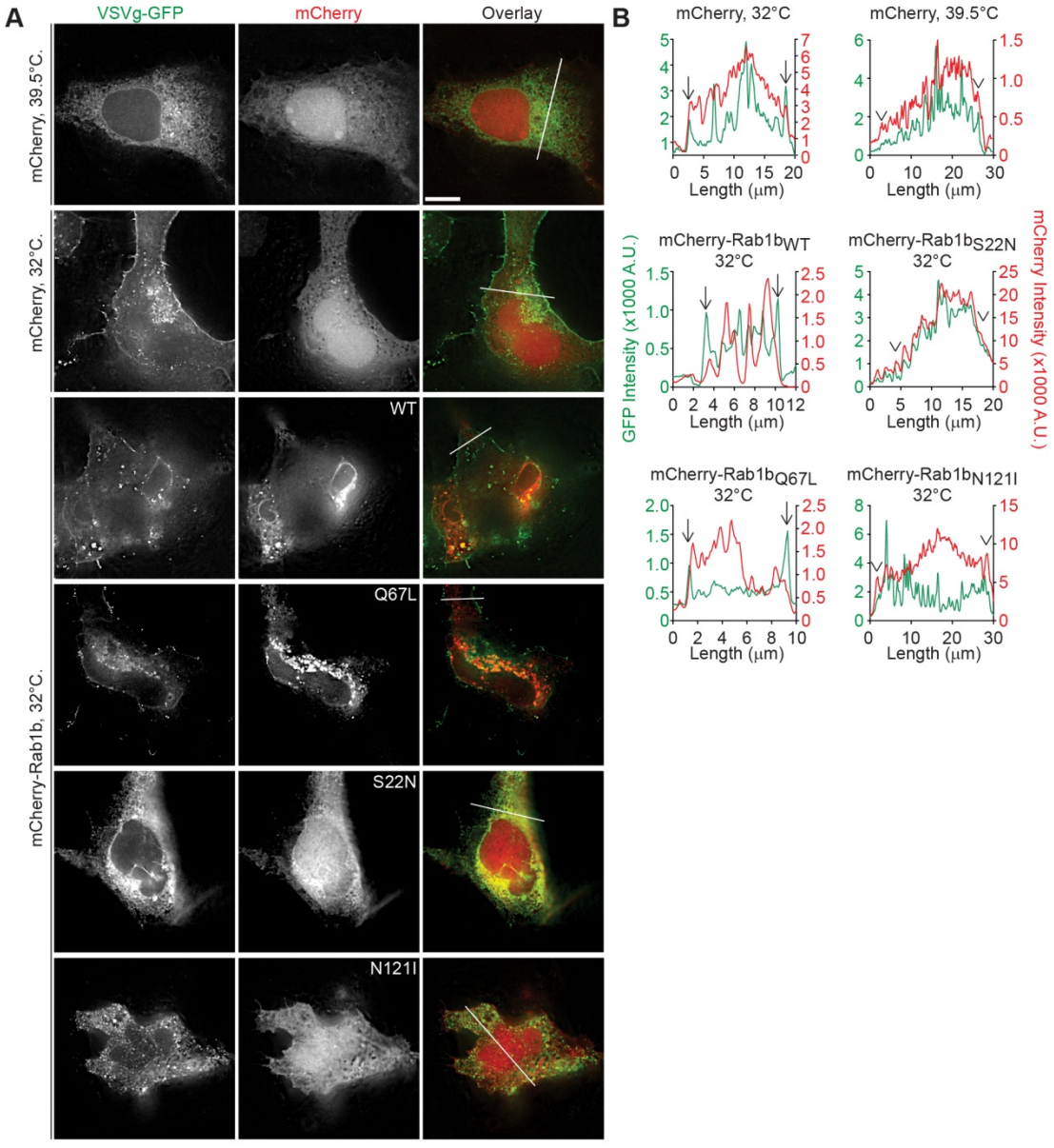
A
VSVg-GFP
mCherry
Overlay
mCherry, 39.5°C.
mCherry, 32°C.
mCherry-Rab1b, 32°C.
WT
Q67L
S22N
N121I
B
mCherry, 32°C
mCherry, 39.5°C
mCherry-Rab1bWT 32°C
mCherry-Rab1bS22N 32°C
mCherry-Rab1bQ67L 32°C
mCherry-Rab1bN121I 32°C
GFP Intensity (x1000 A.U.)
mCherry Intensity (x1000 A.U.)
Length (μm)

5.4. Endocytic activity in the presence of mCherry-Rab1b expression

To alleviate the concern that expression of the DN mCherry-Rab1b constructs affected cargo secretion through general toxic effects on cell physiology, following inhibition of ER to Golgi traffic, I measured the ability of mCherry-Rab1b-expressing cells to endocytose fluorescently labeled transferrin. Transferrin endocytosis is mediated by a membrane transport process that is functionally, mechanistically and topologically divergent from the early exocytic events regulated by Rab1 (Luck and Mason, 2012). I therefore expressed WT or mutant mCherry-Rab1b constructs, or the control mCherry protein alone, in the Huh-7.5 cells, by lentiviral transduction. I detached these cells from the plate using a non-proteolytic method to help preserve integrity of cell surface transferrin receptors. I then allowed the Alexa Fluor 647-labeled transferrin (Tf-AF647) to bind to the cell surface at 4°C and split the cell culture in two samples. I washed one sample while keeping it at 4°C, while I allowed the second sample to undergo endocytic uptake at 37°C, before cooling it and washing it as well. I then quantified the amounts of fluorescent transferrin taken up by the cells in each condition. This transferrin-uptake assay was capable of discerning between non-specific transferrin staining (Figure 5.5A, 4°C trace) and active uptake (Figure 5.5A, 37°C trace). Furthermore, live Huh-7.5 cells transduced with lentiviruses expressing mCherry or mCherry-Rab1b constructs took up transferrin to comparable levels (Figure 5.5B). These findings are consistent with previous reports documenting retention of endocytic activity concurrent with inactivation of ER to Golgi transport (Lippincott-Schwartz et al., 1991; Miller et al., 1992).

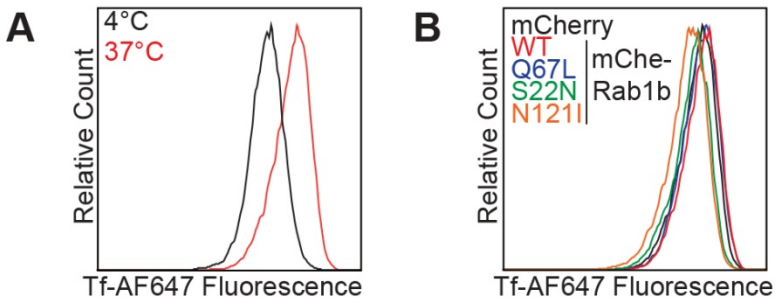

Figure 5.5. Effects of mCherry-Rab1b constructs on transferrin uptake. (A) Huh-7.5 cells were transduced with 25 I.U./cell of a lentivirus expressing mCherry. At 48 h post transduction, the cells were harvested, a fluorescent transferrin uptake assay was performed, and the cells were analyzed by flow cytometry. Traces represent distributions of transferrin staining in live cells after incubation at 4°C (black trace) or 37°C (red trace). (B) Huh-7.5 cells were transduced with 25 I.U./cell of lentiviruses expressing the indicated constructs, then allowed to take up transferrin at 37°C. Traces show distributions of Alexa Fluor 647-labeled transferrin (Tf-AF647) signal levels in single live cells.

5.5. Cell lines inducibly expressing mCherry-Rab1b

To gain better control of the expression of the mCherry-Rab1b constructs, I once again used the Huh-7.5 TetON cells (Figure 2.2). I transduced the Huh-7.5 TetON Clone 9 cell line (Luna et al., 2015), with retroviruses expressing mCherry-Rab1b constructs under the control of a tetracycline response element. I also transduced the resulting cells with a second luciferase-expressing vector to allow estimation of cell culture mass by luciferase activity measurements (Figure 3.2). Doxycycline treatment of these cultures induced mCherry-Rab1b expression in the overwhelming majority of the cells in culture, as detected by microscopy (Figure 5.6A), flow cytometry (Figure 5.6B) and Western blotting (Figure 5.6C). Furthermore, Huh-7.5-specific cell shapes were retained in the cells expressing DN mCherry-Rab1b constructs (Figure 5.6A).

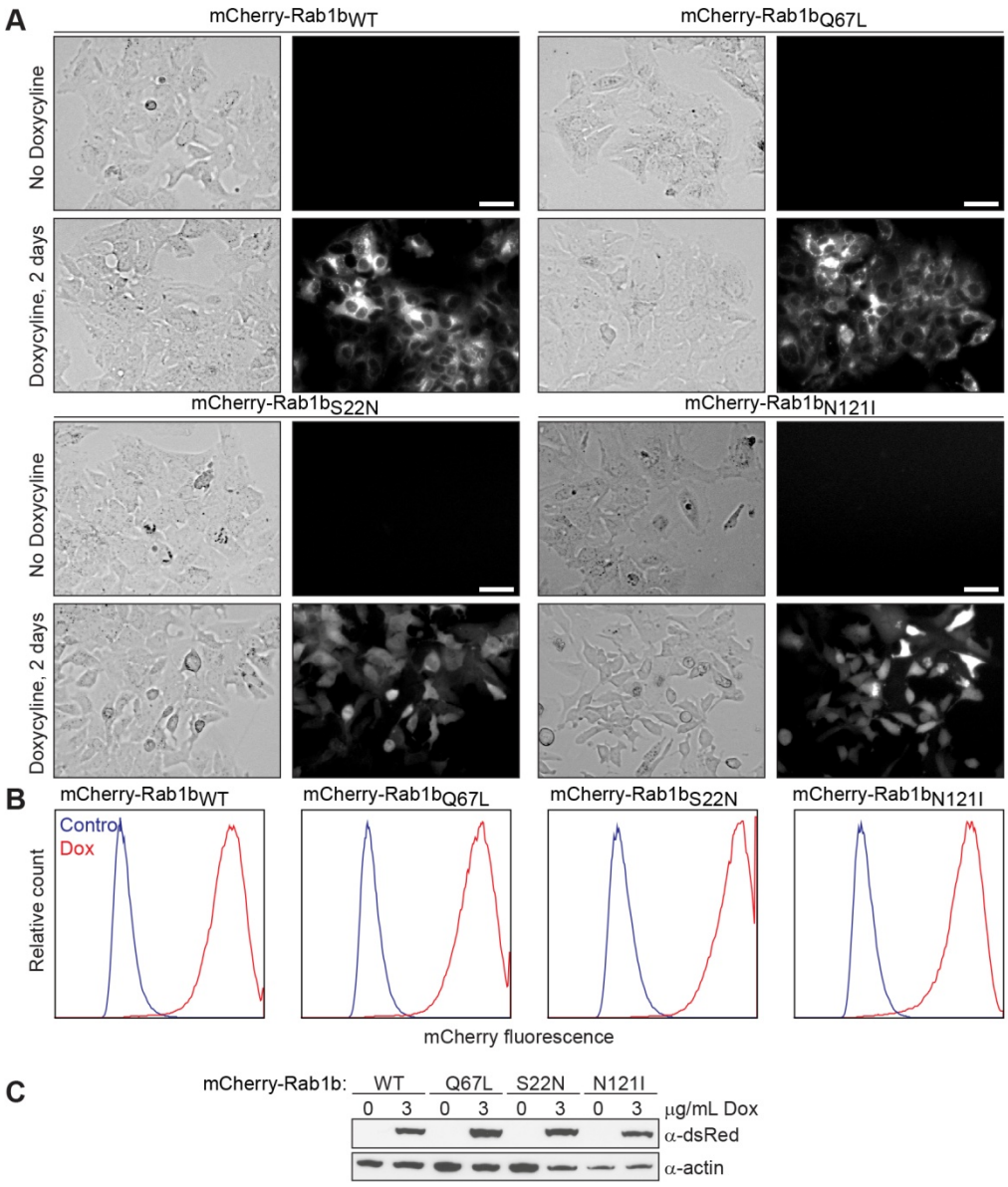

Figure 5.6. Cell lines inducibly expressing mCherry-Rab1b. (A) The cell lines expressing the indicated mCherry-Rab1b constructs were imaged either in the absence of, or after 2 days of treatment with doxycycline. For each cell line, the left column shows brightfield images, while the right column shows epifluorescence images acquired with mCherry-specific filters. Scale bars, 50 µm. (B) The cell lines expressing the indicated mCherry-Rab1b constructs were analyzed by flow cytometry after growth for 24 h in the presence (Dox, red traces) or absence (Control, blue traces) of 3 µg/mL doxycycline. (C) Lysates from these were harvested after 24 h of induction with doxycycline and analyzed by Western blotting with antibodies against dsRed and β-actin.

5.6. Inducible mCherry-Rab1b: cargo secretion normalized to cell lysate luciferase activity

Using the doxycycline-inducible mCherry-Rab1b cell lines, I further investigated the effects of mCherry-Rab1b construct expression on the secretion of albumin, ApoE and ApoB100. Once again I used the luciferase activity of the cell lysates to normalize the ELISA measurements of the cargo amounts secreted in the media. Induction of expression of WT or Q67L mCherry-Rab1b had no detectable effect on the luciferase activity values, while induction of expression of the S22N and N121I mutant constructs caused at most a 2-fold activity decrease over 48 h of growth, when compared to the uninduced condition (Figure 5.7A). When compared to the uninduced control condition, induction of mCherry-Rab1b$_{N121I}$ expression for various lengths of time caused an increase in ApoE secretion, and a decrease in albumin and ApoB100 secretion (Figure 5.7B). This effect was specific for the N121I mutant, since expression of the WT (Figure 5.7C), Q67L (Figure 5.7D) or S22N (Figure 5.7E) constructs only minimally affected, if at all, the secretion of the three cargoes tested, as detected by this method of estimating secretion. These results paralleled those obtained using lentivirus-mediated delivery of the untagged or mCherry-tagged Rab1b constructs (Figure 5.1).

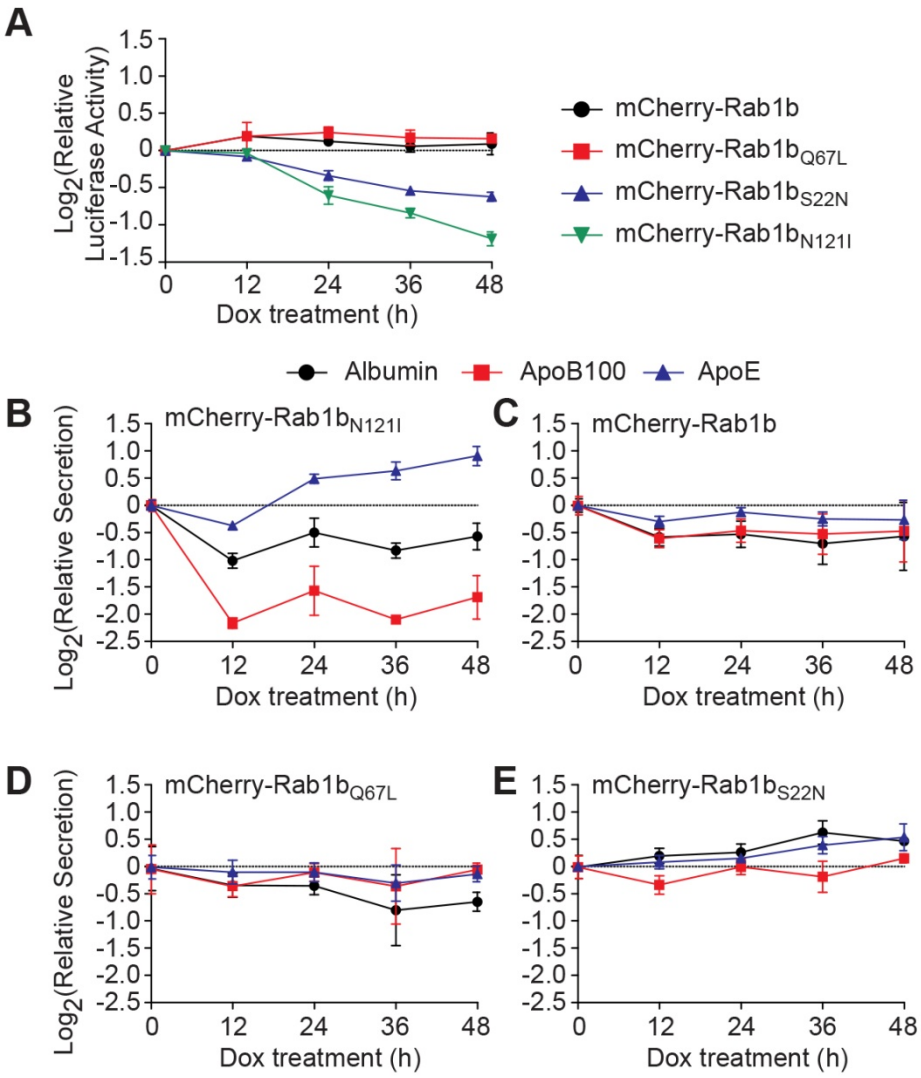

Figure 5.7. Effects of inducible mCherry-Rab1b construct expression on cargo secretion. I: Secretion normalized by cell lysate luciferase activity. (A-E) Inducible cell lines expressing the noted mCherry-Rab1b constructs were treated with doxycycline (Dox) for the indicated durations, or were left untreated, before a 6 h secretion assay was performed and the amounts of albumin, ApoB100, and ApoE secreted in the media from each well were quantified by ELISA, and normalized by the luciferase activity of the corresponding well's cell lysate. The values (mean ± s.d., n=3 parallel wells for secretion assays, and 4 parallel wells for the luciferase assay) are depicted relative to those obtained from uninduced cells, on a Log_2 scale. (A) Relative luciferase activities in the cell lysates harvested at the indicated time points. (B-D) Relative cargo secretion levels in the presence of induction of the indicated constructs.

5.7. mCherry-Rab1b$_{N121I}$ upregulates ApoE and ApoB100 expression

The method that I employed so far to measure cargo secretion accounted for changes in the mass of the cells that were responsible for secretion by normalizing the secreted cargo amounts using the luciferase activity of the cell lysates. However, this method did not account for any cargo expression changes that may be associated with expression of the Rab1 constructs. Rab1 overexpression has been shown to induce transcriptional changes in cells (Romero et al., 2013). To investigate whether such an effect existed in my experimental setting, I quantified, using qRT-PCR, the transcript levels of all three cargoes and of Rab1 in cells induced to express mCherry-Rab1b constructs and compared them to their transcript levels in uninduced cells. As expected, doxycycline-mediated induction of mCherry-Rab1 constructs caused an increase (3-8 fold in magnitude, depending on the construct expressed) in Rab1b message levels (Figure 5.8). I note that the primers used in the qRT-PCR assay are predicted to recognize both the natively-expressed Rab1b and the induced mCherry-Rab1b species. Of note, this level of mRNA overexpression, if translated into protein amount changes, is similar to the amount of excess Rab1b$_{S25N}$ that was used to achieve transport inhibition in a previous *in vitro* study (Nuoffer et al., 1994). In my experimental setup, WT, Q67L or S22N mCherry-Rab1b induction affected ApoE, ApoB and albumin mRNA levels very little, if at all. In contrast, mCherry-Rab1b$_{N121I}$ expression caused an increased (up to 2-fold) expression of ApoE and ApoB100 transcripts, while having little effect on albumin mRNA expression (Figure 5.8). This observation may be explained either by increased transcription of ApoE and ApoB100 mRNAs in the presence of Rab1b$_{N121I}$ expression, or by their increased stability. In a recent study, WT Rab1b overexpression in non-secretory

cell types was shown to cause increased expression of transcripts encoding proteins involved in the functioning of the secretory system (Romero et al., 2013). Under those conditions, $Rab1b_{N121I}$ had no detectable transcription-inducing activity (Romero et al., 2013). The differences between (Romero et al., 2013) and the current findings may be explained by the use of different experimental systems: the secretory cell-derived Huh-7.5 line used here versus the non-secretory cell-derived HeLa line. Alternatively, the complex mechanisms involved in the regulation of lipoprotein transcript expression may be involved (Zannis et al., 2001a; Zannis et al., 2001b). For example, cholesterol loading was shown to cause upregulation of ApoE and ApoB100 mRNA levels (Dashti, 1992; Mazzone et al., 1987). Since $Rab1b_{N121I}$ expression reduced ApoB100 egress (Figures 5.1, 5.7, as well as 5.10 and 5.11 below), it is plausible that it also inhibited ApoB100-mediated cholesterol egress and the resulting accumulation of intracellular cholesterol may be invoked as one of the mechanisms that could explain the observed upregulation of ApoE and ApoB100 mRNA levels.

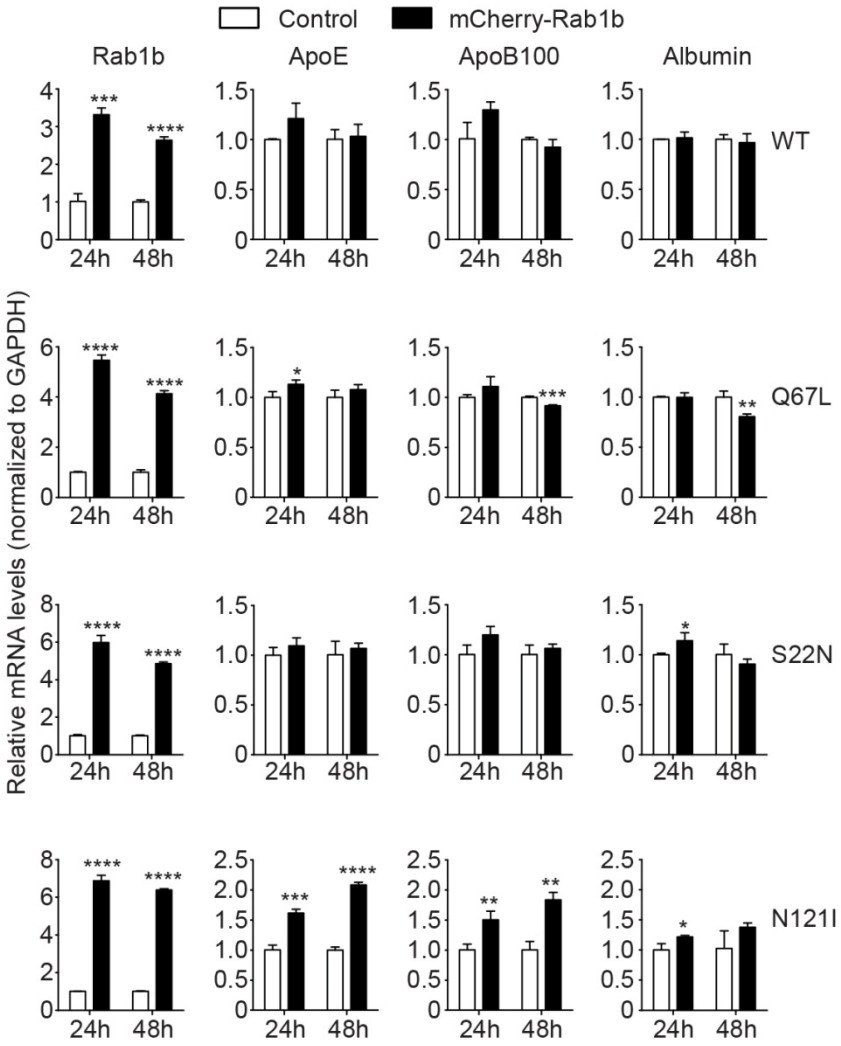

Figure 5.8. Effects of mCherry-Rab1b expression on cargo mRNA levels. Cell lines inducibly expressing the noted mCherry-Rab1b constructs were treated with doxycycline (black bars) or left untreated (white bars) for the indicated durations. mRNA was harvested and analyzed by qRT-PCR. Relative mRNA levels for Rab1b, ApoE, ApoB100 and albumin transcripts are shown (mean ± s.d., n=3 parallel wells). Statistical significance (Student's *t*-test): *, $p<0.05$; **, $p<0.01$; ***, $p<0.001$; ****, $p<0.0001$.

Since mCherry-Rab1b$_{N121I}$ expression caused an increase in the transcript levels of ApoE and ApoB100 (Figure 5.8), I next inquired whether this induction of gene expression manifested itself at the protein level as well. I thank Dr. Ursula Andreo for

performing all radioactivity experiments described here. We compared the relative incorporation of ^{35}S-cysteine and methionine into newly synthesized cargo molecules during a 20-min pulse. In cells expressing mCherry-Rab1b$_{N121I}$ or in control cells, we divided the newly synthesized cargo amounts by the total amounts of newly synthesized protein in the cells, and compared the resulting values. Under these experimental conditions we observed an increase of the relative albumin synthesis, but this increase was not statistically significant (Figure 5.9). In contrast, both ApoE and ApoB100 synthesis was significantly increased, to a magnitude of about two-fold, in the presence of mCherry-Rab1bN$_{121I}$ expression (Figure 5.9). Furthermore, this increase in the relative amount of ApoE and ApoB100 translation closely paralleled the observed elevated mRNA levels for these two species (Figure 5.8).

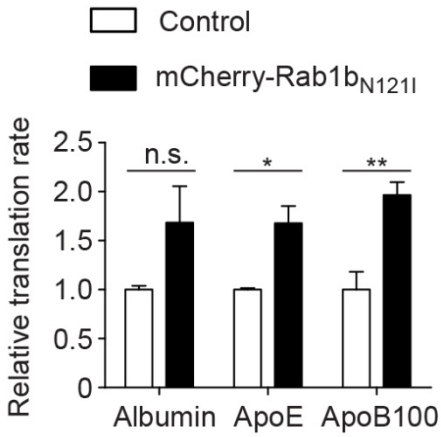

Figure 5.9. Effects of mCherry-Rab1b$_{N121I}$ on cargo translation rate. mCherry-Rab1b$_{N121I}$ expression was induced using 3 μg/mL doxycycline for 24 h (black bars) or left uninduced (control, white bars), then the cells were pulsed with ^{35}S-cysteine and methionine for 20 min and lysed. Albumin, ApoE, and ApoB100-specific incorporation of radiolabeled amino acids was quantified and was reported to the total radioactivity incorporated into the sample. The values (mean ± s.d. of 3 parallel wells) are expressed relative to the control condition. Statistical significance (Student's *t*-test): n.s., non-significant; *, $p<0.05$; **, $p<0.01$.

5.8. Alternative means to quantify cargo secretion

As highlighted above, the use of cell lysate luciferase activity, while accounting for variations of cell mass between wells and experimental conditions, did not account for changes in apparent secretion due to changes in pre-transport processes, such as cargo synthesis. Since mCherry-Rab1b$_{N121I}$ increased the synthesis of ApoB100 and of ApoE (Figures 5.8 and 5.9), it became important to calculate the effective secretion of cargo while taking into account the changes in total cargo mass. I therefore used ELISA to quantify not just the amounts of secreted cargo, but also the amounts cargo that had remained cell-associated at the end of the secretion assay. I then expressed the amount of secreted cargo as fraction of total (secreted + cell-associated) cargo, or calculated a secretion index, defined as the ratio of secreted cargo to cell-associated cargo. Secretion index measurements have previously been used to monitor changes in cargo secretion in other systems (Pan et al., 2008b), and the two measurements are related as follows:

$$Fraction\ secreted = \frac{Secretion\ index}{Secretion\ index + 1}$$

The major difference between the two values is that while the values for the fraction secreted can vary from 0 to 1, the values for the secretion index can vary from 0 to infinity. As such, large changes in the secretion index of a cargo efficiently secreted (for which the secretion fraction is closer to 1) will nonetheless translate into small changes in the cargo's secreted fraction.

Fraction secreted analysis. I once more performed secretion assays in the mCherry-Rab1b inducible cell lines in the presence or absence of doxycycline-mediated mCherry-Rab1b expression. This time I quantified both secreted and cell-associated cargo amounts by ELISA in an attempt to simultaneously account for variations in cell mass as well as cargo expression levels. Expression of mCherry-Rab1b did not alter the secretion of ApoE, ApoB100, or albumin (Figure 5.10A). In contrast, expression of mCherry-Rab1b$_{N121I}$ impaired the secretion of the same set of cargoes (Figure 5.10B). The magnitude of the secretion impairment differed as the ApoE secreted fraction decreased by 18% or 19% from the control value at 24 h or 48 h, respectively. The albumin secreted fraction decreased by 31% or 32%, and the ApoB100 secreted fraction decreased the most, by 39% or 50%, for the 24 h or 48 h time points, respectively (Figure 5.10B). I note that expression of the S22N construct impaired the secretion of albumin and of ApoB100, but not that of ApoE (Figure 5.10C). Lastly, expression of the Q67L construct reproducibly impaired only albumin secretion (Figure 5.10D). Taken together, these results establish the involvement of Rab1 function in the secretion of albumin, ApoE and ApoB100.

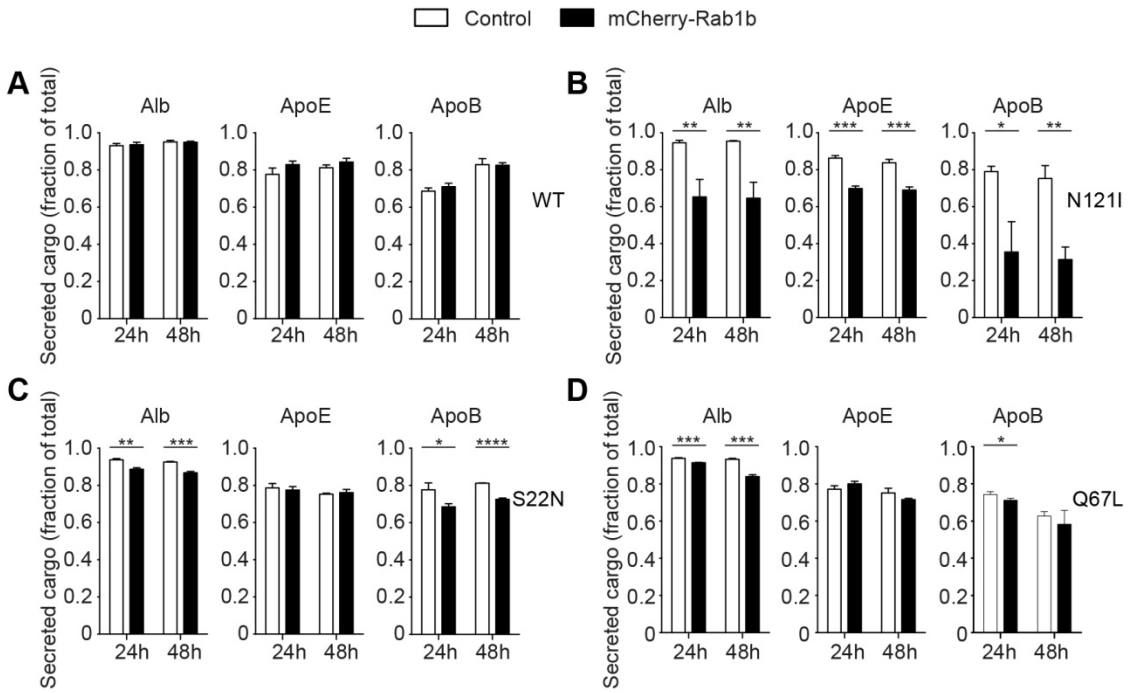

Figure 5.10. Effects of inducible mCherry-Rab1b construct expression on cargo secretion. II: Percent secretion. Cell lines inducibly expressing the noted mCherry-Rab1b constructs were treated with doxycycline for the indicated durations (black bars), or left uninduced (white bars) before a 6 h secretion assay was performed. Secreted and cell-associated amounts of albumin, ApoE and ApoB100 were measured by ELISA and the amounts of secreted cargo were expressed as fraction of total (secreted + cell-associated) amounts. Shown are means ± s.d., n=3 parallel wells. Statistical significance (Student's *t*-test): *, $p<0.05$; **, $p<0.01$; ***, $p<0.001$; ****, $p<0.0001$.

Secretion index analysis. The pattern of the effects of the mCherry-Rab1b mutants on the secretion of the tested cargoes (Figure 5.10) was preserved when secretion indexes were compared (Figure 5.11). Expression of the WT construct did not affect the secretion of either of the three cargoes (Figure 5.11A), while expression of mCherry-Rab1b$_{N121I}$ impaired secretion across the board (Figure 5.11B). Once again, the S22N mutant affected the secretion of both albumin and ApoB, but not that of ApoE while the Q67L mutant affected albumin secretion but not ApoE or ApoB secretion (Figure 5.11C-

D). Since even small, but significant changes in the fractions of cargo secreted (Figure 5.10), corresponded to significant and substantial changes in the cargo secretion indexes (Figure 5.11), I argue that small magnitudes of secreted fraction differences are unlikely to have been caused by technical variations in how the secretion was measured, but are rather true reflections of differences between the secretion capabilities of the cells under these experimental conditions.

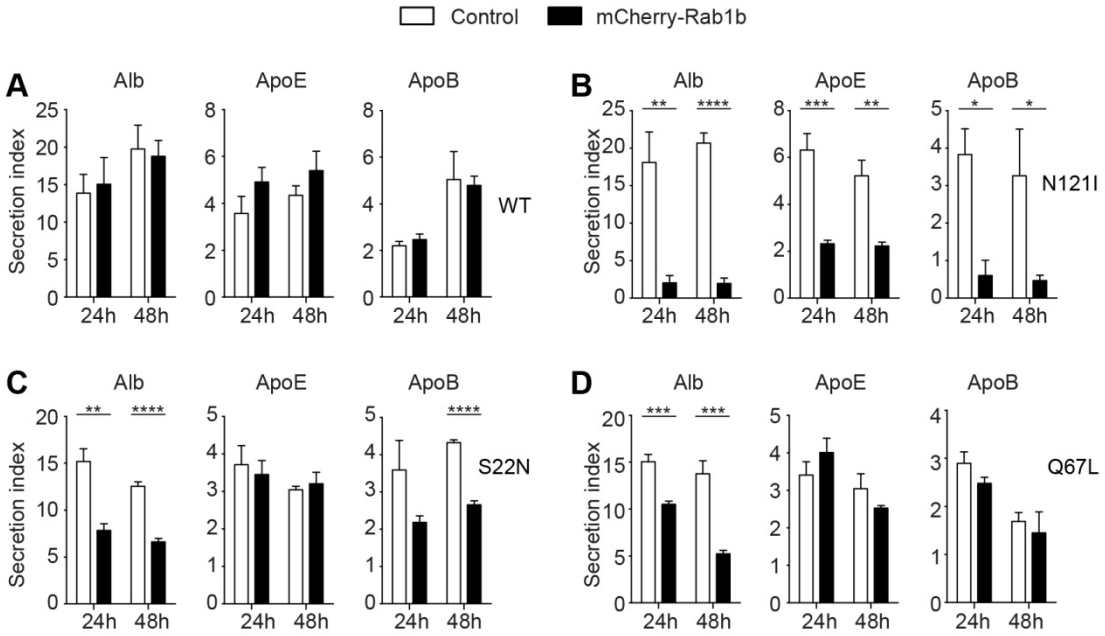

Figure 5.11. Effects of inducible mCherry-Rab1b construct expression on cargo secretion. III: Secretion index analysis. Cell lines inducibly expressing the noted mCherry-Rab1b constructs were treated with doxycycline for the indicated durations (black bars), or left uninduced (white bars) before a 6 h secretion assay was performed. Secretion indexes were calculated by dividing the amounts of cargo secreted by the amounts of cargo that had remained cell-associated. Shown are means ± s.d., n=3 parallel wells. This data was obtained from the same samples as the data shown in Figure 5.10. Statistical significance (Student's *t*-test): *, $p<0.05$; **, $p<0.01$; ***, $p<0.001$; ****, $p<0.0001$.

5.9. mCherry-Rab1b$_{N121I}$ impairs secretion of newly synthesized cargo

I next inquired, again with the help of Dr. Ursula Andreo, whether the observed impairment of cargo secretion caused by mCherry-Rab1b$_{N121I}$ expression (Figures 5.10 and 5.11) was correlated with a decreased rate of secretion of newly synthesized cargo. We thus followed cells that had been pulsed with ^{35}S-cysteine and methionine as they secreted cargo during a chase in the presence of excess cold cysteine, methionine and cycloheximide. At regular time intervals we collected the media and the cell lysates, immunoprecipitated albumin, ApoB100 and ApoE and measured the radioactivity associated with each species. We expressed the amount of newly synthesized cargo species present at any given time point in the cell media as fraction of the total (secreted + cell-associated) amount of newly synthesized cargo recovered at that time point. Using this analysis, we observed that lower fractions of newly synthesized albumin, ApoE and ApoB100 were secreted in the presence of mCherry-Rab1b$_{N121I}$ expression, compared to control, by magnitudes in the range of 10-30% (Figure 5.12). The decrease in total cargo secretion observed in the presence of mCherry-Rab1b$_{N121I}$ expression (Figures 5.10 and 5.11) thus correlates with a decrease in the rate of secretion of newly synthesized cargo (Figure 5.12).

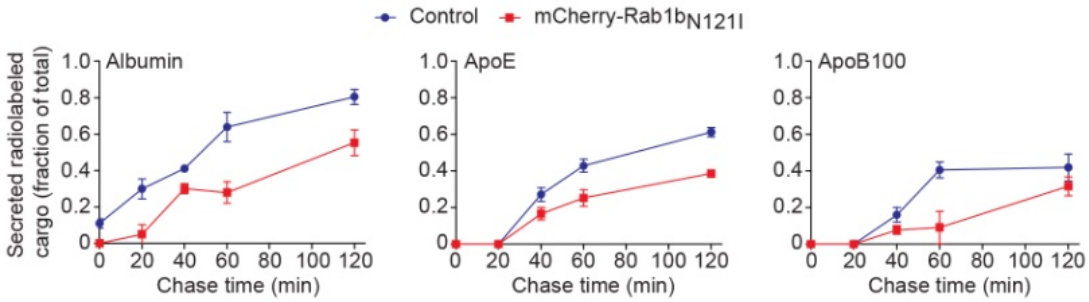

Figure 5.12. Effects of mCherry-Rab1b$_{N121I}$ on the secretion of newly synthesized hepatic cargoes. mCherry-Rab1b$_{N121I}$ expression was induced for 24 h (red trace) or left uninduced (blue trace), then the cells were pulsed with ^{35}S-cysteine and methionine for 20 min and then chased. Newly synthesized amounts of albumin, ApoE and ApoB100 were quantified at the indicated chase time points in both media and cell lysates. The radioactivity of secreted cargo at each time point is expressed as a fraction of the total (secreted + cell-associated) radioactivity of that cargo. Means ± s.d. of 3 parallel wells are depicted.

5.10. Inactivation of endogenous Rab1 function

In the work presented so far, secretion of cargo was impaired by overexpressing DN Rab constructs. To test whether inactivation of endogenous Rab1 function also affected cargo secretion, I engineered the Huh-7.5 TetON cells to inducibly express a *L. pneumophila* protein, DrrA, which has been shown to be exported by the bacterium into the cytosol of infected cells where it interferes with Rab1 function (Machner and Isberg, 2006; Murata et al., 2006). DrrA, also known as SidM (Machner and Isberg, 2006; Murata et al., 2006), possesses several functional domains: a Rab1 AMPylation domain (Hardiman and Roy, 2014; Muller et al., 2010), a Rab1 binding domain and a Rab1 GDF/GEF domain (Ingmundson et al., 2007; Murata et al., 2006; Schoebel et al., 2009; Suh et al., 2010; Zhu et al., 2010) and a phosphatidylinositol 4-phosphate lipid binding domain (Brombacher et al., 2009; Del Campo et al., 2014; Schoebel et al., 2010; Zhu et

al., 2010). The DrrA construct which I used, GFP-DrrA$_{61-647}$, but which I will refer to from here on simply as GFP-DrrA, has part of the AMPylation domain (Muller et al., 2010) deleted and does not exhibit the general cytotoxic effects of full length DrrA (Murata et al., 2006). This construct also preferentially binds and acts on Rab1 GTPases, and its expression interferes with ER to Golgi transport of β-1,4-galactosyl-transferase and disrupts Golgi structure (Machner and Isberg, 2006; Murata et al., 2006), as expected of a Rab1 inhibitor. I also engineered a TetON-GFP control cell line, and I transduced both the GFP-DrrA and GFP cell lines with a luciferase-expressing lentivirus in order to easily monitor the effects of construct expression on cell mass. In secretion assays, GFP expression alone did not affect the secretion of either of the three cargoes tested (Figure 5.13A). In contrast, GFP-DrrA impaired the secretion of albumin and ApoB100, but not that of ApoE (Figure 5.13B), mirroring the effect of mCherry-Rab1b$_{S22N}$ expression (Figures 5.10C and 5.11C). The GFP and the GFP-DrrA proteins were detected in lysates of the respective cell lines only after induction with doxycycline (Figure 5.13C). GFP protein levels were significantly higher than GFP-DrrA levels, since the GFP-DrrA blot required use of a more sensitive chemiluminescence substrate system to allow detection of the GFP-DrrA band. At the same time GFP-DrrA expression did not decrease the luciferase activity of the cell lysates (Figure 5.13D), thus alleviating concerns regarding cytotoxicity, which is consistent with previous findings (Murata et al., 2006). Overall, these results established that inhibition of endogenous Rab1 function impairs hepatic cargo secretion and provided independent confirmation of the results obtained by overexpressing the DN Rab1b constructs.

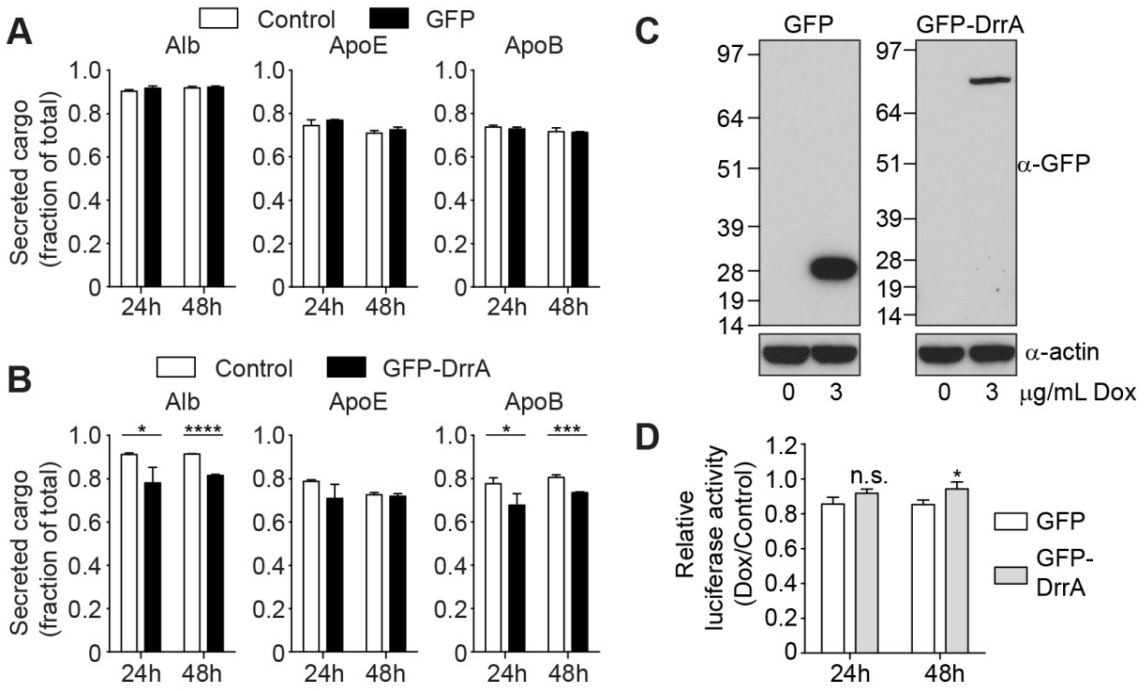

Figure 5.13. Inactivation of endogenous Rab1 function impairs hepatic cargo egress. Cell lines inducibly expressing GFP (A), or GFP-DrrA (B) were induced with doxycycline (black bars) or left uninduced (white bars) for the indicated durations, then a 6 h secretion assay was performed. Secreted and cell-associated amounts of albumin, ApoE and ApoB100 were measured by ELISA and the amounts of secreted cargo were expressed as fraction of total (secreted + cell-associated) amounts. Means ± s.d. of values obtained in three parallel wells are shown. Statistical significance (Student's *t*-test): *, $p<0.05$; **, $p<0.01$; ***, $p<0.001$; ****, $p<0.0001$. (C) Western blotting of cell lysates from inducible GFP or GFP-DrrA cell lines after 2 days of induction with 0 or 3 μg/mL Doxycycline (Dox). Proteins were detected with α-GFP and α-actin antibodies. Molecular weight markers (kDa) are listed at the left of the blots. The GFP blot (top left) and the actin blots (bottom) were developed with the less sensitive ECL Prime detection reagent, while the GFP-DrrA blot (top right) was developed with the more sensitive West Femto reagent. Expected molecular weights: GFP, 27 kDa; GFP-DrrA, 94 kDa.

5.11. Rab1 and HCV secretion

HCV secretion and infectivity requires expression of amphipathic helix-containing apolipoproteins (such as ApoE and ApoB100) by the HCV-producing cells (Fukuhara et al., 2014; Hueging et al., 2014), raising the possibility that HCV employs some of the same secretion route(s) as the lipoproteins. Having established that Rab1 inactivation impairs the secretion of the lipoprotein components ApoE and ApoB100 and of the non-lipoprotein cargo albumin from the Huh-7.5 cell line, I next investigated the effect of Rab1 inactivation on the secretion of HCV. In order to discern between a previously proposed Rab1 function in genome replication (Nevo-Yassaf et al., 2012; Sklan et al., 2007a; Sklan et al., 2007b) and its putative function in virus particle secretion, I allowed the viral genome replication machinery to become established for two days following viral RNA electroporation. Then, I induced mCherry-Rab1b$_{N121I}$ expression to inactivate Rab1 function, and performed secretion assays (Figure 5.14A). I performed several variations of this experiment, by varying either the duration of mCherry-Rab1b$_{N121I}$ expression, or the length of the secretion assay (Figure 5.14A-B) Despite varying these experimental parameters, inhibition of Rab1 function consistently caused a significant increase of the fraction of HCV infectivity that remained cell-associated (Figure 5.14B). This result is consistent with expression of mCherry-Rab1b$_{N121I}$ impairing the transport of newly assembled infectious HCV particles from the ER to the Golgi and causing their concomitant accumulation in an ER-related compartment. These observations are also similar to those noted when anterograde transport of HCV was inhibited by treatment of HCV producing cells with brefeldin A, a potent, widely-used blocker of ER to Golgi transport (Gastaminza et al., 2008;

Lippincott-Schwartz et al., 1989). Furthermore, I found that intracellular HCV RNA levels were also slightly elevated in cells expressing the DN Rab1b construct (Figure 5.14C), consistent with impaired release of HCV RNA via the secretory pathway. Without ruling out a Rab1b function in HCV replication, these results do not favor a massive inhibition of this process by mCherry-Rab1b$_{N121I}$. Lastly, the magnitudes of the sensitivity of ApoE, albumin, and ApoB100 secretion from HCV-infected cells (Figure 5.14D) retained the same relative order as in HCV-free cells (Figures 5.1A-B, 5.7, 5.10 and 5.11). Thus, ApoB100 secretion remained most potently impaired, while ApoE secretion was the least negatively affected, and albumin secretion displayed an intermediate phenotype.

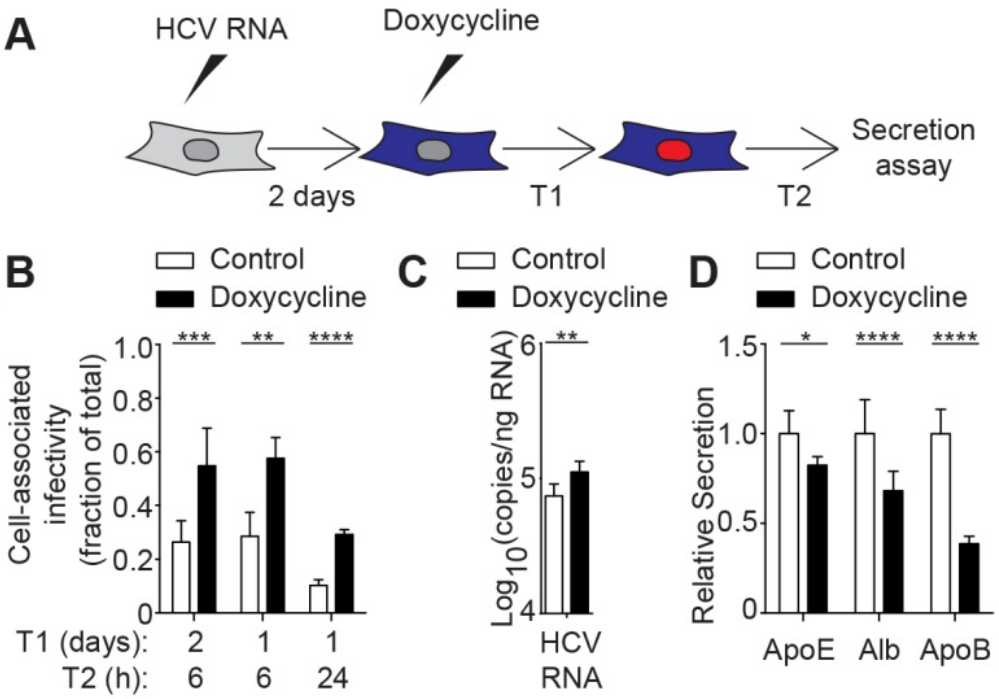

Figure 5.14. Effects of mCherry-Rab1b$_{N121I}$ on HCV infectivity release. (A) Experimental design: cells were electroporated with HCV RNA, allowed to establish HCV infection for 2 days, then induced to express mCherry-Rab1b$_{N121I}$ by treatment with doxycycline for a duration designated T1 (1 or 2 days), then a secretion assay was performed for a period designated T2 (6 or 24 h). Control cells were treated identically except that they were not induced with doxycycline. (B) Effects of mCherry-Rab1b$_{N121I}$ expression on secretion of infectious HCV particles. The experimental format outlined in panel A was followed, while varying T1 and T2, as listed under the graph. For each experiment, 3 parallel HCV RNA electroporations were performed. For each electroporation, 3 wells were induced to express mCherry-Rab1b$_{N121I}$ (black bars) and 3 wells were left uninduced (white bars). Secreted and cell-associated infectivity was measured and the cell-associated infectivity in each well was expressed as fraction of the total infectivity in that well. (C). Total cell-associated HCV RNA was quantified by qRT-PCR in additional wells from the experiment for which T1 = 2 days and T2 = 6 h. (D) Secreted cargo amounts were quantified by ELISA and normalized to the luciferase activity of the corresponding wells (T1 = 2 days and T2 = 6 h). (B-D) Bars represent means ± standard error of the mean for the 3 replicate electroporations. Statistical significance (2-way ANOVA test): *, $p<0.05$; **, $p<0.01$; ***, $p<0.001$; ****, $p<0.0001$.

5.12. Discussion

Technical concerns. Before discussing the general findings of this Rab1-focussed body of work, I wish to address two technical concerns. The first deals with potential toxic effects caused by inhibition of ER-to-Golgi traffic by expression of the DN Rab1b constructs. This concern stems from the knowledge that ER-to-Golgi traffic is essential for cell viability, as evidenced by the findings that Ypt1 loss of function is lethal in yeast (Haubruck et al., 1989; Schmitt et al., 1986; Segev and Botstein, 1987; Segev et al., 1988; Wagner et al., 1987). Rab1 is the mammalian homolog of Ypt1 (Haubruck et al., 1989; Segev et al., 1988; Touchot et al., 1987; Vielh et al., 1989; Zahraoui et al., 1989). Due to this concern I have employed several means to assess cell health. The luciferase activity measurements (Figures 5.1C and 5.7A) did indeed document decreased luciferase activities in cells expressing the DN Rab1b constructs. These decreases were generally no larger than a 2-fold change over 54 h of expression (48 h from the time of lentivirus transduction or doxycycline induction + 6 hours of secretion assay). Such small decreases are inconsistent with massive cell death, but could in turn be caused by growth delays secondary to reduced rates of exocytic transport. Second, effects of DN Rab1 expression on cargo secretion were evident even at early time points after induction (Figure 5.7B), when the luciferase activity in the cell lysates had not changed or had decreased only slightly (Figure 5.7A, 12 and 24 h time points). Third, a divergent membrane transport process, transferrin endocytosis, remained unaffected by expression of various Rab1b constructs, a finding inconsistent with the Rab constructs having caused overwhelming toxicity (Figure 5.5). Fourth, while morphological changes did become noticeable in DN Rab1-expressing cells, many cells in the culture retained the morphology specific to the

Huh-7.5 cell line (Figure 5.6A). Fifth, that cells expressing mCherry-Rab1b$_{N121I}$ synthesized cargo proteins at higher rates than the control cells (Figure 5.9), that this increase in the rate of synthesis correlated with increased expression of cargo messages (Figure 5.8), and that the secretion of the newly synthesized cargoes was decreased in the same conditions (Figure 5.12), served as further evidence that, while affected in some aspects, cell physiology retained a high degree of functionality. I thus argue that, regardless of adverse effects on cell health caused by inhibition of anterograde transport from the ER to the Golgi, the results of the experiments presented above were properly interpreted to yield the conclusion that Rab1 was indeed involved in anterograde transport of these cargoes.

The second technical issue deals with apparent differences between the results obtained using the luciferase activity-based method of normalization (Figures 3.8, 5.1, and 5.7), and those obtained using the normalization method using cell-associated cargo amounts (Figures 5.10, 5.11, and 5.12). Both methods took into account the cell mass responsible for the measured secretion. The later method also accounted for the observed changes in cargo mRNA expression and cargo synthesis (Figures 5.8 and 5.9). For ApoE, a two-fold increase in its translation rate (Figure 5.9) could overcome a 10-20% decrease in transport rate (Figure 5.12), to cause an overall apparent increase in the amount of cargo accumulated in the cell culture media (Figures 3.7, 3.8, 5.1A-B, and 5.7B). For albumin, a smaller increase in expression counteracted by the observed decrease in secretion could account for the relatively small observed net change in secretion amounts (Figures 5.1A-B and 5.7B). ApoB100, in contrast, would have been expected to display a phenotype similar to that of ApoE, since their rates of translation and of secretion had

changed in similar ways in response to DN Rab1b expression (Figures 5.8 and 5.9). However, ApoB100 also undergoes significant degradation associated with the ER (Ginsberg and Fisher, 2009), which does not appear to be the case for ApoE or albumin (Ye et al., 1992; Ye et al., 1993). Thus, although more ApoB100 was being synthesized, if a significant portion of it was degraded along the secretion route, combined with a slower secretion rate overall, these phenomena may well account for the observed overall decrease in secretion. I believe therefore that the results obtained using luciferase-based normalization and those obtained using the cell-associated cargo amounts for normalization, while facially different, were nevertheless consistent with each other as well as with a model in which Rab1 controls the secretion of the analyzed cargoes.

Rab1 functions in hepatic cargo secretion. As described in this chapter, I investigated whether Rab1 mediated ER to Golgi transport of several hepatic secretory cargoes. I found that inactivation of Rab1 function - by expression of DN mutants or of a bacterial effector targeting Rab1 - impaired the secretion of albumin, ApoE, ApoB100 and infectious HCV particles. I propose that Rab1 mediates anterograde transport of these cargoes, as it does for many other cargoes investigated to date (Dong et al., 2012; Dugan et al., 1995; Filipeanu et al., 2004; Filipeanu et al., 2006; Flowerdew and Burgoyne, 2009; Ingmundson et al., 2007; Nachmias et al., 2012; Plutner et al., 1991; Robitaille et al., 2009; Satoh et al., 1997; Wu et al., 2001; Wu et al., 2003; Yamayoshi et al., 2010; Zenner et al., 2011; Zhuang et al., 2010). My findings are consistent with the documented Rab1 association with *in vitro*-made vesicles loaded with VLDL (Rahim et al., 2012). Further corroborating evidence comes from the documented functional association of Rab1 with vesicle coat complexes COPII and COPI implicated in ER to Golgi transport.

COPII mediates sorting of hepatic cargo into anterograde transport vesicles during ER exit (Gusarova et al., 2003; Jones et al., 2003; Siddiqi, 2008; Siddiqi et al., 2003). COPI, in turn, can mediate cargo transport from the ERGIC to the Golgi (Garcia-Mata et al., 2003; Pepperkok et al., 1993; Peter et al., 1993; Shima et al., 1999; Stephens et al., 2000). Rab1 interacts with and may be activated downstream of both COPII and COPI (Kim et al., 2006; Slavin et al., 2011; Yamasaki et al., 2009). Once activated on the surface of transport carriers, Rab1 may interact with a series of effectors, including the Golgi tethering factor p115 (Allan et al., 2000), and GBF1, which is the GEF that activates Arf1 and thus initiates COPI recruitment (Alvarez et al., 2003; Monetta et al., 2007). The ability of mCherry-Rab1b$_{N121I}$ to interfere with hepatic cargo transport could, for example, be mediated through disruption of the function of these effectors. Indeed, expression of Rab1b$_{N121I}$ has been shown to increase the mobility of p115, likely by increasing the rate of its exchange between cytosolic and membrane-bound pools (Brandon et al., 2006). Expression of the N121I mutant construct may also interfere with COPII and/or COPI function in anterograde transport (Alvarez et al., 2003; Monetta et al., 2007; Slavin et al., 2011), which may in turn impair cargo secretion.

Distinct pathways are likely involved in anterograde transport of albumin, ApoE and ApoB100. A recurring observation in the experiments that I presented here was that the various means used to impair Rab1 function differentially affected albumin, ApoE and ApoB100 secretion. This was evident in the different magnitudes of the disruption caused by the N121I mutant (Figures 5.10 and 5.11), and also in the lack of effect of the S22N mutant or of GFP-DrrA on ApoE secretion (Figure 5.13). Since measurements of the amounts of each cargo were performed in parallel in each sample, I

do not view potential variations in cargo quantification efficiencies as a likely explanation of these results. I cannot presently exclude confounding effects of other biological processes, such as cargo degradation known to occur during secretion, or lipoprotein particle maturation processes (Ginsberg and Fisher, 2009; Rutledge et al., 2010; Ye et al., 1992; Ye et al., 1993). I nonetheless note that these results are consistent with a model, supported by *in vitro* experiments (Gusarova et al., 2007; Siddiqi, 2008), in which various hepatic cargoes are transported out of the ER in distinct carriers. Furthermore, a quantitative electron microscopy study has shown that VSVg sorting into ER-derived transport carriers is accompanied by a concentration of this cargo, to levels maintained throughout exocytic transport (Balch et al., 1994). A similar observation was described regarding the transport of human serum albumin from the ER to the Golgi in the HepG2 human hepatoma cell line (Mizuno and Singer, 1993). This packing of cargo in transport carriers, if sufficiently specific, may well yield the different populations of cargo-specific carriers previously identified biochemically (Gusarova et al., 2007; Siddiqi, 2008) and inferred from the different sensitivity of their transport to inhibition of Rab1 function, as described here. Lastly, such differential regulation of anterograde traffic appears not to be limited to hepatocyte function since dendrite and axon growth, respectively, displayed distinct sensitivity to inactivation of the function of the early exocytic regulators Sec23, Sar1 and Rab1 (Ye et al., 2007), while secreted and transmembrane protein transport exhibited distinct sensitivities to GBF1 knockdown (Szul et al., 2007). Further supporting this model, some anterograde cargoes may undergo, under certain experimental conditions, Rab1-independent transport from the ER to the cell periphery (Filipeanu et al., 2006; Wu et al., 2003; Yoo et al., 2002).

Varied effects of the Rab1 inhibition methods. In my hands, albumin secretion was inhibited by all three Rab1 mutants, and by the *L. pneumophila* effector DrrA. ApoB secretion was not inhibited by the Q67L mutant, while ApoE secretion was only inhibited by the N121I mutant. These differences raise questions as to how the various means of blocking Rab1 function actually affected transport. The effect of the Q67L mutant on albumin secretion stands out to begin with, since this mutant does not impair transport of the model cargo VSVg (Tisdale et al., 1992). $Rab1b_{Q67L}$ possesses low intrinsic GTPase activity, but is expected to have normal GAP-stimulated GTPase activity, since this Q67 residue, unlike the equivalent glutamine in other small GTPases, including other Rabs, does not enact GTP hydrolysis in the presence of the cognate Rab1 GAP, TBC1D20 (Gavriljuk et al., 2012). Instead, TBC1D20 provides a catalytic glutamine residue (Gavriljuk et al., 2012). As such, if transport of VSVg, ApoE and ApoB100 primarily involve GAP-mediated GTP hydrolysis, then the lack of effect of the Q67L mutant is unsurprising. Furthermore, it is plausible that albumin transport relies more heavily on unstimulated Rab1 GTPase activity, which may in turn explain the current findings. Alternatively, it is conceivable that Arf1 stabilization on membranes by $Rab1b_{Q67L}$ (Monetta et al., 2007) may affect albumin secretion, although this would raise the question as to why only albumin was affected.

The other means of Rab1 inactivation may affect cargo transport through different mechanisms. $Rab1b_{S22N}$ is likely to compete with endogenous Rab1 for either a Rab1 GEF or for GDI (Nuoffer et al., 1994). GFP-DrrA, a protein which displays Rab1 GEF activity and potentially concurrent Rab1 GDF activity (Ingmundson et al., 2007; Machner and Isberg, 2007; Schoebel et al., 2009; Suh et al., 2010; Zhu et al., 2010), caused similar

changes in cargo secretion as did mCherry-Rab1b$_{S22N}$. DrrA may recruit Rab1 - and activate it - at ectopic, PI4P-containing membranes, such as the plasma membrane (Murata et al., 2006), thereby removing it from the native pathway of ER to Golgi transport. It appears likely, therefore, that the similar effects of the Rab1b$_{S22N}$ and DrrA constructs might be achieved through disruption - in distinct ways - of the activation of Rab1 at the ER. In contrast, the unstable binding of nucleotides by the N121I mutant likely causes a rapid oscillation between the GDP and GTP-bound forms, which likely destabilizes effector recruitment to membranes (Alvarez et al., 2003; Brandon et al., 2006; Monetta et al., 2007; Pind et al., 1994). The pan-cargo effects that we observed when we used the N121I mutant imply that the ability of Rab1 to cycle between GTP- and GDP-bound forms, or to bind effectors for a long-enough duration may be universally required for the transport of Rab1-dependent cargoes. Since the N121I mutant blocks VSVg transport at the ERGIC (Alvarez et al., 2003; Pind et al., 1994; Tisdale et al., 1992), it is likely that the initial, COPII-mediated transport from the ER to the ERGIC does not require lengthy Rab1-effector interaction. This would be further supported by the spatial proximity between ER exit sites and the ERGIC (Bannykh et al., 1996). The S22N, in contrast, causes retention of VSVg in the ER (Alvarez et al., 2003; Nuoffer et al., 1994; Tisdale et al., 1992). VSVg, and likely albumin and ApoB as well, presumably require Rab1 function for their COPII-mediated transport from the ER to the ERGIC. It is surprising that ApoE secretion is insensitive to the Rab1b$_{S22N}$ or DrrA-mediated shift in the GDP-Rab1/GTP-Rab1 balance. Whether ApoE utilizes a novel transport pathway out of the ER may warrant further investigation.

Rab1 functions in infectious HCV particle secretion. By documenting Rab1 involvement in infectious HCV particle secretion, this work complements previous findings implicating Rab1, and its cognate GAP, TBC1D20, in HCV genome replication (Haas et al., 2007; Nevo-Yassaf et al., 2012; Sklan et al., 2007a; Sklan et al., 2007b). TBC1D20 interacts with HCV NS5A (Sklan et al., 2007b). Rab1b (Sklan et al., 2007a) or TBC1D20 (Sklan et al., 2007b) knockdowns decrease HCV genome replication. Expression of GFP-Rab1b$_{N121I}$ caused fragmentation of lipid droplets, organelles implicated in HCV particle assembly (Miyanari et al., 2007), as well as changes in the pattern of NS5A localization (Nevo-Yassaf et al., 2012). However, the effects of Rab1b inactivation on the secretion of infectious HCV particles have not been assessed. Under experimental conditions described above, DN Rab1b expression did not decrease the abundance of cell-associated HCV genomes implying that HCV genome replication was not greatly affected by expression of this mutant, while particle egress was impaired. It is plausible that the Rab1 function in ER to Golgi transport that is inhibited by expression of the N121I mutant be dispensable for HCV genome replication. I did not investigate whether Rab1 function is important for earlier steps of the HCV life cycle, spanning from entry through the establishment of the replication machinery, which could further explain the documented Rab1b knockdown phenotype (Sklan et al., 2007a). Indeed, I inactivated Rab1 function only after allowing replication to become established for 2 days following electroporation of the HCV RNA. Presumably, by this stage, HCV RNA replication has become largely insensitive to (DN-mediated) inhibition of Rab1 function. Another difference between my work and the previous study (Nevo-Yassaf et al., 2012) is the method of DN Rab1 expression. While (Nevo-Yassaf et al., 2012) employed plasmid

transfection, in my hands this method of expression was accompanied by considerable cytotoxic effects, potentially due to high levels of construct overexpression in transfected cells. I was therefore necessitated to employ inducible gene expression from stable cell lines, which may account for some of the observed differences. Nevertheless, our results remain in agreement with previously published studies, and overall document the involvement of Rab1-mediated ER-to-Golgi transport in the secretion of infectious HCV particles.

Chapter 6

Functional Characterization of an ApoE-GFP Fusion

6.1. Introduction

The investigation into how hepatic cargo secretion is regulated, which I described in the previous three chapters, was based primarily on genetic and biochemical assays. To more comprehensively analyze hepatic cargo egress, I wanted to complement these approaches with live cell imaging studies. Live cell imaging assays have the advantage of providing both spatial and temporal dynamic views of the cellular processes studied (Lippincott-Schwartz et al., 2001; Liu et al., 2015; Wouters et al., 2001). Furthermore, live cell imaging of vesicular transport of secreted cargo may provide single-event-level description of this process and therefore reveal unexpected behaviors otherwise lost by the averaging of unsynchronized behaviors, which is inherent to many biochemical approaches (Wennmalm and Simon, 2007). Expression of fluorescent protein-tagged constructs has become a standard and powerful method used to study spatial and temporal dynamics of proteins, membranes and organelles in live cells. The method relies on fusing, in frame, a DNA fragment encoding one of an ever-growing list of fluorescent proteins (Chudakov et al., 2010) to the 5'- or 3'-end of a DNA fragment encoding a protein whose dynamics are to be studied, followed by expression of the resulting chimeric gene. Powerful spatio-temporal studies may be carried out and their results properly interpreted if fluorescent protein tagging does not detectably interfere with the process studied (Jacobs et al., 1999). Unfortunately, fluorescent protein tagging may also

result in DN, non-functional, or mislocalized fusion proteins, as outlined in greater detail in a previous study (Rappoport and Simon, 2008). Thus, to avoid collecting and interpreting artifactual data caused by expression of aberrantly-behaving fluorescent protein fusions, an initial battery of functional tests should be performed (Rappoport and Simon, 2008). I present in this chapter such a functional characterization of an ApoE-GFP fusion protein for use in the investigation of lipoprotein and HCV secretion from hepatic cells.

6.2. A roadmap for investigating ApoE-GFP functionality

Previous studies have described ApoE-GFP constructs that were used to image microtubule-dependent ApoE secretion from macrophages (Kockx et al., 2007), or to colocalize ApoE with fluorescently-labeled HCV Core-containing entities (Coller et al., 2012). In the macrophage study, ApoE-GFP secretion from cells was comparable to that of untagged ApoE. Additionally, its localization at the ER, Golgi, and within secretory vesicles, as well as its movement along microtubules, was consistent with behaviors expected of this secreted protein (Kockx et al., 2007), suggesting that this ApoE-GFP is a good marker for the secretion of ApoE from macrophages. Whether ApoE-GFP is also a useful marker for monitoring ApoE secretion from hepatic cells, in the presence or absence of HCV infection, has not been formally addressed to date.

As I mentioned in Chapter 1, some of the lipid metabolic functions of ApoE are mediated through its interaction with ApoB100-containing VLDL (Blum et al., 1980; Havel et al., 1980). Hepatocyte-made ApoE, in particular, may associate intracellularly with VLDL particles (Dolphin, 1981; Fazio and Yao, 1995; Gusarova et al., 2007), and promote the secretion of VLDL-associated triglycerides (Huang et al., 1998; Kuipers et

al., 1997). Furthermore, ApoE is incorporated into HCV particles that assemble at the ER of infected hepatocytes (Andre et al., 2002; Catanese et al., 2013; Chang et al., 2007; Lindenbach, 2013; Lindenbach and Rice, 2013; Miyanari et al., 2007; Nielsen et al., 2006). This ApoE-HCV association is important for efficient production of HCV particles and for the infectivity of the released virions (Chang et al., 2007; Fukuhara et al., 2014; Hishiki et al., 2010; Hueging et al., 2014; Lee et al., 2014; Long et al., 2011; Vogt et al., 2013).

Given these hepatocyte-specific functions of ApoE in lipoprotein and HCV particle formation and release, I outlined several functional assays that are needed to determine whether ApoE-GFP functionally reproduces the behavior of untagged ApoE with respect to lipoprotein and infectious HCV particle release from hepatic cells. These tests aimed to determine whether: i) ApoE-GFP was properly expressed in cells; ii) ApoE-GFP colocalized with untagged ApoE; iii) ApoE-GFP was secreted from cells with similar efficiency as untagged ApoE; iv) ApoE-GFP associated with secreted lipoprotein particles; and v) tagged ApoE retained the ability to support infectious HCV production. Overall, the results of the experiments designed to address these questions indicated that ApoE-GFP faithfully reproduced known aspects of ApoE association with secreted hepatic lipoproteins, and support its use in future imaging studies aimed at elucidating dynamic spatio-temporal aspects of lipoprotein secretion.

6.3. ApoE-GFP expression

I tagged ApoE with GFP by fusing the fluorescent protein to the carboxyl-terminus of full length human ApoE3. Silent mutations were introduced in the ApoE-coding region to confer resistance to shRNA-mediated knockdown. I am grateful to Dr.

Margaret Scull and Joshua Horwitz for their efforts in making this shRNA-resistant ApoE-expressing cDNA clone. I tagged this ApoE sequence at its carboxyl-terminus with monomeric enhanced GFP (mEGFP), which has a dimerization-disrupting A206K mutation (Zacharias et al., 2002). I used the mEGFP variant to prevent potential GFP-mediated artifactual aggregation of the resulting fusion protein. The linker between ApoE and GFP is predicted to be identical with that found in the ApoE-GFP construct that was previously characterized in macrophages (Kockx et al., 2007). From here on, I refer to the shRNA-resistant ApoE3-mEGFP construct that I made as ApoE-GFP.

To characterize ApoE-GFP, I stably expressed it in human hepatoma Huh-7.5 cells, which secrete both ApoB100- and ApoE-containing lipoproteins and support the complete HCV life cycle (Lindenbach et al., 2005; Meex et al., 2011). Huh-7.5/ApoE-GFP cells expressed both ApoE-GFP (62 kDa predicted unglycosylated molecular weight) and untagged endogenous ApoE (predicted 34 kDa), as detected using a polyclonal α-ApoE antibody (Figure 6.1A). The ApoE-GFP fusion was also detected using an α-GFP antibody (Figure 6.1B), but was not detected using a monoclonal α-ApoE antibody (clone EP1374Y) raised against the C-terminus of ApoE (Figure 6.1C). C-terminal tagging of the ApoE sequence presumably renders this antibody's epitope unrecognizable. ApoE-GFP was not detected in the parental Huh-7.5 cell line, nor in the empty vector (EV) transduced control cell line Huh-7.5/EV Hygro (Figure 6.1A-B). Similar amounts of cell lysate from each of the three cell lines were loaded, as detected by an α-actin antibody (Figure 6.1D).

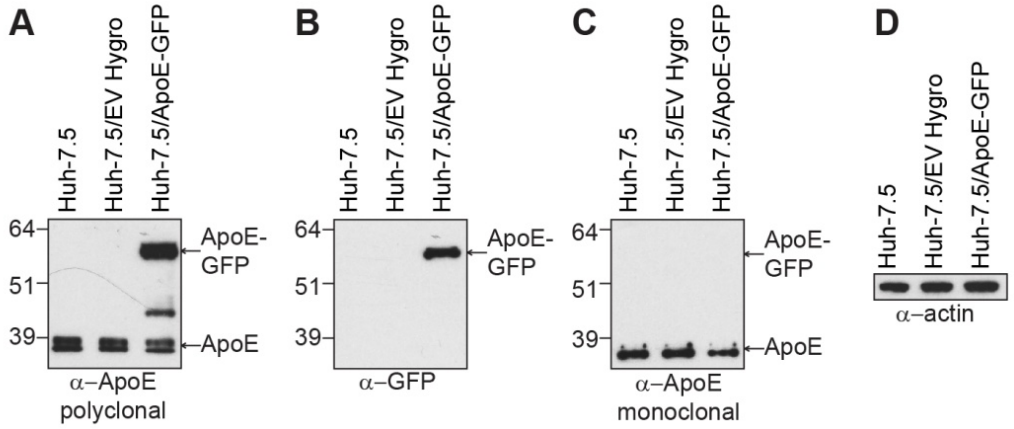

Figure 6.1. Expression of ApoE-GFP in Huh-7.5 cells. Lysates from Huh-7.5 cells, from Huh-7.5/EV Hygro cells, or from Huh-7.5/ApoE-GFP cells were immunoblotted with the following antibodies: (A) α-ApoE, AB947 goat polyclonal, (B) α-GFP, (C) α-ApoE, clone EP1374Y, rabbit monoclonal, and (D) α-actin. Molecular weights (kDa) are listed at the left of the blots. ApoE and ApoE-GFP bands are labeled at the right.

6.4. ApoE-GFP colocalizes with endogenous ApoE

I used the fortuitously discovered EP1374Y monoclonal antibody, which only recognizes the untagged form of ApoE, to characterize the intracellular localization of endogenously-expressed, untagged ApoE, relative to that of ApoE-GFP. We first confirmed that this monoclonal antibody did not recognize ApoE-GFP in immunofluorescence experiments. Neither HeLa cells, which do not express endogenous ApoE (Smith et al., 1988), nor HeLa cells that had been transduced with the ApoE-GFP construct, showed staining with the α-ApoE antibody, while HeLa cells expressing a GFP-ApoE fusion (with GFP at the amino-terminus) became brightly stained under the same conditions (Figure 6.2). Both ApoE-GFP and GFP-ApoE transduced HeLa cells stained with an α-GFP antibody (Figure 6.2). I thank Caroline Gleason for performing this reagent testing-experiment.

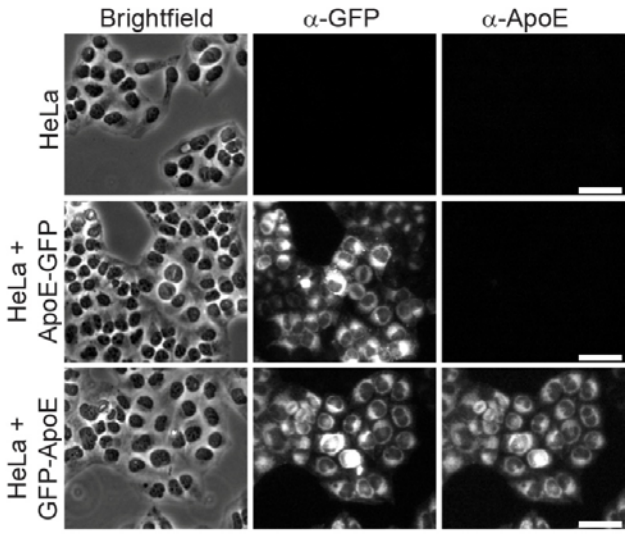

Figure 6.2. An α-ApoE antibody does not recognize ApoE-GFP in immuno-fluorescence assays. The following cells were stained with the rabbit α-ApoE monoclonal antibody EP1374Y: HeLa cells (do not express endogenous ApoE), HeLa cells expressing ApoE-GFP, and HeLa cells expressing GFP-ApoE. An α-GFP antibody was used to boost the GFP signal. While GFP staining occurred in both ApoE-GFP- and GFP-ApoE-expressing cells, ApoE staining occurred only in the GFP-ApoE expressing cells, where the C terminus of ApoE (the immunogen for EP1374Y) presumably remained accessible. No staining was observed in untransduced HeLa. Scale bars, 50 μm.

Since the α-ApoE antibody did not recognize the ApoE-GFP fusion protein in Western blotting (Figure 6.1C) or immunofluorescence (Figure 6.2) experiments, I processed the Huh-7.5/ApoE-GFP cells for immunofluorescence using an α-GFP antibody to boost the signal from the GFP, and with the monoclonal α-ApoE antibody. The resulting signals displayed reticular and punctate distributions (Figure 6.3A), consistent with expected ER and secretory vesicle localization. Perinuclear accumulation of signal consistent with Golgi localization was also apparent. (Figure 6.3A, arrowhead). Importantly, the ApoE-GFP and the ApoE signals overlapped, particularly within puncta that likely represented secretory vesicles (Figure 6.3B, arrowheads).

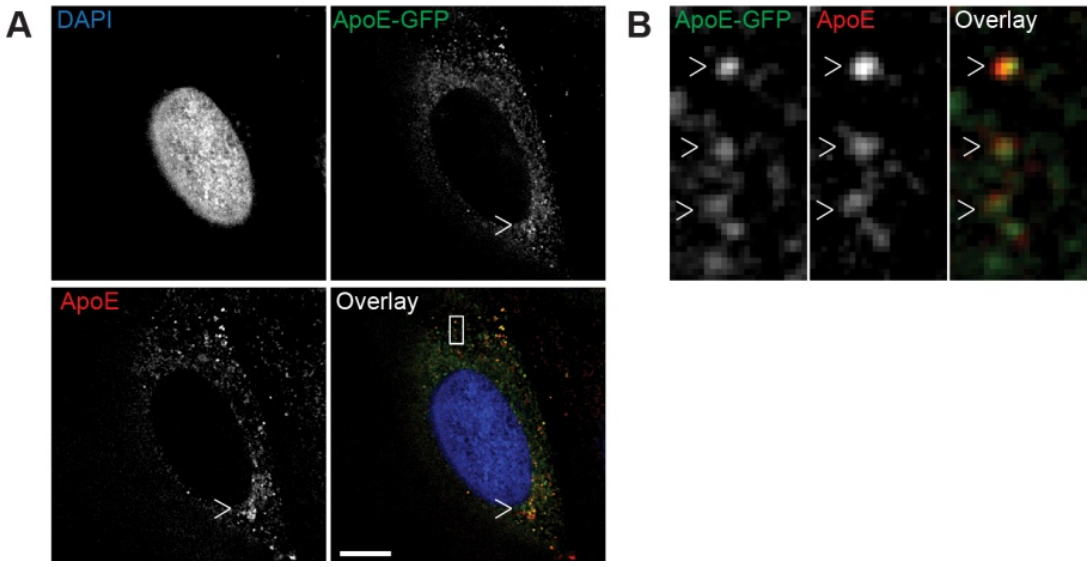

Figure 6.3. ApoE-GFP colocalizes with endogenous ApoE in Huh-7.5 cells. (A) Huh-7.5/ApoE-GFP cells were processed for immunofluorescence using α-ApoE (EP1374Y) and α-GFP (JL-8) and corresponding secondary antibodies. A single deconvolved slice is shown. The GFP and ApoE signals colocalized throughout the cell. Arrow heads indicate perinuclear signal concentrations consistent with Golgi localization. Scale bar, 10 μm. (B) Detail view of the region highlighted in the overlay image of panel A. The arrow heads indicate colocalized ApoE and ApoE-GFP puncta.

6.5. ApoE-GFP and endogenous ApoE secretion rates are indistinguishable

ApoE is a secreted protein (Dashti et al., 1980). To characterize ApoE-GFP's kinetics of secretion from cells, we performed radioactivity pulse-chase experiments in the Huh-7.5/ApoE-GFP cells and in the control Huh-7.5/EV Hygro cells. Once again, I thank Dr. Ursula Andreo for lending to the project her experience with radioactivity pulse-chase assays. After a short ^{35}S-cysteine and methionine pulse, we chased the cells in the absence of label while measuring ApoE- and ApoE-GFP- associated radioactivity in both media and cell lysates at regular intervals. The percent of total ApoE-GFP (Figure 6.4, blue trace) that was recovered from the media was at all times undistinguishable

from the percent of endogenously-expressed ApoE recovered from the same Huh-7.5/ApoE-GFP cells (Figure 6.4, red trace) or from control Huh-7.5/EV Hygro cells (Figure 6.4, black trace). ApoE-GFP thus possessed the same capacity to be secreted from the Huh-7.5 cell line as endogenous ApoE.

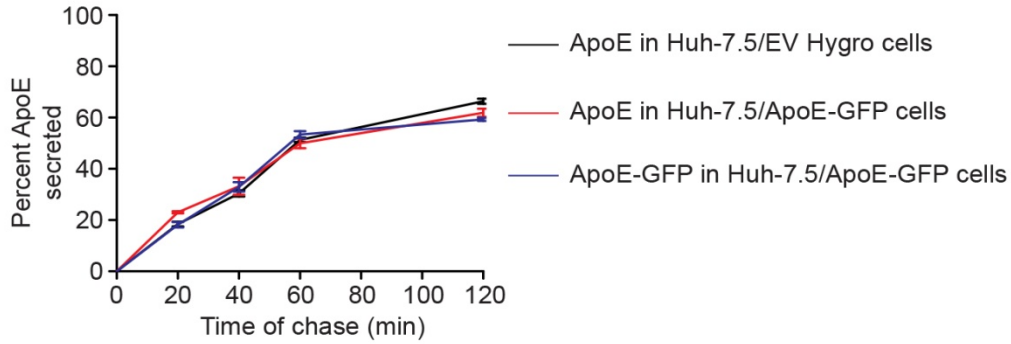

Figure 6.4. ApoE-GFP and ApoE are secreted from cells at undistinguishable rates. The rates of secretion of ApoE and of ApoE-GFP were measured using a radioactivity pulse-chase experiment. At each time point, the amount of secreted radiolabeled cargo is shown as percent of the amount of total (cell-associated + secreted) radiolabeled cargo. ApoE amounts were measured during secretion from Huh-7.5/EV Hygro and Huh-7.5/ApoE-GFP cells, and the ApoE-GFP amounts were measured in Huh-7.5/ApoE-GFP cells, as noted in the legend at the right.

6.6. ApoE-GFP associates with secreted ApoE and ApoB100

ApoE is secreted from cells as lipoprotein particles of various sizes and lipid compositions that include ApoB100-containing VLDL/LDL and ApoB100-free HDL particles (Vance et al., 1984). To be a useful marker of lipoprotein egress, ApoE-GFP should retain untagged ApoE's ability to associate with itself and with secreted ApoB100. To test if this was the case, I performed immunoprecipitation assays on media conditioned by either Huh-7.5/ApoE-GFP cells or control Huh-7.5/EV Hygro cells.

These experiments were done in the absence of detergent, to preserve the integrity of the lipoprotein particles. Immunoprecipitation of Huh-7.5/ApoE-GFP conditioned media with an α-GFP antibody pulled down ApoE-GFP, as expected, but also untagged ApoE and ApoB100 (Figure 6.5A, lane a). Reciprocal immunoprecipitation of the same media with α-ApoB100 pulled down ApoB100, ApoE-GFP, and untagged ApoE (Figure 6.5A, lane b). These results indicate that secreted ApoE-GFP associated with both ApoB100 and untagged ApoE, likely as part of lipoprotein particles. To establish the specificity of the immunoprecipitation assay, I performed a control pull-down with normal species-matched IgG, as well as pull-downs of media conditioned by Huh-7.5/EV with the same sets of antibodies. Immunoprecipitation of ApoE-GFP-free media with the α-ApoB100 antibody resulted in recovery of only untagged ApoE, as expected (Figure 6.5A, lane e), while the other conditions resulted in minimal or no recovery of ApoE, ApoE-GFP or ApoB100 (Figure 6.5A, lanes c, d, and f). I note that the media samples used in these assays were conditioned by similar cellular amounts (Figure 6.5B), and contained comparable total amounts of ApoB100 and ApoE (Figure 6.5C). All in all, these localization, kinetic and biochemical assays established ApoE-GFP as a useful marker for analysis of ApoE-containing lipoprotein secretion.

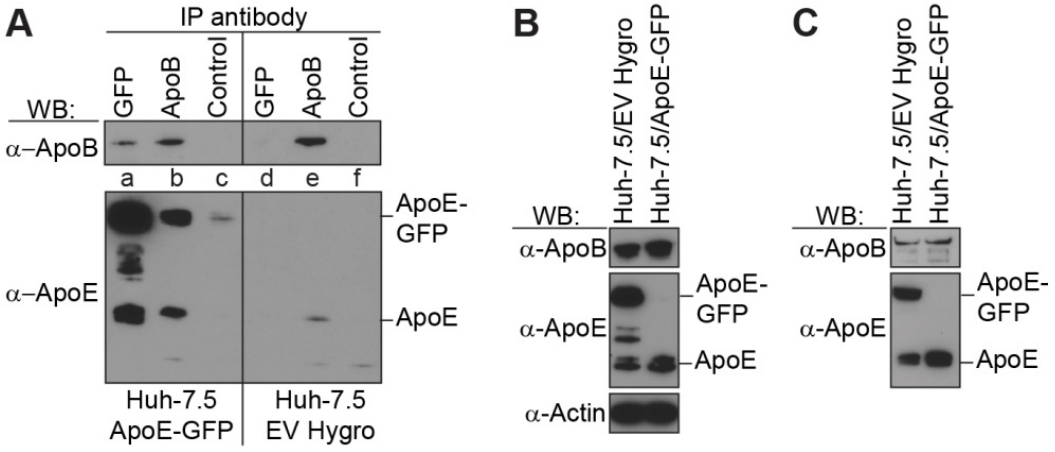

Figure 6.5. ApoE-GFP associates with secreted untagged ApoE and ApoB100. (A) Media was conditioned by Huh-7.5/ApoE-GFP cells or by Huh-7.5/EV Hygro cells, then immunoprecipitated with antibodies listed at the top of the figure. The pulled down material was then blotted using antibodies against ApoB100 and ApoE, as listed at the left. Letters between the two panels correspond to the lane labeling described in the text. (B) The cells that secreted the material analyzed in panel A were lysed and processed by Western blotting using the antibodies listed at the left. (C) Input media used in the immunoprecipitation experiment in panel (A) was processed by Western blotting using the antibodies listed at the left. (A-C) The ApoE and the ApoE-GFP bands are marked at the right of each blot.

6.7. ApoE-GFP and infectious HCV egress

Since ApoE is a functionally important component of infectious HCV particles (Chang et al., 2007; Fukuhara et al., 2014; Hishiki et al., 2010; Hueging et al., 2014; Lee et al., 2014; Long et al., 2011; Vogt et al., 2013), I investigated whether ApoE-GFP expression supported infectious HCV production. To test this, I performed rescue experiments in the context of ApoE knockdown. Dr. Margaret Scull had made and characterized Huh-7.5-derived clonal cell lines in which ApoE expression was knocked

down (clones ApoE KD1 and ApoE KD2, respectively) and a control Huh-7.5 derived clonal cell line transduced with an empty shRNA vector (clone EV KD). She was very gracious in sharing these cell lines with me. The ApoE knockdown cell lines ApoE KD1 and ApoE KD2 expressed barely detectable levels of ApoE, compared to parental Huh-7.5 cells, or to the control knockdown cell line, EV KD (data not shown), consistent with previous reports (Chang et al., 2007; Hishiki et al., 2010; Jiang and Luo, 2009; Lee et al., 2014). I transduced these cell lines with lentiviruses expressing shRNA-resistant untagged ApoE, shRNA-resistant ApoE-GFP, or with an empty control lentivirus (EV). As expected, ApoE expression was not rescued by transduction of these cells with the empty lentiviral expression vector (Figure 6.6A). In contrast, transduction with the lentivirus expressing untagged ApoE resulted in rescue of ApoE expression, and transduction with the lentivirus expressing ApoE-GFP resulted in comparable levels of expression of the fusion protein (Figure 6.6A). I then launched HCV infection in these cells by HCV RNA electroporation. I measured intracellular HCV RNA levels at 6 h and at 72 h post electroporation, and also measured supernatant HCV infectivity titers accumulated over 72 h post electroporation. The expression of ApoE-GFP in the EV KD background, where endogenous ApoE remains expressed (Figure 6.6A), did not significantly change HCV infectivity release compared to control, EV-transduced cells (Figure 6.6B, left pair of bars). I interpret this result to mean that ApoE-GFP did not act as a DN factor with respect to release of infectious HCV particles. Unfortunately, ApoE-GFP expression in the ApoE knockdown cell lines did not rescue infectious HCV particle release (Figure 6.6B), compare second and third black bars to the second and third white bars, respectively). In these cells, the release of infectious HCV particles was

indistinguishable from that observed when the ApoE KD clones were mock-rescued by transduction with an EV (Figure 6.6B, white bars). In contrast, exogenous expression of untagged ApoE partly rescued HCV infectious particle release (Figure 6.6B, compare second and third gray bars to the second and third white bars, respectively). In all but one cell population, intracellular HCV RNA accumulated to similar levels (Figure 6.6C). Comparable HCV RNA amounts were delivered into these cells, as quantified at 6 h post electroporation (Figure 6.6D). Overall, these findings ruled out a major inhibitory effect of ApoE-GFP expression on HCV viral genome replication.

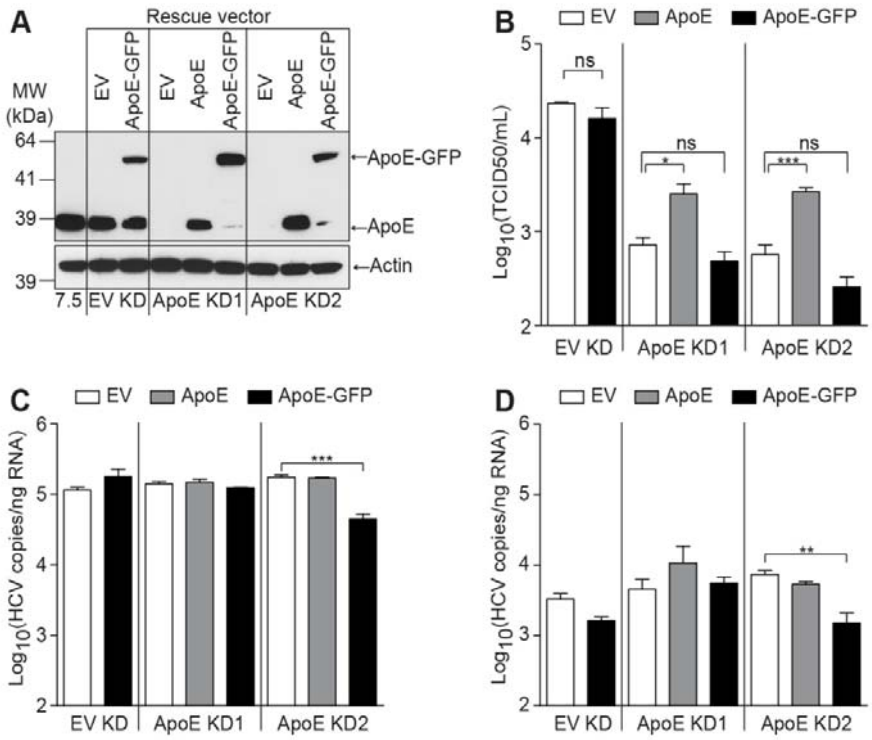

Figure 6.6. ApoE-GFP does not support infectious HCV particle production. (A) Huh-7.5 cells, Huh-7.5 cells engineered to downregulate endogenous ApoE protein expression (clones ApoE KD1 and ApoE KD2) and control knockdown cells (clone EV KD) were transduced with the rescue vectors: empty (EV), ApoE, or ApoE-GFP. Cell lysates were immunoblotted using α-ApoE (top) and α-actin (bottom) antibodies. Molecular weight marker positions (kDa) are at the left of the blots. (B) Infectivity of HCV particles released by the indicated cell lines at 72 h post electroporation. The cells expressed the following rescue vectors: EV (white bars), ApoE (gray bars) or ApoE-GFP (black bars). Shown are means ± standard error of the mean obtained from 2 or 3 independent electroporations, with 3 virus samples analyzed for each electroporation. (C) Cell-associated HCV RNA copies quantified by qRT-PCR at 72 h post electroporation in samples from the experiment presented in panel B. (D) Cell-associated HCV RNA copies quantified by qRT-PCR at 6 h post electroporation in parallel samples to those presented in panels B and C. The lower RNA levels in the ApoE KD2/ApoE-GFP cells both at 6 h (panel D) and at 72 h (panel C) likely reflected a lower electroporation efficiency in that cell background. Statistical differences (Student's *t*-test: ns, $p>0.05$; *, $p<0.05$; **, $p<0.01$; ***, $p<0.001$).

6.8. Discussion

Previous studies have shown that knockdown of ApoE expression results in decrease of infectious HCV release from Huh-7.5 cells (Benga et al., 2010; Chang et al., 2007; Hishiki et al., 2010; Jiang and Luo, 2009; Lee et al., 2014), and that infectivity release may be at least partly rescued by re-expression of knockdown-resistant ApoE (Hishiki et al., 2010; Jiang and Luo, 2009; Lee et al., 2014). Our findings are consistent with these studies. Since in our experimental system ApoE-GFP did not possess any capacity to rescue HCV infectivity release, its usefulness in imaging experiments analyzing spatio-temporal dynamics of HCV particle release may be severely limited. ApoE-GFP might not associate with HCV particles, might associate with HCV particles that are degraded before being released, or might promote the production of ApoE-GFP-containing HCV particles which remain nonetheless non-infectious. A putative defect of ApoE-GFP association with HCV particles would be unsurprising if the GFP tag interfered with ApoE-HCV association. ApoE specifically binds the transmembrane domain of the HCV glycoprotein E2 (Lee et al., 2014) and the GFP tag could cause a conformational change in the ApoE polypeptide that could interfere with the E2 interaction. Alternatively, the relatively bulky GFP tag might sterically clash with the E1E2 glycoprotein ectodomains on the surface of the HCV particle, or might mask lipoprotein or glycoprotein domains involved in entry receptor interaction. If ApoE-GFP associated with HCV particles, and the structure and rate of production of these putative ApoE-GFP-containing HCV non-infectious particles were indistinguishable from the structure and rate of production of infectious ApoE-containing HCV particles, then ApoE-GFP may still be used in the analysis of HCV particle secretion. Unfortunately,

only a small portion of released HCV particles are infectious, and they appear to be difficult to purify and characterize structurally (Catanese et al., 2013; Gastaminza et al., 2010). As such, documenting structural and compositional similarity between infectious ApoE-containing HCV particles and the hypothesized non-infectious ApoE-GFP-containing HCV particles would be challenging at best. I thus conclude that ApoE-GFP is unlikely to be suitable to unambiguously mark and image infectious HCV particles during secretion from hepatic cells.

Nonetheless, the results I present here do document a behavior of ApoE-GFP that closely mirrors that of untagged ApoE with respect to lipoprotein release. We showed that ApoE-GFP and untagged ApoE colocalized intracellularly and were secreted at similar rates. I further showed that ApoE-GFP interacted with both endogenous ApoE and ApoB100, as expected for a proper lipoprotein particle-associated marker. Our findings are further corroborated by a battery of functional tests previously performed in macrophages (Kockx et al., 2007) using the same construct that we used. I propose therefore that ApoE-GFP (or similarly made constructs) may be used in studies aiming, for example, to identify the route(s) of vesicular transport which shuttle ApoE-containing lipoproteins out of producing cells. Colocalization - or lack thereof - between Rabs and intracellular ApoE-GFP, for example, will inform whether a particular Rab protein functions in ApoE-containing lipoprotein egress. Furthermore, quantitative kinetic imaging studies, including the study of whether and how the various ApoE isoforms affected the rates of lipoprotein secretion, may be performed using such fluorescent protein tagged ApoE constructs. Besides characterizing ApoE-GFP behavior, this study provides a framework for testing other fluorescently tagged markers of lipoprotein

particles. Lastly, since ApoE has also been implicated in neurodegenerative diseases (Corder et al., 1994; Corder et al., 1993) and cancer (Pencheva et al., 2012), ApoE-GFP may likely be used in other disease-specific cellular contexts to answer cell biology questions relevant for the understanding of those pathologies.

Chapter 7

Concluding Remarks

Throughout the past several years, aided by wonderfully skilful assistance from my friends and collaborators, I have pursued several lines of investigation, all converging towards a larger unified goal: to molecularly characterize the vesicular transport pathways involved in the secretion of such hepatic cargoes as serum albumin, the lipoprotein components ApoE and ApoB100, and HCV. Some of the avenues of investigation that I followed have yielded interesting results. Other branches of my investigation have established experimental tools and protocols that may prove useful in parsing out the functional details of other cellular processes. Finally, some of the approaches that I initially undertook have failed, or I have chosen not to pursue them further due to time restraints. I will not repeat here the individual discussion points that I have expanded upon at the conclusion of the previous chapters. I will, however, re-emphasize that the DN Rab GTPase screen may be adapted for use in other experimental systems to parse out Rab family involvement in other secretion settings; that an elaborate description of Rab11 and Rab8 function in polarized hepatic cargo secretion may yield interesting revelations on how the hepatocytes handle the tremendous burden of intracellular traffic functions that they must harmoniously juggle; that the peculiar differences in the sensitivities of albumin, ApoE and ApoB100 to Rab1 inhibition may reveal interesting regulation methods of ER to Golgi traffic; and that ApoE-GFP may prove useful in quantitative spatial and temporal analyses of intracellular lipoprotein transport.

Were I to have more time to delve deeper into the investigation of hepatic cargo secretion, not only would I like to continue pursuing the lines of investigation that I have advanced as part of this work, but I would also like to reprise pursuing some other projects that I have envisaged, and even commenced, during my graduate student tenure. I have not included in the results section of this thesis a detailed description of all the bits and pieces of work that I have done as part of the several projects that did not advance significantly, beyond the Rab11 and Rab8 analysis. Those temporarily stalled lines of inquiry may nonetheless be reprised and used to complement the genetic and biochemical analysis of cargo transport that I presented in the pages above. For example, live cell imaging experiments contrasting the transport of fluorescently labeled albumin, ApoE, and HCV particles, with each other and with markers of individual secretion steps, including the Rab GTPases, may provide a trove of information regarding the dynamic spatial and temporal regulation of these model hepatic cargoes. Indeed, with assistance from Caroline Gleason, I have made fluorescent protein-tagged albumin constructs. I have also made HCV genomes expressing fluorescent protein-tagged E2 glycoproteins, or encoding bacteriophage RNA loop arrays (Buxbaum et al., 2015) that may be used to fluorescently label the HCV genome, as a collaboration between the Simon and Bieniasz labs has successfully achieved in the case of the HIV-I genome (Itano et al., 2015; Jouvenet et al., 2008). These fluorescent beacon-tagged constructs would need to be tested in functional assays, as I have described for ApoE-GFP in Chapter 6. Once such characterization is complete, imaging experiments will need to be performed, likely combining several techniques. I am encouraged that such live cell imaging experiments will be facilitated by advances in imaging techniques. Beyond the total internal reflection

microscopy technique that has long been used in the Simon lab (Fix et al., 2004; Jouvenet et al., 2008; Jouvenet et al., 2009; Jouvenet et al., 2011), just recently, super-resolution imaging protocols and multi-focus simultaneous imaging techniques have been developed here and have been successfully applied to address biological questions (Bleck et al., 2014; Itano et al., 2015). These novel experimental techniques, which were not yet available when I started my thesis work, will only hasten the pace of the inquiry. I hope that whoever further pursues this investigation may find useful inspiration in the work that I have done over the past several years, and the work that I have envisaged continuing doing.

I also hope that one day scientists may be able to look back and say: "We know all there is to know about hepatic lipoprotein and HCV secretion by the hepatocyte." This likely is an unachievable dream. But advancements have been made, and will be made. I am happy to think that I may have contributed something useful to the field, yet I am humbled by the realization of how much more still belongs to the great domain of the unknown.

REFERENCES

Agnello, V., Abel, G., Elfahal, M., Knight, G.B., and Zhang, Q.X. (1999). Hepatitis C virus and other flaviviridae viruses enter cells via low density lipoprotein receptor. Proc Natl Acad Sci U S A *96*, 12766-12771.

Ali, K., Middleton, M., Pure, E., and Rader, D.J. (2005). Apolipoprotein E suppresses the type I inflammatory response in vivo. Circ Res *97*, 922-927.

Allaire, P.D., Marat, A.L., Dall'Armi, C., Di Paolo, G., McPherson, P.S., and Ritter, B. (2010). The Connecdenn DENN domain: a GEF for Rab35 mediating cargo-specific exit from early endosomes. Mol Cell *37*, 370-382.

Allan, B.B., Moyer, B.D., and Balch, W.E. (2000). Rab1 recruitment of p115 into a cis-SNARE complex: programming budding COPII vesicles for fusion. Science *289*, 444-448.

Alvarez, C., Garcia-Mata, R., Brandon, E., and Sztul, E. (2003). COPI recruitment is modulated by a Rab1b-dependent mechanism. Mol Biol Cell *14*, 2116-2127.

Alvers, A.L., Ryan, S., Scherz, P.J., Huisken, J., and Bagnat, M. (2014). Single continuous lumen formation in the zebrafish gut is mediated by smoothened-dependent tissue remodeling. Development *141*, 1110-1119.

Amorim, M.J., Bruce, E.A., Read, E.K., Foeglein, A., Mahen, R., Stuart, A.D., and Digard, P. (2011). A Rab11- and microtubule-dependent mechanism for cytoplasmic transport of influenza A virus viral RNA. J Virol *85*, 4143-4156.

Andre, P., Komurian-Pradel, F., Deforges, S., Perret, M., Berland, J.L., Sodoyer, M., Pol, S., Brechot, C., Paranhos-Baccala, G., and Lotteau, V. (2002). Characterization of low- and very-low-density hepatitis C virus RNA-containing particles. J Virol *76*, 6919-6928.

Andrus, L., Marukian, S., Jones, C.T., Catanese, M.T., Sheahan, T.P., Schoggins, J.W., Barry, W.T., Dustin, L.B., Trehan, K., Ploss, A., *et al.* (2011). Expression of paramyxovirus V proteins promotes replication and spread of hepatitis C virus in cultures of primary human fetal liver cells. Hepatology *54*, 1901-1912.

Ang, A.L., Folsch, H., Koivisto, U.M., Pypaert, M., and Mellman, I. (2003). The Rab8 GTPase selectively regulates AP-1B-dependent basolateral transport in polarized Madin-Darby canine kidney cells. J Cell Biol *163*, 339-350.

Ang, A.L., Taguchi, T., Francis, S., Folsch, H., Murrells, L.J., Pypaert, M., Warren, G., and Mellman, I. (2004). Recycling endosomes can serve as intermediates during transport from the Golgi to the plasma membrane of MDCK cells. J Cell Biol *167*, 531-543.

Anitei, M., Wassmer, T., Stange, C., and Hoflack, B. (2010). Bidirectional transport between the trans-Golgi network and the endosomal system. Molecular membrane biology *27*, 443-456.

Appel, N., Zayas, M., Miller, S., Krijnse-Locker, J., Schaller, T., Friebe, P., Kallis, S., Engel, U., and Bartenschlager, R. (2008). Essential role of domain III of nonstructural protein 5A for hepatitis C virus infectious particle assembly. PLoS Pathog *4*, e1000035.

Appenzeller-Herzog, C., and Hauri, H.P. (2006). The ER-Golgi intermediate compartment (ERGIC): in search of its identity and function. J Cell Sci *119*, 2173-2183.

Aridor, M., Bannykh, S.I., Rowe, T., and Balch, W.E. (1995). Sequential coupling between COPII and COPI vesicle coats in endoplasmic reticulum to Golgi transport. J Cell Biol *131*, 875-893.

Armstrong, J., Thompson, N., Squire, J.H., Smith, J., Hayes, B., and Solari, R. (1996). Identification of a novel member of the Rab8 family from the rat basophilic leukaemia cell line, RBL.2H3. J Cell Sci *109 (Pt 6)*, 1265-1274.

Assaker, G., Ramel, D., Wculek, S.K., Gonzalez-Gaitan, M., and Emery, G. (2010). Spatial restriction of receptor tyrosine kinase activity through a polarized endocytic cycle controls border cell migration. Proc Natl Acad Sci U S A *107*, 22558-22563.

Ayoub, W.S., and Tran, T.T. (2015). Regimens for the Hepatitis C Treatment-Naive Patient. Clin Liver Dis *19*, 619-627, v.

Balch, W.E., McCaffery, J.M., Plutner, H., and Farquhar, M.G. (1994). Vesicular stomatitis virus glycoprotein is sorted and concentrated during export from the endoplasmic reticulum. Cell *76*, 841-852.

Bannykh, S.I., Rowe, T., and Balch, W.E. (1996). The organization of endoplasmic reticulum export complexes. J Cell Biol *135*, 19-35.

Banton, M.C., Inder, K.L., Valk, E., Rudd, C.E., and Schneider, H. (2014). Rab8 binding to immune cell-specific adaptor LAX facilitates formation of trans-Golgi network-

proximal CTLA-4 vesicles for surface expression. Molecular and cellular biology *34*, 1486-1499.

Barquera, S., Pedroza-Tobias, A., Medina, C., Hernandez-Barrera, L., Bibbins-Domingo, K., Lozano, R., and Moran, A.E. (2015). Global Overview of the Epidemiology of Atherosclerotic Cardiovascular Disease. Archives of medical research *46*, 328-338.

Barr, F., and Lambright, D.G. (2010). Rab GEFs and GAPs. Current opinion in cell biology *22*, 461-470.

Barr, F.A. (2013). Review series: Rab GTPases and membrane identity: causal or inconsequential? J Cell Biol *202*, 191-199.

Bartenschlager, R., Ahlborn-Laake, L., Mous, J., and Jacobsen, H. (1993). Nonstructural protein 3 of the hepatitis C virus encodes a serine-type proteinase required for cleavage at the NS3/4 and NS4/5 junctions. J Virol *67*, 3835-3844.

Bartenschlager, R., Lohmann, V., Wilkinson, T., and Koch, J.O. (1995). Complex formation between the NS3 serine-type proteinase of the hepatitis C virus and NS4A and its importance for polyprotein maturation. J Virol *69*, 7519-7528.

Bartenschlager, R., Penin, F., Lohmann, V., and Andre, P. (2011). Assembly of infectious hepatitis C virus particles. Trends Microbiol *19*, 95-103.

Bartosch, B., Vitelli, A., Granier, C., Goujon, C., Dubuisson, J., Pascale, S., Scarselli, E., Cortese, R., Nicosia, A., and Cosset, F.L. (2003). Cell entry of hepatitis C virus requires a set of co-receptors that include the CD81 tetraspanin and the SR-B1 scavenger receptor. J Biol Chem *278*, 41624-41630.

Basu, S.K., Brown, M.S., Ho, Y.K., Havel, R.J., and Goldstein, J.L. (1981). Mouse macrophages synthesize and secrete a protein resembling apolipoprotein E. Proc Natl Acad Sci U S A *78*, 7545-7549.

Bathurst, I.C., Brennan, S.O., Carrell, R.W., Cousens, L.S., Brake, A.J., and Barr, P.J. (1987). Yeast KEX2 protease has the properties of a human proalbumin converting enzyme. Science *235*, 348-350.

Bayer, M., Fischer, J., Kremerskothen, J., Ossendorf, E., Matanis, T., Konczal, M., Weide, T., and Barnekow, A. (2005). Identification and characterization of Iporin as a novel interaction partner for rab1. BMC cell biology *6*, 15.

Beard, M., Satoh, A., Shorter, J., and Warren, G. (2005). A cryptic Rab1-binding site in the p115 tethering protein. J Biol Chem *280*, 25840-25848.

Behrens, S.E., Tomei, L., and De Francesco, R. (1996). Identification and properties of the RNA-dependent RNA polymerase of hepatitis C virus. EMBO J *15*, 12-22.

Benedicto, I., Gondar, V., Molina-Jimenez, F., Garcia-Buey, L., Lopez-Cabrera, M., Gastaminza, P., and Majano, P.L. (2015). Clathrin mediates infectious hepatitis C virus particle egress. J Virol *89*, 4180-4190.

Benga, W.J., Krieger, S.E., Dimitrova, M., Zeisel, M.B., Parnot, M., Lupberger, J., Hildt, E., Luo, G., McLauchlan, J., Baumert, T.F.*, et al.* (2010). Apolipoprotein E interacts with hepatitis C virus nonstructural protein 5A and determines assembly of infectious particles. Hepatology *51*, 43-53.

Benoist, F., and Grand-Perret, T. (1997). Co-translational degradation of apolipoprotein B100 by the proteasome is prevented by microsomal triglyceride transfer protein. Synchronized translation studies on HepG2 cells treated with an inhibitor of microsomal triglyceride transfer protein. J Biol Chem *272*, 20435-20442.

Bergmann, J.E. (1989). Using temperature-sensitive mutants of VSV to study membrane protein biogenesis. Methods in cell biology *32*, 85-110.

Bergmann, J.E., Tokuyasu, K.T., and Singer, S.J. (1981). Passage of an integral membrane protein, the vesicular stomatitis virus glycoprotein, through the Golgi apparatus en route to the plasma membrane. Proc Natl Acad Sci U S A *78*, 1746-1750.

Berriot-Varoqueaux, N., Aggerbeck, L.P., Samson-Bouma, M., and Wetterau, J.R. (2000). The role of the microsomal triglygeride transfer protein in abetalipoproteinemia. Annual review of nutrition *20*, 663-697.

Bertuccio, C.A., Lee, S.L., Wu, G., Butterworth, M.B., Hamilton, K.L., and Devor, D.C. (2014). Anterograde trafficking of KCa3.1 in polarized epithelia is Rab1- and Rab8-dependent and recycling endosome-independent. PLoS One *9*, e92013.

Best, J.M., Foell, J.D., Buss, C.R., Delisle, B.P., Balijepalli, R.C., January, C.T., and Kamp, T.J. (2011). Small GTPase Rab11b regulates degradation of surface membrane L-type Cav1.2 channels. Am J Physiol Cell Physiol *300*, C1023-1033.

Beyer, W.R., Westphal, M., Ostertag, W., and von Laer, D. (2002). Oncoretrovirus and lentivirus vectors pseudotyped with lymphocytic choriomeningitis virus glycoprotein: generation, concentration, and broad host range. J Virol *76*, 1488-1495.

Bhatia, S.N., Underhill, G.H., Zaret, K.S., and Fox, I.J. (2014). Cell and tissue engineering for liver disease. Sci Transl Med *6*, 245sr242.

Bieniasz, P.D. (2009). The cell biology of HIV-1 virion genesis. Cell Host Microbe *5*, 550-558.

Bleck, M., Itano, M.S., Johnson, D.S., Thomas, V.K., North, A.J., Bieniasz, P.D., and Simon, S.M. (2014). Temporal and spatial organization of ESCRT protein recruitment during HIV-1 budding. Proc Natl Acad Sci U S A *111*, 12211-12216.

Blight, K.J., McKeating, J.A., and Rice, C.M. (2002). Highly permissive cell lines for subgenomic and genomic hepatitis C virus RNA replication. J Virol *76*, 13001-13014.

Blum, C.B., Aron, L., and Sciacca, R. (1980). Radioimmunoassay studies of human apolipoprotein E. J Clin Invest *66*, 1240-1250.

Blumer, J., Rey, J., Dehmelt, L., Mazel, T., Wu, Y.W., Bastiaens, P., Goody, R.S., and Itzen, A. (2013). RabGEFs are a major determinant for specific Rab membrane targeting. J Cell Biol *200*, 287-300.

Bonecchi, R., Borroni, E.M., Anselmo, A., Doni, A., Savino, B., Mirolo, M., Fabbri, M., Jala, V.R., Haribabu, B., Mantovani, A., *et al.* (2008). Regulation of D6 chemokine scavenging activity by ligand- and Rab11-dependent surface up-regulation. Blood *112*, 493-503.

Bonifacino, J.S., and Glick, B.S. (2004). The mechanisms of vesicle budding and fusion. Cell *116*, 153-166.

Bonifacino, J.S., and Traub, L.M. (2003). Signals for sorting of transmembrane proteins to endosomes and lysosomes. Annu Rev Biochem *72*, 395-447.

Boren, J., Graham, L., Wettesten, M., Scott, J., White, A., and Olofsson, S.O. (1992). The assembly and secretion of ApoB 100-containing lipoproteins in Hep G2 cells. ApoB 100 is cotranslationally integrated into lipoproteins. J Biol Chem *267*, 9858-9867.

Boson, B., Granio, O., Bartenschlager, R., and Cosset, F.L. (2011). A concerted action of hepatitis C virus p7 and nonstructural protein 2 regulates core localization at the endoplasmic reticulum and virus assembly. PLoS Pathog *7*, e1002144.

Boulant, S., Targett-Adams, P., and McLauchlan, J. (2007). Disrupting the association of hepatitis C virus core protein with lipid droplets correlates with a loss in production of infectious virus. J Gen Virol *88*, 2204-2213.

Boyer, J.L. (2013). Bile formation and secretion. Comprehensive Physiology *3*, 1035-1078.

Brandizzi, F., and Barlowe, C. (2013). Organization of the ER-Golgi interface for membrane traffic control. Nature reviews Molecular cell biology *14*, 382-392.

Brandon, E., Szul, T., Alvarez, C., Grabski, R., Benjamin, R., Kawai, R., and Sztul, E. (2006). On and off membrane dynamics of the endoplasmic reticulum-golgi tethering factor p115 in vivo. Mol Biol Cell *17*, 2996-3008.

Bravo-Cordero, J.J., Marrero-Diaz, R., Megias, D., Genis, L., Garcia-Grande, A., Garcia, M.A., Arroyo, A.G., and Montoya, M.C. (2007). MT1-MMP proinvasive activity is regulated by a novel Rab8-dependent exocytic pathway. EMBO J *26*, 1499-1510.

Brennan, S.O., and Peach, R.J. (1988). Calcium-dependent KEX2-like protease found in hepatic secretory vesicles converts proalbumin to albumin. FEBS letters *229*, 167-170.

Breslow, J.L. (2000). Genetics of lipoprotein abnormalities associated with coronary artery disease susceptibility. Annual review of genetics *34*, 233-254.

Breslow, J.L. (2001). Genetic markers for coronary heart disease. Clinical cardiology *24*, II-14-17.

Brombacher, E., Urwyler, S., Ragaz, C., Weber, S.S., Kami, K., Overduin, M., and Hilbi, H. (2009). Rab1 guanine nucleotide exchange factor SidM is a major phosphatidylinositol 4-phosphate-binding effector protein of Legionella pneumophila. J Biol Chem *284*, 4846-4856.

Brown, P.S., Wang, E., Aroeti, B., Chapin, S.J., Mostov, K.E., and Dunn, K.W. (2000). Definition of distinct compartments in polarized Madin-Darby canine kidney (MDCK) cells for membrane-volume sorting, polarized sorting and apical recycling. Traffic *1*, 124-140.

Brown, T.C., Correia, S.S., Petrok, C.N., and Esteban, J.A. (2007). Functional compartmentalization of endosomal trafficking for the synaptic delivery of AMPA receptors during long-term potentiation. The Journal of neuroscience : the official journal of the Society for Neuroscience *27*, 13311-13315.

Bruce, E.A., Digard, P., and Stuart, A.D. (2010). The Rab11 pathway is required for influenza A virus budding and filament formation. J Virol *84*, 5848-5859.

Bryant, D.M., Datta, A., Rodriguez-Fraticelli, A.E., Peranen, J., Martin-Belmonte, F., and Mostov, K.E. (2010). A molecular network for de novo generation of the apical surface and lumen. Nat Cell Biol *12*, 1035-1045.

Bucci, C., Parton, R.G., Mather, I.H., Stunnenberg, H., Simons, K., Hoflack, B., and Zerial, M. (1992). The small GTPase rab5 functions as a regulatory factor in the early endocytic pathway. Cell *70*, 715-728.

Butterworth, M.B., Edinger, R.S., Silvis, M.R., Gallo, L.I., Liang, X., Apodaca, G., Frizzell, R.A., and Johnson, J.P. (2012). Rab11b regulates the trafficking and recycling of the epithelial sodium channel (ENaC). American journal of physiology Renal physiology *302*, F581-590.

Buxbaum, A.R., Haimovich, G., and Singer, R.H. (2015). In the right place at the right time: visualizing and understanding mRNA localization. Nature reviews Molecular cell biology *16*, 95-109.

Calhoun, B.C., and Goldenring, J.R. (1997). Two Rab proteins, vesicle-associated membrane protein 2 (VAMP-2) and secretory carrier membrane proteins (SCAMPs), are present on immunoisolated parietal cell tubulovesicles. Biochem J *325 (Pt 2)*, 559-564.

Calhoun, B.C., Lapierre, L.A., Chew, C.S., and Goldenring, J.R. (1998). Rab11a redistributes to apical secretory canaliculus during stimulation of gastric parietal cells. The American journal of physiology *275*, C163-170.

Campelo, F., and Malhotra, V. (2012). Membrane fission: the biogenesis of transport carriers. Annu Rev Biochem *81*, 407-427.

Campoy, E.M., Zoppino, F.C., and Colombo, M.I. (2011). The early secretory pathway contributes to the growth of the Coxiella-replicative niche. Infect Immun *79*, 402-413.

Cantin, R., Diou, J., Belanger, D., Tremblay, A.M., and Gilbert, C. (2008). Discrimination between exosomes and HIV-1: purification of both vesicles from cell-free supernatants. Journal of immunological methods *338*, 21-30.

Carpio, M.A., Michaud, M., Zhou, W., Fisher, J.K., Walensky, L.D., and Katz, S.G. (2015). BCL-2 family member BOK promotes apoptosis in response to endoplasmic reticulum stress. Proc Natl Acad Sci U S A *112*, 7201-7206.

Casanova, J.E., Wang, X., Kumar, R., Bhartur, S.G., Navarre, J., Woodrum, J.E., Altschuler, Y., Ray, G.S., and Goldenring, J.R. (1999). Association of Rab25 and Rab11a with the apical recycling system of polarized Madin-Darby canine kidney cells. Mol Biol Cell *10*, 47-61.

Catanese, M.T., Uryu, K., Kopp, M., Edwards, T.J., Andrus, L., Rice, W.J., Silvestry, M., Kuhn, R.J., and Rice, C.M. (2013). Ultrastructural analysis of hepatitis C virus particles. Proc Natl Acad Sci U S A *110*, 9505-9510.

Chabrillat, M.L., Wilhelm, C., Wasmeier, C., Sviderskaya, E.V., Louvard, D., and Coudrier, E. (2005). Rab8 regulates the actin-based movement of melanosomes. Mol Biol Cell *16*, 1640-1650.

Chakraborty, A.K., Funasaka, Y., Araki, K., Horikawa, T., and Ichihashi, M. (2003). Evidence that the small GTPase Rab8 is involved in melanosome traffic and dendrite extension in B16 melanoma cells. Cell and tissue research *314*, 381-388.

Chang, K.S., Jiang, J., Cai, Z., and Luo, G. (2007). Human apolipoprotein e is required for infectivity and production of hepatitis C virus in cell culture. J Virol *81*, 13783-13793.

Chavrier, P., Gorvel, J.P., Stelzer, E., Simons, K., Gruenberg, J., and Zerial, M. (1991). Hypervariable C-terminal domain of rab proteins acts as a targeting signal. Nature *353*, 769-772.

Chavrier, P., Parton, R.G., Hauri, H.P., Simons, K., and Zerial, M. (1990a). Localization of low molecular weight GTP binding proteins to exocytic and endocytic compartments. Cell *62*, 317-329.

Chavrier, P., Vingron, M., Sander, C., Simons, K., and Zerial, M. (1990b). Molecular cloning of YPT1/SEC4-related cDNAs from an epithelial cell line. Molecular and cellular biology *10*, 6578-6585.

Chen, S., Liang, M.C., Chia, J.N., Ngsee, J.K., and Ting, A.E. (2001). Rab8b and its interacting partner TRIP8b are involved in regulated secretion in AtT20 cells. J Biol Chem *276*, 13209-13216.

Chen, S.H., Yang, C.Y., Chen, P.F., Setzer, D., Tanimura, M., Li, W.H., Gotto, A.M., Jr., and Chan, L. (1986). The complete cDNA and amino acid sequence of human apolipoprotein B-100. J Biol Chem *261*, 12918-12921.

Chen, T., Han, Y., Yang, M., Zhang, W., Li, N., Wan, T., Guo, J., and Cao, X. (2003). Rab39, a novel Golgi-associated Rab GTPase from human dendritic cells involved in cellular endocytosis. Biochem Biophys Res Commun *303*, 1114-1120.

Chen, W., Feng, Y., Chen, D., and Wandinger-Ness, A. (1998). Rab11 is required for trans-golgi network-to-plasma membrane transport and a preferential target for GDP dissociation inhibitor. Mol Biol Cell *9*, 3241-3257.

Chen, W., and Wandinger-Ness, A. (2001). Expression and functional analyses of Rab8 and Rab11a in exocytic transport from trans-Golgi network. Methods Enzymol *329*, 165-175.

Chen, Y.H., Du, W., Hagemeijer, M.C., Takvorian, P.M., Pau, C., Cali, A., Brantner, C.A., Stempinski, E.S., Connelly, P.S., Ma, H.C., *et al.* (2015). Phosphatidylserine vesicles enable efficient en bloc transmission of enteroviruses. Cell *160*, 619-630.

Chen, Y.T., Holcomb, C., and Moore, H.P. (1993). Expression and localization of two low molecular weight GTP-binding proteins, Rab8 and Rab10, by epitope tag. Proc Natl Acad Sci U S A *90*, 6508-6512.

Chiu, J.H., Hu, C.P., Lui, W.Y., Lo, S.C., and Chang, C.M. (1990). The formation of bile canaliculi in human hepatoma cell lines. Hepatology *11*, 834-842.

Chou, Y.Y., Heaton, N.S., Gao, Q., Palese, P., Singer, R.H., and Lionnet, T. (2013). Colocalization of different influenza viral RNA segments in the cytoplasm before viral budding as shown by single-molecule sensitivity FISH analysis. PLoS Pathog *9*, e1003358.

Choudhury, A., Dominguez, M., Puri, V., Sharma, D.K., Narita, K., Wheatley, C.L., Marks, D.L., and Pagano, R.E. (2002). Rab proteins mediate Golgi transport of caveola-internalized glycosphingolipids and correct lipid trafficking in Niemann-Pick C cells. J Clin Invest *109*, 1541-1550.

Chudakov, D.M., Matz, M.V., Lukyanov, S., and Lukyanov, K.A. (2010). Fluorescent proteins and their applications in imaging living cells and tissues. Physiol Rev *90*, 1103-1163.

Chung, H.Y., Gu, M., Buehler, E., MacDonald, M.R., and Rice, C.M. (2014). Seed sequence-matched controls reveal limitations of small interfering RNA knockdown in functional and structural studies of hepatitis C virus NS5A-MOBKL1B interaction. J Virol *88*, 11022-11033.

Cladaras, C., Hadzopoulou-Cladaras, M., Nolte, R.T., Atkinson, D., and Zannis, V.I. (1986). The complete sequence and structural analysis of human apolipoprotein B-100: relationship between apoB-100 and apoB-48 forms. EMBO J *5*, 3495-3507.

Claude, A., Zhao, B.P., Kuziemsky, C.E., Dahan, S., Berger, S.J., Yan, J.P., Armold, A.D., Sullivan, E.M., and Melancon, P. (1999). GBF1: A novel Golgi-associated BFA-resistant guanine nucleotide exchange factor that displays specificity for ADP-ribosylation factor 5. J Cell Biol *146*, 71-84.

Cocquerel, L., Duvet, S., Meunier, J.C., Pillez, A., Cacan, R., Wychowski, C., and Dubuisson, J. (1999). The transmembrane domain of hepatitis C virus glycoprotein E1 is a signal for static retention in the endoplasmic reticulum. J Virol *73*, 2641-2649.

Cocquerel, L., Meunier, J.C., Pillez, A., Wychowski, C., and Dubuisson, J. (1998). A retention signal necessary and sufficient for endoplasmic reticulum localization maps to the transmembrane domain of hepatitis C virus glycoprotein E2. J Virol *72*, 2183-2191.

Coller, K.E., Berger, K.L., Heaton, N.S., Cooper, J.D., Yoon, R., and Randall, G. (2009). RNA interference and single particle tracking analysis of hepatitis C virus endocytosis. PLoS Pathog *5*, e1000702.

Coller, K.E., Heaton, N.S., Berger, K.L., Cooper, J.D., Saunders, J.L., and Randall, G. (2012). Molecular determinants and dynamics of hepatitis C virus secretion. PLoS Pathog *8*, e1002466.

Corder, E.H., Saunders, A.M., Risch, N.J., Strittmatter, W.J., Schmechel, D.E., Gaskell, P.C., Jr., Rimmler, J.B., Locke, P.A., Conneally, P.M., Schmader, K.E., *et al.* (1994). Protective effect of apolipoprotein E type 2 allele for late onset Alzheimer disease. Nat Genet *7*, 180-184.

Corder, E.H., Saunders, A.M., Strittmatter, W.J., Schmechel, D.E., Gaskell, P.C., Small, G.W., Roses, A.D., Haines, J.L., and Pericak-Vance, M.A. (1993). Gene dose of apolipoprotein E type 4 allele and the risk of Alzheimer's disease in late onset families. Science *261*, 921-923.

Counihan, N.A., Rawlinson, S.M., and Lindenbach, B.D. (2011). Trafficking of hepatitis C virus core protein during virus particle assembly. PLoS Pathog *7*, e1002302.

Cox, D., Lee, D.J., Dale, B.M., Calafat, J., and Greenberg, S. (2000). A Rab11-containing rapidly recycling compartment in macrophages that promotes phagocytosis. Proc Natl Acad Sci U S A *97*, 680-685.

Cox, D.J., Strudwick, N., Ali, A.A., Paton, A.W., Paton, J.C., and Schroder, M. (2011). Measuring signaling by the unfolded protein response. Methods Enzymol *491*, 261-292.

Cramm-Behrens, C.I., Dienst, M., and Jacob, R. (2008). Apical cargo traverses endosomal compartments on the passage to the cell surface. Traffic *9*, 2206-2220.

Cresawn, K.O., Potter, B.A., Oztan, A., Guerriero, C.J., Ihrke, G., Goldenring, J.R., Apodaca, G., and Weisz, O.A. (2007). Differential involvement of endocytic compartments in the biosynthetic traffic of apical proteins. EMBO J *26*, 3737-3748.

Cristea, I.M., Carroll, J.W., Rout, M.P., Rice, C.M., Chait, B.T., and MacDonald, M.R. (2006). Tracking and elucidating alphavirus-host protein interactions. J Biol Chem *281*, 30269-30278.

Dale, L.B., Seachrist, J.L., Babwah, A.V., and Ferguson, S.S. (2004). Regulation of angiotensin II type 1A receptor intracellular retention, degradation, and recycling by Rab5, Rab7, and Rab11 GTPases. J Biol Chem *279*, 13110-13118.

Dancourt, J., and Barlowe, C. (2010). Protein sorting receptors in the early secretory pathway. Annu Rev Biochem *79*, 777-802.

Danta, M., Brown, D., Bhagani, S., Pybus, O.G., Sabin, C.A., Nelson, M., Fisher, M., Johnson, A.M., Dusheiko, G.M., Hiv, *et al.* (2007). Recent epidemic of acute hepatitis C virus in HIV-positive men who have sex with men linked to high-risk sexual behaviours. Aids *21*, 983-991.

Das, A., and Guo, W. (2011). Rabs and the exocyst in ciliogenesis, tubulogenesis and beyond. Trends Cell Biol *21*, 383-386.

Dashti, N. (1992). The effect of low density lipoproteins, cholesterol, and 25-hydroxycholesterol on apolipoprotein B gene expression in HepG2 cells. J Biol Chem *267*, 7160-7169.

Dashti, N., McConathy, W.J., and Ontko, J.A. (1980). Production of apolipoproteins E and A-I by rat hepatocytes in primary culture. Biochim Biophys Acta *618*, 347-358.

Davidson, N.O., and Shelness, G.S. (2000). APOLIPOPROTEIN B: mRNA editing, lipoprotein assembly, and presecretory degradation. Annual review of nutrition *20*, 169-193.

de Graaf, P., Zwart, W.T., van Dijken, R.A., Deneka, M., Schulz, T.K., Geijsen, N., Coffer, P.J., Gadella, B.M., Verkleij, A.J., van der Sluijs, P., *et al.* (2004). Phosphatidylinositol 4-kinasebeta is critical for functional association of rab11 with the Golgi complex. Mol Biol Cell *15*, 2038-2047.

de Saint Basile, G., Menasche, G., and Fischer, A. (2010). Molecular mechanisms of biogenesis and exocytosis of cytotoxic granules. Nature reviews Immunology *10*, 568-579.

Dejgaard, S.Y., Murshid, A., Erman, A., Kizilay, O., Verbich, D., Lodge, R., Dejgaard, K., Ly-Hartig, T.B., Pepperkok, R., Simpson, J.C., *et al.* (2008). Rab18 and Rab43 have key roles in ER-Golgi trafficking. J Cell Sci *121*, 2768-2781.

Del Campo, C.M., Mishra, A.K., Wang, Y.H., Roy, C.R., Janmey, P.A., and Lambright, D.G. (2014). Structural basis for PI(4)P-specific membrane recruitment of the Legionella pneumophila effector DrrA/SidM. Structure *22*, 397-408.

Demir, K., Kirsch, N., Beretta, C.A., Erdmann, G., Ingelfinger, D., Moro, E., Argenton, F., Carl, M., Niehrs, C., and Boutros, M. (2013). RAB8B is required for activity and caveolar endocytosis of LRP6. Cell reports *4*, 1224-1234.

Deng, J., Rudick, V., and Dory, L. (1995). Lysosomal degradation and sorting of apolipoprotein E in macrophages. J Lipid Res *36*, 2129-2140.

Deretic, D., Huber, L.A., Ransom, N., Mancini, M., Simons, K., and Papermaster, D.S. (1995). rab8 in retinal photoreceptors may participate in rhodopsin transport and in rod outer segment disk morphogenesis. J Cell Sci *108 (Pt 1)*, 215-224.

Deretic, D., Puleo-Scheppke, B., and Trippe, C. (1996). Cytoplasmic domain of rhodopsin is essential for post-Golgi vesicle formation in a retinal cell-free system. J Biol Chem *271*, 2279-2286.

Diao, A., Rahman, D., Pappin, D.J., Lucocq, J., and Lowe, M. (2003). The coiled-coil membrane protein golgin-84 is a novel rab effector required for Golgi ribbon formation. J Cell Biol *160*, 201-212.

Diekmann, Y., Seixas, E., Gouw, M., Tavares-Cadete, F., Seabra, M.C., and Pereira-Leal, J.B. (2011). Thousands of rab GTPases for the cell biologist. PLoS computational biology *7*, e1002217.

Doherty, G.J., and McMahon, H.T. (2009). Mechanisms of endocytosis. Annu Rev Biochem *78*, 857-902.

Dolphin, P.J. (1981). Serum and hepatic nascent lipoproteins in normal and hypercholesterolemic rats. J Lipid Res *22*, 971-989.

Dong, C., Yang, L., Zhang, X., Gu, H., Lam, M.L., Claycomb, W.C., Xia, H., and Wu, G. (2010). Rab8 interacts with distinct motifs in alpha2B- and beta2-adrenergic receptors and differentially modulates their transport. J Biol Chem *285*, 20369-20380.

Dong, N., Zhu, Y., Lu, Q., Hu, L., Zheng, Y., and Shao, F. (2012). Structurally distinct bacterial TBC-like GAPs link Arf GTPase to Rab1 inactivation to counteract host defenses. Cell *150*, 1029-1041.

Dugan, J.M., deWit, C., McConlogue, L., and Maltese, W.A. (1995). The Ras-related GTP-binding protein, Rab1B, regulates early steps in exocytic transport and processing of beta-amyloid precursor protein. J Biol Chem *270*, 10982-10989.

Duman, J.G., Tyagarajan, K., Kolsi, M.S., Moore, H.P., and Forte, J.G. (1999). Expression of rab11a N124I in gastric parietal cells inhibits stimulatory recruitment of the H+-K+-ATPase. The American journal of physiology *277*, C361-372.

Dustin, L.B., Cashman, S.B., and Laidlaw, S.M. (2014). Immune control and failure in HCV infection--tipping the balance. Journal of leukocyte biology *96*, 535-548.

Dustin, L.B., and Rice, C.M. (2007). Flying under the radar: the immunobiology of hepatitis C. Annu Rev Immunol *25*, 71-99.

Eggenschwiler, J.T., Espinoza, E., and Anderson, K.V. (2001). Rab23 is an essential negative regulator of the mouse Sonic hedgehog signalling pathway. Nature *412*, 194-198.

Egger, D., Wolk, B., Gosert, R., Bianchi, L., Blum, H.E., Moradpour, D., and Bienz, K. (2002). Expression of hepatitis C virus proteins induces distinct membrane alterations including a candidate viral replication complex. J Virol *76*, 5974-5984.

Ehrenreich, J.H., Bergeron, J.J., Siekevitz, P., and Palade, G.E. (1973). Golgi fractions prepared from rat liver homogenates. I. Isolation procedure and morphological characterization. J Cell Biol *59*, 45-72.

Eisfeld, A.J., Kawakami, E., Watanabe, T., Neumann, G., and Kawaoka, Y. (2011). RAB11A is essential for transport of the influenza virus genome to the plasma membrane. J Virol *85*, 6117-6126.

Emery, G., Hutterer, A., Berdnik, D., Mayer, B., Wirtz-Peitz, F., Gaitan, M.G., and Knoblich, J.A. (2005). Asymmetric Rab 11 endosomes regulate delta recycling and specify cell fate in the Drosophila nervous system. Cell *122*, 763-773.

Ernst, S., Zobiack, N., Boecker, K., Gerke, V., and Rescher, U. (2004). Agonist-induced trafficking of the low-affinity formyl peptide receptor FPRL1. Cell Mol Life Sci *61*, 1684-1692.

Esseltine, J.L., Ribeiro, F.M., and Ferguson, S.S. (2012). Rab8 modulates metabotropic glutamate receptor subtype 1 intracellular trafficking and signaling in a protein kinase C-dependent manner. The Journal of neuroscience : the official journal of the Society for Neuroscience *32*, 16933-16942a.

Evans, M.J., von Hahn, T., Tscherne, D.M., Syder, A.J., Panis, M., Wolk, B., Hatziioannou, T., McKeating, J.A., Bieniasz, P.D., and Rice, C.M. (2007). Claudin-1 is a hepatitis C virus co-receptor required for a late step in entry. Nature *446*, 801-805.

Evans, T.M., Ferguson, C., Wainwright, B.J., Parton, R.G., and Wicking, C. (2003). Rab23, a negative regulator of hedgehog signaling, localizes to the plasma membrane and the endocytic pathway. Traffic *4*, 869-884.

Fan, G.H., Lapierre, L.A., Goldenring, J.R., and Richmond, A. (2003). Differential regulation of CXCR2 trafficking by Rab GTPases. Blood *101*, 2115-2124.

Fan, G.H., Lapierre, L.A., Goldenring, J.R., Sai, J., and Richmond, A. (2004). Rab11-family interacting protein 2 and myosin Vb are required for CXCR2 recycling and receptor-mediated chemotaxis. Mol Biol Cell *15*, 2456-2469.

Farnsworth, C.L., and Feig, L.A. (1991). Dominant inhibitory mutations in the Mg(2+)-binding site of RasH prevent its activation by GTP. Molecular and cellular biology *11*, 4822-4829.

Farquhar, M.G., and Palade, G.E. (1963). Junctional complexes in various epithelia. J Cell Biol *17*, 375-412.

Faust, F., Gomez-Lazaro, M., Borta, H., Agricola, B., and Schrader, M. (2008). Rab8 is involved in zymogen granule formation in pancreatic acinar AR42J cells. Traffic *9*, 964-979.

Fazio, S., and Yao, Z. (1995). The enhanced association of apolipoprotein E with apolipoprotein B-containing lipoproteins in serum-stimulated hepatocytes occurs intracellularly. Arterioscler Thromb Vasc Biol *15*, 593-600.

Feng, S., Knodler, A., Ren, J., Zhang, J., Zhang, X., Hong, Y., Huang, S., Peranen, J., and Guo, W. (2012). A Rab8 guanine nucleotide exchange factor-effector interaction network regulates primary ciliogenesis. J Biol Chem *287*, 15602-15609.

Feng, Y., Press, B., Chen, W., Zimmerman, J., and Wandinger-Ness, A. (2001). Expression and properties of Rab7 in endosome function. Methods Enzymol *329*, 175-187.

Fielding, A.B., Schonteich, E., Matheson, J., Wilson, G., Yu, X., Hickson, G.R., Srivastava, S., Baldwin, S.A., Prekeris, R., and Gould, G.W. (2005). Rab11-FIP3 and FIP4 interact with Arf6 and the exocyst to control membrane traffic in cytokinesis. EMBO J *24*, 3389-3399.

Fielding, A.B., Willox, A.K., Okeke, E., and Royle, S.J. (2012). Clathrin-mediated endocytosis is inhibited during mitosis. Proc Natl Acad Sci U S A *109*, 6572-6577.

Filipeanu, C.M., Zhou, F., Claycomb, W.C., and Wu, G. (2004). Regulation of the cell surface expression and function of angiotensin II type 1 receptor by Rab1-mediated endoplasmic reticulum-to-Golgi transport in cardiac myocytes. J Biol Chem *279*, 41077-41084.

Filipeanu, C.M., Zhou, F., Fugetta, E.K., and Wu, G. (2006). Differential regulation of the cell-surface targeting and function of beta- and alpha1-adrenergic receptors by Rab1 GTPase in cardiac myocytes. Molecular pharmacology *69*, 1571-1578.

Fischer von Mollard, G., Mignery, G.A., Baumert, M., Perin, M.S., Hanson, T.J., Burger, P.M., Jahn, R., and Sudhof, T.C. (1990). rab3 is a small GTP-binding protein exclusively localized to synaptic vesicles. Proc Natl Acad Sci U S A *87*, 1988-1992.

Fischer von Mollard, G., Sudhof, T.C., and Jahn, R. (1991). A small GTP-binding protein dissociates from synaptic vesicles during exocytosis. Nature *349*, 79-81.

Fisher, E.A., Khanna, N.A., and McLeod, R.S. (2011). Ubiquitination regulates the assembly of VLDL in HepG2 cells and is the committing step of the apoB-100 ERAD pathway. J Lipid Res *52*, 1170-1180.

Fisher, E.A., Zhou, M., Mitchell, D.M., Wu, X., Omura, S., Wang, H., Goldberg, A.L., and Ginsberg, H.N. (1997). The degradation of apolipoprotein B100 is mediated by the ubiquitin-proteasome pathway and involves heat shock protein 70. J Biol Chem *272*, 20427-20434.

Fix, M., Melia, T.J., Jaiswal, J.K., Rappoport, J.Z., You, D., Sollner, T.H., Rothman, J.E., and Simon, S.M. (2004). Imaging single membrane fusion events mediated by SNARE proteins. Proc Natl Acad Sci U S A *101*, 7311-7316.

Flowerdew, S.E., and Burgoyne, R.D. (2009). A VAMP7/Vti1a SNARE complex distinguishes a non-conventional traffic route to the cell surface used by KChIP1 and Kv4 potassium channels. Biochem J *418*, 529-540.

Freed, E.O. (2015). HIV-1 assembly, release and maturation. Nat Rev Microbiol *13*, 484-496.

Fuchs, E., Haas, A.K., Spooner, R.A., Yoshimura, S., Lord, J.M., and Barr, F.A. (2007). Specific Rab GTPase-activating proteins define the Shiga toxin and epidermal growth factor uptake pathways. J Cell Biol *177*, 1133-1143.

Fukuda, M. (2008). Regulation of secretory vesicle traffic by Rab small GTPases. Cell Mol Life Sci *65*, 2801-2813.

Fukuhara, T., Wada, M., Nakamura, S., Ono, C., Shiokawa, M., Yamamoto, S., Motomura, T., Okamoto, T., Okuzaki, D., Yamamoto, M.*, et al.* (2014). Amphipathic alpha-helices in apolipoproteins are crucial to the formation of infectious hepatitis C virus particles. PLoS Pathog *10*, e1004534.

Furman, C.A., Lo, C.B., Stokes, S., Esteban, J.A., and Gnegy, M.E. (2009). Rab 11 regulates constitutive dopamine transporter trafficking and function in N2A neuroblastoma cells. Neuroscience letters *463*, 78-81.

Galvez-Santisteban, M., Rodriguez-Fraticelli, A.E., Bryant, D.M., Vergarajauregui, S., Yasuda, T., Banon-Rodriguez, I., Bernascone, I., Datta, A., Spivak, N., Young, K.*, et al.* (2012). Synaptotagmin-like proteins control the formation of a single apical membrane domain in epithelial cells. Nat Cell Biol *14*, 838-849.

Garcia-Mata, R., Szul, T., Alvarez, C., and Sztul, E. (2003). ADP-ribosylation factor/COPI-dependent events at the endoplasmic reticulum-Golgi interface are regulated by the guanine nucleotide exchange factor GBF1. Mol Biol Cell *14*, 2250-2261.

Gardner, L.A., Hajjhussein, H., Frederick-Dyer, K.C., and Bahouth, S.W. (2011). Rab11a and its binding partners regulate the recycling of the ss1-adrenergic receptor. Cellular signalling *23*, 46-57.

Gastaminza, P., Cheng, G., Wieland, S., Zhong, J., Liao, W., and Chisari, F.V. (2008). Cellular determinants of hepatitis C virus assembly, maturation, degradation, and secretion. J Virol *82*, 2120-2129.

Gastaminza, P., Dryden, K.A., Boyd, B., Wood, M.R., Law, M., Yeager, M., and Chisari, F.V. (2010). Ultrastructural and biophysical characterization of hepatitis C virus particles produced in cell culture. J Virol *84*, 10999-11009.

Gastaminza, P., Kapadia, S.B., and Chisari, F.V. (2006). Differential biophysical properties of infectious intracellular and secreted hepatitis C virus particles. J Virol *80*, 11074-11081.

Gavriljuk, K., Gazdag, E.M., Itzen, A., Kotting, C., Goody, R.S., and Gerwert, K. (2012). Catalytic mechanism of a mammalian Rab.RabGAP complex in atomic detail. Proc Natl Acad Sci U S A *109*, 21348-21353.

Gavriljuk, K., Itzen, A., Goody, R.S., Gerwert, K., and Kotting, C. (2013). Membrane extraction of Rab proteins by GDP dissociation inhibitor characterized using attenuated total reflection infrared spectroscopy. Proc Natl Acad Sci U S A *110*, 13380-13385.

Gentzsch, J., Brohm, C., Steinmann, E., Friesland, M., Menzel, N., Vieyres, G., Perin, P.M., Frentzen, A., Kaderali, L., and Pietschmann, T. (2013). hepatitis c Virus p7 is critical for capsid assembly and envelopment. PLoS Pathog *9*, e1003355.

Gentzsch, M., Chang, X.B., Cui, L., Wu, Y., Ozols, V.V., Choudhury, A., Pagano, R.E., and Riordan, J.R. (2004). Endocytic trafficking routes of wild type and DeltaF508 cystic fibrosis transmembrane conductance regulator. Mol Biol Cell *15*, 2684-2696.

Gerges, N.Z., Backos, D.S., and Esteban, J.A. (2004). Local control of AMPA receptor trafficking at the postsynaptic terminal by a small GTPase of the Rab family. J Biol Chem *279*, 43870-43878.

Germi, R., Crance, J.M., Garin, D., Guimet, J., Lortat-Jacob, H., Ruigrok, R.W., Zarski, J.P., and Drouet, E. (2002). Cellular glycosaminoglycans and low density lipoprotein receptor are involved in hepatitis C virus adsorption. J Med Virol *68*, 206-215.

Ghiselli, G., Gregg, R.E., Zech, L.A., Schaefer, E.J., and Brewer, H.B., Jr. (1982a). Phenotype study of apolipoprotein E isoforms in hyperlipoproteinaemic patients. Lancet *2*, 405-407.

Ghiselli, G., Schaefer, E.J., Zech, L.A., Gregg, R.E., and Brewer, H.B., Jr. (1982b). Increased prevalence of apolipoprotein E4 in type V hyperlipoproteinemia. J Clin Invest *70*, 474-477.

Gidon, A., Bardin, S., Cinquin, B., Boulanger, J., Waharte, F., Heliot, L., de la Salle, H., Hanau, D., Kervrann, C., Goud, B., *et al.* (2012). A Rab11A/myosin Vb/Rab11-FIP2 complex frames two late recycling steps of langerin from the ERC to the plasma membrane. Traffic *13*, 815-833.

Gillingham, A.K., and Munro, S. (2007). The small G proteins of the Arf family and their regulators. Annual review of cell and developmental biology *23*, 579-611.

Ginsberg, H.N., and Fisher, E.A. (2009). The ever-expanding role of degradation in the regulation of apolipoprotein B metabolism. J Lipid Res *50 Suppl*, S162-166.

Girard, M., Lacaille, F., Verkarre, V., Mategot, R., Feldmann, G., Grodet, A., Sauvat, F., Irtan, S., Davit-Spraul, A., Jacquemin, E.*, et al.* (2014). MYO5B and bile salt export pump contribute to cholestatic liver disorder in microvillous inclusion disease. Hepatology *60*, 301-310.

Gissen, P., and Arias, I.M. (2015). Structural and functional hepatocyte polarity and liver disease. J Hepatol *63*, 1023-1037.

Glick, B.S., and Nakano, A. (2009). Membrane traffic within the Golgi apparatus. Annual review of cell and developmental biology *25*, 113-132.

Goldenring, J.R. (2013). A central role for vesicle trafficking in epithelial neoplasia: intracellular highways to carcinogenesis. Nature reviews Cancer *13*, 813-820.

Goldenring, J.R. (2015). Recycling endosomes. Current opinion in cell biology *35*, 117-122.

Goldenring, J.R., Smith, J., Vaughan, H.D., Cameron, P., Hawkins, W., and Navarre, J. (1996). Rab11 is an apically located small GTP-binding protein in epithelial tissues. The American journal of physiology *270*, G515-525.

Goldenring, J.R., Soroka, C.J., Shen, K.R., Tang, L.H., Rodriguez, W., Vaughan, H.D., Stoch, S.A., and Modlin, I.M. (1994). Enrichment of rab11, a small GTP-binding protein, in gastric parietal cells. The American journal of physiology *267*, G187-194.

Gorvel, J.P., Chavrier, P., Zerial, M., and Gruenberg, J. (1991). rab5 controls early endosome fusion in vitro. Cell *64*, 915-925.

Goud, B., Zahraoui, A., Tavitian, A., and Saraste, J. (1990). Small GTP-binding protein associated with Golgi cisternae. Nature *345*, 553-556.

Graf, M., Bojak, A., Deml, L., Bieler, K., Wolf, H., and Wagner, R. (2000). Concerted action of multiple cis-acting sequences is required for Rev dependence of late human immunodeficiency virus type 1 gene expression. J Virol *74*, 10822-10826.

Grakoui, A., McCourt, D.W., Wychowski, C., Feinstone, S.M., and Rice, C.M. (1993a). Characterization of the hepatitis C virus-encoded serine proteinase: determination of proteinase-dependent polyprotein cleavage sites. J Virol *67*, 2832-2843.

Grakoui, A., McCourt, D.W., Wychowski, C., Feinstone, S.M., and Rice, C.M. (1993b). A second hepatitis C virus-encoded proteinase. Proc Natl Acad Sci U S A *90*, 10583-10587.

Grakoui, A., Wychowski, C., Lin, C., Feinstone, S.M., and Rice, C.M. (1993c). Expression and identification of hepatitis C virus polyprotein cleavage products. J Virol *67*, 1385-1395.

Grant, B.D., and Donaldson, J.G. (2009). Pathways and mechanisms of endocytic recycling. Nature reviews Molecular cell biology *10*, 597-608.

Greenberg, S.M., Rebeck, G.W., Vonsattel, J.P., Gomez-Isla, T., and Hyman, B.T. (1995). Apolipoprotein E epsilon 4 and cerebral hemorrhage associated with amyloid angiopathy. Ann Neurol *38*, 254-259.

Gregg, R.E., Zech, L.A., Schaefer, E.J., and Brewer, H.B., Jr. (1981). Type III hyperlipoproteinemia: defective metabolism of an abnormal apolipoprotein E. Science *211*, 584-586.

Griffin, B.A., Adams, S.R., and Tsien, R.Y. (1998). Specific covalent labeling of recombinant protein molecules inside live cells. Science *281*, 269-272.

Guo, Y., Sirkis, D.W., and Schekman, R. (2014). Protein sorting at the trans-Golgi network. Annual review of cell and developmental biology *30*, 169-206.

Gurkan, C., Lapp, H., Alory, C., Su, A.I., Hogenesch, J.B., and Balch, W.E. (2005). Large-scale profiling of Rab GTPase trafficking networks: the membrome. Mol Biol Cell *16*, 3847-3864.

Gusarova, V., Brodsky, J.L., and Fisher, E.A. (2003). Apolipoprotein B100 exit from the endoplasmic reticulum (ER) is COPII-dependent, and its lipidation to very low density lipoprotein occurs post-ER. J Biol Chem *278*, 48051-48058.

Gusarova, V., Seo, J., Sullivan, M.L., Watkins, S.C., Brodsky, J.L., and Fisher, E.A. (2007). Golgi-associated maturation of very low density lipoproteins involves conformational changes in apolipoprotein B, but is not dependent on apolipoprotein E. J Biol Chem *282*, 19453-19462.

Ha, C.E., and Bhagavan, N.V. (2013). Novel insights into the pleiotropic effects of human serum albumin in health and disease. Biochim Biophys Acta *1830*, 5486-5493.

Haas, A.K., Yoshimura, S., Stephens, D.J., Preisinger, C., Fuchs, E., and Barr, F.A. (2007). Analysis of GTPase-activating proteins: Rab1 and Rab43 are key Rabs required to maintain a functional Golgi complex in human cells. J Cell Sci *120*, 2997-3010.

Hamelin, E., Theriault, C., Laroche, G., and Parent, J.L. (2005). The intracellular trafficking of the G protein-coupled receptor TPbeta depends on a direct interaction with Rab11. J Biol Chem *280*, 36195-36205.

Hampson, A., O'Connor, A., and Smolenski, A. (2013). Synaptotagmin-like protein 4 and Rab8 interact and increase dense granule release in platelets. Journal of thrombosis and haemostasis : JTH *11*, 161-168.

Hardel, N., Harmel, N., Zolles, G., Fakler, B., and Klocker, N. (2008). Recycling endosomes supply cardiac pacemaker channels for regulated surface expression. Cardiovascular research *79*, 52-60.

Hardiman, C.A., McDonough, J.A., Newton, H.J., and Roy, C.R. (2012). The role of Rab GTPases in the transport of vacuoles containing Legionella pneumophila and Coxiella burnetii. Biochemical Society transactions *40*, 1353-1359.

Hardiman, C.A., and Roy, C.R. (2014). AMPylation is critical for Rab1 localization to vacuoles containing Legionella pneumophila. mBio *5*, e01035-01013.

Hattula, K., Furuhjelm, J., Arffman, A., and Peranen, J. (2002). A Rab8-specific GDP/GTP exchange factor is involved in actin remodeling and polarized membrane transport. Mol Biol Cell *13*, 3268-3280.

Hattula, K., Furuhjelm, J., Tikkanen, J., Tanhuanpaa, K., Laakkonen, P., and Peranen, J. (2006). Characterization of the Rab8-specific membrane traffic route linked to protrusion formation. J Cell Sci *119*, 4866-4877.

Haubruck, H., Prange, R., Vorgias, C., and Gallwitz, D. (1989). The ras-related mouse ypt1 protein can functionally replace the YPT1 gene product in yeast. EMBO J *8*, 1427-1432.

Haugsten, E.M., Brech, A., Liestol, K., Norman, J.C., and Wesche, J. (2014). Photoactivation approaches reveal a role for Rab11 in FGFR4 recycling and signalling. Traffic *15*, 665-683.

Havekes, L., de Wit, E., Leuven, J.G., Klasen, E., Utermann, G., Weber, W., and Beisiegel, U. (1986). Apolipoprotein E3-Leiden. A new variant of human apolipoprotein E associated with familial type III hyperlipoproteinemia. Human genetics *73*, 157-163.

Havel, R.J., Kotite, L., Vigne, J.L., Kane, J.P., Tun, P., Phillips, N., and Chen, G.C. (1980). Radioimmunoassay of human arginine-rich apolipoprotein, apoprotein E. Concentration in blood plasma and lipoproteins as affected by apoprotein E-3 deficiency. J Clin Invest *66*, 1351-1362.

Heeren, J., Grewal, T., Laatsch, A., Rottke, D., Rinninger, F., Enrich, C., and Beisiegel, U. (2003). Recycling of apoprotein E is associated with cholesterol efflux and high density lipoprotein internalization. J Biol Chem *278*, 14370-14378.

Hicks, S.W., and Galan, J.E. (2013). Exploitation of eukaryotic subcellular targeting mechanisms by bacterial effectors. Nat Rev Microbiol *11*, 316-326.

Hijikata, M., Kato, N., Ootsuyama, Y., Nakagawa, M., and Shimotohno, K. (1991). Gene mapping of the putative structural region of the hepatitis C virus genome by in vitro processing analysis. Proc Natl Acad Sci U S A *88*, 5547-5551.

Hijikata, M., Mizushima, H., Akagi, T., Mori, S., Kakiuchi, N., Kato, N., Tanaka, T., Kimura, K., and Shimotohno, K. (1993a). Two distinct proteinase activities required for the processing of a putative nonstructural precursor protein of hepatitis C virus. J Virol *67*, 4665-4675.

Hijikata, M., Mizushima, H., Tanji, Y., Komoda, Y., Hirowatari, Y., Akagi, T., Kato, N., Kimura, K., and Shimotohno, K. (1993b). Proteolytic processing and membrane

association of putative nonstructural proteins of hepatitis C virus. Proc Natl Acad Sci U S A *90*, 10773-10777.

Hirvonen, M.J., Buki, K.G., Sun, Y., Mulari, M.T., Harkonen, P.L., and Vaananen, K.H. (2013). Novel interaction of Rab13 and Rab8 with endospanins. FEBS open bio *3*, 83-88.

Hishiki, T., Shimizu, Y., Tobita, R., Sugiyama, K., Ogawa, K., Funami, K., Ohsaki, Y., Fujimoto, T., Takaku, H., Wakita, T., *et al.* (2010). Infectivity of hepatitis C virus is influenced by association with apolipoprotein E isoforms. J Virol *84*, 12048-12057.

Hiwasa, T., Sawada, T., and Sakiyama, S. (1990). Cysteine proteinase inhibitors and ras gene products share the same biological activities including transforming activity toward NIH3T3 mouse fibroblasts and the differentiation-inducing activity toward PC12 rat pheochromocytoma cells. Carcinogenesis *11*, 75-80.

Hoekstra, D., Tyteca, D., and van, I.S.C. (2004). The subapical compartment: a traffic center in membrane polarity development. J Cell Sci *117*, 2183-2192.

Holmes, J.A., and Thompson, A.J. (2015). Interferon-free combination therapies for the treatment of hepatitis C: current insights. Hepatic medicine : evidence and research *7*, 51-70.

Honegger, J.R., Zhou, Y., and Walker, C.M. (2014). Will there be a vaccine to prevent HCV infection? Semin Liver Dis *34*, 79-88.

Hoofnagle, J.H. (1997). Hepatitis C: the clinical spectrum of disease. Hepatology *26*, 15S-20S.

Horner, S.M., and Gale, M., Jr. (2013). Regulation of hepatic innate immunity by hepatitis C virus. Nat Med *19*, 879-888.

Horwitz, J.A., Dorner, M., Friling, T., Donovan, B.M., Vogt, A., Loureiro, J., Oh, T., Rice, C.M., and Ploss, A. (2013). Expression of heterologous proteins flanked by NS3-4A cleavage sites within the hepatitis C virus polyprotein. Virology *439*, 23-33.

Hsu, C., Morohashi, Y., Yoshimura, S., Manrique-Hoyos, N., Jung, S., Lauterbach, M.A., Bakhti, M., Gronborg, M., Mobius, W., Rhee, J., *et al.* (2010). Regulation of exosome secretion by Rab35 and its GTPase-activating proteins TBC1D10A-C. J Cell Biol *189*, 223-232.

Huang, B., Hubber, A., McDonough, J.A., Roy, C.R., Scidmore, M.A., and Carlyon, J.A. (2010). The Anaplasma phagocytophilum-occupied vacuole selectively recruits Rab-GTPases that are predominantly associated with recycling endosomes. Cell Microbiol *12*, 1292-1307.

Huang, H., Sun, F., Owen, D.M., Li, W., Chen, Y., Gale, M., Jr., and Ye, J. (2007). Hepatitis C virus production by human hepatocytes dependent on assembly and secretion of very low-density lipoproteins. Proc Natl Acad Sci U S A *104*, 5848-5853.

Huang, Y., Liu, X.Q., Rall, S.C., Jr., Taylor, J.M., von Eckardstein, A., Assmann, G., and Mahley, R.W. (1998). Overexpression and accumulation of apolipoprotein E as a cause of hypertriglyceridemia. J Biol Chem *273*, 26388-26393.

Huber, L.A., de Hoop, M.J., Dupree, P., Zerial, M., Simons, K., and Dotti, C. (1993a). Protein transport to the dendritic plasma membrane of cultured neurons is regulated by rab8p. J Cell Biol *123*, 47-55.

Huber, L.A., Dupree, P., and Dotti, C.G. (1995). A deficiency of the small GTPase rab8 inhibits membrane traffic in developing neurons. Molecular and cellular biology *15*, 918-924.

Huber, L.A., Pimplikar, S., Parton, R.G., Virta, H., Zerial, M., and Simons, K. (1993b). Rab8, a small GTPase involved in vesicular traffic between the TGN and the basolateral plasma membrane. J Cell Biol *123*, 35-45.

Hueging, K., Doepke, M., Vieyres, G., Bankwitz, D., Frentzen, A., Doerrbecker, J., Gumz, F., Haid, S., Wolk, B., Kaderali, L., *et al.* (2014). Apolipoprotein E codetermines tissue tropism of hepatitis C virus and is crucial for viral cell-to-cell transmission by contributing to a postenvelopment step of assembly. J Virol *88*, 1433-1446.

Hunyady, L., Baukal, A.J., Gaborik, Z., Olivares-Reyes, J.A., Bor, M., Szaszak, M., Lodge, R., Catt, K.J., and Balla, T. (2002). Differential PI 3-kinase dependence of early and late phases of recycling of the internalized AT1 angiotensin receptor. J Cell Biol *157*, 1211-1222.

Huotari, J., and Helenius, A. (2011). Endosome maturation. EMBO J *30*, 3481-3500.

Hutagalung, A.H., and Novick, P.J. (2011). Role of Rab GTPases in membrane traffic and cell physiology. Physiol Rev *91*, 119-149.

Ignatius, M.J., Gebicke-Harter, P.J., Skene, J.H., Schilling, J.W., Weisgraber, K.H., Mahley, R.W., and Shooter, E.M. (1986). Expression of apolipoprotein E during nerve degeneration and regeneration. Proc Natl Acad Sci U S A *83*, 1125-1129.

Ingmundson, A., Delprato, A., Lambright, D.G., and Roy, C.R. (2007). Legionella pneumophila proteins that regulate Rab1 membrane cycling. Nature *450*, 365-369.

Innamorati, G., Le Gouill, C., Balamotis, M., and Birnbaumer, M. (2001). The long and the short cycle. Alternative intracellular routes for trafficking of G-protein-coupled receptors. J Biol Chem *276*, 13096-13103.

Ishida-Yamamoto, A., Kishibe, M., Takahashi, H., and Iizuka, H. (2007). Rab11 is associated with epidermal lamellar granules. The Journal of investigative dermatology *127*, 2166-2170.

Ishikura, S., and Klip, A. (2008). Muscle cells engage Rab8A and myosin Vb in insulin-dependent GLUT4 translocation. Am J Physiol Cell Physiol *295*, C1016-1025.

Itano, M.S., Bleck, M., Johnson, D.S., and Simon, S.M. (2015). Readily Accessible Multiplane Microscopy: 3D Tracking the HIV-1 Genome in Living Cells. Traffic.

Itoh, T., Fujita, N., Kanno, E., Yamamoto, A., Yoshimori, T., and Fukuda, M. (2008). Golgi-resident small GTPase Rab33B interacts with Atg16L and modulates autophagosome formation. Mol Biol Cell *19*, 2916-2925.

Jacobs, C., Domian, I.J., Maddock, J.R., and Shapiro, L. (1999). Cell cycle-dependent polar localization of an essential bacterial histidine kinase that controls DNA replication and cell division. Cell *97*, 111-120.

Jafar-Nejad, H., Andrews, H.K., Acar, M., Bayat, V., Wirtz-Peitz, F., Mehta, S.Q., Knoblich, J.A., and Bellen, H.J. (2005). Sec15, a component of the exocyst, promotes notch signaling during the asymmetric division of Drosophila sensory organ precursors. Developmental cell *9*, 351-363.

Jenkins, D., Seelow, D., Jehee, F.S., Perlyn, C.A., Alonso, L.G., Bueno, D.F., Donnai, D., Josifova, D., Mathijssen, I.M., Morton, J.E.*, et al.* (2007). RAB23 mutations in Carpenter syndrome imply an unexpected role for hedgehog signaling in cranial-suture development and obesity. American journal of human genetics *80*, 1162-1170.

Jiang, J., and Luo, G. (2009). Apolipoprotein E but not B is required for the formation of infectious hepatitis C virus particles. J Virol *83*, 12680-12691.

Jin, L., Pahuja, K.B., Wickliffe, K.E., Gorur, A., Baumgartel, C., Schekman, R., and Rape, M. (2012). Ubiquitin-dependent regulation of COPII coat size and function. Nature *482*, 495-500.

Jirasko, V., Montserret, R., Lee, J.Y., Gouttenoire, J., Moradpour, D., Penin, F., and Bartenschlager, R. (2010). Structural and functional studies of nonstructural protein 2 of the hepatitis C virus reveal its key role as organizer of virion assembly. PLoS Pathog *6*, e1001233.

Jones, B., Jones, E.L., Bonney, S.A., Patel, H.N., Mensenkamp, A.R., Eichenbaum-Voline, S., Rudling, M., Myrdal, U., Annesi, G., Naik, S., *et al.* (2003). Mutations in a Sar1 GTPase of COPII vesicles are associated with lipid absorption disorders. Nat Genet *34*, 29-31.

Jones, D.M., Atoom, A.M., Zhang, X., Kottilil, S., and Russell, R.S. (2011). A genetic interaction between the core and NS3 proteins of hepatitis C virus is essential for production of infectious virus. J Virol *85*, 12351-12361.

Jones, M.C., Caswell, P.T., and Norman, J.C. (2006). Endocytic recycling pathways: emerging regulators of cell migration. Current opinion in cell biology *18*, 549-557.

Jopling, C.L., Yi, M., Lancaster, A.M., Lemon, S.M., and Sarnow, P. (2005). Modulation of hepatitis C virus RNA abundance by a liver-specific MicroRNA. Science *309*, 1577-1581.

Jouvenet, N., Bieniasz, P.D., and Simon, S.M. (2008). Imaging the biogenesis of individual HIV-1 virions in live cells. Nature *454*, 236-240.

Jouvenet, N., Neil, S.J., Bess, C., Johnson, M.C., Virgen, C.A., Simon, S.M., and Bieniasz, P.D. (2006). Plasma membrane is the site of productive HIV-1 particle assembly. PLoS Biol *4*, e435.

Jouvenet, N., Simon, S.M., and Bieniasz, P.D. (2009). Imaging the interaction of HIV-1 genomes and Gag during assembly of individual viral particles. Proc Natl Acad Sci U S A *106*, 19114-19119.

Jouvenet, N., Zhadina, M., Bieniasz, P.D., and Simon, S.M. (2011). Dynamics of ESCRT protein recruitment during retroviral assembly. Nat Cell Biol *13*, 394-401.

Judah, J.D., Gamble, M., and Steadman, J.H. (1973). Biosynthesis of serum albumin in rat liver. Evidence for the existence of 'proalbumin'. Biochem J *134*, 1083-1091.

Jung, J.J., Tiwari, A., Inamdar, S.M., Thomas, C.P., Goel, A., and Choudhury, A. (2012). Secretion of soluble vascular endothelial growth factor receptor 1 (sVEGFR1/sFlt1) requires Arf1, Arf6, and Rab11 GTPases. PLoS One *7*, e44572.

Kaplan, A., and Reiner, O. (2011). Linking cytoplasmic dynein and transport of Rab8 vesicles to the midbody during cytokinesis by the doublecortin domain-containing 5 protein. J Cell Sci *124*, 3989-4000.

Kapoor, A., Simmonds, P., Gerold, G., Qaisar, N., Jain, K., Henriquez, J.A., Firth, C., Hirschberg, D.L., Rice, C.M., Shields, S., *et al.* (2011). Characterization of a canine homolog of hepatitis C virus. Proc Natl Acad Sci U S A *108*, 11608-11613.

Kapoor, A., Simmonds, P., Scheel, T.K., Hjelle, B., Cullen, J.M., Burbelo, P.D., Chauhan, L.V., Duraisamy, R., Sanchez Leon, M., Jain, K., *et al.* (2013). Identification of rodent homologs of hepatitis C virus and pegiviruses. mBio *4*, e00216-00213.

Kawamoto, K., Yoshida, Y., Tamaki, H., Torii, S., Shinotsuka, C., Yamashina, S., and Nakayama, K. (2002). GBF1, a guanine nucleotide exchange factor for ADP-ribosylation factors, is localized to the cis-Golgi and involved in membrane association of the COPI coat. Traffic *3*, 483-495.

Kelly, E.E., Horgan, C.P., and McCaffrey, M.W. (2012). Rab11 proteins in health and disease. Biochemical Society transactions *40*, 1360-1367.

Kelly, M.E., Clay, M.A., Mistry, M.J., Hsieh-Li, H.M., and Harmony, J.A. (1994). Apolipoprotein E inhibition of proliferation of mitogen-activated T lymphocytes: production of interleukin 2 with reduced biological activity. Cellular immunology *159*, 124-139.

Kessler, D., Gruen, G.C., Heider, D., Morgner, J., Reis, H., Schmid, K.W., and Jendrossek, V. (2012). The action of small GTPases Rab11 and Rab25 in vesicle trafficking during cell migration. Cellular physiology and biochemistry : international journal of experimental cellular physiology, biochemistry, and pharmacology *29*, 647-656.

Khandelwal, P., Prakasam, H.S., Clayton, D.R., Ruiz, W.G., Gallo, L.I., van Roekel, D., Lukianov, S., Peranen, J., Goldenring, J.R., and Apodaca, G. (2013). A Rab11a-Rab8a-Myo5B network promotes stretch-regulated exocytosis in bladder umbrella cells. Mol Biol Cell *24*, 1007-1019.

Khandelwal, P., Ruiz, W.G., Balestreire-Hawryluk, E., Weisz, O.A., Goldenring, J.R., and Apodaca, G. (2008). Rab11a-dependent exocytosis of discoidal/fusiform vesicles in bladder umbrella cells. Proc Natl Acad Sci U S A *105*, 15773-15778.

Khosravi-Far, R., Lutz, R.J., Cox, A.D., Conroy, L., Bourne, J.R., Sinensky, M., Balch, W.E., Buss, J.E., and Der, C.J. (1991). Isoprenoid modification of rab proteins terminating in CC or CXC motifs. Proc Natl Acad Sci U S A *88*, 6264-6268.

Khuroo, M.S., and Khuroo, M.S. (2016). Hepatitis E: an emerging global disease - from discovery towards control and cure. J Viral Hepat *23*, 68-79.

Khvotchev, M.V., Ren, M., Takamori, S., Jahn, R., and Sudhof, T.C. (2003). Divergent functions of neuronal Rab11b in Ca2+-regulated versus constitutive exocytosis. The Journal of neuroscience : the official journal of the Society for Neuroscience *23*, 10531-10539.

Kim, J.L., Morgenstern, K.A., Lin, C., Fox, T., Dwyer, M.D., Landro, J.A., Chambers, S.P., Markland, W., Lepre, C.A., O'Malley, E.T.*, et al.* (1996). Crystal structure of the hepatitis C virus NS3 protease domain complexed with a synthetic NS4A cofactor peptide. Cell *87*, 343-355.

Kim, S., Welsch, C., Yi, M., and Lemon, S.M. (2011). Regulation of the production of infectious genotype 1a hepatitis C virus by NS5A domain III. J Virol *85*, 6645-6656.

Kim, Y.G., Raunser, S., Munger, C., Wagner, J., Song, Y.L., Cygler, M., Walz, T., Oh, B.H., and Sacher, M. (2006). The architecture of the multisubunit TRAPP I complex suggests a model for vesicle tethering. Cell *127*, 817-830.

Knipe, D.M., and Howley, P.M. (2013). Fields virology, 6th edn (Philadelphia, PA: Wolters Kluwer/Lippincott Williams & Wilkins Health).

Knodler, A., Feng, S., Zhang, J., Zhang, X., Das, A., Peranen, J., and Guo, W. (2010). Coordination of Rab8 and Rab11 in primary ciliogenesis. Proc Natl Acad Sci U S A *107*, 6346-6351.

Knowles, B.C., Roland, J.T., Krishnan, M., Tyska, M.J., Lapierre, L.A., Dickman, P.S., Goldenring, J.R., and Shub, M.D. (2014). Myosin Vb uncoupling from RAB8A and RAB11A elicits microvillus inclusion disease. J Clin Invest *124*, 2947-2962.

Knowles, B.C., Weis, V.G., Yu, S., Roland, J.T., Williams, J.A., Alvarado, G.S., Lapierre, L.A., Shub, M.D., Gao, N., and Goldenring, J.R. (2015). Rab11a regulates syntaxin 3 localization and microvillus assembly in enterocytes. J Cell Sci *128*, 1617-1626.

Kockx, M., Guo, D.L., Huby, T., Lesnik, P., Kay, J., Sabaretnam, T., Jary, E., Hill, M., Gaus, K., Chapman, J., *et al.* (2007). Secretion of apolipoprotein E from macrophages occurs via a protein kinase A and calcium-dependent pathway along the microtubule network. Circ Res *101*, 607-616.

Kohan, A.B. (2015). Apolipoprotein C-III: a potent modulator of hypertriglyceridemia and cardiovascular disease. Current opinion in endocrinology, diabetes, and obesity *22*, 119-125.

Kohan, A.B., Wang, F., Lo, C.M., Liu, M., and Tso, P. (2015). ApoA-IV: current and emerging roles in intestinal lipid metabolism, glucose homeostasis, and satiety. American journal of physiology Gastrointestinal and liver physiology *308*, G472-481.

Kothapalli, D., Fuki, I., Ali, K., Stewart, S.A., Zhao, L., Yahil, R., Kwiatkowski, D., Hawthorne, E.A., FitzGerald, G.A., Phillips, M.C., *et al.* (2004). Antimitogenic effects of HDL and APOE mediated by Cox-2-dependent IP activation. J Clin Invest *113*, 609-618.

Kouranti, I., Sachse, M., Arouche, N., Goud, B., and Echard, A. (2006). Rab35 regulates an endocytic recycling pathway essential for the terminal steps of cytokinesis. Curr Biol *16*, 1719-1725.

Krautkramer, E., Lehmann, M.J., Bollinger, V., and Zeier, M. (2012). Polar release of pathogenic Old World hantaviruses from renal tubular epithelial cells. Virol J *9*, 299.

Kreis, T.E., and Lodish, H.F. (1986). Oligomerization is essential for transport of vesicular stomatitis viral glycoprotein to the cell surface. Cell *46*, 929-937.

Kuge, O., Dascher, C., Orci, L., Rowe, T., Amherdt, M., Plutner, H., Ravazzola, M., Tanigawa, G., Rothman, J.E., and Balch, W.E. (1994). Sar1 promotes vesicle budding from the endoplasmic reticulum but not Golgi compartments. J Cell Biol *125*, 51-65.

Kuhn, R.J., Zhang, W., Rossmann, M.G., Pletnev, S.V., Corver, J., Lenches, E., Jones, C.T., Mukhopadhyay, S., Chipman, P.R., Strauss, E.G., *et al.* (2002). Structure of dengue virus: implications for flavivirus organization, maturation, and fusion. Cell *108*, 717-725.

Kuipers, F., Jong, M.C., Lin, Y., Eck, M., Havinga, R., Bloks, V., Verkade, H.J., Hofker, M.H., Moshage, H., Berkel, T.J., *et al.* (1997). Impaired secretion of very low density lipoprotein-triglycerides by apolipoprotein E- deficient mouse hepatocytes. J Clin Invest *100*, 2915-2922.

Laatsch, A., Panteli, M., Sornsakrin, M., Hoffzimmer, B., Grewal, T., and Heeren, J. (2012). Low density lipoprotein receptor-related protein 1 dependent endosomal trapping and recycling of apolipoprotein E. PLoS One *7*, e29385.

Law, S.W., Grant, S.M., Higuchi, K., Hospattankar, A., Lackner, K., Lee, N., and Brewer, H.B., Jr. (1986). Human liver apolipoprotein B-100 cDNA: complete nucleic acid and derived amino acid sequence. Proc Natl Acad Sci U S A *83*, 8142-8146.

Lee, J., Tauscher, A., Seo, D.W., Oram, J.F., and Kuver, R. (2003). Cultured gallbladder epithelial cells synthesize apolipoproteins A-I and E. American journal of physiology Gastrointestinal and liver physiology *285*, G630-641.

Lee, J.Y., Acosta, E.G., Stoeck, I.K., Long, G., Hiet, M.S., Mueller, B., Fackler, O.T., Kallis, S., and Bartenschlager, R. (2014). Apolipoprotein E likely contributes to a maturation step of infectious hepatitis C virus particles and interacts with viral envelope glycoproteins. J Virol *88*, 12422-12437.

Lesburg, C.A., Cable, M.B., Ferrari, E., Hong, Z., Mannarino, A.F., and Weber, P.C. (1999). Crystal structure of the RNA-dependent RNA polymerase from hepatitis C virus reveals a fully encircled active site. Nat Struct Biol *6*, 937-943.

Leung, K.F., Baron, R., and Seabra, M.C. (2006). Thematic review series: lipid posttranslational modifications. geranylgeranylation of Rab GTPases. J Lipid Res *47*, 467-475.

Leung, S.M., Ruiz, W.G., and Apodaca, G. (2000). Sorting of membrane and fluid at the apical pole of polarized Madin-Darby canine kidney cells. Mol Biol Cell *11*, 2131-2150.

Lewis, M.J., and Pelham, H.R. (1992). Ligand-induced redistribution of a human KDEL receptor from the Golgi complex to the endoplasmic reticulum. Cell *68*, 353-364.

Li, B.X., Satoh, A.K., and Ready, D.F. (2007). Myosin V, Rab11, and dRip11 direct apical secretion and cellular morphogenesis in developing Drosophila photoreceptors. J Cell Biol *177*, 659-669.

Li, Y., Wang, G., Lin, K., Yin, H., Zhou, C., Liu, T., Wu, G., and Qian, G. (2010). Rab1 GTPase promotes expression of beta-adrenergic receptors in rat pulmonary microvascular endothelial cells. The international journal of biochemistry & cell biology *42*, 1201-1209.

Lilly-Stauderman, M., Brown, T.L., Balasubramaniam, A., and Harmony, J.A. (1993). Heparin releases newly synthesized cell surface-associated apolipoprotein E from HepG2 cells. J Lipid Res *34*, 190-200.

Lin, C., Lindenbach, B.D., Pragai, B.M., McCourt, D.W., and Rice, C.M. (1994). Processing in the hepatitis C virus E2-NS2 region: identification of p7 and two distinct E2-specific products with different C termini. J Virol *68*, 5063-5073.

Lin, C., Thomson, J.A., and Rice, C.M. (1995). A central region in the hepatitis C virus NS4A protein allows formation of an active NS3-NS4A serine proteinase complex in vivo and in vitro. J Virol *69*, 4373-4380.

Lindenbach, B.D. (2013). Virion assembly and release. Current topics in microbiology and immunology *369*, 199-218.

Lindenbach, B.D., Evans, M.J., Syder, A.J., Wolk, B., Tellinghuisen, T.L., Liu, C.C., Maruyama, T., Hynes, R.O., Burton, D.R., McKeating, J.A., *et al.* (2005). Complete replication of hepatitis C virus in cell culture. Science *309*, 623-626.

Lindenbach, B.D., Meuleman, P., Ploss, A., Vanwolleghem, T., Syder, A.J., McKeating, J.A., Lanford, R.E., Feinstone, S.M., Major, M.E., Leroux-Roels, G., *et al.* (2006). Cell culture-grown hepatitis C virus is infectious in vivo and can be recultured in vitro. Proc Natl Acad Sci U S A *103*, 3805-3809.

Lindenbach, B.D., and Rice, C.M. (2013). The ins and outs of hepatitis C virus entry and assembly. Nat Rev Microbiol *11*, 688-700.

Linder, M.D., Mayranpaa, M.I., Peranen, J., Pietila, T.E., Pietiainen, V.M., Uronen, R.L., Olkkonen, V.M., Kovanen, P.T., and Ikonen, E. (2009). Rab8 regulates ABCA1 cell surface expression and facilitates cholesterol efflux in primary human macrophages. Arterioscler Thromb Vasc Biol *29*, 883-888.

Linder, M.D., Uronen, R.L., Holtta-Vuori, M., van der Sluijs, P., Peranen, J., and Ikonen, E. (2007). Rab8-dependent recycling promotes endosomal cholesterol removal in normal and sphingolipidosis cells. Mol Biol Cell *18*, 47-56.

Lippincott-Schwartz, J., Snapp, E., and Kenworthy, A. (2001). Studying protein dynamics in living cells. Nature reviews Molecular cell biology *2*, 444-456.

Lippincott-Schwartz, J., Yuan, L., Tipper, C., Amherdt, M., Orci, L., and Klausner, R.D. (1991). Brefeldin A's effects on endosomes, lysosomes, and the TGN suggest a general mechanism for regulating organelle structure and membrane traffic. Cell *67*, 601-616.

Lippincott-Schwartz, J., Yuan, L.C., Bonifacino, J.S., and Klausner, R.D. (1989). Rapid redistribution of Golgi proteins into the ER in cells treated with brefeldin A: evidence for membrane cycling from Golgi to ER. Cell *56*, 801-813.

Liu, Z., Lavis, L.D., and Betzig, E. (2015). Imaging live-cell dynamics and structure at the single-molecule level. Mol Cell *58*, 644-659.

Livak, K.J., and Schmittgen, T.D. (2001). Analysis of relative gene expression data using real-time quantitative PCR and the 2(-Delta Delta C(T)) Method. Methods *25*, 402-408.

Lock, J.G., and Stow, J.L. (2005). Rab11 in recycling endosomes regulates the sorting and basolateral transport of E-cadherin. Mol Biol Cell *16*, 1744-1755.

Lohmann, V. (2013). Hepatitis C virus RNA replication. Current topics in microbiology and immunology *369*, 167-198.

Lohmann, V., Korner, F., Koch, J., Herian, U., Theilmann, L., and Bartenschlager, R. (1999). Replication of subgenomic hepatitis C virus RNAs in a hepatoma cell line. Science *285*, 110-113.

Lombardi, D., Soldati, T., Riederer, M.A., Goda, Y., Zerial, M., and Pfeffer, S.R. (1993). Rab9 functions in transport between late endosomes and the trans Golgi network. EMBO J *12*, 677-682.

Long, G., Hiet, M.S., Windisch, M.P., Lee, J.Y., Lohmann, V., and Bartenschlager, R. (2011). Mouse hepatic cells support assembly of infectious hepatitis C virus particles. Gastroenterology *141*, 1057-1066.

Lorenz, I.C., Marcotrigiano, J., Dentzer, T.G., and Rice, C.M. (2006). Structure of the catalytic domain of the hepatitis C virus NS2-3 protease. Nature *442*, 831-835.

Love, R.A., Brodsky, O., Hickey, M.J., Wells, P.A., and Cronin, C.N. (2009). Crystal structure of a novel dimeric form of NS5A domain I protein from hepatitis C virus. J Virol *83*, 4395-4403.

Love, R.A., Parge, H.E., Wickersham, J.A., Hostomsky, Z., Habuka, N., Moomaw, E.W., Adachi, T., and Hostomska, Z. (1996). The crystal structure of hepatitis C virus NS3 proteinase reveals a trypsin-like fold and a structural zinc binding site. Cell *87*, 331-342.

Luck, A.N., and Mason, A.B. (2012). Transferrin-mediated cellular iron delivery. Current topics in membranes *69*, 3-35.

Luna, J.M., Scheel, T.K., Danino, T., Shaw, K.S., Mele, A., Fak, J.J., Nishiuchi, E., Takacs, C.N., Catanese, M.T., de Jong, Y.P.*, et al.* (2015). Hepatitis C Virus RNA Functionally Sequesters miR-122. Cell *160*, 1099-1110.

Lupberger, J., Zeisel, M.B., Xiao, F., Thumann, C., Fofana, I., Zona, L., Davis, C., Mee, C.J., Turek, M., Gorke, S.*, et al.* (2011). EGFR and EphA2 are host factors for hepatitis C virus entry and possible targets for antiviral therapy. Nat Med *17*, 589-595.

Lusis, A.J., Mar, R., and Pajukanta, P. (2004). Genetics of atherosclerosis. Annual review of genomics and human genetics *5*, 189-218.

Luzio, J.P., Pryor, P.R., and Bright, N.A. (2007). Lysosomes: fusion and function. Nature reviews Molecular cell biology *8*, 622-632.

Ma, Y., Yates, J., Liang, Y., Lemon, S.M., and Yi, M. (2008). NS3 helicase domains involved in infectious intracellular hepatitis C virus particle assembly. J Virol *82*, 7624-7639.

Machner, M.P., and Isberg, R.R. (2006). Targeting of host Rab GTPase function by the intravacuolar pathogen Legionella pneumophila. Developmental cell *11*, 47-56.

Machner, M.P., and Isberg, R.R. (2007). A bifunctional bacterial protein links GDI displacement to Rab1 activation. Science *318*, 974-977.

MacLachlan, J.H., and Cowie, B.C. (2015). Hepatitis B virus epidemiology. Cold Spring Harbor perspectives in medicine *5*, a021410.

MacLachlan, J.H., Locarnini, S., and Cowie, B.C. (2015). Estimating the global prevalence of hepatitis B. Lancet *386*, 1515-1517.

Macro, L., Jaiswal, J.K., and Simon, S.M. (2012). Dynamics of clathrin-mediated endocytosis and its requirement for organelle biogenesis in Dictyostelium. J Cell Sci *125*, 5721-5732.

Madara, J.L. (1998). Regulation of the movement of solutes across tight junctions. Annual review of physiology *60*, 143-159.

Mahley, R.W. (1988). Apolipoprotein E: cholesterol transport protein with expanding role in cell biology. Science *240*, 622-630.

Mahley, R.W., Huang, Y., and Rall, S.C., Jr. (1999). Pathogenesis of type III hyperlipoproteinemia (dysbetalipoproteinemia). Questions, quandaries, and paradoxes. J Lipid Res *40*, 1933-1949.

Mahley, R.W., Innerarity, T.L., Rall, S.C., Jr., and Weisgraber, K.H. (1984). Plasma lipoproteins: apolipoprotein structure and function. J Lipid Res *25*, 1277-1294.

Maiga, S.F., Kalopissis, A.D., and Chabert, M. (2014). Apolipoprotein A-II is a key regulatory factor of HDL metabolism as appears from studies with transgenic animals and clinical outcomes. Biochimie *96*, 56-66.

Mansbach, C.M., and Siddiqi, S.A. (2010). The biogenesis of chylomicrons. Annual review of physiology *72*, 315-333.

Marchiando, A.M., Graham, W.V., and Turner, J.R. (2010). Epithelial barriers in homeostasis and disease. Annu Rev Pathol *5*, 119-144.

Martens, S., and McMahon, H.T. (2008). Mechanisms of membrane fusion: disparate players and common principles. Nature reviews Molecular cell biology *9*, 543-556.

Martinez, M., Brice, A., Vaughan, J.R., Zimprich, A., Breteler, M.M., Meco, G., Filla, A., Farrer, M.J., Betard, C., Singleton, A., *et al.* (2005). Apolipoprotein E4 is probably

responsible for the chromosome 19 linkage peak for Parkinson's disease. Am J Med Genet B Neuropsychiatr Genet *136B*, 72-74.

Martinez, O., Schmidt, A., Salamero, J., Hoflack, B., Roa, M., and Goud, B. (1994). The small GTP-binding protein rab6 functions in intra-Golgi transport. J Cell Biol *127*, 1575-1588.

Marukian, S., Andrus, L., Sheahan, T.P., Jones, C.T., Charles, E.D., Ploss, A., Rice, C.M., and Dustin, L.B. (2011). Hepatitis C virus induces interferon-lambda and interferon-stimulated genes in primary liver cultures. Hepatology *54*, 1913-1923.

Marzesco, A.M., Dunia, I., Pandjaitan, R., Recouvreur, M., Dauzonne, D., Benedetti, E.L., Louvard, D., and Zahraoui, A. (2002). The small GTPase Rab13 regulates assembly of functional tight junctions in epithelial cells. Mol Biol Cell *13*, 1819-1831.

Masaki, T., Suzuki, R., Murakami, K., Aizaki, H., Ishii, K., Murayama, A., Date, T., Matsuura, Y., Miyamura, T., Wakita, T., *et al.* (2008). Interaction of hepatitis C virus nonstructural protein 5A with core protein is critical for the production of infectious virus particles. J Virol *82*, 7964-7976.

Matheny, S.C., and Kingery, J.E. (2012). Hepatitis A. American family physician *86*, 1027-1034; quiz 1010-1022.

Matsui, T., Itoh, T., and Fukuda, M. (2011). Small GTPase Rab12 regulates constitutive degradation of transferrin receptor. Traffic *12*, 1432-1443.

Mattila, P.E., Raghavan, V., Rbaibi, Y., Baty, C.J., and Weisz, O.A. (2014). Rab11a-positive compartments in proximal tubule cells sort fluid-phase and membrane cargo. Am J Physiol Cell Physiol *306*, C441-449.

Mazelova, J., Astuto-Gribble, L., Inoue, H., Tam, B.M., Schonteich, E., Prekeris, R., Moritz, O.L., Randazzo, P.A., and Deretic, D. (2009a). Ciliary targeting motif VxPx directs assembly of a trafficking module through Arf4. EMBO J *28*, 183-192.

Mazelova, J., Ransom, N., Astuto-Gribble, L., Wilson, M.C., and Deretic, D. (2009b). Syntaxin 3 and SNAP-25 pairing, regulated by omega-3 docosahexaenoic acid, controls the delivery of rhodopsin for the biogenesis of cilia-derived sensory organelles, the rod outer segments. J Cell Sci *122*, 2003-2013.

Mazzone, T., Gump, H., Diller, P., and Getz, G.S. (1987). Macrophage free cholesterol content regulates apolipoprotein E synthesis. J Biol Chem *262*, 11657-11662.

McEwen, D.P., Schumacher, S.M., Li, Q., Benson, M.D., Iniguez-Lluhi, J.A., Van Genderen, K.M., and Martens, J.R. (2007). Rab-GTPase-dependent endocytic recycling of Kv1.5 in atrial myocytes. J Biol Chem *282*, 29612-29620.

McLauchlan, J., Lemberg, M.K., Hope, G., and Martoglio, B. (2002). Intramembrane proteolysis promotes trafficking of hepatitis C virus core protein to lipid droplets. EMBO J *21*, 3980-3988.

Meex, S.J., Andreo, U., Sparks, J.D., and Fisher, E.A. (2011). Huh-7 or HepG2 cells: which is the better model for studying human apolipoprotein-B100 assembly and secretion? J Lipid Res *52*, 152-158.

Mensenkamp, A.R., Havekes, L.M., Romijn, J.A., and Kuipers, F. (2001). Hepatic steatosis and very low density lipoprotein secretion: the involvement of apolipoprotein E. J Hepatol *35*, 816-822.

Merz, A., Long, G., Hiet, M.S., Brugger, B., Chlanda, P., Andre, P., Wieland, F., Krijnse-Locker, J., and Bartenschlager, R. (2011). Biochemical and morphological properties of hepatitis C virus particles and determination of their lipidome. J Biol Chem *286*, 3018-3032.

Merzlyak, E.M., Goedhart, J., Shcherbo, D., Bulina, M.E., Shcheglov, A.S., Fradkov, A.F., Gaintzeva, A., Lukyanov, K.A., Lukyanov, S., Gadella, T.W., *et al.* (2007). Bright monomeric red fluorescent protein with an extended fluorescence lifetime. Nat Methods *4*, 555-557.

Mesa, R., Salomon, C., Roggero, M., Stahl, P.D., and Mayorga, L.S. (2001). Rab22a affects the morphology and function of the endocytic pathway. J Cell Sci *114*, 4041-4049.

Mihai Gazdag, E., Streller, A., Haneburger, I., Hilbi, H., Vetter, I.R., Goody, R.S., and Itzen, A. (2013). Mechanism of Rab1b deactivation by the Legionella pneumophila GAP LepB. EMBO Rep *14*, 199-205.

Miller, E.A., and Schekman, R. (2013). COPII - a flexible vesicle formation system. Current opinion in cell biology *25*, 420-427.

Miller, S.G., Carnell, L., and Moore, H.H. (1992). Post-Golgi membrane traffic: brefeldin A inhibits export from distal Golgi compartments to the cell surface but not recycling. J Cell Biol *118*, 267-283.

Mishra, A.K., Del Campo, C.M., Collins, R.E., Roy, C.R., and Lambright, D.G. (2013). The Legionella pneumophila GTPase activating protein LepB accelerates Rab1 deactivation by a non-canonical hydrolytic mechanism. J Biol Chem *288*, 24000-24011.

Mitchell, H., Choudhury, A., Pagano, R.E., and Leof, E.B. (2004). Ligand-dependent and -independent transforming growth factor-beta receptor recycling regulated by clathrin-mediated endocytosis and Rab11. Mol Biol Cell *15*, 4166-4178.

Miyanari, Y., Atsuzawa, K., Usuda, N., Watashi, K., Hishiki, T., Zayas, M., Bartenschlager, R., Wakita, T., Hijikata, M., and Shimotohno, K. (2007). The lipid droplet is an important organelle for hepatitis C virus production. Nat Cell Biol *9*, 1089-1097.

Mizuno, M., and Singer, S.J. (1993). A soluble secretory protein is first concentrated in the endoplasmic reticulum before transfer to the Golgi apparatus. Proc Natl Acad Sci U S A *90*, 5732-5736.

Mizushima, H., Hijikata, M., Asabe, S., Hirota, M., Kimura, K., and Shimotohno, K. (1994a). Two hepatitis C virus glycoprotein E2 products with different C termini. J Virol *68*, 6215-6222.

Mizushima, H., Hijikata, M., Tanji, Y., Kimura, K., and Shimotohno, K. (1994b). Analysis of N-terminal processing of hepatitis C virus nonstructural protein 2. J Virol *68*, 2731-2734.

Mohd Hanafiah, K., Groeger, J., Flaxman, A.D., and Wiersma, S.T. (2013). Global epidemiology of hepatitis C virus infection: new estimates of age-specific antibody to HCV seroprevalence. Hepatology *57*, 1333-1342.

Momose, F., Sekimoto, T., Ohkura, T., Jo, S., Kawaguchi, A., Nagata, K., and Morikawa, Y. (2011). Apical transport of influenza A virus ribonucleoprotein requires Rab11-positive recycling endosome. PLoS One *6*, e21123.

Monazahian, M., Bohme, I., Bonk, S., Koch, A., Scholz, C., Grethe, S., and Thomssen, R. (1999). Low density lipoprotein receptor as a candidate receptor for hepatitis C virus. J Med Virol *57*, 223-229.

Monetta, P., Slavin, I., Romero, N., and Alvarez, C. (2007). Rab1b interacts with GBF1 and modulates both ARF1 dynamics and COPI association. Mol Biol Cell *18*, 2400-2410.

Monks, J., and Neville, M.C. (2004). Albumin transcytosis across the epithelium of the lactating mouse mammary gland. The Journal of physiology *560*, 267-280.

Moore, R.H., Millman, E.E., Alpizar-Foster, E., Dai, W., and Knoll, B.J. (2004). Rab11 regulates the recycling and lysosome targeting of beta2-adrenergic receptors. J Cell Sci *117*, 3107-3117.

Moradpour, D., Evans, M.J., Gosert, R., Yuan, Z., Blum, H.E., Goff, S.P., Lindenbach, B.D., and Rice, C.M. (2004). Insertion of green fluorescent protein into nonstructural protein 5A allows direct visualization of functional hepatitis C virus replication complexes. J Virol *78*, 7400-7409.

Moradpour, D., Gosert, R., Egger, D., Penin, F., Blum, H.E., and Bienz, K. (2003). Membrane association of hepatitis C virus nonstructural proteins and identification of the membrane alteration that harbors the viral replication complex. Antiviral Res *60*, 103-109.

Moradpour, D., Penin, F., and Rice, C.M. (2007). Replication of hepatitis C virus. Nat Rev Microbiol *5*, 453-463.

Morimoto, S., Nishimura, N., Terai, T., Manabe, S., Yamamoto, Y., Shinahara, W., Miyake, H., Tashiro, S., Shimada, M., and Sasaki, T. (2005). Rab13 mediates the continuous endocytic recycling of occludin to the cell surface. J Biol Chem *280*, 2220-2228.

Moritz, O.L., Tam, B.M., Hurd, L.L., Peranen, J., Deretic, D., and Papermaster, D.S. (2001). Mutant rab8 Impairs docking and fusion of rhodopsin-bearing post-Golgi membranes and causes cell death of transgenic Xenopus rods. Mol Biol Cell *12*, 2341-2351.

Morlot, S., and Roux, A. (2013). Mechanics of dynamin-mediated membrane fission. Annual review of biophysics *42*, 629-649.

Moyer, B.D., Allan, B.B., and Balch, W.E. (2001a). Rab1 interaction with a GM130 effector complex regulates COPII vesicle cis--Golgi tethering. Traffic *2*, 268-276.

Moyer, B.D., Matteson, J., and Balch, W.E. (2001b). Expression of wild-type and mutant green fluorescent protein-Rab1 for fluorescence microscopy analysis. Methods Enzymol *329*, 6-14.

Mukhopadhyay, S., Kim, B.S., Chipman, P.R., Rossmann, M.G., and Kuhn, R.J. (2003). Structure of West Nile virus. Science *302*, 248.

Mukhopadhyay, S., Kuhn, R.J., and Rossmann, M.G. (2005). A structural perspective of the flavivirus life cycle. Nat Rev Microbiol *3*, 13-22.

Muller, M.P., Peters, H., Blumer, J., Blankenfeldt, W., Goody, R.S., and Itzen, A. (2010). The Legionella effector protein DrrA AMPylates the membrane traffic regulator Rab1b. Science *329*, 946-949.

Munafo, D.B., and Colombo, M.I. (2002). Induction of autophagy causes dramatic changes in the subcellular distribution of GFP-Rab24. Traffic *3*, 472-482.

Murakami, M., Ushio, Y., Morino, Y., Ohta, T., and Matsukado, Y. (1988). Immunohistochemical localization of apolipoprotein E in human glial neoplasms. J Clin Invest *82*, 177-188.

Murata, T., Delprato, A., Ingmundson, A., Toomre, D.K., Lambright, D.G., and Roy, C.R. (2006). The Legionella pneumophila effector protein DrrA is a Rab1 guanine nucleotide-exchange factor. Nat Cell Biol *8*, 971-977.

Murray, C.L., Jones, C.T., and Rice, C.M. (2008). Architects of assembly: roles of Flaviviridae non-structural proteins in virion morphogenesis. Nat Rev Microbiol *6*, 699-708.

Murray, C.L., Jones, C.T., Tassello, J., and Rice, C.M. (2007). Alanine scanning of the hepatitis C virus core protein reveals numerous residues essential for production of infectious virus. J Virol *81*, 10220-10231.

Musch, A. (2014). The unique polarity phenotype of hepatocytes. Experimental cell research *328*, 276-283.

Nachmias, D., Sklan, E.H., Ehrlich, M., and Bacharach, E. (2012). Human immunodeficiency virus type 1 envelope proteins traffic toward virion assembly sites via a TBC1D20/Rab1-regulated pathway. Retrovirology *9*, 7.

Nachury, M.V., Loktev, A.V., Zhang, Q., Westlake, C.J., Peranen, J., Merdes, A., Slusarski, D.C., Scheller, R.H., Bazan, J.F., Sheffield, V.C., *et al.* (2007). A core complex of BBS proteins cooperates with the GTPase Rab8 to promote ciliary membrane biogenesis. Cell *129*, 1201-1213.

Nakano, A., and Muramatsu, M. (1989). A novel GTP-binding protein, Sar1p, is involved in transport from the endoplasmic reticulum to the Golgi apparatus. J Cell Biol *109*, 2677-2691.

Namba, T., Funahashi, Y., Nakamuta, S., Xu, C., Takano, T., and Kaibuchi, K. (2015). Extracellular and Intracellular Signaling for Neuronal Polarity. Physiol Rev *95*, 995-1024.

Neto, H., Balmer, G., and Gould, G. (2013). Exocyst proteins in cytokinesis: Regulation by Rab11. Communicative & integrative biology *6*, e27635.

Neuberger, J. (2016). An update on liver transplantation: A critical review. Journal of autoimmunity *66*, 51-59.

Nevo-Yassaf, I., Yaffe, Y., Asher, M., Ravid, O., Eizenberg, S., Henis, Y.I., Nahmias, Y., Hirschberg, K., and Sklan, E.H. (2012). Role for TBC1D20 and Rab1 in hepatitis C virus replication via interaction with lipid droplet-bound nonstructural protein 5A. J Virol *86*, 6491-6502.

Nguyen, A.W., and Daugherty, P.S. (2005). Evolutionary optimization of fluorescent proteins for intracellular FRET. Nat Biotechnol *23*, 355-360.

Nielsen, S.U., Bassendine, M.F., Burt, A.D., Martin, C., Pumeechockchai, W., and Toms, G.L. (2006). Association between hepatitis C virus and very-low-density lipoprotein (VLDL)/LDL analyzed in iodixanol density gradients. J Virol *80*, 2418-2428.

Niu, T.K., Pfeifer, A.C., Lippincott-Schwartz, J., and Jackson, C.L. (2005). Dynamics of GBF1, a Brefeldin A-sensitive Arf1 exchange factor at the Golgi. Mol Biol Cell *16*, 1213-1222.

Nokes, R.L., Fields, I.C., Collins, R.N., and Folsch, H. (2008). Rab13 regulates membrane trafficking between TGN and recycling endosomes in polarized epithelial cells. J Cell Biol *182*, 845-853.

Norata, G.D., Tsimikas, S., Pirillo, A., and Catapano, A.L. (2015). Apolipoprotein C-III: From Pathophysiology to Pharmacology. Trends in pharmacological sciences *36*, 675-687.

Nuoffer, C., Davidson, H.W., Matteson, J., Meinkoth, J., and Balch, W.E. (1994). A GDP-bound of rab1 inhibits protein export from the endoplasmic reticulum and transport between Golgi compartments. J Cell Biol *125*, 225-237.

Ogawa, K., Medline, A., and Farber, E. (1979). Sequential analysis of hepatic carcinogenesis: the comparative architecture of preneoplastic, malignant, prenatal, postnatal and regenerating liver. British journal of cancer *40*, 782-790.

Olofsson, S.O., and Boren, J. (2005). Apolipoprotein B: a clinically important apolipoprotein which assembles atherogenic lipoproteins and promotes the development of atherosclerosis. J Intern Med *258*, 395-410.

Omori, Y., Zhao, C., Saras, A., Mukhopadhyay, S., Kim, W., Furukawa, T., Sengupta, P., Veraksa, A., and Malicki, J. (2008). Elipsa is an early determinant of ciliogenesis that links the IFT particle to membrane-associated small GTPase Rab8. Nat Cell Biol *10*, 437-444.

Ossipova, O., Chuykin, I., Chu, C.W., and Sokol, S.Y. (2015). Vangl2 cooperates with Rab11 and Myosin V to regulate apical constriction during vertebrate gastrulation. Development *142*, 99-107.

Ossipova, O., Kim, K., Lake, B.B., Itoh, K., Ioannou, A., and Sokol, S.Y. (2014). Role of Rab11 in planar cell polarity and apical constriction during vertebrate neural tube closure. Nature communications *5*, 3734.

Padula, P., Figueroa, R., Navarrete, M., Pizarro, E., Cadiz, R., Bellomo, C., Jofre, C., Zaror, L., Rodriguez, E., and Murua, R. (2004). Transmission study of Andes hantavirus infection in wild sigmodontine rodents. J Virol *78*, 11972-11979.

Palade, G. (1975). Intracellular aspects of the process of protein synthesis. Science *189*, 347-358.

Pan, M., Maitin, V., Parathath, S., Andreo, U., Lin, S.X., St Germain, C., Yao, Z., Maxfield, F.R., Williams, K.J., and Fisher, E.A. (2008a). Presecretory oxidation, aggregation, and autophagic destruction of apoprotein-B: a pathway for late-stage quality control. Proc Natl Acad Sci U S A *105*, 5862-5867.

Pan, X., Luhrmann, A., Satoh, A., Laskowski-Arce, M.A., and Roy, C.R. (2008b). Ankyrin repeat proteins comprise a diverse family of bacterial type IV effectors. Science *320*, 1651-1654.

Patino-Lopez, G., Dong, X., Ben-Aissa, K., Bernot, K.M., Itoh, T., Fukuda, M., Kruhlak, M.J., Samelson, L.E., and Shaw, S. (2008). Rab35 and its GAP EPI64C in T cells regulate receptor recycling and immunological synapse formation. J Biol Chem *283*, 18323-18330.

Pelkmans, L. (2005). Viruses as probes for systems analysis of cellular signalling, cytoskeleton reorganization and endocytosis. Curr Opin Microbiol *8*, 331-337.

Pencheva, N., Tran, H., Buss, C., Huh, D., Drobnjak, M., Busam, K., and Tavazoie, S.F. (2012). Convergent multi-miRNA targeting of ApoE drives LRP1/LRP8-dependent melanoma metastasis and angiogenesis. Cell *151*, 1068-1082.

Pepperkok, R., Scheel, J., Horstmann, H., Hauri, H.P., Griffiths, G., and Kreis, T.E. (1993). Beta-COP is essential for biosynthetic membrane transport from the endoplasmic reticulum to the Golgi complex in vivo. Cell *74*, 71-82.

Peranen, J. (2011). Rab8 GTPase as a regulator of cell shape. Cytoskeleton *68*, 527-539.

Peranen, J., Auvinen, P., Virta, H., Wepf, R., and Simons, K. (1996). Rab8 promotes polarized membrane transport through reorganization of actin and microtubules in fibroblasts. J Cell Biol *135*, 153-167.

Peranen, J., and Furuhjelm, J. (2001). Expression, purification, and properties of Rab8 function in actin cortical skeleton organization and polarized transport. Methods Enzymol *329*, 188-196.

Perez-Gracia, M.T., Suay, B., and Mateos-Lindemann, M.L. (2014). Hepatitis E: an emerging disease. Infection, genetics and evolution : journal of molecular epidemiology and evolutionary genetics in infectious diseases *22*, 40-59.

Peter, F., Plutner, H., Zhu, H., Kreis, T.E., and Balch, W.E. (1993). Beta-COP is essential for transport of protein from the endoplasmic reticulum to the Golgi in vitro. J Cell Biol *122*, 1155-1167.

Petrie, R.J., Doyle, A.D., and Yamada, K.M. (2009). Random versus directionally persistent cell migration. Nature reviews Molecular cell biology *10*, 538-549.

Pfeffer, S.R. (2013). Rab GTPase regulation of membrane identity. Current opinion in cell biology *25*, 414-419.

Phillips, M.C. (2014). Apolipoprotein E isoforms and lipoprotein metabolism. IUBMB life *66*, 616-623.

Pileri, P., Uematsu, Y., Campagnoli, S., Galli, G., Falugi, F., Petracca, R., Weiner, A.J., Houghton, M., Rosa, D., Grandi, G.*, et al.* (1998). Binding of hepatitis C virus to CD81. Science *282*, 938-941.

Pilli, M., Arko-Mensah, J., Ponpuak, M., Roberts, E., Master, S., Mandell, M.A., Dupont, N., Ornatowski, W., Jiang, S., Bradfute, S.B.*, et al.* (2012). TBK-1 promotes autophagy-mediated antimicrobial defense by controlling autophagosome maturation. Immunity *37*, 223-234.

Pind, S.N., Nuoffer, C., McCaffery, J.M., Plutner, H., Davidson, H.W., Farquhar, M.G., and Balch, W.E. (1994). Rab1 and Ca2+ are required for the fusion of carrier vesicles mediating endoplasmic reticulum to Golgi transport. J Cell Biol *125*, 239-252.

Pitas, R.E., Boyles, J.K., Lee, S.H., Foss, D., and Mahley, R.W. (1987). Astrocytes synthesize apolipoprotein E and metabolize apolipoprotein E-containing lipoproteins. Biochim Biophys Acta *917*, 148-161.

Ploss, A., Evans, M.J., Gaysinskaya, V.A., Panis, M., You, H., de Jong, Y.P., and Rice, C.M. (2009). Human occludin is a hepatitis C virus entry factor required for infection of mouse cells. Nature *457*, 882-886.

Ploss, A., Khetani, S.R., Jones, C.T., Syder, A.J., Trehan, K., Gaysinskaya, V.A., Mu, K., Ritola, K., Rice, C.M., and Bhatia, S.N. (2010). Persistent hepatitis C virus infection in microscale primary human hepatocyte cultures. Proc Natl Acad Sci U S A *107*, 3141-3145.

Ploss, A., and Rice, C.M. (2009). Towards a small animal model for hepatitis C. EMBO Rep *10*, 1220-1227.

Plump, A.S., Smith, J.D., Hayek, T., Aalto-Setala, K., Walsh, A., Verstuyft, J.G., Rubin, E.M., and Breslow, J.L. (1992). Severe hypercholesterolemia and atherosclerosis in apolipoprotein E-deficient mice created by homologous recombination in ES cells. Cell *71*, 343-353.

Plutner, H., Cox, A.D., Pind, S., Khosravi-Far, R., Bourne, J.R., Schwaninger, R., Der, C.J., and Balch, W.E. (1991). Rab1b regulates vesicular transport between the endoplasmic reticulum and successive Golgi compartments. J Cell Biol *115*, 31-43.

Popescu, C.I., Callens, N., Trinel, D., Roingeard, P., Moradpour, D., Descamps, V., Duverlie, G., Penin, F., Heliot, L., Rouille, Y., *et al.* (2011). NS2 protein of hepatitis C virus interacts with structural and non-structural proteins towards virus assembly. PLoS Pathog *7*, e1001278.

Powell, R.R., and Temesvari, L.A. (2004). Involvement of a Rab8-like protein of Dictyostelium discoideum, Sas1, in the formation of membrane extensions, secretion and adhesion during development. Microbiology *150*, 2513-2525.

Presley, J.F., Cole, N.B., Schroer, T.A., Hirschberg, K., Zaal, K.J., and Lippincott-Schwartz, J. (1997). ER-to-Golgi transport visualized in living cells. Nature *389*, 81-85.

Presley, J.F., Ward, T.H., Pfeifer, A.C., Siggia, E.D., Phair, R.D., and Lippincott-Schwartz, J. (2002). Dissection of COPI and Arf1 dynamics in vivo and role in Golgi membrane transport. Nature *417*, 187-193.

Preston, J.E., Joan Abbott, N., and Begley, D.J. (2014). Transcytosis of macromolecules at the blood-brain barrier. Advances in pharmacology *71*, 147-163.

Prigozhina, N.L., and Waterman-Storer, C.M. (2006). Decreased polarity and increased random motility in PtK1 epithelial cells correlate with inhibition of endosomal recycling. J Cell Sci *119*, 3571-3582.

Protzer, U., Maini, M.K., and Knolle, P.A. (2012). Living in the liver: hepatic infections. Nature reviews Immunology *12*, 201-213.

Pybus, O.G., Markov, P.V., Wu, A., and Tatem, A.J. (2007). Investigating the endemic transmission of the hepatitis C virus. International journal for parasitology *37*, 839-849.

Pybus, O.G., and Theze, J. (2015). Hepacivirus cross-species transmission and the origins of the hepatitis C virus. Current opinion in virology *16*, 1-7.

Pylypenko, O., Rak, A., Durek, T., Kushnir, S., Dursina, B.E., Thomae, N.H., Constantinescu, A.T., Brunsveld, L., Watzke, A., Waldmann, H.*, et al.* (2006). Structure of doubly prenylated Ypt1:GDI complex and the mechanism of GDI-mediated Rab recycling. EMBO J *25*, 13-23.

Quinlan, G.J., Martin, G.S., and Evans, T.W. (2005). Albumin: biochemical properties and therapeutic potential. Hepatology *41*, 1211-1219.

Quinn, P.S., Gamble, M., and Judah, J.D. (1975). Biosynthesis of serum albumin in rat liver. Isolation and probable structure of 'proalbumin' from rat liver. Biochem J *146*, 389-393.

Rahim, A., Nafi-valencia, E., Siddiqi, S., Basha, R., Runyon, C.C., and Siddiqi, S.A. (2012). Proteomic analysis of the very low density lipoprotein (VLDL) transport vesicles. Journal of proteomics *75*, 2225-2235.

Rak, A., Pylypenko, O., Durek, T., Watzke, A., Kushnir, S., Brunsveld, L., Waldmann, H., Goody, R.S., and Alexandrov, K. (2003). Structure of Rab GDP-dissociation inhibitor in complex with prenylated YPT1 GTPase. Science *302*, 646-650.

Rall, S.C., Jr., Weisgraber, K.H., and Mahley, R.W. (1982). Human apolipoprotein E. The complete amino acid sequence. J Biol Chem *257*, 4171-4178.

Randhawa, V.K., Ishikura, S., Talior-Volodarsky, I., Cheng, A.W., Patel, N., Hartwig, J.H., and Klip, A. (2008). GLUT4 vesicle recruitment and fusion are differentially regulated by Rac, AS160, and Rab8A in muscle cells. J Biol Chem *283*, 27208-27219.

Raney, K.D., Sharma, S.D., Moustafa, I.M., and Cameron, C.E. (2010). Hepatitis C virus non-structural protein 3 (HCV NS3): a multifunctional antiviral target. J Biol Chem *285*, 22725-22731.

Raposo, G., Marks, M.S., and Cutler, D.F. (2007). Lysosome-related organelles: driving post-Golgi compartments into specialisation. Current opinion in cell biology *19*, 394-401.

Rappoport, J.Z., and Simon, S.M. (2008). A functional GFP fusion for imaging clathrin-mediated endocytosis. Traffic *9*, 1250-1255.

Rappoport, J.Z., and Simon, S.M. (2009). Endocytic trafficking of activated EGFR is AP-2 dependent and occurs through preformed clathrin spots. J Cell Sci *122*, 1301-1305.

Ravkov, E.V., Nichol, S.T., and Compans, R.W. (1997). Polarized entry and release in epithelial cells of Black Creek Canal virus, a New World hantavirus. J Virol *71*, 1147-1154.

Reardon, C.A., Blachowicz, L., Watson, K.M., Barr, E., and Getz, G.S. (1998). Association of human apolipoprotein E with lipoproteins secreted by transfected McA RH7777 cells. J Lipid Res *39*, 1372-1381.

Reefman, E., Kay, J.G., Wood, S.M., Offenhauser, C., Brown, D.L., Roy, S., Stanley, A.C., Low, P.C., Manderson, A.P., and Stow, J.L. (2010). Cytokine secretion is distinct from secretion of cytotoxic granules in NK cells. J Immunol *184*, 4852-4862.

Ren, M., Xu, G., Zeng, J., De Lemos-Chiarandini, C., Adesnik, M., and Sabatini, D.D. (1998). Hydrolysis of GTP on rab11 is required for the direct delivery of transferrin from the pericentriolar recycling compartment to the cell surface but not from sorting endosomes. Proc Natl Acad Sci U S A *95*, 6187-6192.

Rizo, J., and Rosenmund, C. (2008). Synaptic vesicle fusion. Nat Struct Mol Biol *15*, 665-674.

Rizo, J., and Xu, J. (2015). The Synaptic Vesicle Release Machinery. Annual review of biophysics *44*, 339-367.

Rizzetto, M. (2015). Hepatitis D Virus: Introduction and Epidemiology. Cold Spring Harbor perspectives in medicine *5*, a021576.

Robitaille, M., Ramakrishnan, N., Baragli, A., and Hebert, T.E. (2009). Intracellular trafficking and assembly of specific Kir3 channel/G protein complexes. Cellular signalling *21*, 488-501.

Rodriguez-Boulan, E., and Macara, I.G. (2014). Organization and execution of the epithelial polarity programme. Nature reviews Molecular cell biology *15*, 225-242.

Rodriguez Boulan, E., and Pendergast, M. (1980). Polarized distribution of viral envelope proteins in the plasma membrane of infected epithelial cells. Cell *20*, 45-54.

Rodriguez Boulan, E., and Sabatini, D.D. (1978). Asymmetric budding of viruses in epithelial monlayers: a model system for study of epithelial polarity. Proc Natl Acad Sci U S A *75*, 5071-5075.

Rojas, R., and Apodaca, G. (2002). Immunoglobulin transport across polarized epithelial cells. Nature reviews Molecular cell biology *3*, 944-955.

Romero-Brey, I., and Bartenschlager, R. (2014). Membranous replication factories induced by plus-strand RNA viruses. Viruses *6*, 2826-2857.

Romero-Brey, I., Merz, A., Chiramel, A., Lee, J.Y., Chlanda, P., Haselman, U., Santarella-Mellwig, R., Habermann, A., Hoppe, S., Kallis, S., *et al.* (2012). Three-dimensional architecture and biogenesis of membrane structures associated with hepatitis C virus replication. PLoS Pathog *8*, e1003056.

Romero, N., Dumur, C.I., Martinez, H., Garcia, I.A., Monetta, P., Slavin, I., Sampieri, L., Koritschoner, N., Mironov, A.A., De Matteis, M.A., *et al.* (2013). Rab1b overexpression modifies Golgi size and gene expression in HeLa cells and modulates the thyrotrophin response in thyroid cells in culture. Mol Biol Cell *24*, 617-632.

Roosterman, D., Schmidlin, F., and Bunnett, N.W. (2003). Rab5a and rab11a mediate agonist-induced trafficking of protease-activated receptor 2. Am J Physiol Cell Physiol *284*, C1319-1329.

Rothschild, M.A., Oratz, M., and Schreiber, S.S. (1988). Serum albumin. Hepatology *8*, 385-401.

Rowe, R.K., and Pekosz, A. (2006). Bidirectional virus secretion and nonciliated cell tropism following Andes virus infection of primary airway epithelial cell cultures. J Virol *80*, 1087-1097.

Rowe, R.K., Suszko, J.W., and Pekosz, A. (2008). Roles for the recycling endosome, Rab8, and Rab11 in hantavirus release from epithelial cells. Virology *382*, 239-249.

Rustaeus, S., Lindberg, K., Boren, J., and Olofsson, S.O. (1995). Brefeldin A reversibly inhibits the assembly of apoB containing lipoproteins in McA-RH7777 cells. J Biol Chem *270*, 28879-28886.

Rutledge, A.C., Su, Q., and Adeli, K. (2010). Apolipoprotein B100 biogenesis: a complex array of intracellular mechanisms regulating folding, stability, and lipoprotein assembly. Biochemistry and cell biology = Biochimie et biologie cellulaire *88*, 251-267.

Rzomp, K.A., Scholtes, L.D., Briggs, B.J., Whittaker, G.R., and Scidmore, M.A. (2003). Rab GTPases are recruited to chlamydial inclusions in both a species-dependent and species-independent manner. Infect Immun *71*, 5855-5870.

Sacks, F.M. (2015). The crucial roles of apolipoproteins E and C-III in apoB lipoprotein metabolism in normolipidemia and hypertriglyceridemia. Current opinion in lipidology *26*, 56-63.

Sainz, B., Jr., Barretto, N., Martin, D.N., Hiraga, N., Imamura, M., Hussain, S., Marsh, K.A., Yu, X., Chayama, K., Alrefai, W.A., *et al.* (2012). Identification of the Niemann-Pick C1-like 1 cholesterol absorption receptor as a new hepatitis C virus entry factor. Nat Med *18*, 281-285.

Salamero, J., Bausinger, H., Mommaas, A.M., Lipsker, D., Proamer, F., Cazenave, J.P., Goud, B., de la Salle, H., and Hanau, D. (2001). CD1a molecules traffic through the early recycling endosomal pathway in human Langerhans cells. The Journal of investigative dermatology *116*, 401-408.

Saraste, J., Lahtinen, U., and Goud, B. (1995). Localization of the small GTP-binding protein rab1p to early compartments of the secretory pathway. J Cell Sci *108 (Pt 4)*, 1541-1552.

Sastry, L., Johnson, T., Hobson, M.J., Smucker, B., and Cornetta, K. (2002). Titering lentiviral vectors: comparison of DNA, RNA and marker expression methods. Gene therapy *9*, 1155-1162.

Sato, T., Iwano, T., Kunii, M., Matsuda, S., Mizuguchi, R., Jung, Y., Hagiwara, H., Yoshihara, Y., Yuzaki, M., Harada, R., *et al.* (2014). Rab8a and Rab8b are essential for several apical transport pathways but insufficient for ciliogenesis. J Cell Sci *127*, 422-431.

Sato, T., Mushiake, S., Kato, Y., Sato, K., Sato, M., Takeda, N., Ozono, K., Miki, K., Kubo, Y., Tsuji, A., *et al.* (2007). The Rab8 GTPase regulates apical protein localization in intestinal cells. Nature *448*, 366-369.

Satoh, A., Tokunaga, F., Kawamura, S., and Ozaki, K. (1997). In situ inhibition of vesicle transport and protein processing in the dominant negative Rab1 mutant of Drosophila. J Cell Sci *110 (Pt 23)*, 2943-2953.

Satoh, A., Wang, Y., Malsam, J., Beard, M.B., and Warren, G. (2003). Golgin-84 is a rab1 binding partner involved in Golgi structure. Traffic *4*, 153-161.

Satoh, A.K., O'Tousa, J.E., Ozaki, K., and Ready, D.F. (2005). Rab11 mediates post-Golgi trafficking of rhodopsin to the photosensitive apical membrane of Drosophila photoreceptors. Development *132*, 1487-1497.

Savina, A., Fader, C.M., Damiani, M.T., and Colombo, M.I. (2005). Rab11 promotes docking and fusion of multivesicular bodies in a calcium-dependent manner. Traffic *6*, 131-143.

Savina, A., Vidal, M., and Colombo, M.I. (2002). The exosome pathway in K562 cells is regulated by Rab11. J Cell Sci *115*, 2505-2515.

Sayed, I.M., Vercouter, A.S., Abdelwahab, S.F., Vercauteren, K., and Meuleman, P. (2015). Is hepatitis E virus an emerging problem in industrialized countries? Hepatology *62*, 1883-1892.

Scarselli, E., Ansuini, H., Cerino, R., Roccasecca, R.M., Acali, S., Filocamo, G., Traboni, C., Nicosia, A., Cortese, R., and Vitelli, A. (2002). The human scavenger receptor class B type I is a novel candidate receptor for the hepatitis C virus. EMBO J *21*, 5017-5025.

Scheel, T.K., and Rice, C.M. (2013). Understanding the hepatitis C virus life cycle paves the way for highly effective therapies. Nat Med *19*, 837-849.

Schiavo, G., and van der Goot, F.G. (2001). The bacterial toxin toolkit. Nature reviews Molecular cell biology *2*, 530-537.

Schindelin, J., Arganda-Carreras, I., Frise, E., Kaynig, V., Longair, M., Pietzsch, T., Preibisch, S., Rueden, C., Saalfeld, S., Schmid, B., *et al.* (2012). Fiji: an open-source platform for biological-image analysis. Nat Methods *9*, 676-682.

Schmid, B., Rinas, M., Ruggieri, A., Acosta, E.G., Bartenschlager, M., Reuter, A., Fischl, W., Harder, N., Bergeest, J.P., Flossdorf, M., *et al.* (2015). Live Cell Analysis and

Mathematical Modeling Identify Determinants of Attenuation of Dengue Virus 2'-O-Methylation Mutant. PLoS Pathog *11*, e1005345.

Schmidt, A.J., Rockstroh, J.K., Vogel, M., An der Heiden, M., Baillot, A., Krznaric, I., and Radun, D. (2011). Trouble with bleeding: risk factors for acute hepatitis C among HIV-positive gay men from Germany--a case-control study. PLoS One *6*, e17781.

Schmitt, H.D., Wagner, P., Pfaff, E., and Gallwitz, D. (1986). The ras-related YPT1 gene product in yeast: a GTP-binding protein that might be involved in microtubule organization. Cell *47*, 401-412.

Schoebel, S., Blankenfeldt, W., Goody, R.S., and Itzen, A. (2010). High-affinity binding of phosphatidylinositol 4-phosphate by Legionella pneumophila DrrA. EMBO Rep *11*, 598-604.

Schoebel, S., Oesterlin, L.K., Blankenfeldt, W., Goody, R.S., and Itzen, A. (2009). RabGDI displacement by DrrA from Legionella is a consequence of its guanine nucleotide exchange activity. Mol Cell *36*, 1060-1072.

Schonfeld, G. (2003). Familial hypobetalipoproteinemia: a review. J Lipid Res *44*, 878-883.

Schonfeld, G., Lin, X., and Yue, P. (2005). Familial hypobetalipoproteinemia: genetics and metabolism. Cell Mol Life Sci *62*, 1372-1378.

Schuck, S., Gerl, M.J., Ang, A., Manninen, A., Keller, P., Mellman, I., and Simons, K. (2007). Rab10 is involved in basolateral transport in polarized Madin-Darby canine kidney cells. Traffic *8*, 47-60.

Schwaninger, R., Beckers, C.J., and Balch, W.E. (1991). Sequential transport of protein between the endoplasmic reticulum and successive Golgi compartments in semi-intact cells. J Biol Chem *266*, 13055-13063.

Seebohm, G., Strutz-Seebohm, N., Birkin, R., Dell, G., Bucci, C., Spinosa, M.R., Baltaev, R., Mack, A.F., Korniychuk, G., Choudhury, A., *et al.* (2007). Regulation of endocytic recycling of KCNQ1/KCNE1 potassium channels. Circ Res *100*, 686-692.

Segev, N., and Botstein, D. (1987). The ras-like yeast YPT1 gene is itself essential for growth, sporulation, and starvation response. Molecular and cellular biology *7*, 2367-2377.

Segev, N., Mulholland, J., and Botstein, D. (1988). The yeast GTP-binding YPT1 protein and a mammalian counterpart are associated with the secretion machinery. Cell *52*, 915-924.

Segrest, J.P., Jones, M.K., De Loof, H., Brouillette, C.G., Venkatachalapathi, Y.V., and Anantharamaiah, G.M. (1992). The amphipathic helix in the exchangeable apolipoproteins: a review of secondary structure and function. J Lipid Res *33*, 141-166.

Sheff, D.R., Daro, E.A., Hull, M., and Mellman, I. (1999). The receptor recycling pathway contains two distinct populations of early endosomes with different sorting functions. J Cell Biol *145*, 123-139.

Shima, D.T., Scales, S.J., Kreis, T.E., and Pepperkok, R. (1999). Segregation of COPI-rich and anterograde-cargo-rich domains in endoplasmic-reticulum-to-Golgi transport complexes. Curr Biol *9*, 821-824.

Shin, H.W., Hayashi, M., Christoforidis, S., Lacas-Gervais, S., Hoepfner, S., Wenk, M.R., Modregger, J., Uttenweiler-Joseph, S., Wilm, M., Nystuen, A., *et al.* (2005). An enzymatic cascade of Rab5 effectors regulates phosphoinositide turnover in the endocytic pathway. J Cell Biol *170*, 607-618.

Shin, K., Fogg, V.C., and Margolis, B. (2006). Tight junctions and cell polarity. Annual review of cell and developmental biology *22*, 207-235.

Shrivastava, S., Devhare, P., Sujijantarat, N., Steele, R., Kwon, Y.C., Ray, R., and Ray, R.B. (2015). Knockdown of Autophagy Inhibits Infectious Hepatitis C Virus Release by the Exosomal Pathway. J Virol *90*, 1387-1396.

Siddiqi, S.A. (2008). VLDL exits from the endoplasmic reticulum in a specialized vesicle, the VLDL transport vesicle, in rat primary hepatocytes. Biochem J *413*, 333-342.

Siddiqi, S.A., Gorelick, F.S., Mahan, J.T., and Mansbach, C.M., 2nd (2003). COPII proteins are required for Golgi fusion but not for endoplasmic reticulum budding of the pre-chylomicron transport vesicle. J Cell Sci *116*, 415-427.

Silvis, M.R., Bertrand, C.A., Ameen, N., Golin-Bisello, F., Butterworth, M.B., Frizzell, R.A., and Bradbury, N.A. (2009). Rab11b regulates the apical recycling of the cystic fibrosis transmembrane conductance regulator in polarized intestinal epithelial cells. Mol Biol Cell *20*, 2337-2350.

Simons, M., Saffrich, R., Reiser, J., and Mundel, P. (1999). Directed membrane transport is involved in process formation in cultured podocytes. Journal of the American Society of Nephrology : JASN *10*, 1633-1639.

Simpson, J.C., Griffiths, G., Wessling-Resnick, M., Fransen, J.A., Bennett, H., and Jones, A.T. (2004). A role for the small GTPase Rab21 in the early endocytic pathway. J Cell Sci *117*, 6297-6311.

Sklan, E.H., Serrano, R.L., Einav, S., Pfeffer, S.R., Lambright, D.G., and Glenn, J.S. (2007a). TBC1D20 is a Rab1 GTPase-activating protein that mediates hepatitis C virus replication. J Biol Chem *282*, 36354-36361.

Sklan, E.H., Staschke, K., Oakes, T.M., Elazar, M., Winters, M., Aroeti, B., Danieli, T., and Glenn, J.S. (2007b). A Rab-GAP TBC domain protein binds hepatitis C virus NS5A and mediates viral replication. J Virol *81*, 11096-11105.

Slavin, I., Garcia, I.A., Monetta, P., Martinez, H., Romero, N., and Alvarez, C. (2011). Role of Rab1b in COPII dynamics and function. European journal of cell biology *90*, 301-311.

Smith, J.D., Melian, A., Leff, T., and Breslow, J.L. (1988). Expression of the human apolipoprotein E gene is regulated by multiple positive and negative elements. J Biol Chem *263*, 8300-8308.

Snipes, G.J., McGuire, C.B., Norden, J.J., and Freeman, J.A. (1986). Nerve injury stimulates the secretion of apolipoprotein E by nonneuronal cells. Proc Natl Acad Sci U S A *83*, 1130-1134.

Sobajima, T., Yoshimura, S., Iwano, T., Kunii, M., Watanabe, M., Atik, N., Mushiake, S., Morii, E., Koyama, Y., Miyoshi, E.*, et al.* (2014). Rab11a is required for apical protein localisation in the intestine. Biology open *4*, 86-94.

Sonnichsen, B., De Renzis, S., Nielsen, E., Rietdorf, J., and Zerial, M. (2000). Distinct membrane domains on endosomes in the recycling pathway visualized by multicolor imaging of Rab4, Rab5, and Rab11. J Cell Biol *149*, 901-914.

Spano, S., and Galan, J.E. (2012). A Rab32-dependent pathway contributes to Salmonella typhi host restriction. Science *338*, 960-963.

Srinivas, R.V., Balachandran, N., Alonso-Caplen, F.V., and Compans, R.W. (1986). Expression of herpes simplex virus glycoproteins in polarized epithelial cells. J Virol *58*, 689-693.

Stagg, S.M., Gurkan, C., Fowler, D.M., LaPointe, P., Foss, T.R., Potter, C.S., Carragher, B., and Balch, W.E. (2006). Structure of the Sec13/31 COPII coat cage. Nature *439*, 234-238.

Stagg, S.M., LaPointe, P., Razvi, A., Gurkan, C., Potter, C.S., Carragher, B., and Balch, W.E. (2008). Structural basis for cargo regulation of COPII coat assembly. Cell *134*, 474-484.

Stearns, T., Willingham, M.C., Botstein, D., and Kahn, R.A. (1990). ADP-ribosylation factor is functionally and physically associated with the Golgi complex. Proc Natl Acad Sci U S A *87*, 1238-1242.

Stenmark, H. (2009). Rab GTPases as coordinators of vesicle traffic. Nature reviews Molecular cell biology *10*, 513-525.

Stephens, D.J., Lin-Marq, N., Pagano, A., Pepperkok, R., and Paccaud, J.P. (2000). COPI-coated ER-to-Golgi transport complexes segregate from COPII in close proximity to ER exit sites. J Cell Sci *113 (Pt 12)*, 2177-2185.

Strain, A.J., and Neuberger, J.M. (2002). A bioartificial liver--state of the art. Science *295*, 1005-1009.

Struck, D.K., Siuta, P.B., Lane, M.D., and Lennarz, W.J. (1978). Effect of tunicamycin on the secretion of serum proteins by primary cultures of rat and chick hepatocytes. Studies on transferrin, very low density lipoprotein, and serum albumin. J Biol Chem *253*, 5332-5337.

Sudhof, T.C. (2004). The synaptic vesicle cycle. Annual review of neuroscience *27*, 509-547.

Sugawara, K., Shibasaki, T., Mizoguchi, A., Saito, T., and Seino, S. (2009). Rab11 and its effector Rip11 participate in regulation of insulin granule exocytosis. Genes to cells : devoted to molecular & cellular mechanisms *14*, 445-456.

Suh, H.Y., Lee, D.W., Lee, K.H., Ku, B., Choi, S.J., Woo, J.S., Kim, Y.G., and Oh, B.H. (2010). Structural insights into the dual nucleotide exchange and GDI displacement activity of SidM/DrrA. EMBO J *29*, 496-504.

Sun, Q., Westphal, W., Wong, K.N., Tan, I., and Zhong, Q. (2010a). Rubicon controls endosome maturation as a Rab7 effector. Proc Natl Acad Sci U S A *107*, 19338-19343.

Sun, Y., Bilan, P.J., Liu, Z., and Klip, A. (2010b). Rab8A and Rab13 are activated by insulin and regulate GLUT4 translocation in muscle cells. Proc Natl Acad Sci U S A *107*, 19909-19914.

Sun, Y., Chiu, T.T., Foley, K.P., Bilan, P.J., and Klip, A. (2014). Myosin Va mediates Rab8A-regulated GLUT4 vesicle exocytosis in insulin-stimulated muscle cells. Mol Biol Cell *25*, 1159-1170.

Sundaram, M., and Yao, Z. (2010). Recent progress in understanding protein and lipid factors affecting hepatic VLDL assembly and secretion. Nutrition & metabolism *7*, 35.

Sundaram, M., and Yao, Z. (2012). Intrahepatic role of exchangeable apolipoproteins in lipoprotein assembly and secretion. Arterioscler Thromb Vasc Biol *32*, 1073-1078.

Swiatecka-Urban, A., Brown, A., Moreau-Marquis, S., Renuka, J., Coutermarsh, B., Barnaby, R., Karlson, K.H., Flotte, T.R., Fukuda, M., Langford, G.M., *et al.* (2005). The short apical membrane half-life of rescued {Delta}F508-cystic fibrosis transmembrane conductance regulator (CFTR) results from accelerated endocytosis of {Delta}F508-CFTR in polarized human airway epithelial cells. J Biol Chem *280*, 36762-36772.

Swiatecka-Urban, A., Talebian, L., Kanno, E., Moreau-Marquis, S., Coutermarsh, B., Hansen, K., Karlson, K.H., Barnaby, R., Cheney, R.E., Langford, G.M., *et al.* (2007). Myosin Vb is required for trafficking of the cystic fibrosis transmembrane conductance regulator in Rab11a-specific apical recycling endosomes in polarized human airway epithelial cells. J Biol Chem *282*, 23725-23736.

Szul, T., Garcia-Mata, R., Brandon, E., Shestopal, S., Alvarez, C., and Sztul, E. (2005). Dissection of membrane dynamics of the ARF-guanine nucleotide exchange factor GBF1. Traffic *6*, 374-385.

Szul, T., Grabski, R., Lyons, S., Morohashi, Y., Shestopal, S., Lowe, M., and Sztul, E. (2007). Dissecting the role of the ARF guanine nucleotide exchange factor GBF1 in Golgi biogenesis and protein trafficking. J Cell Sci *120*, 3929-3940.

Takai, Y., Sasaki, T., and Matozaki, T. (2001). Small GTP-binding proteins. Physiol Rev *81*, 153-208.

Takano, T., Tomomura, M., Yoshioka, N., Tsutsumi, K., Terasawa, Y., Saito, T., Kawano, H., Kamiguchi, H., Fukuda, M., and Hisanaga, S. (2012). LMTK1/AATYK1 is a novel regulator of axonal outgrowth that acts via Rab11 in a Cdk5-dependent manner. The Journal of neuroscience : the official journal of the Society for Neuroscience *32*, 6587-6599.

Takano, T., Urushibara, T., Yoshioka, N., Saito, T., Fukuda, M., Tomomura, M., and Hisanaga, S. (2014). LMTK1 regulates dendritic formation by regulating movement of Rab11A-positive endosomes. Mol Biol Cell *25*, 1755-1768.

Takeuchi, H., Furuta, N., Morisaki, I., and Amano, A. (2011). Exit of intracellular Porphyromonas gingivalis from gingival epithelial cells is mediated by endocytic recycling pathway. Cell Microbiol *13*, 677-691.

Takikawa, S., Ishii, K., Aizaki, H., Suzuki, T., Asakura, H., Matsuura, Y., and Miyamura, T. (2000). Cell fusion activity of hepatitis C virus envelope proteins. J Virol *74*, 5066-5074.

Tarafder, A.K., Bolasco, G., Correia, M.S., Pereira, F.J., Iannone, L., Hume, A.N., Kirkpatrick, N., Picardo, M., Torrisi, M.R., Rodrigues, I.P., *et al.* (2014). Rab11b mediates melanin transfer between donor melanocytes and acceptor keratinocytes via coupled exo/endocytosis. The Journal of investigative dermatology *134*, 1056-1066.

Targett-Adams, P., Hope, G., Boulant, S., and McLauchlan, J. (2008). Maturation of hepatitis C virus core protein by signal peptide peptidase is required for virus production. J Biol Chem *283*, 16850-16859.

Tellinghuisen, T.L., Foss, K.L., Treadaway, J.C., and Rice, C.M. (2008). Identification of residues required for RNA replication in domains II and III of the hepatitis C virus NS5A protein. J Virol *82*, 1073-1083.

Tellinghuisen, T.L., Marcotrigiano, J., Gorbalenya, A.E., and Rice, C.M. (2004). The NS5A protein of hepatitis C virus is a zinc metalloprotein. J Biol Chem *279*, 48576-48587.

Tellinghuisen, T.L., Marcotrigiano, J., and Rice, C.M. (2005). Structure of the zinc-binding domain of an essential component of the hepatitis C virus replicase. Nature *435*, 374-379.

Teng, B., Burant, C.F., and Davidson, N.O. (1993). Molecular cloning of an apolipoprotein B messenger RNA editing protein. Science *260*, 1816-1819.

Tennyson, G.E., Sabatos, C.A., Higuchi, K., Meglin, N., and Brewer, H.B., Jr. (1989). Expression of apolipoprotein B mRNAs encoding higher- and lower-molecular weight isoproteins in rat liver and intestine. Proc Natl Acad Sci U S A *86*, 500-504.

Terai, T., Nishimura, N., Kanda, I., Yasui, N., and Sasaki, T. (2006). JRAB/MICAL-L2 is a junctional Rab13-binding protein mediating the endocytic recycling of occludin. Mol Biol Cell *17*, 2465-2475.

Theendakara, V., Peters-Libeu, C.A., Spilman, P., Poksay, K.S., Bredesen, D.E., and Rao, R.V. (2016). Direct Transcriptional Effects of Apolipoprotein E. The Journal of neuroscience : the official journal of the Society for Neuroscience *36*, 685-700.

Theriault, C., Rochdi, M.D., and Parent, J.L. (2004). Role of the Rab11-associated intracellular pool of receptors formed by constitutive endocytosis of the beta isoform of the thromboxane A2 receptor (TP beta). Biochemistry *43*, 5600-5607.

Thomas, C., Rousset, R., and Noselli, S. (2009). JNK signalling influences intracellular trafficking during Drosophila morphogenesis through regulation of the novel target gene Rab30. Developmental biology *331*, 250-260.

Thomas, D.L. (2000). Hepatitis C epidemiology. Current topics in microbiology and immunology *242*, 25-41.

Thomas, D.L. (2013). Global control of hepatitis C: where challenge meets opportunity. Nat Med *19*, 850-858.

Thompson, A., Nessler, R., Wisco, D., Anderson, E., Winckler, B., and Sheff, D. (2007). Recycling endosomes of polarized epithelial cells actively sort apical and basolateral cargos into separate subdomains. Mol Biol Cell *18*, 2687-2697.

Thuenauer, R., Hsu, Y.C., Carvajal-Gonzalez, J.M., Deborde, S., Chuang, J.Z., Romer, W., Sonnleitner, A., Rodriguez-Boulan, E., and Sung, C.H. (2014). Four-dimensional live imaging of apical biosynthetic trafficking reveals a post-Golgi sorting role of apical endosomal intermediates. Proc Natl Acad Sci U S A *111*, 4127-4132.

Tisdale, E.J., and Balch, W.E. (1996). Rab2 is essential for the maturation of pre-Golgi intermediates. J Biol Chem *271*, 29372-29379.

Tisdale, E.J., Bourne, J.R., Khosravi-Far, R., Der, C.J., and Balch, W.E. (1992). GTP-binding mutants of rab1 and rab2 are potent inhibitors of vesicular transport from the endoplasmic reticulum to the Golgi complex. J Cell Biol *119*, 749-761.

Tiwari, S., and Siddiqi, S.A. (2012). Intracellular trafficking and secretion of VLDL. Arterioscler Thromb Vasc Biol *32*, 1079-1086.

Tomei, L., Failla, C., Santolini, E., De Francesco, R., and La Monica, N. (1993). NS3 is a serine protease required for processing of hepatitis C virus polyprotein. J Virol *67*, 4017-4026.

Touchot, N., Chardin, P., and Tavitian, A. (1987). Four additional members of the ras gene superfamily isolated by an oligonucleotide strategy: molecular cloning of YPT-related cDNAs from a rat brain library. Proc Natl Acad Sci U S A *84*, 8210-8214.

Traber, M.G., Kayden, H.J., and Rindler, M.J. (1987). Polarized secretion of newly synthesized lipoproteins by the Caco-2 human intestinal cell line. J Lipid Res *28*, 1350-1363.

Tran, K., Thorne-Tjomsland, G., DeLong, C.J., Cui, Z., Shan, J., Burton, L., Jamieson, J.C., and Yao, Z. (2002). Intracellular assembly of very low density lipoproteins containing apolipoprotein B100 in rat hepatoma McA-RH7777 cells. J Biol Chem *277*, 31187-31200.

Treyer, A., and Musch, A. (2013). Hepatocyte polarity. Comprehensive Physiology *3*, 243-287.

Tsukiyama-Kohara, K., Iizuka, N., Kohara, M., and Nomoto, A. (1992). Internal ribosome entry site within hepatitis C virus RNA. J Virol *66*, 1476-1483.

Tzaban, S., Massol, R.H., Yen, E., Hamman, W., Frank, S.R., Lapierre, L.A., Hansen, S.H., Goldenring, J.R., Blumberg, R.S., and Lencer, W.I. (2009). The recycling and transcytotic pathways for IgG transport by FcRn are distinct and display an inherent polarity. J Cell Biol *185*, 673-684.

Udayar, V., Buggia-Prevot, V., Guerreiro, R.L., Siegel, G., Rambabu, N., Soohoo, A.L., Ponnusamy, M., Siegenthaler, B., Bali, J., Aesg, *et al.* (2013). A paired RNAi and RabGAP overexpression screen identifies Rab11 as a regulator of beta-amyloid production. Cell reports *5*, 1536-1551.

Uhlig, M., Passlack, W., and Eckel, J. (2005). Functional role of Rab11 in GLUT4 trafficking in cardiomyocytes. Molecular and cellular endocrinology *235*, 1-9.

Ullrich, O., Reinsch, S., Urbe, S., Zerial, M., and Parton, R.G. (1996). Rab11 regulates recycling through the pericentriolar recycling endosome. J Cell Biol *135*, 913-924.

Urbanus, A.T., van de Laar, T.J., Stolte, I.G., Schinkel, J., Heijman, T., Coutinho, R.A., and Prins, M. (2009). Hepatitis C virus infections among HIV-infected men who have sex with men: an expanding epidemic. Aids *23*, F1-7.

Utermann, G. (1975). Isolation and partial characterization of an arginine-rich apolipoprotein from human plasma very-low-density lipoproteins: apolipoprotein E. Hoppe-Seyler's Zeitschrift fur physiologische Chemie *356*, 1113-1121.

Utermann, G., Hees, M., and Steinmetz, A. (1977). Polymorphism of apolipoprotein E and occurrence of dysbetalipoproteinaemia in man. Nature *269*, 604-607.

Uzan-Gafsou, S., Bausinger, H., Proamer, F., Monier, S., Lipsker, D., Cazenave, J.P., Goud, B., de la Salle, H., Hanau, D., and Salamero, J. (2007). Rab11A controls the biogenesis of Birbeck granules by regulating Langerin recycling and stability. Mol Biol Cell *18*, 3169-3179.

Vaibhava, V., Nagabhushana, A., Chalasani, M.L., Sudhakar, C., Kumari, A., and Swarup, G. (2012). Optineurin mediates a negative regulation of Rab8 by the GTPase-activating protein TBC1D17. J Cell Sci *125*, 5026-5039.

Valadi, H., Ekstrom, K., Bossios, A., Sjostrand, M., Lee, J.J., and Lotvall, J.O. (2007). Exosome-mediated transfer of mRNAs and microRNAs is a novel mechanism of genetic exchange between cells. Nat Cell Biol *9*, 654-659.

van de Graaf, S.F., Chang, Q., Mensenkamp, A.R., Hoenderop, J.G., and Bindels, R.J. (2006). Direct interaction with Rab11a targets the epithelial Ca2+ channels TRPV5 and TRPV6 to the plasma membrane. Molecular and cellular biology *26*, 303-312.

van de Laar, T., Pybus, O., Bruisten, S., Brown, D., Nelson, M., Bhagani, S., Vogel, M., Baumgarten, A., Chaix, M.L., Fisher, M.*, et al.* (2009). Evidence of a large, international network of HCV transmission in HIV-positive men who have sex with men. Gastroenterology *136*, 1609-1617.

van de Laar, T.J., Matthews, G.V., Prins, M., and Danta, M. (2010). Acute hepatitis C in HIV-infected men who have sex with men: an emerging sexually transmitted infection. Aids *24*, 1799-1812.

van de Laar, T.J., van der Bij, A.K., Prins, M., Bruisten, S.M., Brinkman, K., Ruys, T.A., van der Meer, J.T., de Vries, H.J., Mulder, J.W., van Agtmael, M.*, et al.* (2007). Increase in HCV incidence among men who have sex with men in Amsterdam most likely caused by sexual transmission. J Infect Dis *196*, 230-238.

van den Elzen, P., Garg, S., Leon, L., Brigl, M., Leadbetter, E.A., Gumperz, J.E., Dascher, C.C., Cheng, T.Y., Sacks, F.M., Illarionov, P.A.*, et al.* (2005). Apolipoprotein-mediated pathways of lipid antigen presentation. Nature *437*, 906-910.

van der Sluijs, P., Hull, M., Webster, P., Male, P., Goud, B., and Mellman, I. (1992). The small GTP-binding protein rab4 controls an early sorting event on the endocytic pathway. Cell *70*, 729-740.

Van Der Sluijs, P., Hull, M., Zahraoui, A., Tavitian, A., Goud, B., and Mellman, I. (1991). The small GTP-binding protein rab4 is associated with early endosomes. Proc Natl Acad Sci U S A *88*, 6313-6317.

Vance, D.E., Weinstein, D.B., and Steinberg, D. (1984). Isolation and analysis of lipoproteins secreted by rat liver hepatocytes. Biochim Biophys Acta *792*, 39-47.

Vance, J.E., and Hayashi, H. (2010). Formation and function of apolipoprotein E-containing lipoproteins in the nervous system. Biochim Biophys Acta *1801*, 806-818.

Varthakavi, V., Smith, R.M., Martin, K.L., Derdowski, A., Lapierre, L.A., Goldenring, J.R., and Spearman, P. (2006). The pericentriolar recycling endosome plays a key role in Vpu-mediated enhancement of HIV-1 particle release. Traffic *7*, 298-307.

Vielh, E., Touchot, N., Zahraoui, A., and Tavitian, A. (1989). Nucleotide sequence of a rat cDNA: rab1B, encoding a rab1-YPT related protein. Nucleic Acids Res *17*, 1770.

Vieyres, G., Thomas, X., Descamps, V., Duverlie, G., Patel, A.H., and Dubuisson, J. (2010). Characterization of the envelope glycoproteins associated with infectious hepatitis C virus. J Virol *84*, 10159-10168.

Vogt, A., Scull, M.A., Friling, T., Horwitz, J.A., Donovan, B.M., Dorner, M., Gerold, G., Labitt, R.N., Rice, C.M., and Ploss, A. (2013). Recapitulation of the hepatitis C virus life-cycle in engineered murine cell lines. Virology *444*, 1-11.

Volpicelli, L.A., Lah, J.J., Fang, G., Goldenring, J.R., and Levey, A.I. (2002). Rab11a and myosin Vb regulate recycling of the M4 muscarinic acetylcholine receptor. The Journal of neuroscience : the official journal of the Society for Neuroscience *22*, 9776-9784.

Wagner, P., Molenaar, C.M., Rauh, A.J., Brokel, R., Schmitt, H.D., and Gallwitz, D. (1987). Biochemical properties of the ras-related YPT protein in yeast: a mutational analysis. EMBO J *6*, 2373-2379.

Wakabayashi, Y., Dutt, P., Lippincott-Schwartz, J., and Arias, I.M. (2005). Rab11a and myosin Vb are required for bile canalicular formation in WIF-B9 cells. Proc Natl Acad Sci U S A *102*, 15087-15092.

Wakabayashi, Y., Lippincott-Schwartz, J., and Arias, I.M. (2004). Intracellular trafficking of bile salt export pump (ABCB11) in polarized hepatic cells: constitutive cycling between the canalicular membrane and rab11-positive endosomes. Mol Biol Cell *15*, 3485-3496.

Walker, C.M., and Grakoui, A. (2015). Hepatitis C virus: why do we need a vaccine to prevent a curable persistent infection? Current opinion in immunology *35*, 137-143.

Walter, M., Clark, S.G., and Levinson, A.D. (1986). The oncogenic activation of human p21ras by a novel mechanism. Science *233*, 649-652.

Wang, F., Chen, X., Zhang, X., and Ma, L. (2008). Phosphorylation state of mu-opioid receptor determines the alternative recycling of receptor via Rab4 or Rab11 pathway. Molecular endocrinology *22*, 1881-1892.

Wang, H., Chen, X., and Fisher, E.A. (1993). N-3 fatty acids stimulate intracellular degradation of apoprotein B in rat hepatocytes. J Clin Invest *91*, 1380-1389.

Wang, J., Morita, Y., Mazelova, J., and Deretic, D. (2012). The Arf GAP ASAP1 provides a platform to regulate Arf4- and Rab11-Rab8-mediated ciliary receptor targeting. EMBO J *31*, 4057-4071.

Wang, X., Kumar, R., Navarre, J., Casanova, J.E., and Goldenring, J.R. (2000). Regulation of vesicle trafficking in madin-darby canine kidney cells by Rab11a and Rab25. J Biol Chem *275*, 29138-29146.

Wang, Y., Ng, E.L., and Tang, B.L. (2006). Rab23: what exactly does it traffic? Traffic *7*, 746-750.

Ward, E.S., Martinez, C., Vaccaro, C., Zhou, J., Tang, Q., and Ober, R.J. (2005). From sorting endosomes to exocytosis: association of Rab4 and Rab11 GTPases with the Fc receptor, FcRn, during recycling. Mol Biol Cell *16*, 2028-2038.

Ward, H.H., Brown-Glaberman, U., Wang, J., Morita, Y., Alper, S.L., Bedrick, E.J., Gattone, V.H., 2nd, Deretic, D., and Wandinger-Ness, A. (2011). A conserved signal and GTPase complex are required for the ciliary transport of polycystin-1. Mol Biol Cell *22*, 3289-3305.

Weide, T., Bayer, M., Koster, M., Siebrasse, J.P., Peters, R., and Barnekow, A. (2001). The Golgi matrix protein GM130: a specific interacting partner of the small GTPase rab1b. EMBO Rep *2*, 336-341.

Weide, T., Teuber, J., Bayer, M., and Barnekow, A. (2003). MICAL-1 isoforms, novel rab1 interacting proteins. Biochem Biophys Res Commun *306*, 79-86.

Weisgraber, K.H., Rall, S.C., Jr., and Mahley, R.W. (1981). Human E apoprotein heterogeneity. Cysteine-arginine interchanges in the amino acid sequence of the apo-E isoforms. J Biol Chem *256*, 9077-9083.

Welte, M.A. (2015). Expanding roles for lipid droplets. Curr Biol *25*, R470-481.

Welz, T., Wellbourne-Wood, J., and Kerkhoff, E. (2014). Orchestration of cell surface proteins by Rab11. Trends Cell Biol *24*, 407-415.

Wennmalm, S., and Simon, S.M. (2007). Studying individual events in biology. Annu Rev Biochem *76*, 419-446.

Wernette-Hammond, M.E., Lauer, S.J., Corsini, A., Walker, D., Taylor, J.M., and Rall, S.C., Jr. (1989). Glycosylation of human apolipoprotein E. The carbohydrate attachment site is threonine 194. J Biol Chem *264*, 9094-9101.

Westlake, C.J., Baye, L.M., Nachury, M.V., Wright, K.J., Ervin, K.E., Phu, L., Chalouni, C., Beck, J.S., Kirkpatrick, D.S., Slusarski, D.C.*, et al.* (2011). Primary cilia membrane assembly is initiated by Rab11 and transport protein particle II (TRAPPII) complex-dependent trafficking of Rabin8 to the centrosome. Proc Natl Acad Sci U S A *108*, 2759-2764.

Wetterau, J.R., Aggerbeck, L.P., Bouma, M.E., Eisenberg, C., Munck, A., Hermier, M., Schmitz, J., Gay, G., Rader, D.J., and Gregg, R.E. (1992). Absence of microsomal triglyceride transfer protein in individuals with abetalipoproteinemia. Science *258*, 999-1001.

Wickner, W., and Schekman, R. (2008). Membrane fusion. Nat Struct Mol Biol *15*, 658-664.

Wilcke, M., Johannes, L., Galli, T., Mayau, V., Goud, B., and Salamero, J. (2000). Rab11 regulates the compartmentalization of early endosomes required for efficient transport from early endosomes to the trans-golgi network. J Cell Biol *151*, 1207-1220.

Wilcox, H.G., and Heimberg, M. (1987). Secretion and uptake of nascent hepatic very low density lipoprotein by perfused livers from fed and fasted rats. J Lipid Res *28*, 351-360.

Wilfling, F., Haas, J.T., Walther, T.C., and Farese, R.V., Jr. (2014). Lipid droplet biogenesis. Current opinion in cell biology *29*, 39-45.

Wilson, C., Wardell, M.R., Weisgraber, K.H., Mahley, R.W., and Agard, D.A. (1991). Three-dimensional structure of the LDL receptor-binding domain of human apolipoprotein E. Science *252*, 1817-1822.

Wilson, G.M., Fielding, A.B., Simon, G.C., Yu, X., Andrews, P.D., Hames, R.S., Frey, A.M., Peden, A.A., Gould, G.W., and Prekeris, R. (2005). The FIP3-Rab11 protein complex regulates recycling endosome targeting to the cleavage furrow during late cytokinesis. Mol Biol Cell *16*, 849-860.

Winslow, A.R., Chen, C.W., Corrochano, S., Acevedo-Arozena, A., Gordon, D.E., Peden, A.A., Lichtenberg, M., Menzies, F.M., Ravikumar, B., Imarisio, S., *et al.* (2010). alpha-Synuclein impairs macroautophagy: implications for Parkinson's disease. J Cell Biol *190*, 1023-1037.

Wittinghofer, A., and Vetter, I.R. (2011). Structure-function relationships of the G domain, a canonical switch motif. Annu Rev Biochem *80*, 943-971.

Wolk, B., Sansonno, D., Krausslich, H.G., Dammacco, F., Rice, C.M., Blum, H.E., and Moradpour, D. (2000). Subcellular localization, stability, and trans-cleavage competence of the hepatitis C virus NS3-NS4A complex expressed in tetracycline-regulated cell lines. J Virol *74*, 2293-2304.

Wouters, F.S., Verveer, P.J., and Bastiaens, P.I. (2001). Imaging biochemistry inside cells. Trends Cell Biol *11*, 203-211.

Wu, G., Yussman, M.G., Barrett, T.J., Hahn, H.S., Osinska, H., Hilliard, G.M., Wang, X., Toyokawa, T., Yatani, A., Lynch, R.A., *et al.* (2001). Increased myocardial Rab GTPase expression: a consequence and cause of cardiomyopathy. Circ Res *89*, 1130-1137.

Wu, G., Zhao, G., and He, Y. (2003). Distinct pathways for the trafficking of angiotensin II and adrenergic receptors from the endoplasmic reticulum to the cell surface: Rab1-independent transport of a G protein-coupled receptor. J Biol Chem *278*, 47062-47069.

Xu, D., and Hay, J.C. (2004). Reconstitution of COPII vesicle fusion to generate a pre-Golgi intermediate compartment. J Cell Biol *167*, 997-1003.

Xu, S., Edman, M., Kothawala, M.S., Sun, G., Chiang, L., Mircheff, A., Zhu, L., Okamoto, C., and Hamm-Alvarez, S. (2011). A Rab11a-enriched subapical membrane compartment regulates a cytoskeleton-dependent transcytotic pathway in secretory epithelial cells of the lacrimal gland. J Cell Sci *124*, 3503-3514.

Xu, S., Ma, L., Evans, E., Okamoto, C.T., and Hamm-Alvarez, S.F. (2013). Polymeric immunoglobulin receptor traffics through two distinct apically targeted pathways in primary lacrimal gland acinar cells. J Cell Sci *126*, 2704-2717.

Xu, X.F., Chen, Z.T., Gao, N., Zhang, J.L., and An, J. (2009). Myosin Vc, a member of the actin motor family associated with Rab8, is involved in the release of DV2 from HepG2 cells. Intervirology *52*, 258-265.

Xu, X.F., Chen, Z.T., Zhang, J.L., Chen, W., Wang, J.L., Tian, Y.P., Gao, N., and An, J. (2008). Rab8, a vesicular traffic regulator, is involved in dengue virus infection in HepG2 cells. Intervirology *51*, 182-188.

Yamamura, R., Nishimura, N., Nakatsuji, H., Arase, S., and Sasaki, T. (2008). The interaction of JRAB/MICAL-L2 with Rab8 and Rab13 coordinates the assembly of tight junctions and adherens junctions. Mol Biol Cell *19*, 971-983.

Yamasaki, A., Menon, S., Yu, S., Barrowman, J., Meerloo, T., Oorschot, V., Klumperman, J., Satoh, A., and Ferro-Novick, S. (2009). mTrs130 is a component of a mammalian TRAPPII complex, a Rab1 GEF that binds to COPI-coated vesicles. Mol Biol Cell *20*, 4205-4215.

Yamasaki, K., Chuang, V.T., Maruyama, T., and Otagiri, M. (2013). Albumin-drug interaction and its clinical implication. Biochim Biophys Acta *1830*, 5435-5443.

Yamayoshi, S., Neumann, G., and Kawaoka, Y. (2010). Role of the GTPase Rab1b in ebolavirus particle formation. J Virol *84*, 4816-4820.

Yang, C.Y., Chen, S.H., Gianturco, S.H., Bradley, W.A., Sparrow, J.T., Tanimura, M., Li, W.H., Sparrow, D.A., DeLoof, H., Rosseneu, M., *et al.* (1986). Sequence, structure, receptor-binding domains and internal repeats of human apolipoprotein B-100. Nature *323*, 738-742.

Yang, X., Boehm, J.S., Yang, X., Salehi-Ashtiani, K., Hao, T., Shen, Y., Lubonja, R., Thomas, S.R., Alkan, O., Bhimdi, T., *et al.* (2011). A public genome-scale lentiviral expression library of human ORFs. Nat Methods *8*, 659-661.

Ye, B., Zhang, Y., Song, W., Younger, S.H., Jan, L.Y., and Jan, Y.N. (2007). Growing dendrites and axons differ in their reliance on the secretory pathway. Cell *130*, 717-729.

Ye, S.Q., Olson, L.M., Reardon, C.A., and Getz, G.S. (1992). Human plasma lipoproteins regulate apolipoprotein E secretion from a post-Golgi compartment. J Biol Chem *267*, 21961-21966.

Ye, S.Q., Reardon, C.A., and Getz, G.S. (1993). Inhibition of apolipoprotein E degradation in a post-Golgi compartment by a cysteine protease inhibitor. J Biol Chem *268*, 8497-8502.

Yin, H., Li, Q., Qian, G., Wang, Y., Li, Y., Wu, G., and Wang, G. (2011). Rab1 GTPase regulates phenotypic modulation of pulmonary artery smooth muscle cells by mediating the transport of angiotensin II type 1 receptor under hypoxia. The international journal of biochemistry & cell biology *43*, 401-408.

Yoneda, A., and Doering, T.L. (2006). A eukaryotic capsular polysaccharide is synthesized intracellularly and secreted via exocytosis. Mol Biol Cell *17*, 5131-5140.

Yoo, J.S., Moyer, B.D., Bannykh, S., Yoo, H.M., Riordan, J.R., and Balch, W.E. (2002). Non-conventional trafficking of the cystic fibrosis transmembrane conductance regulator through the early secretory pathway. J Biol Chem *277*, 11401-11409.

Yoshimura, S., Gerondopoulos, A., Linford, A., Rigden, D.J., and Barr, F.A. (2010). Family-wide characterization of the DENN domain Rab GDP-GTP exchange factors. J Cell Biol *191*, 367-381.

Young, S.G., Hubl, S.T., Chappell, D.A., Smith, R.S., Claiborne, F., Snyder, S.M., and Terdiman, J.F. (1989). Familial hypobetalipoproteinemia associated with a mutant species of apolipoprotein B (B-46). The New England journal of medicine *320*, 1604-1610.

Yu, Q., Hu, L., Yao, Q., Zhu, Y., Dong, N., Wang, D.C., and Shao, F. (2013). Structural analyses of Legionella LepB reveal a new GAP fold that catalytically mimics eukaryotic RasGAP. Cell research *23*, 775-787.

Yu, S., Yehia, G., Wang, J., Stypulkowski, E., Sakamori, R., Jiang, P., Hernandez-Enriquez, B., Tran, T.S., Bonder, E.M., Guo, W.*, et al.* (2014). Global ablation of the mouse Rab11a gene impairs early embryogenesis and matrix metalloproteinase secretion. J Biol Chem *289*, 32030-32043.

Yu, X., Qiao, M., Atanasov, I., Hu, Z., Kato, T., Liang, T.J., and Zhou, Z.H. (2007). Cryo-electron microscopy and three-dimensional reconstructions of hepatitis C virus particles. Virology *367*, 126-134.

Zacharias, D.A., Violin, J.D., Newton, A.C., and Tsien, R.Y. (2002). Partitioning of lipid-modified monomeric GFPs into membrane microdomains of live cells. Science *296*, 913-916.

Zahraoui, A., Joberty, G., Arpin, M., Fontaine, J.J., Hellio, R., Tavitian, A., and Louvard, D. (1994). A small rab GTPase is distributed in cytoplasmic vesicles in non polarized cells but colocalizes with the tight junction marker ZO-1 in polarized epithelial cells. J Cell Biol *124*, 101-115.

Zahraoui, A., Touchot, N., Chardin, P., and Tavitian, A. (1989). The human Rab genes encode a family of GTP-binding proteins related to yeast YPT1 and SEC4 products involved in secretion. J Biol Chem *264*, 12394-12401.

Zanni, E.E., Kouvatsi, A., Hadzopoulou-Cladaras, M., Krieger, M., and Zannis, V.I. (1989). Expression of ApoE gene in Chinese hamster cells with a reversible defect in O-glycosylation. Glycosylation is not required for apoE secretion. J Biol Chem *264*, 9137-9140.

Zannis, V.I., Fotakis, P., Koukos, G., Kardassis, D., Ehnholm, C., Jauhiainen, M., and Chroni, A. (2015). HDL biogenesis, remodeling, and catabolism. Handbook of experimental pharmacology *224*, 53-111.

Zannis, V.I., Kan, H.Y., Kritis, A., Zanni, E., and Kardassis, D. (2001a). Transcriptional regulation of the human apolipoprotein genes. Front Biosci *6*, D456-504.

Zannis, V.I., Kan, H.Y., Kritis, A., Zanni, E.E., and Kardassis, D. (2001b). Transcriptional regulatory mechanisms of the human apolipoprotein genes in vitro and in vivo. Current opinion in lipidology *12*, 181-207.

Zenner, H.L., Yoshimura, S., Barr, F.A., and Crump, C.M. (2011). Analysis of Rab GTPase-activating proteins indicates that Rab1a/b and Rab43 are important for herpes simplex virus 1 secondary envelopment. J Virol *85*, 8012-8021.

Zennou, V., Perez-Caballero, D., Gottlinger, H., and Bieniasz, P.D. (2004). APOBEC3G incorporation into human immunodeficiency virus type 1 particles. J Virol *78*, 12058-12061.

Zhang, S.H., Reddick, R.L., Piedrahita, J.A., and Maeda, N. (1992). Spontaneous hypercholesterolemia and arterial lesions in mice lacking apolipoprotein E. Science *258*, 468-471.

Zhang, W., Chipman, P.R., Corver, J., Johnson, P.R., Zhang, Y., Mukhopadhyay, S., Baker, T.S., Strauss, J.H., Rossmann, M.G., and Kuhn, R.J. (2003a). Visualization of membrane protein domains by cryo-electron microscopy of dengue virus. Nat Struct Biol *10*, 907-912.

Zhang, Y., Corver, J., Chipman, P.R., Zhang, W., Pletnev, S.V., Sedlak, D., Baker, T.S., Strauss, J.H., Kuhn, R.J., and Rossmann, M.G. (2003b). Structures of immature flavivirus particles. EMBO J *22*, 2604-2613.

Zhao, X., Lasell, T.K., and Melancon, P. (2002). Localization of large ADP-ribosylation factor-guanine nucleotide exchange factors to different Golgi compartments: evidence for distinct functions in protein traffic. Mol Biol Cell *13*, 119-133.

Zheng, J.Y., Koda, T., Fujiwara, T., Kishi, M., Ikehara, Y., and Kakinuma, M. (1998). A novel Rab GTPase, Rab33B, is ubiquitously expressed and localized to the medial Golgi cisternae. J Cell Sci *111 (Pt 8)*, 1061-1069.

Zhou, D., Zhang, Y., Li, Q., Chen, Y., He, B., Yang, J., Tu, H., Lei, L., and Yan, H. (2011). Matrix protein-specific IgA antibody inhibits measles virus replication by intracellular neutralization. J Virol *85*, 11090-11097.

Zhou, M., Fisher, E.A., and Ginsberg, H.N. (1998). Regulated Co-translational ubiquitination of apolipoprotein B100. A new paradigm for proteasomal degradation of a secretory protein. J Biol Chem *273*, 24649-24653.

Zhu, Y., Hu, L., Zhou, Y., Yao, Q., Liu, L., and Shao, F. (2010). Structural mechanism of host Rab1 activation by the bifunctional Legionella type IV effector SidM/DrrA. Proc Natl Acad Sci U S A *107*, 4699-4704.

Zhuang, X., Adipietro, K.A., Datta, S., Northup, J.K., and Ray, K. (2010). Rab1 small GTP-binding protein regulates cell surface trafficking of the human calcium-sensing receptor. Endocrinology *151*, 5114-5123.

Zoppino, F.C., Militello, R.D., Slavin, I., Alvarez, C., and Colombo, M.I. (2010). Autophagosome formation depends on the small GTPase Rab1 and functional ER exit sites. Traffic *11*, 1246-1261.